MINERAL PRECIPITATION AND DEPOSITION IN COOLING SYSTEMS USING IMPAIRED WATERS: MECHANISMS, KINETICS, AND INHIBITION

by

Heng Li

B.S.E., Tsinghua University, 1999

M.Phil., University of Hong Kong, 2001

M.S., University of Arizona, 2003

Submitted to the Graduate Faculty of

Swanson School of Engineering in partial fulfillment

of the requirements for the degree of

Doctor of Philosophy

University of Pittsburgh

2010

UNIVERSITY OF PITTSBURGH

SWANSON SCHOOL OF ENGINEERING

This dissertation was presented

by

Heng Li

It was defended on

July 27, 2010

and approved by

Radisav D. Vidic, Professor, Civil and Environmental Engineering Department

David A. Dzombak, Professor, Civil and Environmental Engineering Department (CMU)

Willie F. Harper, Jr., Associate Professor, Civil and Environmental Engineering Department

Di Gao, Assistant Professor, Chemical and Petroleum Engineering Department

Jason D. Monnell, Research Assistant Professor, Civil and Environmental Engineering

Department

Dissertation Director: Radisav D. Vidic, Professor

MINERAL PRECIPITATION AND DEPOSITION IN COOLING SYSTEMS USING

IMPAIRED WATERS: MECHANISMS, KINETICS, AND INHIBITION

Heng Li, Ph.D.

University of Pittsburgh, 2010

Given the increasing water shortage and growing energy demand, novel approaches to water reuse are critical to ensuring sufficient water supply for cooling in thermoelectric power plants. Major challenges arise from complicated chemistries of the waters under consideration and changing operating conditions in open recirculating cooling systems, both of which lead to accelerated mineral precipitation/deposition (mineral scaling). This study evaluated three impaired waters, namely, secondary-treated municipal wastewater, passively-treated abandoned mine drainage, and coal-ash transport water for their use in cooling water systems. The focus of the study was on understanding the mechanisms, kinetics, and inhibition of scaling from both fundamental and applied perspective.

Scaling inhibition with a variety of antiscalants was investigated and polymaleic acid (PMA) was the most effective antiscalant in all three waters. Scale control with PMA is achieved through retardation of mineral precipitation via PMA's competitive interactions with crystallizing ions, and stabilization of suspended mineral particles via surface adsorption of negatively-charged PMA molecules. Nevertheless, biofouling and corrosion, two other main technical challenges in water reuse for cooling, compromised the effectiveness of PMA for scaling control.

Equilibrium-based chemical modeling for scaling prediction exhibited limited success for cooling systems using impaired waters. The model that considered CO_2 degassing, NH_3 stripping, and kinetically-limited solids formation captured the underlying mechanisms dictating the pH changes observed in pilot-scale cooling towers.

Electrochemical Impedance Spectroscopy (EIS) was developed as an in situ, sensitive approach for monitoring scaling rates by measuring the electrical impedance at the solid-liquid interface. The EIS capacitance correlated very well with the mass of mineral deposits and was independent of the chemical composition of the deposits. The applicability of the method was successfully expanded to systems with multiple minerals and broader water chemistries, including secondary treated municipal wastewater.

The key findings of this study indicate that it is possible to control scaling of several impaired waters used as makeup water in cooling systems. The chemical treatment approach demonstrated in this study offers an alternative to costly pre-treatment that is often suggested when impaired waters are used in cooling systems.

TABLE OF CONTENTS

LIST OF TABLES

LIST OF FIGURES

ACRONYMS AND NOMENCLATURE

AAS   Atomic Absorption Spectroscopy

AC   Alternating Current

ALK   Alkalinity (as $CaCO_3$)

AMD   Abandoned Mine Drainage

ANOVA   Analysis Of Variance

APW   Ash-settling Pond Water

atm   Atmosphere (air pressure)

BGD   Billion Gallons per Day

BOD   Biological Oxygen Demand

CCS/CCR   Carbon Capture and Sequestration/Recovery

CE   Counter Electrode

CFU   Colony Forming Unit

C.I.   Confidence Interval

CoC   Cycles of Concentration

COD   Chemical Oxygen Demand

CPE   Constant-Phase Element

DBPs   Disinfection Byproducts

DC	Direct Current
DLVO Theory	Derjaguin, Landau, Verwey, and Overbeek Theory
DO	Dissolved Oxygen
EDS (EDX)	Energy Dispersive X-ray Spectroscopy
EEC	Equivalent Electric Circuit
EIS	Electrochemical Impedance Spectroscopy
EPS	Extracellular Polymeric Substance
GOF	Goodness Of Fit
GPM	Gallons Per Minute
HAP	Hydroxyapatite
HPC	Heterotrophic Plate Count
IAP	Ionic Activity Product
ICP-MS	Inductively Coupled Plasma-Mass Spectroscopy
K-K	Kramers-Kronig
kWh	kilowatt hour
LCA	Life Cycle Assessment (Analysis)
LSI	Langelier Saturation Index
MCA	Monochloramine
MGD	Million Gallons per Day
MIC	Microbiologically Influenced (Induced) Corrosion
MPY	Mils (milli-inches) Per Year
MWW	Municipal Wastewater

NOM	Natural Organic Matter
OCP (OCV)	Open Circuit Potential (Voltage)
ORP	Oxidation Reduction Potential
PAA	Polyacrylic Acid
PBTC	2-Phosphonobutane-1,2,5-tricarboxylic Acid
PE	Polyethylene
PMA	Polymaleic Acid
POTWs	Publicly Owned Treatment Works
PVC	Polyvinyl Chloride
rms	root-mean square
RE	Reference Electrode
RPM (rpm)	Round Per Minute
RSI	Ryzner Scaling/Stability Index
SCE	Saturated Calomel Electrode
SD (sd)	Standard Deviation
SEM	Scanning Electron Microscopy
SS	Stainless Steel
TDS	Total Dissolved Solids
TKPP	Tetrapotassium Pyrophosphate
TOC	Total Organic Carbon
TSS	Total Suspended Solids
TTA	Tolyltriazole

WE	Working Electrode
XRD	X-ray Diffraction

A	Scale Forming Area, m^2
C	Capacitance, farad
C_{dl}	Double-layer Capacitance, farad
d	Scale Coating Thickness, m
E_H^0	Standard Redox/Oxidation Potential, volt (V) or mV
f	AC Frequency, Hz
ΔG_j	Free Energy of Mineral Nucleation with i-mer
ΔG_{bulk}	Bulk Energy Gain of Mineral Nucleation
ΔG_{surf}	Energy Loss due to Mineral Surface Creation
i	The Imaginary Unit, $\sqrt{-1}$
k_f	Nucleation Rate Constant
K_{SP}	Solubility Production Constant
$\mathrm{pH_{iep}}$	Isoelectric Point of pH
r	Radius of Mineral Nucleus, m
r_j^*	Critical Size of Mineral Nucleus, m
R	Ideal Gas Constant
R_P	Polarization Resistance, ohm (Ω)
R_S	Solution Resistance, ohm (Ω)
S	Supersaturation Ratio

T	Temperature, °F, °C, or K
V_M	Molar Volume of Solid Phase, m^3/mole
$V(\omega)$	AC Voltage, volt
ω	Angular Velocity, rad/sec
$I(\omega)$	AC Current, amp
$Z(\omega)$	Impedance, ohm (Ω)
Z_R	Resistive Impedance, ohm (Ω)
Z_C	Capacitive Impedance, ohm (Ω)
Y_0	CPE Constant
ε_r	Dielectric Constant
γ	Surface Tension, mJ/m^2

ACKNOWLEDGEMENTS

I am deeply grateful to my advisor and mentor, Professor Radisav Vidic, for giving me the opportunity to work on a research project that is of both fundamental and applied importance. My doctoral studies under his direction have been an unforgettable journey full of challenge, inspiration, and reward. The profound knowledge and scholarship I have gained from Radisav and the unreserved support I have received are invaluable assets for my continued pursuit of a professional career in environmental engineering and science.

I thank my Ph.D. committee members: Professors David Dzombak, Willie Harper, Di Gao, and Jason Monnell. Professor Dzombak (Carnegie Mellon University) has collaborated with Professor Vidic in a number of projects and directed my work related to those projects. His guidance and critiques were instrumental for the completion of several manuscripts based on this PhD work. Professor Gao (Chemical Engineering) provided valuable discussions on surface treatment as a novel scaling control strategy. His knowledge and experiences were remarkably useful. Professor Harper offered me several teaching opportunities and assistance with my research, and he was a pleasure to work with. Professor Monnell was indispensable to many laboratory-based investigations, especially during the initial stages of my dissertation work.

Dr. Natasa Vidic (Industrial Engineering) provided help with the statistical analysis of the EIS data. Professors Judith Yang (Mechanical Engineering and Materials Science) and Nathaniel Rosi (Chemistry) provided insights about the mechanisms of precipitation inhibition by the

polymer PMA. I also want to thank Professor Uziel Landau at Case Western Reserve University, Professor Ray Taylor at the University of Texas, and Professor Rudy Buchheit at Ohio State University, for their helpful discussions on the promising application of impedance-based electrochemical approaches for mineral deposition detection.

My studies at Pittsburgh would not be as joyful and productive without the countless interactions and mutual learning with my student colleagues and laboratory collaborators: Ming-Kai Hsieh, Shih-Hsiang Chien, Indranil Chowdhury, David Sanchez, Yinghua Feng, Wenshi Liu, Dr. Elise Barbot, Scott Duda, Dr. Matthew Ernest, Briana Niblick, Meng Li, Liangliang Cao, Jiamin Wu, Kent Pu, Maria Jaime, Mahbuboor Choudhury, and Ranjani Theregowda.

I greatly appreciate my wife, Lisa Bai. Her love, understanding, support, and cheer have carried me through the more than 1,000 unrelenting days. My parents in China have always believed in me in whatever I set out to do and have endured for so many years the absence of my company and care. I am forever indebted to them. My dear friends Darren Wilson, Jack Giles, and Alan Reznik at Pittsburgh were always there to provide excellent assistance in editing and proof-reading this document (any errors and omissions are still entirely mine though).

"If there is magic on this planet, it is contained in water."

—Loren Eiseley

"… He will guide them to the springs of waters of life."

—*Revelation* 7:17

1.0   INTRODUCTION

1.1   BACKGROUND AND MOTIVATION

The growing demand for freshwater, driven by population growth and improved living standards, is becoming a great challenge of the 21st century [1, 2]. The current trend of global climate change also affects that demand [3-5]. The need for adequate water supplies has prompted governments, businesses, and communities to act forcefully and embrace water recycling and reuse. Wastewater—water after initial human use—is now being recognized as a significant source of water for many purposes, such as process cooling and agriculture [6, 7]. Process cooling, having surpassed agriculture since 2005, is now the single largest domestic use of freshwater, accounting for 41% of all freshwater withdrawals in the US [8, 9].

Many types of wastewater have been successfully reused in various applications, with the specific applications depending on both the quantity and quality of the wastewater [10]. Treated municipal wastewater (MWW) effluent, for example, represents an abundant and widely available source of water that has been employed as cooling-system makeup water, although only in a handful of cases [7]. MWW contains low to moderate amounts of total suspended solids (TSS) and organic matter, as well as moderate amounts of common mineral ions, such as calcium, carbonates, and phosphates [7]. In a typical recirculating cooling system, which includes elevated temperature and evaporative loss of water, mineral precipitation and deposition

1

(mineral scaling) on piping and heat exchanger surfaces are among the primary problems (the other main issues include corrosion and biofouling). Knowledge about the scaling problem caused by MWW or other types of wastewater is, therefore, of critical importance for their successful reuse in cooling and other applications. Better understanding of the deposition process is of critical importance for the design of effective scale-control measures.

Besides the importance of scale deposition control when using wastewater for cooling, mineral precipitation and deposition are frequently encountered in numerous other water-based processes and have historically resulted in large economic losses. For example, the problem of scale deposition is responsible for 43% of the cost arising from heat exchanger fouling [11]. Also, 4% of the total cost of drinking water supply goes to scale deposition control [12]. Scaling in geothermal heat pump systems for building heating and cooling has been a lingering problem that impedes the wide adoption of this system in many states [13].

Given the increasing interests in water reuse and the ubiquity of the mineral scaling problem in most water-based processes, advancing the understanding of the scale deposition phenomena and scale interactions with antiscaling chemicals, and improving techniques to monitor scale formation and scaling kinetics, become more critical for engineering effective scaling control strategies.

1.2   RESEARCH OBJECTIVES

The overall goal of this study was to evaluate the feasibility of using impaired waters as alternative sources of makeup water for cooling in thermoelectric power generation, with a focus on both fundamental and applied aspects of the behavior of mineral precipitation and deposition

2

(scaling) in the context of impaired water reuse in recirculating cooling systems. The following questions regarding the scaling process are crucial in understanding, quantifying, and solving the scaling problem through well-informed engineering solutions:

- What are the opportunities and challenges in using impaired waters for power plant cooling?

- What kinds of impaired waters are available for power plant cooling? What are the water quality characteristics pertaining to mineral scaling? How severe is the scaling problem in cooling systems using different types of impaired waters?

- What chemical control strategies can be used to mitigate/inhibit scaling in the impaired waters under conditions relevant to recirculating cooling?

- How does simultaneous control of corrosion and biofouling affect scaling control?

- What are the fundamental mechanisms of chemical antiscaling?

- Can chemical equilibrium modeling be useful to facilitate the understanding of scaling and/or the water behavior in recirculating cooling systems?

- Can a better detection method be developed for scaling rate measurements to replace the traditional gravimetric method of mineral mass determination that is crude, unreliable, and time-consuming?

This study was designed and carried out to find answers to these questions. Specifically, experimental investigations were directed towards the following five interconnected objectives:

1) Employ custom-built experimental systems at both laboratory and pilot-scale to examine the scaling behaviors of three impaired waters, secondary-treated municipal wastewater,

passively-treated abandoned mine drainage, and clarified ash pond water, in cooling water pipes under conditions representing open recirculating cooling in power plants.

2) Systematically evaluate antiscaling chemicals to identify effective ones for use with the three impaired waters. Examine the key water quality parameters that impact the performance of the antiscalants. Assess the potentially antagonistic goals of biofouling and corrosion control with regard to scaling control.

3) Evaluate the use of comprehensive chemical modeling in predicting scaling behavior and/or changes of water chemistries of the impaired waters under cooling system operating conditions. Based on experimental findings, propose approaches to improve the modeling.

4) Explore the fundamental mechanisms of scaling inhibition by a chemical that proves to be effective for the impaired waters. The understanding of and insights into the antiscaling mechanisms will help in selecting/developing proper antiscalants for future use.

5) Develop a new scaling detection approach that is convenient and sensitive for use in quantifying scaling rates. Test the robustness of the approach under practically-relevant cooling water conditions, namely, complex water chemistries with chemical additives for simultaneous control of scaling, corrosion, and biofouling.

1.3   SCOPE AND ORGANIZATION OF DISSERTATION

Following the present chapter (Chapter 1) with overall introduction of the dissertation, Chapters 2-9 were each organized as individual manuscripts for journal publication. Chapter 2 provides a

general overview of the escalating water demands for energy production, the potential for use of impair water, and the need to study the technical problems associated with such water use. This investigation is important because, compared to the typical quality of freshwater sources, the lower quality of impaired water in cooling systems can pose several major technical difficulties, including mineral precipitation and deposition (mineral scaling), corrosion, and biofouling.

Many types of impaired water can be potentially used to replace freshwater as cooling system makeup water. Chief among those are secondary-treated municipal wastewater (MWW), passively-treated abandoned mine drainage (AMD), and clarified coal-ash transport and settling pond effluent (APW) within coal-fired power plants. The secondary-treated MWW is potentially the most widely available and geographically accessible source of impaired water for power plant cooling. However, the mineral scaling problems can be a significant impediment to the viability of this water reuse. The control of mineral scale deposition in cooling systems using secondary-treated MWW is the subject of Chapter 3. Theoretical, laboratory, and field studies were conducted to evaluate the mineral deposition propensities of MWW and associated chemical strategies for deposition control under conditions relevant to typical power plant cooling. Chapters 4 and 5 include comprehensive information of the feasibility and challenges of using the passively-treated AMD and the clarified APW in recirculating cooling systems, respectively. Experimental studies showed that polymaleic acid (PMA) effectively decreased the settlability of suspended solids in AMD, thus rendering the solids less prone to deposition in the pipe flow sections of the cooling system. Modeling and laboratory results show that scaling in APW was much less severe than in AMD, even without chemical amendments.

Besides the chemical complexities of the impaired waters, the pH behavior of the cooling water can impact many aspects of proper operations and chemical control regimens in a cooling

system. In Chapter 6, a new modeling approach for reliable prediction of the pH changes in open cooling systems using MWW was presented. The modeling approach greatly improves one's ability to forecast the cooling water pH at various cycles of concentration, even without knowing the recirculating water alkalinity, which was previously a key parameter for pH predictions by other empirical models.

Inspired by the observation of the drastically varied effectiveness of different antiscalants, Chapter 7 investigated the impact of PMA, a polymer that had been repeatedly observed to be very effective in all the three types of impaired water tested, on the kinetics and mechanisms of mineral precipitation and deposition. It was found that the polymer can alter mineral precipitation pathways or even completely inhibit mineral precipitation. The inhibition is based primarily on the retardation of precipitation induction but also on electrostatic repulsions between the polymer-adsorbed mineral colloids and negatively-charged substrate surfaces. Further analysis showed that PMA molecules complexed more strongly with Mg^{2+} than Ca^{2+}. Under the influence of PMA, Mg was incorporated in the amorphous precipitates, which were slower to form than Mg-free crystalline precipitates. These findings improve our fundamental understanding of the antiscaling processes of polymer antiscalants like PMA, and help remove the empiricism in the design of new anti-deposition polymers.

Existing studies of mineral scaling have often relied on simple measurements of bulk water chemistries and/or mineral mass accumulations on substrate surfaces. Chapter 8 presents a new measurement approach based on Electrochemical Impedance Spectroscopy (EIS) to monitor the process of mineral deposition in situ and with requisite sensitivity, both highly valuable traits for detection method. The method was validated in several commonly encountered single-mineral suspensions by comparing and quantitatively correlating with a standard method for

deposition rate measurement via mineral mass determination. Furthermore, the applicability of the EIS method for mineral deposition monitoring was expanded in Chapter 9 under broader water chemistries, including multiple-mineral systems and potential complications of chemical additives for scaling, corrosion, and biofouling control. It was demonstrated that the EIS is a nondestructive method that allows in situ semi-continuous measurement of overall mineral deposition; its sensitivity (< 0.1 mg of deposit detectable) may afford means of early detection of mineral deposition. The method also holds great potential as a surface-based sensor to help elucidate the mechanisms of mineral surface deposition. In addition, it is possible to use narrow ranges of AC scanning frequencies to obtain essentially the same amount of useful information for scale detection, thereby saving measurement time and the EIS device cost.

Chapter 10 provides the main conclusions of this dissertation work and lists the key contributions. Overall, a better understanding of mineral precipitation and deposition processes and a more advanced deposition detection method contribute to informed decision-making for using impaired waters in cooling systems and even broader applications. Extrapolation of this work can be considered for more general areas of geochemical mineralogy and biogeochemistry of environmental concerns, such as mineral-mediated transport and removal of contaminants in ground water environments. The information and insights presented in this work can also add to the understanding of mineral fouling control in membrane filtration and desalination application. Nevertheless, more specific future work that can be directly branched out from this dissertation is given in the final chapter, Chapter 11.

2.0 ESCALATING WATER DEMANDS FOR ENERGY PRODUCTION AND THE POTENTIAL FOR USE OF TREATED MUNICIPAL WASTEWATER

The use of alternative water sources to replace freshwater for cooling will inevitably be a critical requirement to ensure sufficient thermoelectric power production in the future. This chapter discusses the opportunities and challenges of using treated municipal wastewater (MWW) for wet-cooling in thermoelectric power plants. Statistical analysis on the availability of MWW showed that secondary-treated MWW is promising in terms of its quantity and geographical proximity to power plants. Half of the existing coal-fired power plants in the US can meet their cooling water needs using MWW effluent from only 1 or 2 fairly large sewer treatment works that are located within a 10-mile radius. Compared to the typical quality of freshwater, MWW's lower quality can pose several technical difficulties, including scaling, corrosion, and biofouling in cooling systems. The complicated water chemistry of MWW and the varying operating conditions of open recirculating cooling systems pose great challenges for the traditional approaches of using chemicals to control scaling, corrosion, and biofouling. New research is needed to provide technical support for more suitable control strategies to mitigate these problems when MWW is used as makeup water. Although existing federal regulations do not prohibit using impaired waters for power plant cooling, and the state regulations impose a minimal set of additional environmental requirements for such practices, forward-thinking

strategies should be proposed and evaluated to ensure protection of the public and the environment as the use of MWW in power plant cooling systems becomes more common.

2.1 INTRODUCTION

Water and energy are inseparable in many ways. For instance, water supply and wastewater treatment both require energy input. On the other hand, water is needed in power plant cooling to drive the thermoelectric energy generation. According to the latest survey, total water withdrawal in the US reached 410 billion gallons per day (BGD) in 2005, of which 349 BGD was freshwater and the rest (15%) was saline water [1]. Among the major freshwater uses, thermoelectric power generation has surpassed agriculture to become the number one use (41%) since 2005. Reliable and abundant water sources are required to ensure sufficient power generation in the future. However, the increasing water shortages and the global warming effect further exacerbate the fierce competition for water among various users [2].

In the effort to reduce green house gas emissions, implementation of carbon capture and sequestration/reuse (CCS/CCR) has been the focus of policy enforcement. However, the adoption of CCS/CCR will increase water consumption by 76-90% in a fossil-fuel power plant due to the decrease in power generation efficiency and the need of water for the CCS/CCR processes [3].

Coal, natural gas, and nuclear power, added together, account for nearly 90% of the world's electricity produced in thermoelectric power plants [4]. Regardless of the cooling technology used in these power plants, either recirculating cooling or once-through cooling, water is critical to cool and condense the steam in the boiler water loop [5].

9

Several cases in arid regions, such as Arizona and Texas, have shown that the lack of available cooling water resulted in suspension for existing power plants and permit denial for constructing new plants [6, 7]. Rising demand for electricity in those areas will lead to difficult decisions in water allocating priorities and finding reliable water sources for electricity production. The use of alternative water sources for power plant cooling will likely be an inevitable requirement to ensure sufficient energy production in the future. Moreover, tightening regulation of water intake structures imposed by the Clean Water Act (CWA) to protect fish and other aquatic life (CWA section 316(b)) has put the power plants and other industrial facilities in a challenging position for natural water withdrawal. Indeed, the ability to use alternative water sources for cooling may provide a competitive advantage for new power plants with respect to siting and construction permits [8].

Many types of nontraditional water sources may be considered for power plant cooling. However, their use may be restricted by drastically varied availability and quality. For instance, passively-treated coal mine drainage is most abundant in Pennsylvania and West Virginia, while the most severe water constraints for cooling are more likely to lie in western US [9]. Water is used to transport either fly ash or bottom ash generated from coal combustion and the effluent from ash settling pond is readily available for reuse. However, it is shown that ash pond water can only serve for emergency use due to its limited amount. At best, this water can satisfy 25% of the need for cooling water makeup [10-12]. Among all the alternatives, treated municipal wastewater (MWW) is considered as the most promising water owing to its ubiquitous availability and fairly steady quality [13].

Although using treated municipal wastewater to replace freshwater withdrawal for power plant cooling seems to be feasible based on its availability, use of this impaired water can pose

several technical difficulties in cooling systems because of its lower quality compared to typical freshwater sources. Metal corrosion, mineral scaling, and biofouling are the major technical challenges.

Besides the technical challenges with the use of MWW, legal basis for wastewater reuse for power plant cooling needs to be considered. Whether the cooling systems are new or being retrofitted, any water reuse program needs to comply with federal, state, and local regulations. The issue of water ownership and right of use may also complicate the use of treated MWW if interstate water transportation is involved. In addition to legal considerations, potential air-borne pollution and proper blowdown discharge from the cooling systems using concentrated wastewater are among the public concerns that must be addressed.

2.2   ABUNDANCE AND ACCESSIBILITY OF MWW FOR POWER PLANTS

Treated MWW holds the great potential to be the most promising alternative water sources for power plant cooling in the US. Therefore, the analysis of the quantity, availability, and geographical proximity of treated MWW for power plants is critically needed and should precede technical assessment of the feasibility of MWW reuse for cooling.

It is estimated that a total volume of 30-40 billion gallons of municipal wastewater is treated per day in the US [14]. However, this amount of water is not evenly distributed and the effluent discharge rates may vary significantly from site to site. For the analysis of MWW availability for power plant cooling, a comparison must be performed between the location and amount of water supply and prospective water consumption. The publicly owned treatment works (POTWs), which are the most reliable and accessible point water sources regulated by the

11

National Pollutant Discharge Elimination System (NPDES) permit program [15], are considered here as the major water providers. Based on NPDES, MWW effluents must reach at least the secondary treatment level and be disinfected prior to discharge from the treatment facilities. A database containing water flowrates and geographical locations of 33,852 NPDES permitted discharges has been constructed by the US EPA since 1996, of which 17,864 are POTWs in the lower 48 states and can be considered as potential water providers for power plant cooling.

The amount of water withdrawal for power plant cooling system makeup can be very different, depending on the particular cooling technology used in the power plant. For a once-through cooling system, 20–50 gallons of water are used to generate one kWh of electricity. On the other hand, modern recirculating cooling towers need 0.2-0.6 gallons of water to generate each kWh of electricity [11]. However, the construction of once-through cooling systems is no longer permitted by CWA 316(b), and the focus of this study was on recirculating cooling systems.

Among all thermoelectric power plants in the lower 48 states, 407 coal-fired power plants are selected to represent potential users of treated MWW for cooling. It is assumed that the cooling systems in these 407 power plants are recirculating systems, regardless of their current actual configurations. The cooling water demand is then estimated by using a conversion factor of 0.6 gallons of water per kWh of electricity produced.

The correlation between the water providers and water users are determined using geospatial analysis (ArcGIS version 9.2, ESRI, Redlands, CA). The number of POTWs required to satisfy the water needs of a power plant within a specified radius is determined. Coverage of 10 and 25 mile radius is examined to ensure reasonable transportation distance of the treated MWW from the POTWs to power plant.

The GIS data show that in Pennsylvania, for example, there are 11.7 POTWs on average within a 10-mile radius around each existing power plant, and 62.5 POTWs when the range is extended to 25 miles. Nationwide, about 50% of existing power plants can obtain sufficient amount of cooling water from POTWs located within a 10-mile radius. Furthermore, for these power plants only 1.14 POTWs can supply enough water to meet their water demand. On the other hand, 76% of the power plants can have sufficient cooling water supply from an average of 1.46 POTWs if the radius is extended to 25 miles. It is important to note that only one or two water conveyance pipes of reasonable length (less than 25 miles) are required between a power plant and the POTWs to supply sufficient amount of cooling water to replace more than 50% of current freshwater withdrawal for power plant cooling. The use of MWW as an alternative makeup water for power plant cooling is particularly meaningful for the development of coal-fired power plants in regions where freshwater sources are not readily available.

2.3   TECHNICAL CHALLENGES

2.3.1   Inorganic Scaling

Given the relatively high levels of both dissolved and suspended solids, alkalinity, and hardness in typical secondary-treated MWW (Table 2.1), a primary concern when using the wastewater for recirculating cooling is the potentially severe mineral scaling problems. Scale formation in cooling systems causes a multitude of operational problems, chief among which are the hindrance of heat transfer, the obstruction of pipe flow, pump failures, and accelerated fall-down of cooling tower fills [16]. The bottom line is that scaling causes large economic losses in

virtually all water-based industrial processes. The control of scaling is imperative to ensure proper operations of these processes.

Table 2.1. Quality of secondary-treated municipal wastewater (typical ranges of concentration)

Parameter	Range
pH	7-8
BOD (mg/L)	3-30
COD (mg/L)	40-80
TDS (mg/L)	130-1600
TSS (mg/L)	10-50
Alkalinity (mg/L as $CaCO_3$)	100-500
Ca (mg/L)	28-185
Mg (mg/L)	23-150
NH_3-N (mg/L)	3-73
NO_3-N (mg/L)	10-30
SO_4 (mg/L)	60-293
PO_4 (mg/L)	0.6-51
Conductivity (mS/cm)	0.2-1.2

An important operational parameter in recirculating cooling is Cycles of Concentration, or CoC, which is the primary cause of mineral precipitation and scaling. In a recirculating cooling system, there are basically two water loops. One is a closed loop for boiler water and the other is an open loop for cooling water. Heat from the closed loop is transferred to the open loop at the heat exchanger. The warm water coming from the heat exchanger is distributed at the top of the cooling tower. Airflow in the counter direction (or cross-flow direction, depending on the specific tower configuration) takes the heat out through evaporative water losses, and the cooled

14

water is cycled back to the heat exchanger. During the cooling water cycling, the evaporative water losses lead to increased concentration of mineral salts in the cooling water. Assuming there is no loss of the dissolved species to either evaporation or deposition, the CoC can be calculated by either the volume of evaporative water loss or by the level of the salt concentration increase. However, some salts eventually become supersaturated and precipitate out of solution to form scales. In this case, the volume-based CoC calculation is more appropriate that salt concentration based. Moreover, the elevated temperature of the bulk water may exaggerate mineral scaling, especially for some common minerals such as calcium carbonates. To avoid excessive scaling, a portion of the concentrated bulk water is removed through blowdown. At steady state operation, feedwater is brought in to make up the volume loss due to evaporation and blowdown.

Power plant cooling using freshwater may generally encounter only minor scaling problems, especially when the system is operated at low CoC [17]. However, in the case of using MWW as makeup water, the cooling tower performance could be significantly compromised by scaling problems when the water chemistry is not properly managed. A better understanding of the mineral deposition processes and mechanisms of MWW in cooling systems is therefore required before sound control technologies can be developed and implemented to inhibit mineral deposition.

The development of inorganic solids from an aqueous solution starts with the nucleation of minerals from their constituting ions which, based on their ionic complementarity, form small clusters. These clusters undergo a dynamic process of growth and disintegration governed by the counterplay between the energy penalty incurred by surface generation and the energy gain related to the formation of a crystal lattice [18, 19]. At the point where the surface energy cost is counterbalanced by the energy of crystal phase formation, a critical size is reached. Afterwards,

continued growth leads to a reduction of the Gibbs energy of the system as the further decrease of the lattice energy over-compensates for the increase in surface energy. As the spontaneous growth ensues, a critical nucleus develops into a primary nanoparticle. These nanoparticles further develop into larger particles either by the addition of ions or by the oriented attachment of multiple particles. This entire process manifests in the bulk solution as mineral precipitation.

A substantial amount of research has already been devoted to the thermodynamics and kinetics of mineral precipitation and dissolution in bulk solutions. Characterization of single minerals (e.g., calcium carbonates, calcium sulfates, iron oxides) in relatively simple solutions is well documented in the literature. However, the knowledge acquired from these studies can be inadequate for elucidating mineral precipitation behaviors of MWW, which contains a whole array of inorganic and organic chemical constituents, as well as certain amount of particulate matter. The effects of co-existing chemical species on the precipitation behavior of a particular mineral, being either synergistic or antagonistic, have not been studied extensively. Attempts to apply the specific data obtained from simple aqueous systems to more complex ones containing multiple chemical constituents is likely to achieve limited success.

Thermodynamic calculations indicate the formation of dolomite ($CaMg(CO_3)_2$) in a solution supersaturated with calcium, magnesium, and carbonate. However, direct dolomite precipitation in laboratories and natural waters under normal conditions (temperature, pressure, and salinity) has rarely been observed; the phases that actually form consist of aragonite and magnesian calcite (a solid solution) [20, 21]. Thus, great care must be taken in using simple thermodynamic calculations to predict behaviors of complex water systems, such as concentrated municipal wastewater, where carbonate minerals are dominated by metastable phases and

16

deposition reactions may be governed by uncharacterized foreign surfaces or poorly understood phases whose properties differ significantly from underlying bulk mineral.

A number of common ions present in aqueous solution can pose inhibitory effects to Ca-based mineral precipitation. The presence of Mg^{2+} appears to cause the precipitation of beta-tricalcium phosphate rather than apatite and the precipitation of magnesian calcium carbonate rather than calcite [22-25]. In the case of Ca-P precipitation, the net effect of Mg^{2+} is to increase the phosphate solubility at pH below 9, but to decrease it at higher pH due to Mg precipitation as $Mg(OH)_2$. The inhibition effect of Mg^{2+} results from its incorporation into the Ca-P solid lattice, which prevents the formation of a well-crystalline Ca-P structure [26, 27].

Natural organic matter (NOM) and organic acids are known to inhibit mineral precipitation [28-34]. However, the chemical and physical processes involved in the inhibition are not well understood because of the complexity of the chemistry and structural variabilities of the dissolved organic matter. The inhibitory effects of organic acids on precipitation of Ca-P have been generally attributed to their adsorption onto newly formed Ca-P nuclei, thereby blocking the active sites for further crystal growth. Aqueous complexation of the acids with Ca could also have inhibitory effects by lowering free Ca concentration in solution and thus reducing its supersaturation levels with respect to phosphate or carbonate anions. However, such direct complexation mechanism is noted to be less important compared to the effect of adsorption onto nucleus growth sites [31].

Commonly used methods for monitoring scale formation are electrical conductivity and turbidity measurements [35]. However, the response from both these techniques is dominated by mineral precipitation events in the bulk suspension. In effect, neither technique is able to detect mineral deposition, which is a surface process. Therefore, to study scale inhibitors and their

ability to prevent scale formation, it is critical to use a detection method that is able to differentiate between the bulk and surface processes and is able to quantify the scale deposition on a given surface. In addition, in the context of using treated MWW as a source of industrial cooling water, the effect of disinfectants, which are commonly added for bio-control, on mineral scaling has not been studied. Lack of understanding of these issues hinders the development of control strategies for mineral deposition that are pre-requisite for successful reuse of MWW for cooling.

2.3.2 Biological Fouling

Although the treatment processes employed in most POTWs remove large portion of biodegradable organic content, treated MWW still contains appreciable levels of phosphorus, nitrogen, and residual organic matter. Warm, moist, and nutrient-rich environment in recirculating cooling systems is conducive to continued biological growth, including a wide range of microorganisms such as bacteria, fungi, and algae [36]. Typical cooling operation, such as temperature at 35-45°C, pH 6-9, continuous aeration, and sunlight exposure, makes the cooling system a favorable habitat for biological growth. The CoC effect concentrates the organic matter and other nutrients in the bulk cooling water, which renders the biological growth control even more challenging.

Biological growth can quickly lead to biomass/slime accumulation on equipment surfaces, a process known as biological fouling (biofouling). For example, biofouling is able to develop on heat exchanger surfaces within 4-8 hr [37]. The resulting biofilm can bind with suspended solids, silt, corrosion products, and organic and inorganic deposits, which greatly exaggerates mineral scaling and corrosion (microbial induced corrosion underneath biofilm) problems [38].

Control of biofouling can be achieved through chemical or physical methods. Application of proper chemical biocides is a widely adopted approach based on cooling system design and the makeup water quality. Chemical biocides work through three primary mechanisms: 1) damage the microbial membrane and cell structures, 2) disrupt the microbial metabolic functions, and 3) interrupt the biosynthesis of crucial substances [39]. The disinfection efficiency is affected by water temperature, pH, redox condition, chemicals added for corrosion and scaling control [37, 39]. A general guideline of acceptable biofouling control is 10^4 CFU/mL (CFU: Colony Forming Unit) for planktonic bacteria or 10^4 CFU/cm^2 for sessile bacteria measured by the standard heterotrophic plate counts (HPC) [38].

Chlorination is the most common chemical program used in cooling systems to control biogrowth because of its high efficiency, easy accessibility, and low cost [36]. Biofouling can be well mitigated by maintaining a proper disinfectant residual concentration in the bulk water. However, elevated organic content and ammonia concentration in cooling systems using MWW can greatly increase the free chlorine dose required to achieve breakpoint chlorination. Moreover, free chlorine tends to react with natural organic matter to form undesirable disinfection byproducts (DBPs), which can endanger public health when they are discharged into surface waters.

Monochloramine has been demonstrated to be as effective as free chlorine in biofouling control when secondary-treated MWW is used in cooling systems [40]. Application of monochloramine was shown to be more effective than free chlorine in preventing the development of biofilm in a cooling system [41]. Chloramination usually requires higher residual concentrations than chlorination (1-3 ppm higher) to achieve comparable disinfection effectiveness. Nevertheless, monochloramine is more stable with lower decomposition rates

compared to free chlorine [42, 43]. As such, the overall chemical consumption can be potentially lower with chloramination than chlorination.

Our study [13] indicated that monochloramine can be very effective in controlling biofouling in pilot-scale cooling tower systems using secondary-treated MWW and operating at CoC 4. Results from bench-scale experiments indicate that carbonate, phosphate, or sulfate did not significantly interfere with the in situ formation of monochloramine in the wastewater. However, all of these constituents increased monochloramine decomposition rate. Natural organic matter also slightly increased the decomposition rate through redox and substitution reactions. Overall, the results from our bench studies are in agreement with the work presented by Rao et al. [40]. However, the results from our pilot tests indicated that in situ chloramine formation through the reaction between ammonia present in the MWW and sodium hypochlorite added to the cooling tower was not reliable. To maintain the total chlorine level above 1 ppm (as Cl_2), pre-formed monochloramine had to be added to reduce HPC in planktonic and sessile phases below the respective target biocontrol criteria.

In conclusion, monochloramine can be used to replace free chlorine as an effective disinfectant in cooling systems using secondary-treated MWW as makeup water. It is essential to continuously dose pre-formed monochloramine to maintain target residual disinfectant (2-3 ppm) and keep the bioactivity under control.

2.3.3   Corrosion

Another challenge when using treated municipal wastewater as makeup water in recirculating cooling water systems comes from corrosion of metal heat-transfer surfaces and conveyance pipes due to degraded quality of the wastewater and is exacerbated by mineral scaling and

biofouling. As a result, knowledge of traditional corrosion control approaches built on the experience with freshwater as cooling system makeup water needs to be re-evaluated.

Among the many water quality parameters influencing corrosion in cooling systems using MWW, phosphate and ammonia are of the great interests. Ammonia and phosphate concentrations in secondary-treated MWW can reach up to 70 and 50 mg/L, respectively (Table 2.1). Ammonia is a strong complexing agent toward many metals and metal alloys and can be very corrosive [44]. It is recommended that the ammonia concentration in cooling systems should not exceed 2 mg/L (as NH_3) [45]. Although the ammonia in the makeup water (MWW) can be high, several studies reported that the ammonia in recirculating cooling water was low [46-48]. Such findings are most likely due to stripping and nitrification in cooling towers, where high water temperature (40-50°C), high pH (8-9), and active aeration are all in favor of evaporative loss of ammonia. The knowledge of ammonia stripping and nitrification in cooling towers is important for determining corrosion control strategies to overcome the aggressiveness of ammonia. However, the study of ammonia stripping and nitrification in cooling towers has not yet been conducted.

Phosphate can adsorb onto the surface of metals and metal alloys to form a protective thin film against corrosion [49] and has been used as a corrosion inhibitor in cooling systems. Calcium phosphate has limited solubility and its precipitation and surface deposition help to mitigate corrosion. However, excessive phosphate precipitation can be a problem when the water contains high hardness. Preliminary results of the stability of phosphate and phosphate-based corrosion inhibitors currently being studied in our laboratory show that these inhibitors tend to precipitate in treated MWW. Furthermore, acid addition to the cooling water is still commonly practiced to control mineral precipitation. The decreased pH raises the corrosivity of the cooling

21

water. Therefore, pH control-based scaling mitigation can compromise the potential advantage of using mineral precipitation for corrosion inhibition. Studies on the optimal acidification strategies that balance scaling and corrosion problems would be of great interest.

As discussed in the previous section, cooling systems using MWW can have high biofouling potential, which can cause microbiologically influenced corrosion (MIC). Traditional approaches of maintaining free chlorine residuals for biofouling control may cause higher corrosion rates due to the direct attack of free chlorine on metals and metal alloys. Free chlorine also degrades tolyltriazole (TTA), a commonly used copper corrosion inhibitor. Instead of free chlorine, monochloramine may be more appropriate for use in cooling systems using MWW, but its influence on the corrosion of metal alloys and the corrosion inhibitors needs to be further evaluated.

Chemical additives for the control of corrosion are still the most widely employed approach in recirculating cooling systems. When a cooling system switches its makeup water source from freshwater to treated MWW, traditionally proven corrosion control approaches may not work well and need to be re-evaluated taking into account degraded water quality and the scaling/biofouling phenomena and associated control strategies.

2.4   REGULATORY ISSUES AND COMMUNITY ACCEPTANCE

A number of power plants have already blended MWW with freshwater as a cooling makeup [11, 15], but the blend ratio varies significantly. Only a few power plants have operated their cooling towers with treated MWW as the dominant makeup water. One notable example is the Redhawk Power Plant in Arizona that uses over 90% of MWW as its makeup water. The 6.46

MGD of wastewater used by the facility is transported 40 miles from a wastewater treatment facility, which is located at a higher elevation than the power plant. However, the MWW received at the power plant has been further treated before feeding into the cooling towers. Power plants usually do not use 100% MWW as cooling system makeup due to a lack of technical knowledge and legal framework to support such practices.

Currently, the US federal government does not directly regulate any practices of water reuse, including the reuse of treated MWW as power plant cooling water. EPA has recommended guidelines of minimum treatment requirements and desired water quality for water discharge programs for industrial cooling systems [15]. Effluent (blowdown) leaving the cooling water system should meet the technology-based limits on BOD_5, TSS, and pH. Fecal coliforms are also restricted with a minimum chlorine residual requirement to limit the bacterial activity in the drift, which has high potential to enter the human respiration system and cause health problems.

In addition to the federal EPA water reuse guidelines, several states have been developing regulations applicable to wastewater reuse in power plant cooling systems. The state regulations largely focus on the reduction of water aerosols emitted from cooling tower drift, which may contain elevated concentrations of pollutants and microorganisms and pose a health risk to the public. Generally speaking, however, there are no major impediments for the use of treated MWW from POTWs to meet the growing cooling water needs of thermoelectric power plants.

2.5   SUMMARY: STATUS AND POTENTIAL

Increasing population and economic development will continue to drive the demand for electric power in the years ahead. According to the U.N. Environment Program, the global

energy demand will increase by 49% from 2007 to 2035 [50]. Despite growth in renewable energy sources, most of the electricity generating capacity in the decades ahead will still be from coal-fired and nuclear thermoelectric power plants. In most thermoelectric power production, water is used for cooling. About half of the existing power plants in the US employ once-through cooling, which will not be an option for proposed new power plants and may not be available for re-permitted plants. In recent years, water withdrawal for power plant cooling has surpassed agriculture to become the number one use of freshwater in the US. Meeting the freshwater demand of new power generation capacity will be very difficult in parts of the country that already have limitations on available freshwater, most notably in the west and southwest regions of the US. A number of proposed power plants were denied permits due to the lack of sufficient freshwater for cooling.

Waters of impaired quality can be used as alternative sources of makeup water for recirculating cooling systems in electric power plants. Some alternative sources include treated municipal wastewater, abandoned mine drainage, and industrial process wastewater. Treated municipal wastewater is the most widely available and easily accessible water source.

Under typical cooling tower operating conditions, i.e., elevated temperature and evaporative loss of water that leads to concentration of minerals during water recirculation, mineral precipitation and deposition, commonly referred to as mineral scaling, is among the primary concerns when treated MWW is used as cooling tower makeup water. Control of algae, bacteria, fungi, and other organisms is also essential for efficient cooling tower operation due to health concerns for people in the vicinity of the power plants using MWW in cooling systems (disease-causing organisms may escape with aerosols). Given the potentially high levels of

ammonia and phosphate in the source water, intensive protection of all metals in contact with the cooling water from corrosion is necessary.

The feasibility of using chemical inhibitors in combination with advanced treatment to manage the cooling water quality need to be examined to ensure successful use of treated MWW for power plant cooling. Systematic investigations employing both bench-scale systems and pilot-scale cooling towers are needed to explore optimal chemical treatment strategies for controlling corrosion, scaling, and biofouling before the most promising strategies can be tested in the field. Tertiary treatment, such as nitrification and/or filtration, may be required to reduce levels of suspended solids, bioactivity, organic matter, and alkalinity. Studies to determine the most cost effective approaches for managing MWW in cooling systems are critical. Changing regulatory issues, e.g., more controls on inter-basin transfers, concerns for extra contaminants in drift, need to be considered.

The environmental impacts during delivery, treatment, use, and discharge of MWW for cooling need to be investigated. In this regard, a comparative Life Cycle Assessment (LCA) of alternative pre-treatment and operating strategies is needed to inform sustainable design and decision-making. Social and institutional barriers to reuse of this water for power plant cooling may exist and work should be undertaken to identify such barriers and develop approaches to overcome them to ensure further development of power generation capacity in the future.

3.0   CONTROL OF MINERAL SCALE DEPOSITION IN COOLING SYSTEMS USING SECONDARY-TREATED MUNICIPAL WASTEWATER

Secondary-treated municipal wastewater (MWW) is a promising alternative to freshwater as power plant cooling-system makeup water, especially in arid regions. A prominent challenge for the successful use of MWW for cooling is potentially severe mineral deposition (scaling) on pipe surfaces. In this study, theoretical, laboratory, and field work were conducted to evaluate the mineral deposition potential of MWW and its deposition control strategies under conditions relevant to power plant cooling systems. Polymaleic acid (PMA) was found to effectively reduce scale formation when the makeup water was concentrated four times in a recirculating cooling system. It was the most effective deposition inhibitor of those studied when applied at 10 mg/L dosing level in a synthetic MWW. However, the deposition inhibition by PMA was compromised by free chlorine added for biogrowth control. Ammonia present in the wastewater suppressed the reaction of the free chlorine with PMA through the formation of chloramines. Monochloramine, an alternative to free chlorine, was found to be less reactive with PMA than free chlorine. In pilot tests, scaling control was more complex due to the inevitable occurrence of biofouling even with effective disinfection. Phosphorous-based corrosion inhibitors are not appropriate due to their significant loss through precipitation reactions with calcium. Chemical equilibrium modeling helped with interpretation of mineral precipitation behavior but must be

used with caution for recirculating cooling systems, especially with use of MWW, where kinetic limitations and complex water chemistries often prevail.

3.1   INTRODUCTION

With increasing shortages of freshwater, wastewater is now being recognized as a significant source of water for non-potable uses [1, 2]. Among different types of wastewater, secondary-treated municipal wastewater (MWW) is of increasing interest, primarily because it holds promise as a viable alternative source of cooling water in terms of quantity and geographical proximity to existing and future power plants in the US [3]. A number of power plants already use MWW as makeup water in their recirculating cooling water systems [4, 5]. The majority of these power plants are in regions of the US most susceptible to freshwater constraints, i.e., the southwest and Florida. These power plants typically use MWW only as a fraction of the total makeup water needed or only after significant additional treatment to obtain better water quality.

The primary challenges with MWW reuse for cooling arise from its low quality. Secondary-treated MWW usually contains appreciable amounts of hardness, phosphate, ammonia, dissolved solids, and organic matter compared to the amounts in freshwater [6, 7]. In recirculating cooling systems, the water constituents become concentrated many times (typically 4-8 times) because of the evaporative loss of water. The elevated concentrations and high water temperature can cause severe mineral deposition (scaling) problems, along with the problems of corrosion and biofouling. Because of these challenges, intensive chemical control programs are usually implemented [8]. Neither the mineral deposition characteristics of MWW under cooling system conditions nor the feasibility of controlling deposit formation through chemical addition

when using MWW as the sole source of makeup water in a recirculating cooling system have been studied.

Presently, three types of deposit inhibition chemicals—antiscalants—are widely used to prevent mineral deposition on pipe and heat exchanger surfaces in cooling systems: carboxylic polymers, such as polyacrylic acid (PAA), polyacrylamid, and polymaleic acid (PMA); phosphonates; and polyphosphates. Polymeric antiscalants often incorporate functional groups in addition to carboxylate such as sulfonate or benzenesulfonate [9, 10].

Multiple antiscaling mechanisms working together contribute to the effectiveness of the antiscaling chemicals. First, the precipitation propensity of minerals is mitigated through complexation with antiscalant molecules to increase the operational solubility of cationic species, primarily Ca and Mg, the most common potential scale forming species in water [11]. Second, the antiscalants can interact with newly formed mineral nuclei to disrupt the crystallization process, thereby hindering the growth of the precipitating particles [9, 12]. Antiscalants for which this mechanism is dominant are commonly referred to as threshold inhibitors. Third, antiscalant molecules can stabilize the mineral particulates through electrostatic and/or steric interactions to keep them dispersed in the aqueous suspension, rendering them less prone to sedimentation or deposition [11]. A fourth mechanism of scale inhibition involves adsorption of antiscalants onto pipe surfaces to prevent mineral deposition onto the surfaces. For example, phosphorous-bearing groups exhibit strong interactions with surfaces of metals and metal oxides [13]. Based on the similar mechanism of surface adsorption, some phosphonates and polyphosphates are used as corrosion inhibitors as well because a surface layer of these molecules retards surface redox reactions [14]. However, many of the phosphorous-based compounds, particularly the polyphosphates, suffer from hydrolysis reactions that produce

orthophosphate [15], potentially exacerbating phosphate scaling when the water contains significant hardness. The effectiveness and fate of phosphorous-based inhibitors when applied in cooling systems using MWW has not been well studied.

Numerous polymer antiscalants with varied molecular weight, structural features, and effectiveness in different waters are available commercially. PMA was selected in this study as a model polymer antiscalant based on a literature survey and consultation with practitioners in cooling system design and operation. PMA is believed to act as both a colloid dispersant and a crystal distorter, particularly for Ca-containing precipitates, the potentially dominant scale formers in MWW [2, 5, 16-18]. Besides PMA, representative antiscalants containing phosphonates or polyphosphates, including 3-phosphonobutane-1,2,4-tricarboxylic acid (PBTC) and tetra-potassium pyrophosphate (TKPP), were also tested for their effectiveness in MWW.

The influence of orthophosphate and ammonia present in MWW on scaling control is of particular interest. Both ortho- and polyphosphate (much less abundant than orthophosphate) may precipitate with di- and trivalent cations. Ammonia is a strong complexing agent, especially for copper and iron, both of which are common pipe/heat exchanger materials in cooling systems [19]. Another concern with the use of MWW for cooling lies in the need to control biogrowth. The use of chlorine as a biocide may potentially compromise the effectiveness of organic antiscalants because free chlorine, a strong oxidant, is aggressive toward many aqueous organic compounds and pipe materials. For example, studies show that large doses of chlorine significantly increase mild steel corrosion [20], which leads to iron dissolution and precipitation on the pipe surface. Ammonia, on the other hand, can combine with free chlorine to form chloramines, which pose less risk for metal alloy corrosion [21]. The influence of chloramines on scaling control in cooling systems that use treated MWW has not been investigated in detail.

Quantitative analytical methods for studying mineral scaling in cooling systems are not readily available in the literature. There is a general lack of well-documented methods suitable for in situ measurements of mineral deposition kinetics. Most established techniques pertaining to mineral scaling phenomena confine themselves to means of static observations and analysis only after solid scales have formed and been collected. For example, ASTM standard methods D 1245-84, D 2331-80, D 933-84, D 934-80, and D 887-82 only deal with the procedures of removing water-formed deposits from sample tubes by specified mechanical or chemical means, and with qualitative identification of deposits by spectroscopy-based analysis. Very limited effort has been devoted to the study of mineral scaling kinetics in terms of how scales form, at what rate(s) they form, and the mechanisms and conditions influencing their formation in waters of varying quality.

The objectives of this study were to investigate the effects of orthophosphate and ammonia on the performance of scaling control by PMA in cooling systems using treated MWW, and to test the feasibility of biocontrol by chlorine and corrosion control by phosphorous-bearing chemicals without interfering with scale inhibition under recirculating cooling conditions. Chemical equilibrium calculations were performed to evaluate the mineral deposition potential of MWW under a range of cooling water conditions. Laboratory studies were conducted to determine effective deposition control strategies under conditions relevant to industrial cooling systems, i.e., elevated temperature, circulating flow, and concentrated water constituents. In addition, pilot-scale cooling tower tests were conducted to study the effectiveness of the model polymer antiscalant, PMA, and the potential applicability and implications of an integrated chemical regimen for the successful control of scaling, corrosion, and biofouling in using treated MWW for cooling.

3.2   MATERIALS AND METHODS

3.2.1   Secondary-Treated Municipal Wastewater

A secondary-treated municipal wastewater effluent (i.e., biological trickling filter followed by secondary clarification) was collected for use in bench-scale experiments. The effluent was at the Franklin Township Municipal Sanitary Authority wastewater treatment plant located in Murrysville, PA. Polyethylene (PE) containers (1-L bottles or 5-gallon jars) were used for temporary storage of the MWW before experiments. Typical storage time was less than 24 hours, otherwise the water was refrigerated.

To characterize the water quality of secondary-treated MWW, both filtered (0.45-µm) and unfiltered water samples were collected and transferred to different PE containers that were prepared with the addition of appropriate acid preservatives. Metal concentrations were determined by inductively coupled plasma mass spectroscopy (ICP-MS) at a commercial laboratory (Test America Analytical Services, Pittsburgh, PA). Other water quality parameters were determined either in our laboratories at the University of Pittsburgh or at the commercial lab, using appropriate standard test procedures. The concentrations of calcium and magnesium, the two principal cationic species, were measured by Atomic Absorption Spectroscopy (AAS). The water quality data for secondary-treated MWW are provided in Table 3.1.

For bench-scale experiments, the wastewater effluent sample was concentrated in the laboratory by evaporation at 40°C to reach 4 cycles of concentration (CoC 4) as determined by 75% volume reduction, prior to use in a bench-scale water recirculating system (Figure 3.1). However, it was discovered from preliminary tests that pre-concentrating the MWW resulted in a loss of mineral content due to precipitation that took place during the concentration step. This

31

premature precipitation made the concentrated water less representative of MWW at CoC 4. As such, a synthetic municipal wastewater was prepared that truly represented CoC 4 in terms of its mineral content (i.e., four times more concentrated than the MWW) for detailed investigation in the bench-scale studies. The synthetic MWW (CoC 4) was made using DI water (resistivity > 18 MΩ-cm) with the addition of desired chemical constituents (reagent grade or better). The chemical recipe of the synthetic MWW (CoC 4) is provided in Table 3.2.
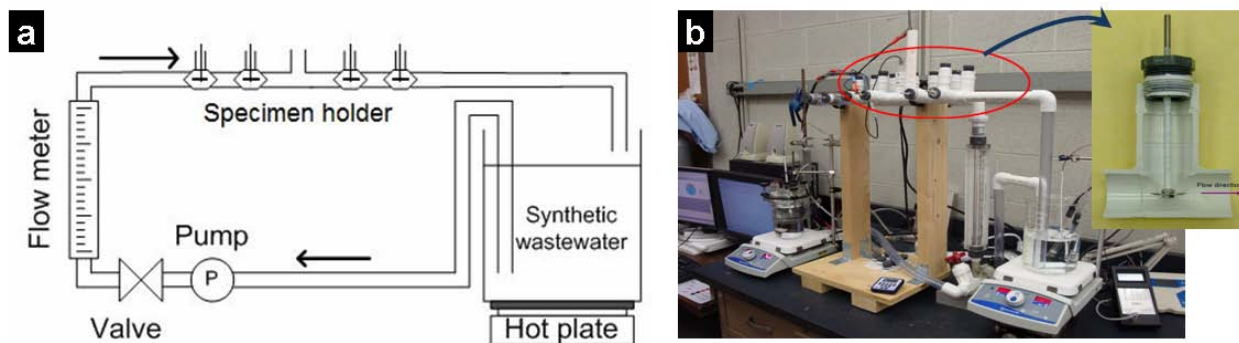
Figure 3.1 Customized bench-scale water recirculation system for examining mineral deposition..

(a) Schematic flow chart. (b) Picture of the experimental setup with a pipe flow section showing the circular metal disc used to collect mineral deposits.

Table 3.1 Chemical composition of the secondary-treated municipal wastewater (MWW) from Franklin Township
Municipal Sanitary Authority, Murrysville, PA

Analyte	Unit	Result (unfiltered)	(filtered)	Analysis limit
Al	mg/L	0.2	-	0.2
Ca	mg/L	42	41	5
Cu	mg/L	0.028	-	0.025
Fe	mg/L	0.5	0.37	0.1
K	mg/L	16.3	NA*	5
Mg	mg/L	10.7	10	5
Mn	mg/L	0.32	-	0.015
Na	mg/L	94	NA	5
SiO_2	mg/L	8.54	NA	1.07
Zn	mg/L	0.07	NA	0.02
pH		7.1	7.2	
NH_3	mg N/L	21.0	NA	0.5
NO_3	mg N/L	3.6	NA	0.1
HCO_3 Alkalinity	mg $CaCO_3$/L	177	NA	5
Total Alkalinity	mg $CaCO_3$/L	177	NA	5
BOD	mg/L	32	NA	2
Cl	mg/L	106	NA	10
SO_4	mg/L	86	NA	1
Total P	mg P/L	4.5	NA	0.5
TOC	mg/L	27	NA	1
TDS	mg/L	661	NA	10
TSS	mg/L	NA	41	5
Conductance	mS/cm	1.03	1.02	0.01
Turbidity	NTU	16.7	NA	1

*NA: Not Analyzed.

Table 3.2 Chemical composition of synthetic MWW (simulating CoC 4) used for MINEQL+ modeling
calculations and bench-scale experiments

Cation	Concentration mM	mg/L	Anion	Concentration mM	mg/L
Ca^{2+}	7.60	305	SO_4^{3-}	2.84	273
Mg^{2+}	7.16	174	HCO_3^-	13.44	820
Na^+	26.88	618	Cl^-	31.13	1105
K^+	0.70	27	PO_4^{3-}	0.21	20
NH_4^+ (as N)	7.01	98			

The initial level of TDS of the water, before any precipitation takes place, is 3,455 mg/L.

3.2.2 Antiscalants and Other Chemicals

PMA and PBTC, both in 50% active content, were provided by Kroff Chemical Company (Pittsburgh, PA). TKPP (48% active content) was provided by Crown Solutions/Veolia Water ((Vandalia, OH). Free chlorine was used as concentrated sodium hypochlorite (NaOCl) solution (5%). Monochloramine was pre-formed by mixing NaOCl and ammonium chloride (NH_4Cl) at 4:1 Cl_2:NH_3 mass ratio and was used immediately.

PMA concentrations were determined colorimetrically at 505 nm using a commercial test kit (MCI analytical test procedure, Masters Company, Wood Dale, IL). The concentrations of PBTC and TKPP were monitored by following Standard Method 4500-P (American Public Health, American Water Works Association et al. 1998). Free chlorine and monochloramine were measured with a chlorine photometer (HF Scientific Inc., FL).

3.2.3 Scaling Study in Bench Tests

A customized bench-scale water recirculating system was equipped with removable stainless steel (SS316) circular disc specimens to provide surfaces for scaling/deposition in the recirculating water (Figure 3.1). Mineral mass deposited on the SS surfaces (5.61 cm^2 per disc) was determined to track the scaling process with varied water chemistries and scaling control strategies. Water temperature and flowrate were 40°C (105°F) and 11.4 L/min (3 GPM), respectively, to reflect actual conditions of industrial cooling systems. In a typical test, the recirculating water was exposed to air so that the alkalinity may approach equilibrium with

$CO_2(g)$, as is the case with actual cooling system operation. Before use, the SS specimens were cleaned by ultrasonic wash for 5 min in an acetone/ethanol solution (1:1 v/v ratio), rinsed with DI water and air-dried in a laminar flow hood. At predetermined time intervals during an experiment, the SS specimens were taken out of the recirculating water through the sampling ports. The water remaining on the disc surface was carefully removed by paper tissue without disturbing the solid deposits on the surface. The discs were then air-dried for at least 48 hr and the mass of each disc was measured using an analytical balance (Mettler AE163, detection limit 0.01 mg). Final weighing was performed only after a constant mass was achieved (mass measurement variation < 0.05 mg/hr). Three measurements were taken for each specimen and the average value was reported as the mineral mass on the disc.

After weighing, the morphology of the scale samples were inspected using Scanning Electron Microscopy (SEM, Philips XL30, FEI Co., Hillsboro, OR), and the scale elemental compositions were determined by Energy Dispersive X-ray Spectroscopy (EDS, EDAX Inc., Mahwah, NJ). These examinations were useful to identify the scale characteristics and facilitated the selection of effective scaling control approaches. For example, the identification of the mineral deposits by SEM/EDS provided evidence for the selection of the appropriate antiscaling chemicals to inhibit the formation of the specific minerals identified in the scales.

After each experiment, the recirculating system was cleaned by running HCl solution (pH 2-3) for about 1 hr, followed by DI water rinsing for three times, with 0.5 hr of water recirculation each time.

3.2.4   Pilot-Scale Cooling Tower Tests

Pilot-scale cooling towers were constructed and operated with secondary-treated MWW (Figure 3.2) to test the optimal chemical treatment regimen that was identified from the bench-scale experiments. The pipe section for scale collection on disc specimens had a similar design as used in the bench-scale tests. For simultaneous evaluation of different scaling control programs, three towers were operated side by side at the wastewater treatment plant of the Franklin Township Municipal Sanitary Authority (Murrysville, PA). Chemical control of biofouling and corrosion was also implemented. All three towers were operated at CoC 4, using a flowrate of 11.4 L/min (3 GPM). The temperature of water entering the tower was 40°C (105°F) and leaving the tower was 35°C (95°F).
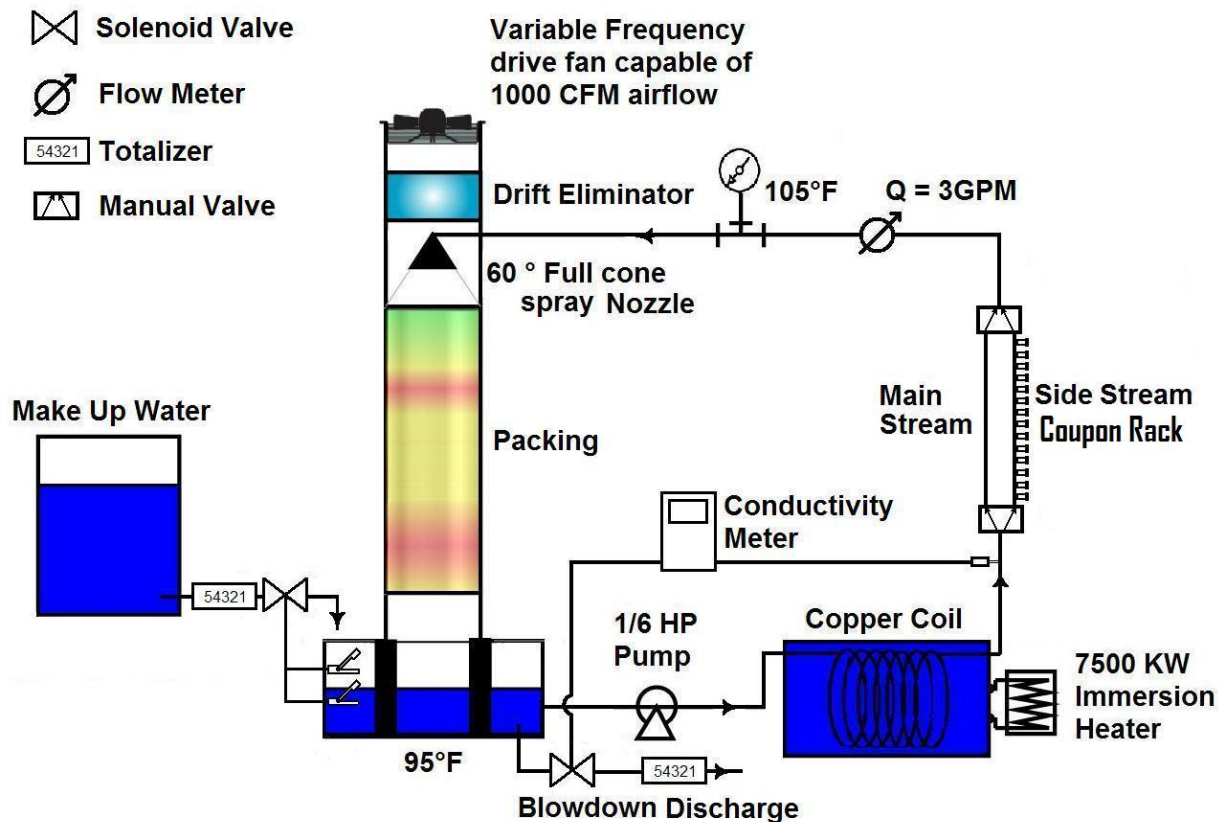
Figure 3.2 Schematic of pilot-scale cooling tower. The disc coupon rack had a similar design as in the bench-scale recirculation system (Figure 3.1).

The cooling towers were tested for two consecutive 21-day periods. The first run was a full operation with all three towers and the second run used two towers. The primary purpose for the second run was to test the biocontrol by pre-formed monochloramine instead of free chlorine [22]. Between the two tests, the towers were cleaned with an acetic-acid solution and disinfected by free chlorine. Detailed information on tower operations was recorded, including the water temperature profile at different locations, the airflow rate inside the cooling tower, the conductivity of circulating water, the flowrates of makeup water, recirculating water, and

blowdown stream, as well as the ambient conditions (weather, air temperature, relative humidity, etc.). The rates of solid deposition on stainless steel disc specimens were measured during both runs. In addition, the corrosion of selected metal alloys and the bioactivity in the towers were monitored by a coupon weight loss method [23] and by heterotrophic planktonic/sessile bacteria counts [22], respectively.

3.3   RESULTS AND DISCUSSION

3.3.1   Bench-Scale Recirculating Experiments with Synthetic MWW (CoC 4)

The use of a synthetic municipal wastewater allowed the representation of the recirculating cooling conditions in which secondary-treated MWW as the sole makeup water was concentrated to CoC 4. A series of experiments was conducted to test the effectiveness of the antiscalants PMA and PBTC at CoC 4 and to evaluate the impact of chlorine disinfectants, ammonia, and phosphate on the performance of the antiscalants.

Effect of antiscalants. Without antiscalants addition, the mineral deposits collected on a disc specimen at CoC 4 during the recirculation of the synthetic MWW were, on average, more than 2 mg (Figure 3.3). As a comparison, the deposits collected at CoC 1 were between 0 and 0.2 mg (data not shown in figure). The antiscalant PBTC dosed at 10 mg/L suppressed deposition to about 0.2 mg, which was more effective than when dosed at 5 mg/L (Figure 3.3), suggesting that the MWW concentrated to CoC 4 demands higher doses of antiscalants for scaling control, as compared with typical values used for freshwater [16, 18]. PMA dosed at 10 mg/L inhibited

scaling nearly completely, demonstrating its superior antiscaling effect in the synthetic MWW (CoC 4).
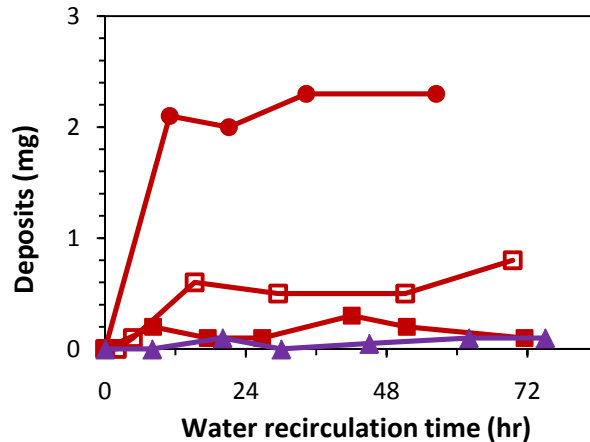
Figure 3.3 Scaling behavior of a synthetic municipal wastewater (CoC 4) in bench-scale tests with inhibitors at different dosing (40°C).

No inhibitors (●), 5 mg/L of PBTC (□), 10 mg/L of PBTC (■), 10 mg/L of PMA (▲).

Influence of ammonia and phosphate. As can be seen in Figure 3.4, the removal of ammonia, which was present as 100 mg-N/L in the other tests, resulted in significant scale formation compared with the case in which the addition of antiscalants substantially reduced scaling in the presence of ammonia. Conversely, the removal of orthophosphate (as 20 mg-PO_4/L) did not exhibit a profound impact on scaling control by PBTC, which implies that the addition of the antiscalant (10 mg/L of PBTC) was sufficient to reduce phosphate mineral scale formation. The beneficial role of ammonia for scaling inhibition was due to both complexation reactions between ammonia and calcium (confirmed by chemical equilibrium modeling) and ammonia adsorption onto mineral surfaces to disrupt particle growth [24]. Also, given the predominance of ammonium ions in the experimental pH range (pH 7.5-8) where the water

recirculating system was operated, some complexation between NH_4^+ and carbonate species could also occur to further decrease the precipitation potential of carbonate minerals.
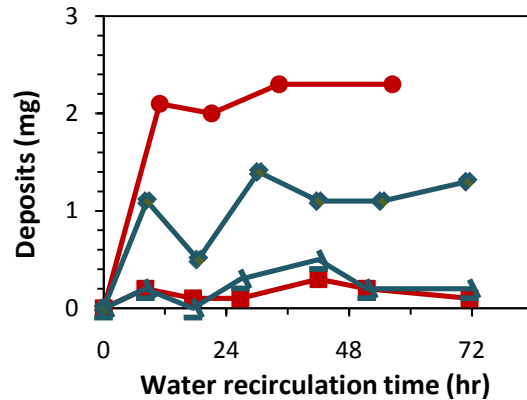
Figure 3.4 Influence of ammonia and phosphate on scaling control in bench tests with a synthetic MWW at CoC 4 (40°C)

No inhibitors (●), 10 mg/L of PBTC (■), 10 mg/L of PBTC, no ammonia (♦), 10 mg/L of PBTC, no phosphate (Δ).

Interference of chlorine biocides. As shown in Figure 3.5, the addition of chlorine biocides for biogrowth control negatively impacted scaling inhibition by either PBTC or PMA. In the absence of the biocides, PBTC substantially inhibited scale formation while PMA nearly completely inhibited scaling. However, the addition of free chlorine caused a significant decrease in the antiscaling efficiency, Both of the antiscalants were significantly impaired by the oxidizing biocides. It is noteworthy that free chlorine was more detrimental than monochloramine to compromise the antiscaling effects of PBTC and PMA, even for the case with elevated dosing of 20 mg/L of PMA (Figure 3.6).
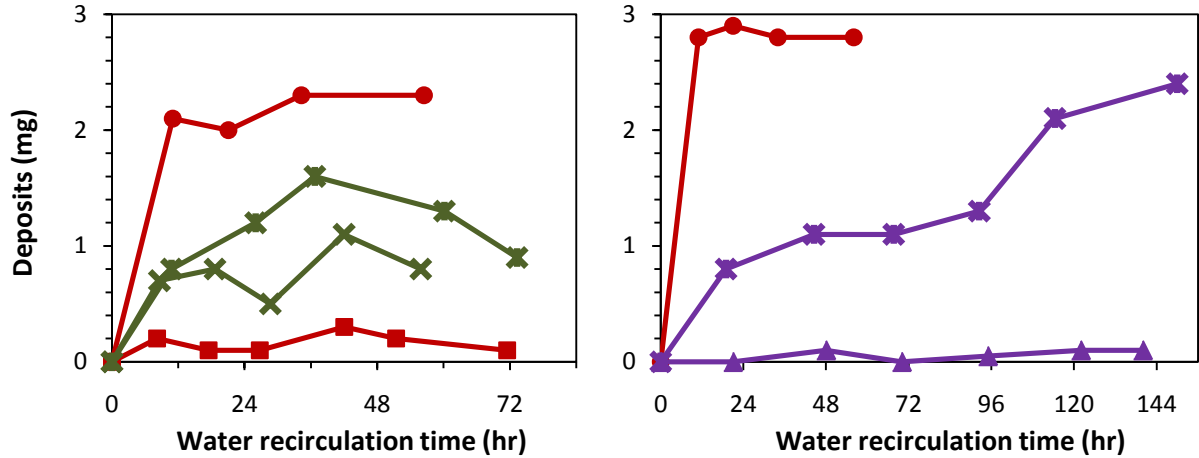
Figure 3.5 Interference of chlorine-based biocides on scaling control in bench tests with a synthetic MWW at CoC 4 (40°C).

Upper: No inhibitors, no biocides (●), 10 mg/L of PBTC, no biocides (■), 10 mg/L of PBTC, 1 mg/L of free chlorine (*), 10 mg/L of PBTC, 1 mg/L of monochloramine (×).

Lower: No inhibitors, no biocides (●), 10 mg/L of PMA, no biocides (▲), 10 mg/L of PMA, 1 mg/L of free chlorine (*), 10 mg/L of PMA, 1 mg/L of monochloramine (×).
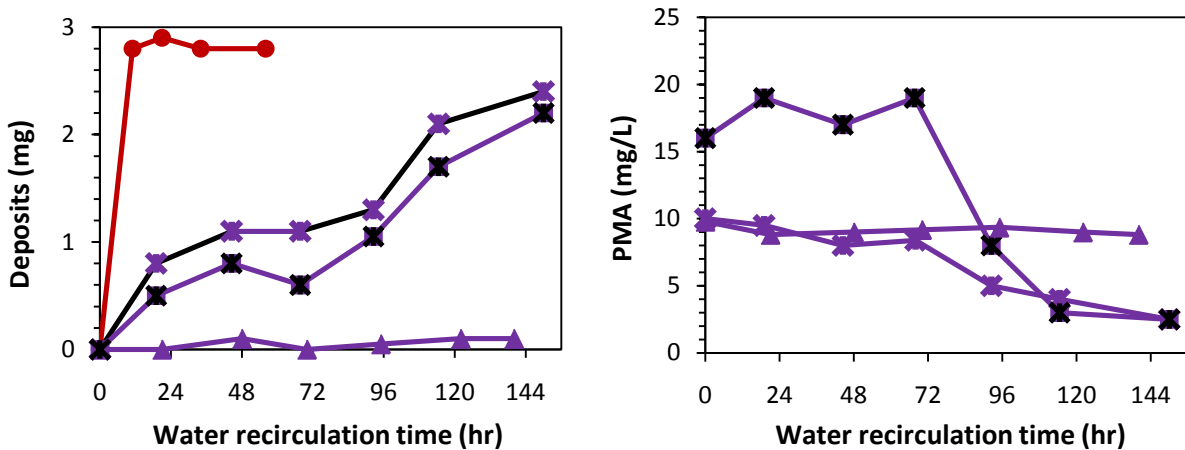
Figure 3.6 Interference of chlorine biocides with PMA on scaling control in bench tests with a synthetic MWW at CoC 4 (40°C).

No inhibitors, no biocides (●), 10 mg/L of PMA, no biocides (▲), 10 mg/L of PMA, 1 mg/L of free chlorine (*), 20 mg/L of PMA, 1 mg/L of free chlorine (✱).

41

The interaction between PMA and free chlorine is explained by the data shown in Figure 3.6. In the absence of free chlorine, the PMA concentration remained stable during the entire period of experiment (6 days). After 3 days of interaction with free chlorine, PMA started to deplete for both doses tested. Furthermore, during the experiment with 20 mg/L of PMA addition, total chlorine demand was much greater than in the experiment with 10 mg/L of PMA. To maintain a constant level of chlorine in solution, i.e., 1 mg/L, a total of 26 mg/L of chlorine was added over the 6 days of the experiment. In comparison, only 6 mg/L of chlorine was needed to maintain the 1 mg/L concentration level over the same period of experiment with 10 mg/L of PMA addition. This explains, at least in part, the sharp decrease in PMA after day 3. PMA was substantially consumed by chlorine, especially after 3 days, and consequently, the scaling inhibition efficiency was greatly reduced, as evidenced by the appreciable increase in the mineral mass deposited on test coupons after 3 days. A number of studies have used PMA as a model compound of natural organic matter (NOM) owing to its resemblance of the chemical and structural characteristics of natural humic and fulvic acids [25-27]. It is hence not surprising to observe the destruction of PMA by free chlorine, given the extensively-studied formation pathways of disinfection by products (DBPs) from NOM and chlorine biocides [28-33]. Separate batch tests of PBTC in the presence of chlorine additives showed stability of PBTC up to 150 hours. As such, deposit data beyond 72 hours were not collected in Figure 3.5.

3.3.2   Pilot-Scale Study with Secondary-Treated MWW

3.3.2.1 Changes of water chemistry due to scaling

Table 3.3 shows the chemical treatment program for simultaneous control of scaling, corrosion, and biofouling in pilot-scale cooling towers. The program included the addition of

PMA and PBTC as scaling inhibitors, TKPP and Tolyltriazole (TTA) as corrosion inhibitors, and free chlorine (the first run) or monochloramine (the second run) as biocides. The results of the pilot-scale studies provided evidence for the effectiveness of PMA, PBTC, and TKPP in preventing scaling from the MWW at larger scale.

Table 3.3 Chemical treatment program (target concentrations) for pilot-scale cooling tower tests with secondary-treated MWW at Franklin Township, PA (unit: mg/L)

Chemical addition		First Run			Second Run	
		Tower A	Tower B	Tower C	Tower A	Tower B
Corrosion Control	TTA	1	2	2	1	2
	TKPP	0	10	10	0	0
Scaling Control	PMA	0	10	20	0	10
	PBTC	0	5	10	0	0
Biocontrol	Free Cl_2	1.5	1.5	1.5	0	0
	MCA	0	0	0	3	3

TTA: tolyltriazole; TKPP: tetrapotassium pyrophosphate; PMA: polymaleic acid; PBTC: 3-phosphonobutane-1,2,4-tricarboxylic acid; MCA: monochloramine.

Water samples, obtained from the recirculating loop of each cooling tower operated at steady state, were analyzed for key constituents and chemical parameters (Table 3.4 and Table 3.5). Before reaching the steady state of CoC 4, a sharp increase of water pH from ~7.2 of the makeup water (secondary effluent) to ~8.3 was observed in each tower, primarily due to an aeration effect of the cooling towers that liberated CO_2 from the water. It is well known that effluent from the secondary clarifier in a wastewater treatment plant is commonly oversaturated with CO_2 yielded by the continuing aerobic biodegradation of residual organic carbon [34-37]. We analyzed the pH behavior of the cooling towers through measurements and modeling. Detailed description about the pH changes will be reported separately (Chapter 6). After reaching CoC 4, the alkalinity in the recirculating water was generally 3-4 times higher than in the

makeup water, further raising the pH to 8.5-9. The concentration factor of 3-4 for alkalinity was lower than the volume-based CoC because part of the alkalinity was lost to the precipitation of carbonate solids.

Table 3.4 Concentrations of cationic species and PMA in makeup water (secondary effluent) and recirculating water (CoC 4-5) in field testing with pilot-scale cooling towers (unit: mg/L)

| Species | | Raw water | First Run | | | Second Run | |
			Tower A	Tower B	Tower C	Tower A	Tower B
Ca	Total	35.2±1.5	97±7	112±8	111±10	105±3	113±7
	Filterable	34.5±1.1	91±7	100±9	102±11	98±4	103±6
Mg	Total	10±1	47±8	58±5	57±5	46±3	43±3
	Filterable	10±1	45±8	55±4	54±5	44±3	42±3
Fe	Total	0.37±0.11	0.59±0.23	0.81±0.25	0.68±0.25	0.74±0.24	0.86±0.28
	Filterable	0.12±0.03	0.06±0.02	0.05±0.04	0.07±0.03	0.06±0.03	0.08±0.05
Cu	Total	0.06±0.03	0.12±0.03	0.13±0.03	0.13±0.04	0.28±0.14	0.22±0.09
	Filterable	0.06±0.03	0.10±0.03	0.10±0.03	0.11±0.04	0.23±0.11	0.18±0.09
PMA	Total	--	--	6.8±1.9	14.6±2.6	--	6.9±1.6
	Filterable	--	--	4.3±1.3	9.7±2.1	--	4.5±1.3

Data are mean values ± 1 sd. Sample size for raw water n = 7. Samples for recirculating water in the cooling towers were from day 4 to day 24 during the tower operation (sample size for tower A: 10, tower B: 10, tower C: 11).

Concentrations of chloride in the cooling water were typically 6-7 times higher than in the makeup water. This ratio is higher than the expected ratio based on the water volume reduction (i.e., CoC 4-5). The extra chloride of some 350 mg/L (estimation based on Table 3.5) in the recirculating water came from the addition of chlorine biocides (either free chlorine for the first run or monochloramine for the second run).

Concentrations of sulfate in the cooling water were generally 4-5 times higher than in the makeup water, which corresponded well to the volume-based CoC because there was no additional sink or source for sulfate, and as such, sulfate behaved as a conservative species.

Table 3.5 Concentrations of anionic species and other chemical additives (for corrosion and biofouling control) in makeup water (secondary effluent) and recirculating water (CoC 4-5) in field testing with pilot-scale cooling towers (unit: mg/L)

Species	Raw water	First Run			Second Run	
		Tower A	Tower B	Tower C	Tower A	Tower B
ALK	113±34	283±54	364±53	324±25	232±68	244±79
SO$_4$	75±7	357±39	388±49	378±76	323±30	356±27
Cl	142±22	955±135	937±74	917±152	859±133	1050±115
PO$_4$	11.5±1.8	5.9±1.1	4.1±1.0	5.2±0.6	7.5±2.7	8.1±3.3
TKPP	--	--	0.6±0.4	0.6±0.4	--	--
PBTC	--	--	0.8±0.3	0.9±0.7	--	--
TTA	--	1.0±0.8	2.0±0.9	1.8±1.0	--	1.8±1.0
Total Cl$_2$	--	1.2±0.9	1.0±0.7	1.5±0.8	3.2±1.3	3.6±2.2

For ALK, the unit is mg /L as CaCO$_3$.

Total phosphate concentrations in the tower water were much lower than that in the makeup water—nearly 90% of the phosphate precipitated out of water due to its low solubility in the presence of high calcium (~100 mg/L, or 2.5 mM) under the cooling tower conditions investigated. For example, TKPP, a polyphosphate, was added primarily as a corrosion inhibitor (10 mg/L as PO$_4$). However, the measured TKPP concentration in the recirculating water was less than 1 mg/L—most of it precipitated and became unavailable for corrosion control. Therefore, the feasibility of using phosphate-based corrosion inhibitors such as TKPP in secondary-treated municipal wastewater is questionable because it may only add to more challenges for scaling control.

Tower A, which received no PMA or PBTC for scaling inhibition, precipitated the greatest amount of calcium. The amount of calcium in the recirculating water accounted for 60-70% of the amount fed with the makeup water, i.e., 30-40% of the calcium precipitated. The degree of calcium removal by precipitation will be discussed in more detail.

Similar to sulfate, magnesium was 4-5 times more concentrated in the cooling water than in the makeup water, suggesting that magnesium precipitation was minimal. This was confirmed by the EDS analysis, which revealed nearly undetectable amount of magnesium in the collected solids.

PMA was added to Towers B and C for scaling control during the first run. The concentrations and fate of PMA were monitored periodically. The target levels of PMA in Towers B and C were 10 mg/L and 20 mg/L, respectively (daily addition was based on the volume of blowdown water). Detected PMA in Tower A, however, was 7 mg/L on average, suggesting that about 30% of the PMA was removed with precipitated mineral solids and settled out of the liquid phase, or was degraded by chlorine. Furthermore, free PMA (the filterable fraction) accounted for about 60% of total aqueous PMA. The rest (40%) was most likely associated with suspended solids. Studies have shown that anionic polyelectrolytes such as PMA tend to adsorb onto mineral particles and prevent solids settling by providing an electrostatic and/or steric stabilization mechanism [11, 27, 38, 39].

3.3.2.2 Mass deposition measurement

Figure 3.7 shows the accumulated scale solids deposited on stainless steel disc specimens in the three cooling towers with different chemical dosing strategies. Tower A, as a control tower, received no antiscaling chemicals. In Tower B, the addition of 10 mg/L of PMA and 5 mg/L of PBTC resulted in the least scaling among the three towers. However, when the dosing of

PMA and PBTC was doubled in Tower C, expected better scaling inhibition was not observed and actually the scales accumulated as much as those in the control tower without antiscaling treatment (Tower A). It appeared that overdosing had occurred. Given the small increment between the two dosings, the ionic strength of the cooling water was not increased significantly, and as such, compression of the electrical double layer of suspended particles was unlikely to be important in destabilizing them in Tower C. Also, the additional 10 mg/L of PMA in Tower C did not change the water pH. It is more likely, however, that interparticle bridging due to the double dosing of PMA might cause particle destabilization and subsequent deposition (scaling), an effect similar to enhanced coagulation by polymers.
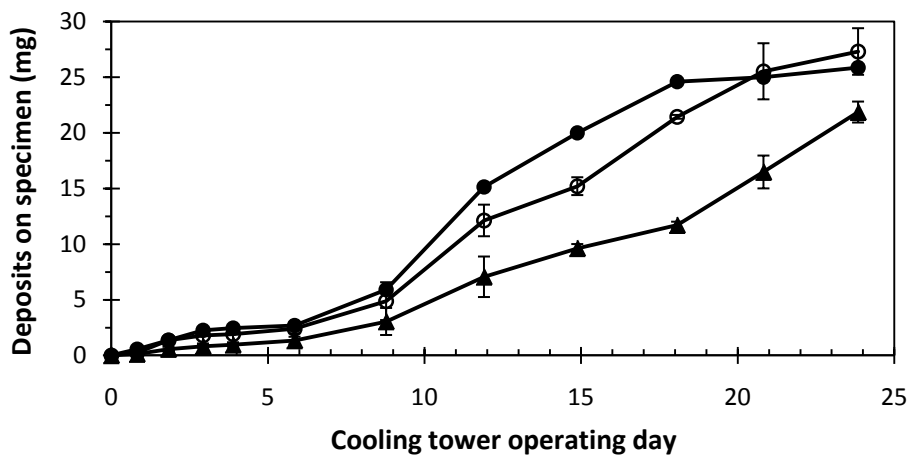
Figure 3.7 Deposit mass measurements in the pilot-scale cooling tower tests using secondary-treated MWW.

Tower A, no inhibitors (○), Tower B, 10 mg/L of PMA (▲), Tower C, 20 mg/L of PMA (●).

Deposits were collected on stainless steel disc specimens immersed in recirculating pipe flow. Effective collection area 5.61 cm^2, flow velocity 0.57 m/s (3 GPM flowrate in 3/4" pipe), water temperature $40 \pm 1°C$ ($104 \pm 2°F$), pH 8.5 ± 0.3 (open to air condition). Error bars indicate the data range of measurements from duplicate tower tests.

After day 8 (or 4 days after reaching steady state of CoC 4), an accelerated mass accumulation of solids on the coupon discs in all three towers was obvious. An analysis of solid

composition revealed that biomass (the fraction burnable at 500°C) accounted for 30-50% of the total accumulated solids, indicating that biofilm growth played an important role in surface fouling in the cooling towers using secondary-treated MWW. Indeed, the dynamic process of simultaneous biofouling and mineral scaling might enhance each other mutually—the mineral scales can provide a coating layer conducive to biofilm development compared to a smooth metal surface, and at the same time the organic matrix consisting of extracellular polymeric substances (EPS) of the biofilm can help trap more mineral solids. For example, the inorganic mineral fraction of EPS can be as much as 77% of the EPS dry weight [40].

3.3.3   Experimental Observation vs. Equilibrium Prediction

The use of chemical equilibrium modeling with the model MINEQL+ [41, 42] allowed estimation of the mineral precipitation potential, the chemical composition of solid precipitates, and their relative abundance. In this study, mineral precipitates predicted by MINEQL+ were compared with the actual species that comprised the deposits collected from experiments conducted at both bench-scale water recirculating systems and pilot-scale cooling towers.

The precipitated solids from the bench- and pilot-scale tests were inspected using Scanning Electron Microscopy (SEM) and their elemental composition determined by Energy Dispersive X-ray Spectroscopy (EDS) analyses. The total mass of the solids collected in various tests was also compared to the amount predicted by MINEQL+ for the conditions tested. The information obtained from these comparisons was used to discuss the usefulness of the equilibrium modeling as a predictive tool in assessing the cooling water scaling behavior.

Based on the chemical composition of the synthetic MWW (Table 3.2), chemical equilibrium modeling predicted that hydroxyapatite (HAP) and dolomite would precipitate at

48

CoC 4 (modeling condition: ionic strength corrected, 40°C, and closed system) with the following amounts:

HAP [$Ca_5(PO_4)_3OH$](s):   0.07 mM (35.2 mg/L)

Dolomite [$CaMg(CO_3)_2$](s): 6.44 mM (1187.5 mg/L)

Based on the modeling results, the elemental composition of the predicted solids is shown in Table 3.6 (Condition (1)).

For the simulations of synthetic MWW, the initial TDS of the water (CoC 4) was 3,455 mg/L, of which 1,223 mg/L were predicted to precipitate at equilibrium (35.4 wt%), leaving 65% of the initial TDS in solution (roughly, a 1:2 distribution in terms of precipitated vs. soluble total solids). Of particular interest is the distribution of Ca and Mg at equilibrium: precipitated, complexed, and free ions. Equilibrium prediction by MINEQL+ for synthetic MWW illustrated that almost 90% of the initial Ca and Mg should precipitate out of solution. Ca and Mg are thus disproportionately removed from the solution comparing to other aqueous species.

Table 3.6 Elemental composition of the precipitates from synthetic MWW: Modeling prediction vs. experimental observation

Condition		Elemental Percentage					
		Ca	Mg	P	C	O	H
Modeling without kinetic constraints (1)	Molar	10.3	9.8	0.3	19.5	60.0	0.1
	Mass	22.3	12.8	0.5	12.7	51.8	0.0
Modeling with kinetic constraints (2)*	Molar	20.1	0	0.6	19.2	60.0	0.2
	Mass	40.0	0	0.9	11.4	47.7	0.0
Observed in bench experiments (3)	Molar	28.7	1.3	0.0	24.2	45.8	0.0
	Mass	52.2	1.4	0.0	13.2	33.2	0.0

* No Mg precipitation.

Stainless steel disc specimens immersed in the bench-scale recirculating system using the synthetic MWW were used to collect mineral deposits. After 6 days, the discs were removed from the recirculating water and air-dried prior to SEM/EDS analysis. The SEM image shows well-shaped crystalline morphologies of calcite (Figure 3.8). Based on the EDS analysis, the average abundance of the elements in the collected solids is listed in Table 3.6 (Condition (3)). Comparing to the model prediction (Table 3.6 Condition (1)), the sampled solids contained excess Ca but were deficient in Mg. This observation that Mg did not participate in the solids formation was confirmed by the essentially unchanged aqueous concentration of Mg over the course of experiment (Figure 3.9). What the model predicted may be the most stable crystalline phases under equilibrium conditions. Deposits precipitated from the experimental water, while ultimately driven by thermodynamics, can experience different pathways of mineral formation which involved different kinetic constraints and/or inhibitory factors imposed by water chemistry amendments.
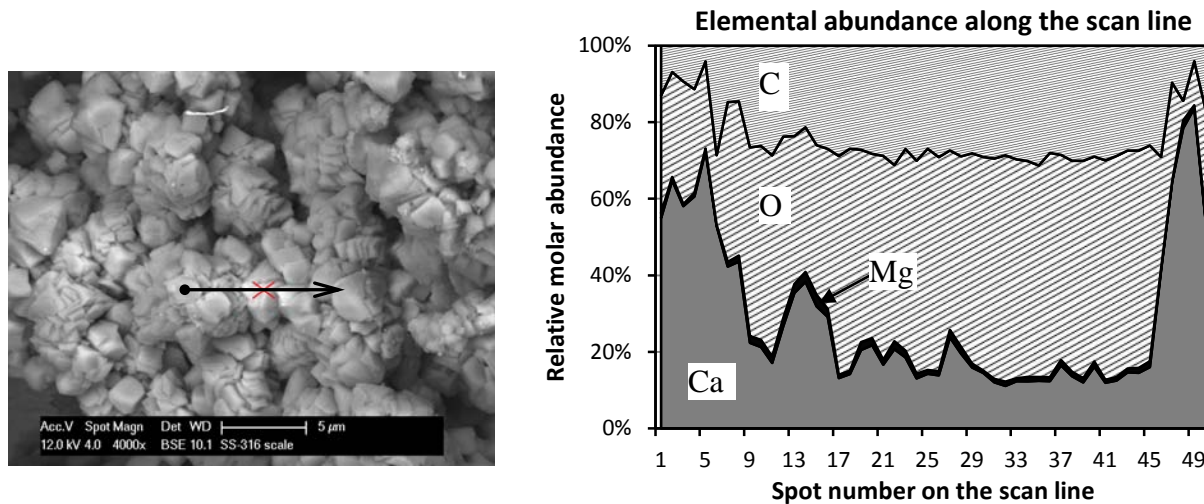
Figure 3.8 SEM image (left) and quantitative 1D EDS analysis (right) of the deposits collected on a stainless steel disc immersed in synthetic MWW in bench-scale water recirculating system.

The arrow line (10 μm in length) on the SEM image indicates the scan line for the EDS analysis of elemental abundance. P and H are not detected.

Since Mg was only marginally observed in the collected deposits, a second set of modeling calculations was performed with the added modeling constraints: 1) Mg-containing solids (e.g., dolomite, huntite, artinite, brusite, and magnesite) were not allowed to form, and 2) Calcium carbonate takes the form of aragonite, a faster-forming crystalline phase of $CaCO_3(s)$ that is also more soluble than calcite [43, 44]. Under these conditions, a total of 759 mg/L of precipitates in the form of HAP and aragonite were predicted to form, resulting in a 22% decrease in solution TDS.

HAP [$Ca_5(PO_4)_3OH$](s):   0.07 mM (35.2 mg/L)

Aragonite [$CaCO_3$](s):   7.23 mM (723.6 mg/L)

The elemental composition of the solids predicted under these conditions is shown in Table 3.6 (Condition (2)). The result is in a closer agreement with the experimental observation

in terms of elemental composition. However, the total amount of solids predicted by modeling (759 mg/L) was still significantly greater than that precipitated experimentally (150-200 mg/L), implying that precipitation equilibrium had not been established during the experimental conditions, i.e., 3-4 days of limiting hydraulic residence time in the cooling water.

Compared to the modeling prediction of 90% Ca precipitation, only about 35% of Ca actually precipitated during the 6 days of bench-scale tests with synthetic MWW (Figure 3.9). A similar percentage of Ca precipitation (35-40%) was observed in pilot-scale cooling tower tests with secondary-treated MWW. Tower A, which received no PMA, precipitated the greatest amount of Ca, while Towers B and C, with PMA addition, retained higher amounts of Ca in water. This suggests that PMA retarded Ca precipitation, resulting in higher Ca concentrations during the course of tower tests. It is clear therefore that kinetic constraints of precipitation exerted by the PMA addition are not captured by the equilibrium modeling that is entirely based on thermodynamic calculations.
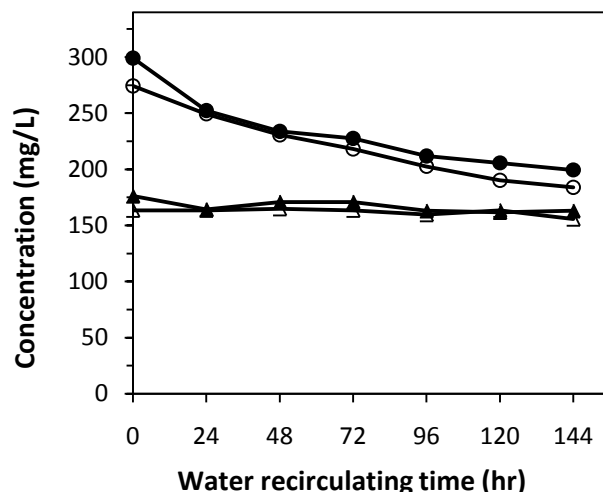
Figure 3.9 Changes in the aqueous concentrations of Ca and Mg in bench-scale water recirculating system using a synthetic MWW (without chemical addition).

Closed data points represent concentrations of unfiltered water samples while open points filtered samples. The filtration is carried out using 0.45 μm HA type membrane filters (Millipore) to remove suspended solids. Ca unfiltered (●), Ca filtered (○), Mg unfiltered (▲), Mg filtered (Δ).

For pilot-scale cooling tower experiments, SEM/EDS analyses were performed on deposits collected from Tower A after 6 days of operation at CoC 4 (Figure 3.10). The EDS spectra show very low amounts of Mg, thereby confirming the results shown in Figure 3.8 and Figure 3.9 from bench tests with synthetic MWW. However, the SEM data indicated solids of more amorphous character as opposed to those depicted in Figure 3.8. Alvarez et al. [45] observed that the Ca-P complexes preferentially precipitate in amorphous forms in the presence of soil organic matter. In addition, amorphous $CaCO_3(s)$ has been collected on steel surfaces when organic additives are present in solution [46-49]. The interactions of mineral precipitates with organic matter present in the actual MWW suggest more complex chemistries occurring in pilot-scale cooling tower water than in the bench-scale system where synthetic MWW was used to simulate only the inorganic constituents.

53
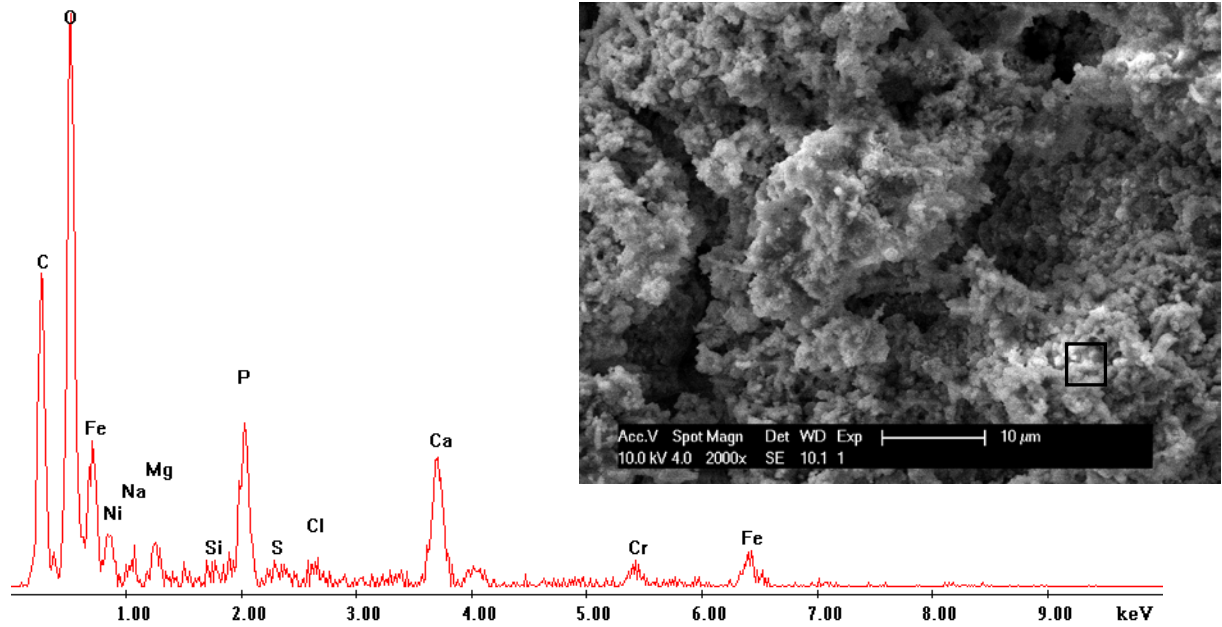
Figure 3.10 SEM image and the elemental composition of the solid deposits collected on a stainless steel disc immersed in the secondary-treated MWW in the pilot-scale cooling tower (Tower A) operated at CoC 4. EDS scan was performed on the area outlined by the square box on the SEM image.

The EDS analyses conducted on the solids collected from pilot experiments indicate that the deposits consisted primarily of calcium carbonates and phosphates, which is in qualitative agreement with the revised model predictions discussed earlier. However, the quantity of phosphates appears to be greatly enriched when compared to that in the deposits collected from the bench-sale studies using synthetic MWW. This is likely because of the higher P concentration in the actual MWW (i.e., 12 mg/L vs. 5 mg/L in the synthetic water). In addition, P-containing chemicals, in the form of TKPP (10 mg/L) and PBTC (5 mg/L), were also added to the cooling towers for corrosion/scaling control. Chemical analyses indicated that these added

54

phosphates quickly became undetectable in the liquid phase, suggesting their precipitation that further contributed to the relatively high P signal in the EDS spectra (Figure 3.10).

3.4   CONCLUSIONS

This study demonstrates the feasibility and challenges of using secondary-treated municipal wastewater as an alternative cooling system makeup water to replace freshwater. The scaling behavior and control of it in recirculating cooling systems was evaluated. Based on the results from bench-scale experiments performed in this study, it was determined that commonly used polymer-based scaling inhibitors can be effective in controlling potentially severe scaling when using this impaired water as makeup in recirculating cooling systems. PMA worked very well at scaling inhibition in the absence of chlorine disinfectants but only partially effective in the presence of chlorine. Ammonia present in the wastewater could suppress the aggressiveness of free chlorine on PMA. Pre-formed monochloramine was found to be less aggressive than free chlorine, while still being an effective biocide. Pilot-scale cooling tower experiments suggested that mineral scaling control by PMA was much more challenging due to biofouling.

Overall, for scaling control of MWW that is concentrated to CoC 4 in recirculating cooling systems, 1) PMA can be applied at 10 mg/L level for effective mineral scaling inhibition in the absence of biofouling, 2) monochloramine is better suited as biocide than free chlorine because of the reduced impact of monochloramine on antiscaling programs, and 3) phosphorous based scaling and corrosion inhibitors are not appropriate due to their precipitation with Ca.

4.0   SCALING CONTROL FOR REUSE OF PASSIVELY-TREATED ABANDONED MINE DRAINAGE IN RECIRCULATING COOLING SYSTEMS

In coal mining regions where substantial coal-based power generation takes place, significant quantities of abandoned mine water that exists in mine voids represent a potential for use as a stable, large volume supply of cooling water. Reusing passively-treated abandoned mine drainage (AMD) can avoid surface water contamination that can otherwise occur due to the overflow of the AMD from mine pools, which is usually acidic and contains high concentrations of metals, especially iron and manganese. However, since using AMD for cooling is not widely practiced, knowledge about the proper control of scaling issues in cooling systems using AMD is limited. The use of AMD is predicated on being pre-treated with aeration/settling ponds to remove Fe/Mn and suspended solids. In this study, the scaling behaviors of passively-treated AMD and scaling mitigation in cooling water systems were investigated through laboratory and pilot-scale experiments. Bench-scale recirculating systems and three pilot-scale cooling towers were employed for testing various chemical control schemes for scaling control in AMD. The tests were conducted under conditions of temperature, flow velocities, and water constituent concentrations similar to those in a recirculating cooling water system. The effectiveness of chemical treatment strategies in inhibiting mineral scaling was evaluated through exposure and monitoring of specially designed disc specimens in extended experimental tests. Polymaleic acid (PMA) effectively decreased the settling of suspended solids and rendered the solids less prone

to deposition onto the surfaces immersed in the pipe flow sections. In the absence of PMA, significant amounts of solids settled in the sumps of pilot-scale cooling towers where flow velocity was minimal. The PVC and stainless steel surfaces exhibited different affinities for scaling; PVC was determined to yield increased deposition in bench-scale recirculation systems. The observation implies that varied severity of scaling problems can take place in recirculating sections of a cooling system made of different materials, which was also observed in the pilot-scale cooling towers using the same type of passively-treated AMD.

4.1   INTRODUCTION

Abandoned mine drainage (AMD) refers to the release of the contaminated groundwater produced by dissolution of sulfide minerals (especially pyrite FeS_2(s)) and commonly found in the areas adjacent to abandoned mine sites [1]. AMD is characterized by low pH, high content of iron hydroxides, as well as elevated levels of heavy metals [2]. These characteristics are manifested in streams impacted by AMD through sediment color ranging from red to orange or yellow due to iron precipitation, and significant endangerment of aquatic and benthic life [3].

Coal mining produces the bulk of AMD. This is especially true in Pennsylvania where more than 25% of the nation's total coal output was produced over the past 200 years [4]. As such, AMD has been a major water-pollution problem in Pennsylvania where over 3,000 miles of streams and associated ground waters have been contaminated [4]. Other areas in the US with large volumes of AMD include the other Appalachian coal-producing states and the Illinois-Indiana coal mining region [5]. AMD is also generated in the hard-rock mining areas of the western US, although such water was not examined in this study.

57

Given the large quantity of AMD available, it may be possible to use it for cooling purposes in areas of the US where freshwater shortages occur frequently [6, 7]. This practice may significantly impact water conservation as consumptive withdrawal of freshwater by thermoelectric power generation cooling water systems can contribute significantly to the water shortage problem in some areas. In the US, thermoelectric power generation consumed 3.3 BGD of freshwater in 1995, mainly through evaporative loss from cooling towers [8].

Waters of impaired quality, such as AMD, are of increasing interest as alternative sources to freshwater for thermoelectric power plant recirculating cooling water systems. The AMD represents significant quantities of possible cooling system makeup water in coal mining regions where substantial coal-based power generation takes place [9, 10]. It was estimated that there is approximately 250 billion gallons of mine pool volume in West Virginia and Pennsylvania [9]. In addition to supplementing withdrawal of surface water for cooling, other benefits of reusing mine pool water in power plants are the prevention of AMD-related surface water contamination, and additional flexibility in siting new power plants. Although active pretreatment might be necessary to raise the water quality of AMD to allow reuse (treatments typically raise pH, reduce metal concentration and total dissolved solids), the development and successful implementation of passive treatment systems makes it promising to access AMD with better quality [11, 12]. Further, AMD chemical compositions often evolve over time to become less acidic and can approach neutral pH in many cases, as well as have lower loads of dissolved solids over time [13]. Such AMD can be treated with temporary retention in ponds to allow oxidation and iron precipitation. Passively-treated, near-neutral pH AMD waters are good candidates for use in power plant cooling systems. Indeed, there is already some experience with operating their cooling systems totally or partially with treated AMD in Pennsylvania [14].

However, mineral precipitation and subsequent surface scaling remains one of the main challenges for AMD reuse in recirculating cooling water systems. Up to date, knowledge in the literature concerning mineral scaling in cooling systems caused by AMD is limited due to the fact that using AMD as cooling tower makeup is not widely practiced.

The goal of this study was to evaluate the technical feasibility of reusing AMD in power plant cooling tower systems. Specifically, the objectives of this study were to 1) simulate scale formation under cooling tower operation conditions at different cycles of concentration via chemical equilibrium modeling, 2) test the effectiveness of different chemical treatment programs on scaling inhibition in bench-scale water recirculating systems, and 3) determine the viability of using AMD as cooling water makeup through testing in a pilot-scale cooling tower system.

4.2   MATERIALS AND METHODS

4.2.1   Passively-treated AMD characterization and preparation for laboratory and field testing

Passively-treated AMD from the St. Vincent College mine drainage site (Latrobe, PA) was chosen for testing in laboratory experiments and in pilot-scale cooling towers. Passive treatment at the St. Vincent site is accomplished through a system of constructed wetlands to reduce iron content. A total of 7,000 gallon of the AMD for use as makeup water in tests with pilot-scale cooling towers was collected and transported to our test site at the Franklin Township Municipal Sanitary Authority (Murrysville, PA) by a steel tanker truck on September 30, 2008. The AMD

was transferred to a covered and lined steel roll-off container stored outside at ambient temperature and was used as needed.

Table 4.1 Characteristics of the passively-treated abandoned mine drainage from St. Vincent College mine drainage site (sampled on November 4, 2008). Unit: mg/L

Analyte	Result	Reporting limit
Al	ND	0.4
Ca	228	10
Cu	ND	0.05
Fe	ND	0.2
K	5.21 B	10
Mg	61.8	10
Mn	0.172	0.03
Na	96.4	10
SiO_2	14.9	2.14
Zn	0.0281 B	0.04
pH	7.8	
NH_3-N	0.34 J	0.1
Bicarbonate Alkalinity	117 J	5
BOD	ND	2
Cl	56.1	1
NO_3-N	0.32	0.05
SO_4	656 J	25
Total P	0.056 B	0.1
Total Alkalinity	117 J	5
TOC	1.7	1
TDS	991	10
TSS	ND	4

Notes: J: Method blank contamination. The associated method blank contains the target analyte at a reportable level. B: Estimated result. Result is less than reporting limit. ND: Not detected.

Water samples were taken from the roll-off container before testing and intermittently during testing to serve as baselines for comparison purposes. These samples were collected with 1-L polyethylene sample bottles and transferred to appropriate polyethylene or glass sample containers provided by the commercial laboratory, TestAmerica (Pittsburgh, PA). Appropriate preservatives were added to the sample bottles prior to sampling. Results from the analysis are reported in Table 4.1.

Samples of the AMD were collected for laboratory experiments. The AMD was concentrated in the laboratory by evaporation at 35-40°C to reach 4 cycles of concentration (CoC 4) as determined by 75 % water volume reduction.

4.2.2 Equilibrium modeling of AMD scaling potentials

The chemistry of AMD cooling water at different CoC was modeled using MINEQL+ version 4.5 [15, 16] to predict the effects of CoC on scaling. The primary objective for this effort was to estimate the amount and composition of mineral solids that would precipitate from the solution in the pilot cooling units as a function of CoC, and to understand and interpret the chemistries observed in the pilot tests. In addition, the major constituents and their chemical speciation in solution were assessed and the dominant scale-producing reactions were identified.

The following four operational conditions were tested for the AMD water:

1) The aqueous system was open to the atmosphere ($P_{CO2} = 10^{-3.5}$ atm) to allow the alkalinity to be in equilibrium with $CO_2(g)$ and solids were allowed to precipitate.

2) The aqueous system was open to the atmosphere ($P_{CO2} = 10^{-3.5}$ atm) to allow the alkalinity to be in equilibrium with $CO_2(g)$ and solids were not allowed to precipitate (i.e., water can be super-saturated).

3) The aqueous system was closed to the atmosphere with total alkalinity fixed and solids were allowed to precipitate.

4) The aqueous system was closed to the atmosphere with total alkalinity fixed and solids were not allowed to precipitate.

The four conditions represent the extreme effects of atmospheric CO_2 and solution supersaturation. It is reasonable to expect that the actual conditions for field testing would fall within these boundary conditions.

4.2.3   Scaling inhibition in bench-scale tests

Methods for studying scaling in cooling tower systems were not readily available in the literature. A well-documented method to measure scaling deposition and kinetics in-situ was not found in the course of this research. Most established techniques pertaining to scaling phenomena confine themselves to means of static observations and analysis once solid scales have formed and have been collected [17-19]. Very limited effort has been devoted to the study of scaling dynamics and kinetics in terms of how scales form and at what rate(s) they form. In addition, there is no quantitative knowledge of conditions influencing and mechanisms dictating scale forming processes.

A method to study scale formation tendency and kinetics for AMD and other impaired waters was developed in this study. Bench-scale water circulating systems similar to those employed in the corrosion studies were constructed and were dedicated to investigate scaling. Stainless steel circular coupon discs were inserted through sampling ports into the recirculating water to provide collecting surfaces for scaling/deposition, as shown in Figure 4.1. A mass gain method, similar to the mass loss method for corrosion, was used as a straightforward means to

record the scale forming quantities at different water chemistries and scaling control conditions. Scaling kinetics of the AMD was studied at varying cycles of concentration (CoC) in the bench-scale water recirculating systems. Water temperature was fixed at 104°F (40°C) and the flow rate was adjusted at 3 GPM. The system was open to air so that the alkalinity may approach equilibrium with the atmospheric CO_2, which is similar to conditions in actual cooling tower operation.
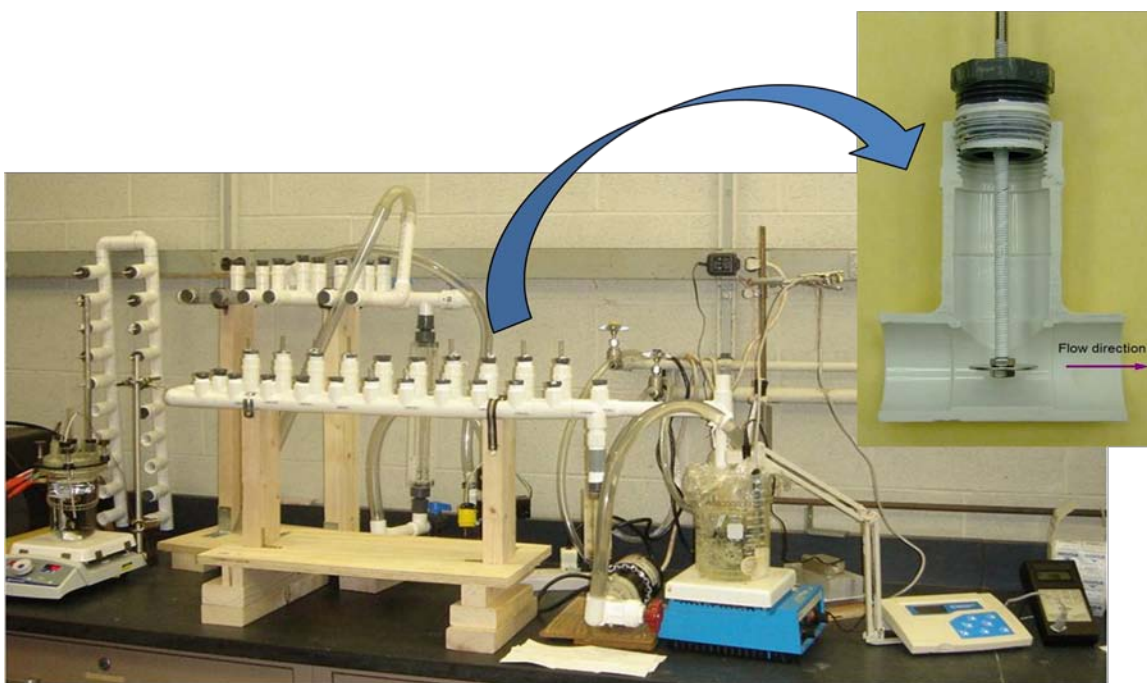
Figure 4.1 Bench-scale water recirculating system with inserted stainless steel circular disc specimens for scale collection and subsequent mass gain measurement.

Inset shows a pipe T-section where stainless steel circular disc specimens were inserted. Actual AMD water collected from St. Vincent College site (Latrobe, PA) was tested.

The scale samples collected on the test discs over time were air-dried and weighed with analytical balance to obtain mass data.

Scaling inhibitors tested in this study included tetra-potassium polyphosphate (TKPP, also a corrosion inhibitor), polymaleic acid (PMA), Aquatreat AR-540 and AR-545 (terpolymers manufactured by Alco Chemicals, Chattanooga, TN), and Acumer 2100 (a carboxylic acid/sulonic acid copolymer manufactured by Rohm & Haas, Philadelphia, PA). TKPP and PMA were obtained from The National Colloid Company (Steubenville, OH). Monochloramine was prepared by mixing sodium hypochlorite (5% stock solution) and ammonium chloride (Fisher) at $Cl_2:NH_3$-N of 4:1 wt. ratio and was used as a biomass control agent in the pilot-scale testing. In addition to TKPP, dedicated corrosion inhibitors in the form of tolyltriazole (TTA) and di-potassium phosphate (DKP) (The National Colloid Company, Steubenville, OH) were tested in this study.

Varied amounts of adsorption and adhesion of solids were observed on different materials in the pilot scale cooling towers. It was hypothesized that surfaces have different degrees of affinity toward suspended solids and thus lead to varied amounts of adsorption and adhesion of these solids. To test this hypothesis, both stainless steel and plastic coupon discs were used as collecting surfaces in bench-scale water recirculating systems. The plastic material selected for the experiment was the PVC that was used in the manufacture of the packing material used in the pilot-scale cooling towers, so that the information obtained from the bench-scale testing can be applied to the pilot-scale experiments.

4.2.4 Pilot-scale cooling tower tests

Three pilot-scale cooling towers were designed and constructed to test in the field the optimal chemical control regimen determined from bench-scale experiments. The towers were transported to the Franklin Township Municipal Sanitary Authority for side-by-side evaluation of different corrosion/scaling/biofouling control programs. The three towers were operated with the following target conditions: 1) CoC 4; 2) flow rate 3 GPM (passing through a 0.75" ID PVC pipe); and 3) temperature 105°F of the recirculating water entering the tower and 95°F exiting the tower.

The cooling towers were operated using passively-treated abandoned mine drainage collected from the St. Vincent College wetland site. The preliminary run started on October 8, 2008 and ended on October 17, 2008. The final run started on October 18, 2008 and ended on November 9, 2008. In both runs, all towers were using 100% of the passively-treated abandoned mine drainage as makeup water. The objective of the initial 12-day run was to evaluate the influence of high alkalinity and high conductivity of the makeup water on the operation of the pilot scale cooling towers. It was found that solids deposition during this run was excessively high (the scaling coupons immersed in water were completely covered by a thick layer of deposits), primarily because of the malfunctioning of the conductivity-based blowdown control. It was concluded that the in-line conductivity meter was not a reliable indicator of the actual CoC in the towers for the AMD water. Instead, the blowdown volume was fixed at 10 gallons per day to achieve CoC of 4.5 as the total daily makeup water addition averaged 45 gallons.

Prior to the final run, the towers were cleaned with acetic-acid solution and disinfected by free chlorine. Detailed information on tower operations, including the temperature of water at specific locations, airflow rate inside the cooling tower, the conductivity of recirculating system,

makeup water volume, blowdown volume, water flowrate, and ambient condition (weather, temperature, relative humidity), was recorded throughout the run. It was documented that the towers were able to perform according to design specifications and adequately simulate the operation of full-scale cooling towers in thermoelectric power plants.

Different levels of polymaleic acid (PMA) were added to each tower to determine its effect on controlling scale formation. Towers A and C were dosed at 15 and 25 ppm levels, respectively, while Tower B was used as a study control and received no PMA treatment. Scaling behavior as monitored with the mass gain of stainless steel coupon discs was analyzed by using a mass balance approach for the entire cooling tower recirculating system. Solid (scale) deposition rates on the stainless steel coupon surfaces were documented during all runs (along with corrosion weight loss of metal alloys, and heterotrophic planktonic/sessile bacteria). Water chemistry parameters were monitored to obtain detailed understanding of the cooling tower behavior.

4.3   RESULTS AND DISCUSSION

4.3.1   Precipitation modeling with equilibrium calculations

MINEQL+ [15, 16] was used to evaluate the scaling potentials of the AMD at different cycles of concentration. In addition, two most commonly referenced practical saturation indexes (Langelier Saturation Index and Ryznar Stability Index) were calculated as direct predictors of precipitation formation. The pH values with respect to cycles of concentration were also calculated.
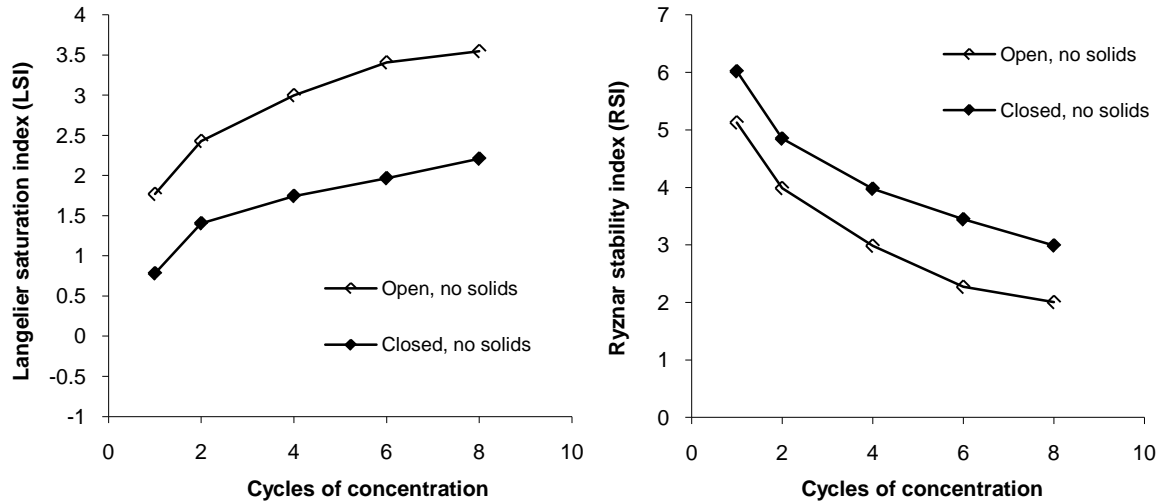
Figure 4.2 Modeling results of LSI (left) and RSI (right) for both open and closed to air cases without solids precipitation.

Detailed modeling results, as a function of increasing CoC, consist of the following:

The Langelier Saturation Index (LSI) and Ryznar Stability Index (RSI) under open/closed conditions (Figure 4.2);

The amount and form of solid precipitates under open/closed conditions (Figure 4.3);

Changes of aqueous pH (Figure 4.4).

The Langelier Saturation Index (LSI) increased with cycles of concentration, so did the scaling potential of the water. Ryznar Stability Index (RSI) was calculated by a different formula and usually exhibited an opposite trend with cycles of concentration compared to the LSI. The RSI values in Figure 4.2 decreased with the cycles of concentration and were below 6 under all conditions, which indicates mild to severe scaling potentials.

a. Open to air
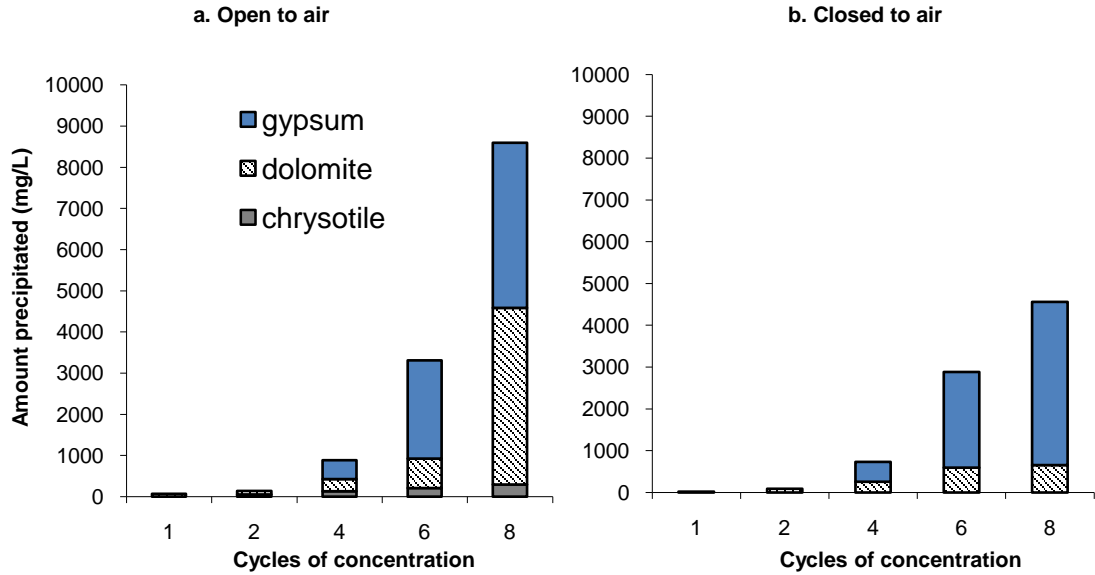
b. Closed to air

Figure 4.3 Predicted solid precipitation from the St. Vincent College Abandoned Mine Drainage calculated by MINEQL+.
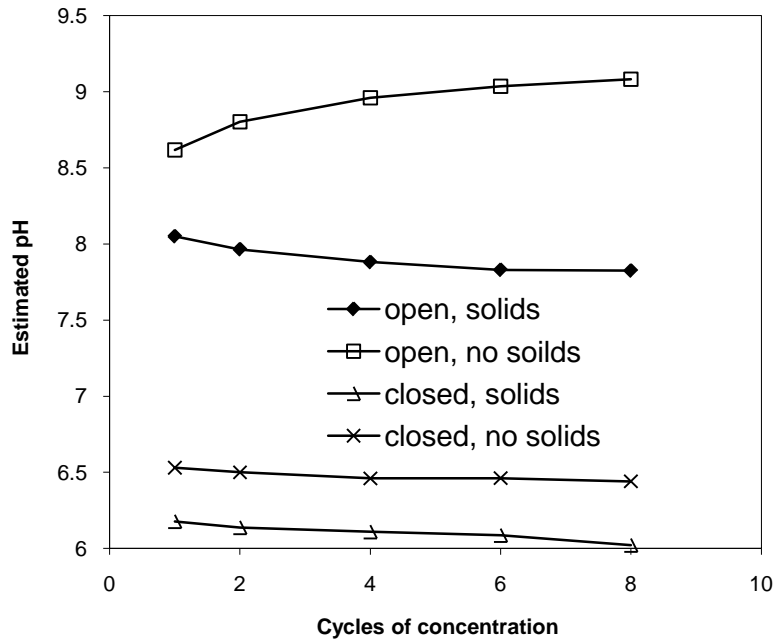
Figure 4.4 Predicted solution pH at different CoC under four different operation scenarios (open or closed to air; with and without solid precipitation).

MINEQL+ modeling results suggest that gypsum and dolomite are the major solid precipitates to form from the St. Vincent College abandoned mine drainage under recirculating cooling tower conditions. More solids were predicted to precipitate under open-to-air condition because of the abundant supply of carbonation. As shown in Figure 4.3, a significant amount of otherwise dissolved solids could precipitate and contribute to solids accumulation when the towers operate at high cycles of concentration. The amount of solids precipitation at equilibrium was predicted to be 7-10 times more at CoC 8 than at CoC 4.

When the calculations allowed water to be open to the atmosphere and to equilibrate with $CO_2(g)$, the pH values ranged between 8 and 9. When the calculations were performed in the absence of exposure to the atmosphere, the water was predicted to become acidic. Under the open condition, the calculated pH tended to increase with increasing CoC, when no solids were allowed to form. Such behavior was due to the accumulation of alkalinity with CoC. On the other hand, the pH tended to decrease with increasing CoC when solids formation was allowed to take place because the alkalinity was consumed through dolomite formation.

4.3.2   Bench-scale recirculating system experiments

Two bench-scale water recirculating systems were used to determine the scaling behavior of the actual SVAMD water at CoC 4 when inhibitors (i.e., PMA or AR-545) were added. The SVAMD water in both systems was treated with 15 ppm anti-scalant: System A with AR-545 and System B with PMA. SVAMD samples were added to the two water recirculating system and the water volume was reduced by 75% to CoC 4 with a heat source in about 5 days.

Concentration cycles, as determined by solution conductivity (which was the approach for field testing), took a longer time to reach CoC 4 than that based on water volume reduction

(Figure 4.5). This suggests that the dissolved solids that precipitated during the concentrating process do not contribute to the conductivity measurements. The 1:1 trend line defines an ideal behavior by which all dissolved solids remain in solution during evaporative concentration. A deviation from the 1:1 line indicates that part of the dissolved solids has precipitated out of the solution during concentration. In the presence of anti-scalants, the degree of deviation from the ideal line indicates the effectiveness of the added antiscalants to hold the solids in solution. Using this criterion, it was determined that PMA was more effective.
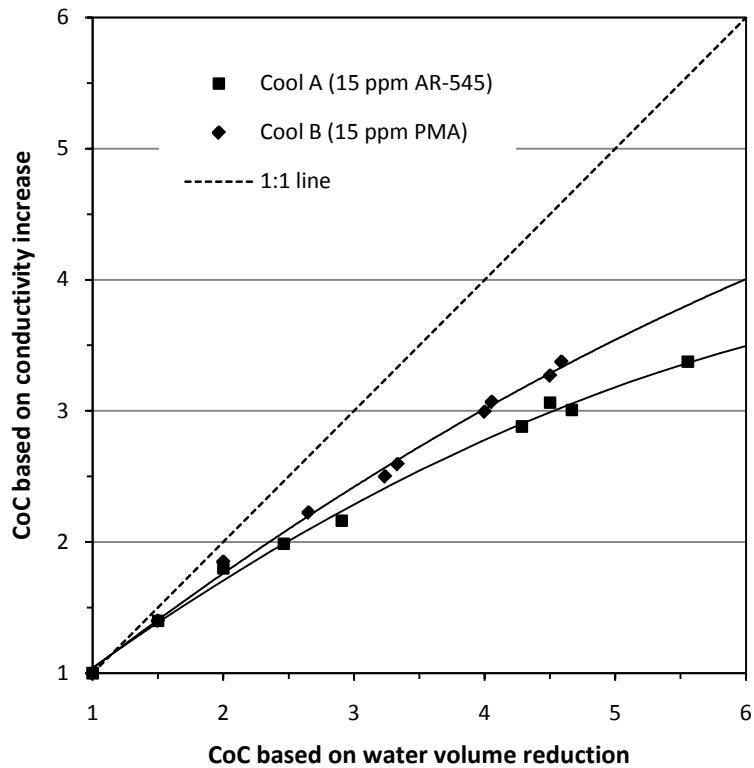
Figure 4.5 Correlation of concentration cycles determined by water volume reduction and conductivity measurements.

Coupon discs immersed in the SVAMD water treated with 15 ppm of AR-545 collected more solids after 8 days than those immersed in the SVAMD water treated with 15 ppm of PMA,

suggesting that PMA performed better in such water (Figure 4.6). In addition, the turbidity of the AR-545-treated SVAMD water started to increase from ca. 2 NTU to greater than 10 NTU after 5 days, while the PMA-treated water remained relatively clear (< 4 NTU). By day 10, the difference in turbidity between these two waters grew to more than 35 NTU.
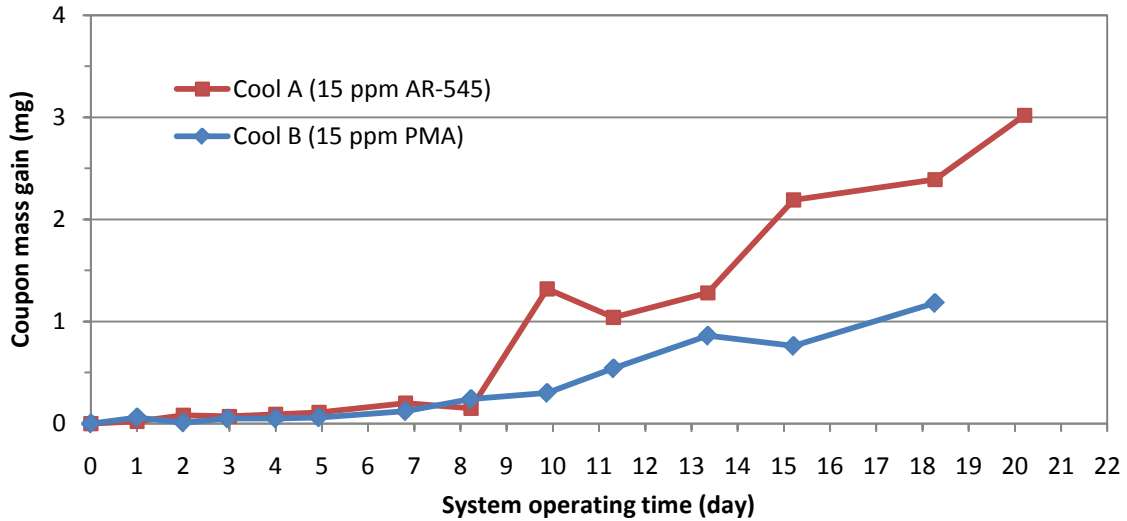
Figure 4.6 Coupon mass gain measurements for bench-scale water recirculating systems operated with the SVAMD (the water was stored in lab for a week prior to test). Recirculation conditions: 3 GPM, 40°C, pH 8.5.

Beaker tests with other anti-scalants (Acumer 2100 and AR-540) did not generate significantly better scaling inhibition performance than that of PMA (Figure 4.7) since the TDS of all solutions was approximately the same after reaching 75% volume reduction. These results suggest that PMA should be an effective scaling inhibitor for SVAMD water at 15-25 ppm dosage level. The effectiveness of PMA at both 15 ppm and 25 ppm concentrations were tested in pilot-scale experiments.
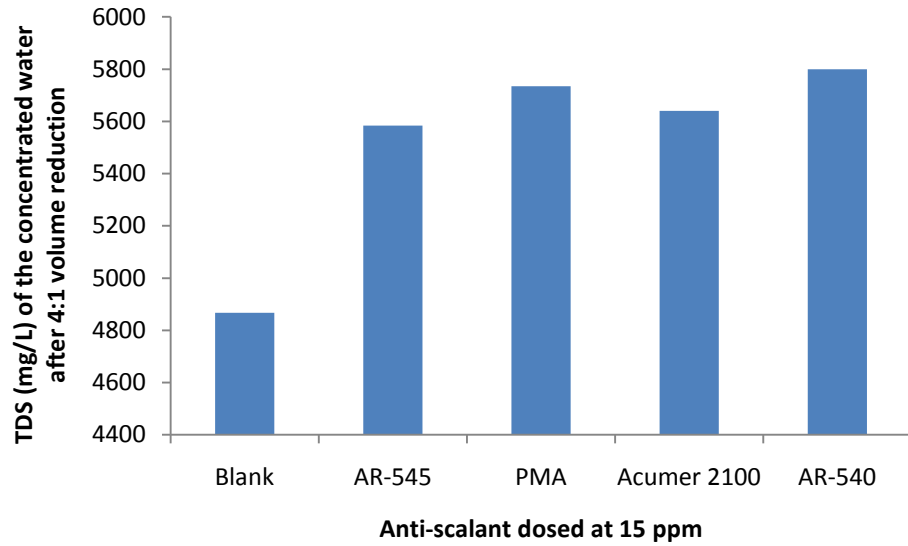
Figure 4.7 Effectiveness of different antiscalants in beaker tests at 40-45°C.

Initial water volume was 1.00 L, final volume for TDS measurements was 0.25 L. Water was heated in a water bath and bubbled with air to facilitate evaporation. It took 1-1.5 days for the water to reach CoC 4 (i.e., water volume reduction from 1.00 L to 0.25 L).

Figure 4.8 shows that the PVC discs collected more solids from water, especially in the absence of PMA, than the stainless steel coupons. On average, 3-4 times more solids were collected on the PVC than on the stainless steel.
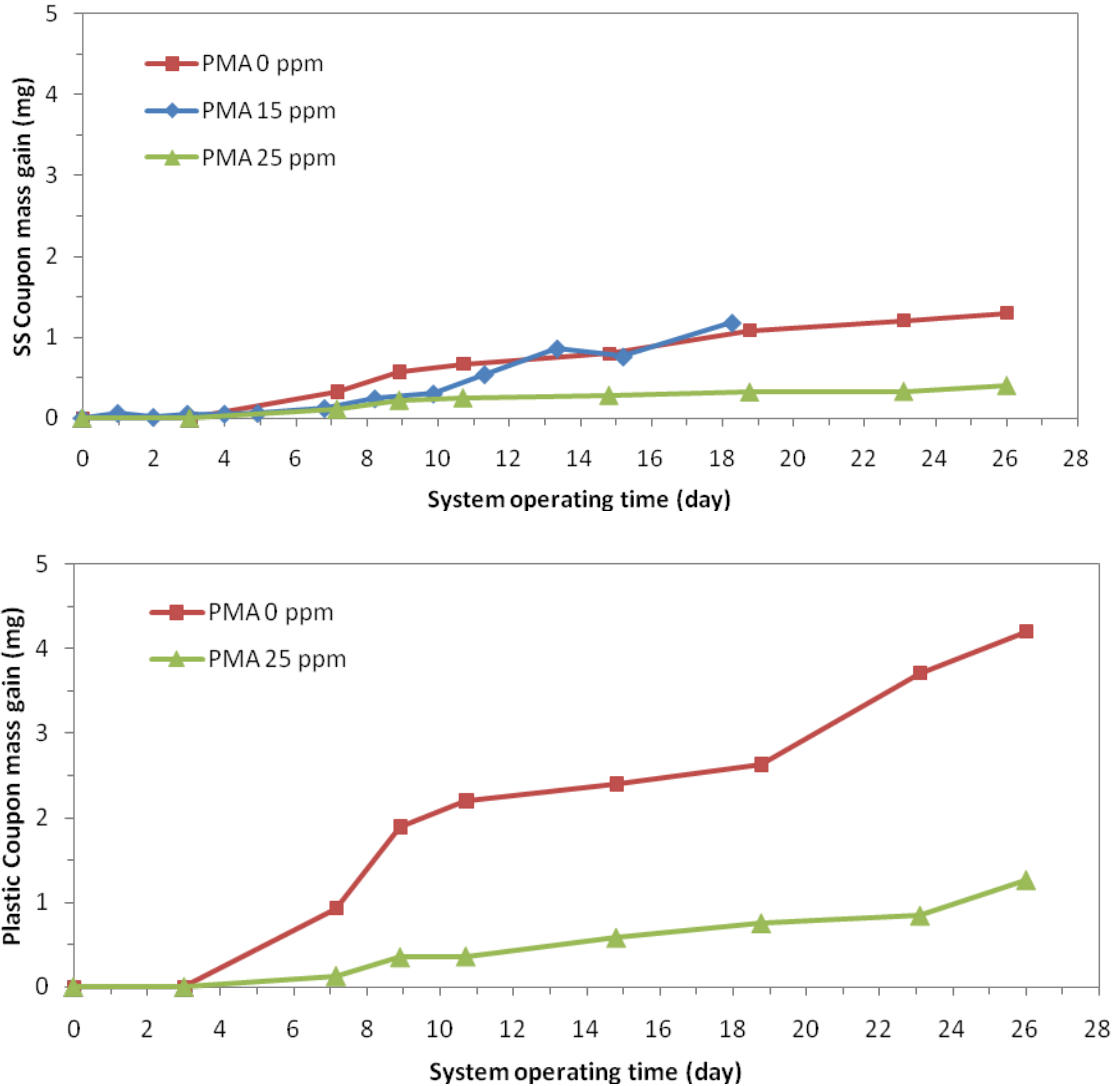
Figure 4.8 Coupon mass gain measurement for bench-scale water recirculating systems fed with the SVAMD water. The system was operated at 3 GPM, 40°C, and CoC 4. Upper panel: measured with stainless steel coupon discs. Lower panel: measured with PVC coupon discs.

The bench-scale experiments led to two basic conclusions: a) PMA performed satisfactorily well for scaling inhibition under the operating conditions employed; and b) Conductivity-based control of concentration cycles could deviate significantly from the concentration cycles determined based on water volume reduction.

Table 4.2 Cooling tower water quality in the field testing using the passively-treated AMD from St. Vincent College mine drainage site

The recirculating tower water analyzed was operated at CoC 4 (the run from October 18, 2008 to November 9, 2008). Unit: mg/L

Analyte	Result (unfiltered)		
	Tower A	Tower B	Tower C
Al	ND	ND	ND
Ca	825	674	796
Cu	0.0629	0.0303 B	0.0344 B
Fe	ND	ND	ND
K	29.3	23.4	26.3
Mg	254	251	235
Mn	0.578	0.109	0.595
Na	446	450	418
SiO_2	59.1	57.9	54.9
Zn	0.0567	0.101	0.0531
NH_3-N	0.57 J	0.74 J	0.64
Bicarbonate Alkalinity	276 J	92.3 J	257 [J]
BOD	ND	ND	ND
Cl	216	239	223
NO_3-N	1.1	1.1	1.1
SO_4	2930 J	2910 J	2850 [J]
Total P	0.64	0.032 B	0.65
Total Alkalinity	407	92.3 J	400 [J]
TOC	13.8	6	17

Notes: J: Method blank contamination. The associated method blank contains the target analyte at a reportable level. B: Estimated result. Result is less than reporting limit. ND: Not detected.

4.3.3　Pilot-scale study

Bulk water chemistry in cooling towers. The water quality data for the three cooling towers are summarized in Table 4.2, and discussed in detail below.

pH – The pH values in towers treated for scaling inhibition by PMA (along with other chemical additives for simultaneous corrosion and biofouling control) were different from those in the control tower. The control tower (Tower B) that had no PMA addition had an average pH of 8.2, whereas the two towers that received chemical treatments for scaling, corrosion, and biofouling control had an average pH value of 8.7 for Tower A and 8.8 for Tower C. As a reference, the raw SVAMD had an average pH of 7.8. The comparatively higher pH levels in the treated towers were related to the higher levels of solution alkalinity that was retained by PMA.

Chloride – Chloride concentrations in the recirculating water were generally 6-8 times greater than those in the makeup water (i.e., 400 mg/L in recirculating vs. 60 mg/L in makeup). As such, the values of CoC based on the chloride concentration were also greater than the volume-based values of CoC 4-5. The extra amount of chloride input was from the addition of chlorine-based biocide (i.e., in the form of monochloramine).

Sulfate – Sulfate concentrations in the towers were generally 4-5 times higher than those in the makeup water. This ratio was close to the volume-based CoC since there was no additional sink or source of sulfate (gypsum was not found in solid deposits).

Phosphate – Orthophosphate was added as a corrosion inhibitor. The target phosphate concentration was 5 ppm as PO_4^{3-} but it was not strictly maintained due to its low solubility in the presence of high concentration of calcium. Consequently, phosphate concentrations in the bulk water remained below 1 ppm. Corrosion studies showed that the added phosphate (in the

form of pyrophosphate) was ineffective to prevent corrosion. Rather, the addition of phosphate produced more phosphate-containing scales.

Alkalinity – Alkalinities in Towers A and C were around 4 times higher than those in the makeup water, close to the volume-based CoC. However, in Tower B, the alkalinity was close to makeup water. The significant difference in alkalinities between the test towers and the control tower is attributed to the addition of PMA. Without PMA addition in Tower B, alkalinity was consumed by the formation of calcium carbonate precipitates. In Towers A and C, PMA successfully inhibited the formation of calcium carbonates and as a result, most of the alkalinity remained in the aqueous phase.

Mass deposition over time. During the pilot-scale testing with the SVAMD water, a preliminary run was conducted for a period of 12 days as a test run to obtain critical data for cooling tower performance. Figure 4.9 (upper panel) depicts the time course of scale mass deposited on stainless steel coupon discs in the three towers during the preliminary run. The scale accumulation on the coupon discs was excessive- the entire coupon surface was covered by a thick layer of deposits (ca. 2 mm thick). The excessive solids deposition was caused by the towers operating at much higher cycles of concentration than originally planned. The towers were operated at higher CoC because the conductivity probes in each tower that were used to monitor the conductivity of the recirculating water and to trigger blowdown at preset values failed to function properly. The experiment was designed to operate with raw SVAMD with an average conductivity of 1.91 mS/cm, which means that the recirculating water in each tower should have conductivity values between 7.5-9.5 mS/cm to maintain a target CoC of 4-5. However, tower blowdown was not successfully triggered at these predetermined conductivity

levels and the towers were actually operating at CoC 8-10 based on water volume reduction. The excessive mass deposition observed was consistent with modeling predictions (Figure 4.3).
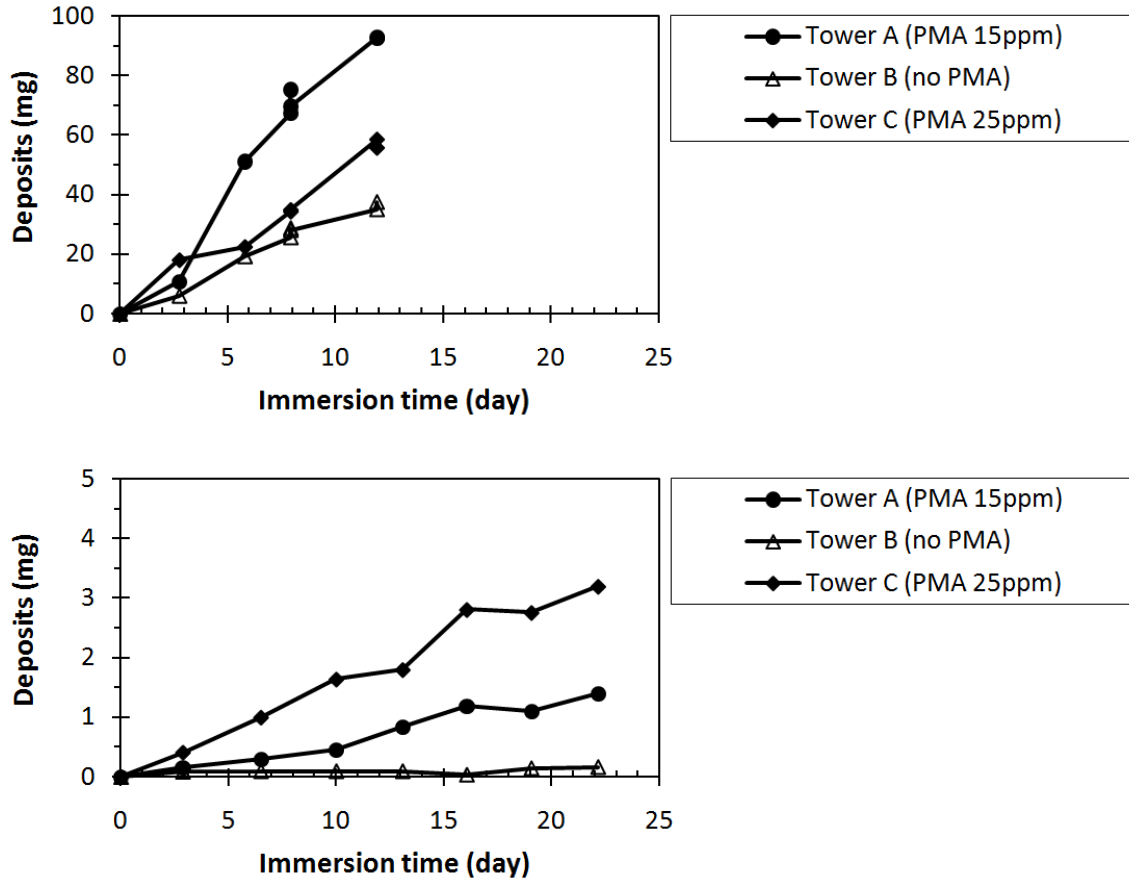
Figure 4.9 Mass gain measurements in pilot-scale cooling towers operated with SVAMD water at FTMSA site. Upper: preliminary test run (CoC 8-10); Lower: final run (CoC 4-5). Deposits were collected on stainless steel coupon discs immersed in pipe flow. Effective collection area 5.61 cm^2, flow velocity 1.9 ft/sec (3 GPM in 3/4" ID pipe), water temperature $104 \pm 2°F$ in the pipe section, open recirculating cooling system.

Upon completion of the preliminary run, the conductivity probes were either calibrated or replaced to ensure proper function prior to the final run. To guarantee proper blowdown when the towers reached CoC 4, daily check up on the blowdown volume was performed throughout the run. When the volume of blowdown based on the conductivity measurements was less than a

quarter of the makeup water volume, manual blowdown was executed to maintain CoC 4 in each tower. The time course of scale mass deposited for the three towers during the final run is shown in Figure 4.9 (lower panel). Comparing with data from the preliminary run where CoC 4 was not maintained (Figure 4.9 upper panel), scale deposition was significantly reduced when CoC was maintained around 4.

However, the coupon mass gain measurements showed that the most scale formed on discs in water treated with the highest dosage of PMA, which is contrary to expectation. According to the data for scale build up over time (Figure 4.9), coupon discs immersed in Tower B that was not dosed with PMA collected the smallest amount of scale whereas the coupon discs in Tower C with 25 ppm PMA addition collected the largest amount. This outcome of scaling behavior is exactly the opposite of the intuitive expectation that addition of PMA would inhibit scaling and that higher PMA dosing would perform better. To understand these observations in the coupon mass gain measurements, a series of experiments were carried out at the pilot-scale and bench-scale and the results are discussed below.

Effectiveness of PMA to control scaling. The residual PMA concentration in the recirculating water was measured and compared to the amount added and then correlated to scale formation to determine the effectiveness of the PMA treatment. As shown in Figure 4.10, total measureable PMA in both Towers A and C was lower than the added concentration, suggesting that a fraction of the added PMA was removed from the aqueous phase. This removal was most likely through coprecipitation with solids. The dissolved (aqueous) PMA in water accounted for about 50-60% of total PMA in both towers. The remaining 40-50% was associated with suspended solids, thereby exerting repulsive forces between suspended particles to discourage

solids settling (PMA molecules are generally negatively charged due to dissociation of carboxylic groups).
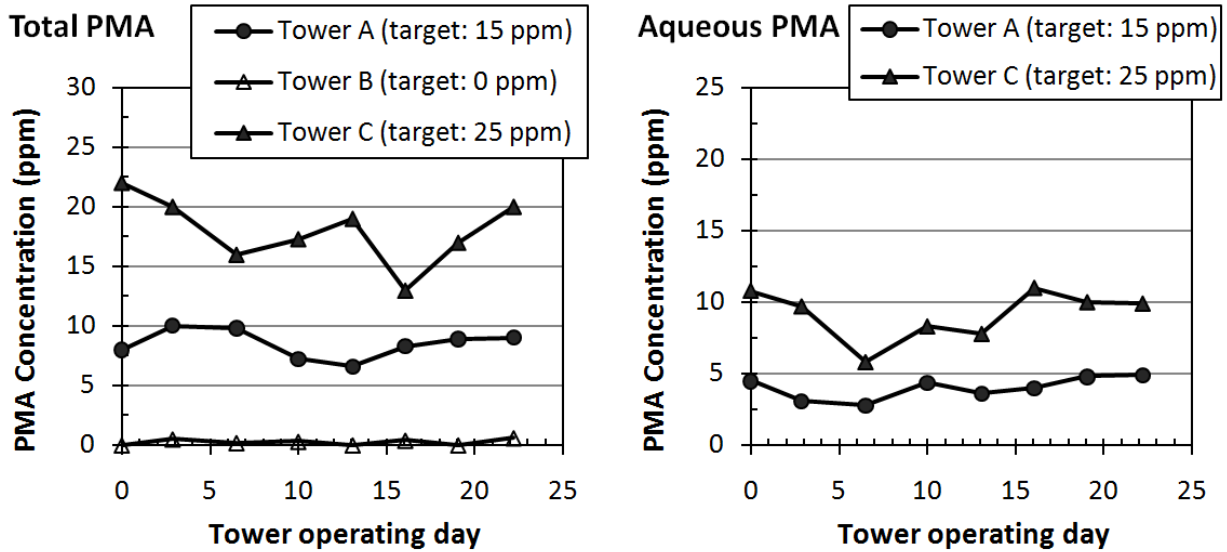
Figure 4.10 Total PMA (left panel) and dissolved (aqueous) PMA (right panel) concentrations in the recirculating water of the cooling towers as measured after daily addition of PMA (with 0.5 hr delay).

PMA dose was based on water blowdown volume. The aqueous PMA concentration was obtained by filtering the water sample through a 0.22-μm filter. Background readings were corrected using water sampled from Tower B where no PMA was added.

The effect of PMA as an antiscalant was contrary to the original hypothesis that PMA would reduce scale formation; higher concentrations of PMA in the recirculating water resulted in more scale deposition on the steel coupons. Additional experiments determined that a significant amount of solids were precipitated on the packing in Tower B, which did not receive any antiscalant (the PVC surface exhibited significant affinity for the SVAMD solids) and that the turbidity of the recirculating water in Tower B was close to that of the makeup water (Figure 4.11). The large error bars (one standard deviation) of the turbidity measurements (Figure 4.11)

with waters in Towers A and C suggest that the differences in turbidity of the two waters are statistically insignificant: both waters contained appreciable amount of suspended solids. Such findings suggest that the solids formed in Tower B were easily separated from the liquid phase and removed from the system. This was evidenced by the mass balance on four main sections of the recirculating cooling tower system (Table 4.3). At the bottom sumps of the towers, significant amounts of solids were accumulated under slow flow condition. For Tower B without PMA treatment, solids buildup became the most serious in the tower packing section where evaporative concentration led to precipitation-induced deposition. In Towers A and C, the influence of flow rate in the bottom sump and the evaporation on the tower packing were mitigated by the presence of PMA, which impeded solids deposition. Higher levels of suspended solids in Towers A and C resulted in higher water turbidities and a greater chance for the suspended solids to deposit on the pipe and coil sections. It is noteworthy that the ranking order of the solids deposition at the pipe and coil section of the three cooling towers calculated based on the mass balance analysis (i.e., C > A > B) is in agreement with the scaling trends measured by the coupon mass gain (Figure 4.9).
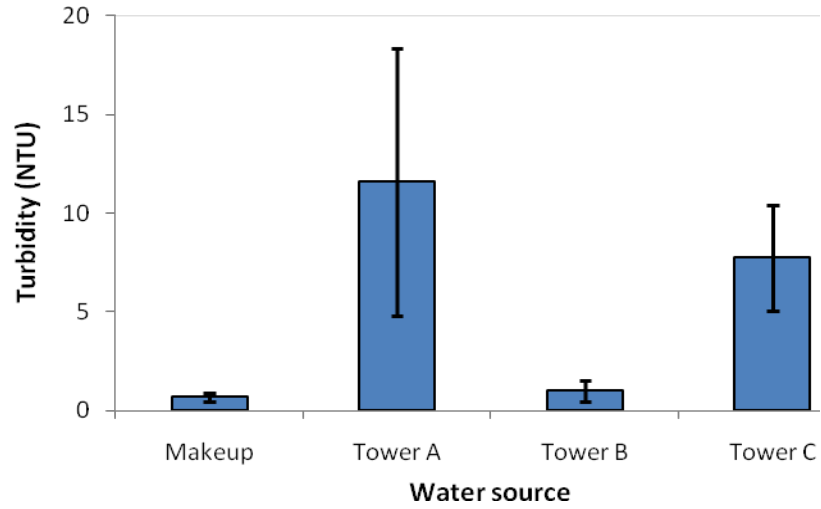
Figure 4.11 Turbidity of the makeup water and the recirculating water in the cooling towers during the CoC 4 operation.

The column represents mean values of seven measurements over the course of tower operation; error bars represent 1 standard deviation of the seven measurements for each tower.

Table 4.3 Mass balance analysis of solids deposition in different sections of the cooling towers operated with SVAMD water at CoC 4 for 25 days (the final run). All units are in grams

Cooling Tower	A	B	C
Solids input with makeup water (1)	6183	6126	6488
Solids output with blowdown (2)	4939	4574	5301
Net solids input to tower system (3) = (1) – (2)	**1244**	**1552**	**1187**
Solids accumulated in bottom sump (4)	491	557	469
Solids accumulated on tower packing (5)	506	936	220
Solids accumulated in the pipe and coil sections (6) = (3) – (4) – (5)	**247**	**59**	**498**

Overall, PMA was not very effective at keeping high levels of dissolved solids present in SVAMD in solution under the pilot testing conditions and the doses applied. The solids content of the SVAMD water at four cycles of concentration was extremely high and inhibition of precipitation by PMA was not effective.

4.4   CONCLUSIONS

The scaling behavior and control of wetland-treated abandoned mine drainage in recirculating cooling systems was evaluated in this study. Results from the pilot-scale experiments determined that the addition of commonly used polymer-based scaling inhibitors alone was ineffective for

scaling control. The high concentration of total dissolved solids requires more comprehensive pretreatment and scaling controls. Nevertheless, the added PMA, at concentrations of 15 to 25 ppm, lent some stability to suspended mineral solids (high water turbidities) and there was less deposition in the pipe flow sections of the cooling towers.

Deposits from the SVAMD concentrated to CoC 4 in recirculating cooling systems exhibited varied affinities to different surfaces. More deposits were collected on the PVC surfaces that were used as the tower packing material. Hydrodynamics also played a role in deposition. Low flow velocities encountered in the plastic packing and bottom sump sections of cooling tower resulted in greater sedimentation. Indeed, significant amount of deposits were observed at the bottom of the tower sump, especially in the tower receiving no PMA treatment. The finding suggests that scaling took place in a nonuniform manner throughout the cooling tower system. Therefore, it is suggested that scaling measurements should be performed at tower sections where deposition is of concern. Also, similar materials of test coupon should be used for scale deposition to provide substrate surfaces representative of the building materials of cooling tower.

5.0 SCALING CONTROL IN ASH TRANSPORT/SETTLING POND WATER INTERNALLY USED IN COAL-FIRED POWER PLANT COOLING SYSTEMS

Water sluicing systems are commonly used at coal-fired electric power plants to remove combustion residues, i.e., fly ash and bottom ash, from the plant. Water is used to transport the ash to sedimentation ponds where the ash is hydraulically settled and the supernatant—ash pond effluent (APW)—is discharged. APW is a promising alternative to freshwater as a cooling water makeup for coal-fired power plants, as it is internally available at many plants. The amounts of APW available at a coal-fired power plant can generally satisfy the cooling water makeup needs in a recirculating cooling system. The reuse of APW, which contains a variety of soluble chemicals originated from coal-ash leaching, can avoid their direct discharge to natural waters, which can be potentially problematic since the APW contains a variety of soluble chemical contaminants originated from the leaching of the sluiced coal ash. But concentrated APW in recirculating cooling systems may cause scaling problems. In this study, the feasibility of controlling scaling when using clarified APW, the pond effluent after the ash solids are settled, in cooling water systems was investigated through laboratory experiments. Bench-scale recirculating experiments were conducted to test chemical control schemes for scaling in systems APW. The testing was conducted at temperature, flow velocity conditions as well as water constituent concentrations similar to those in a recirculating cooling system. The effectiveness of chemical treatment strategies in inhibiting scaling was studied through exposure and monitoring

84

of specially designed disc specimens in extended duration tests. The mineral scaling resulting from the use of the APW was much less severe than from the previously tested two other impaired waters (i.e., secondary-treated municipal wastewater and passively-treated abandoned mine drainage). The addition of PMA (10 ppm) effectively inhibited scale formation, while without PMA treatment the scale formed consisted of primarily calcium solids. In addition, this study demonstrated that the corrosion products from the metallic components of cooling towers could potentially lead to elevated amounts of scales due to the re-deposition of the corrosion product solids, especially under the conditions where large metallic surface is in contract with the APW cooling water.

5.1   INTRODUCTION

Ash transport water is typically regarded as expendable waste because after sedimentation, the sluicing water effluent from the sedimentation ponds is usually discharged into receiving waters. A variety of soluble chemical species are present in ash transport water as a result of leaching from the fly bottom ashes and in some cases from addition of plant liquid wastes to the sluice water. Fly ash and bottom ash generally contain little organic matter. The chemical constituents of most concern in ash transport water with respect to discharge are inorganic, in particular metals [1, 2]. These are derived from leaching of ash particles, which consist primarily of oxides of silicon, aluminum, and iron, but also contain a number of other metals at lower levels.

Impaired waters are of increasing interest as alternative sources of makeup water for thermoelectric power plant recirculating cooling water systems. Ash transport water has the potential for use in cooling systems at coal-based power plants. The large amounts of water

involved in these processes represent a substantial opportunity for internal water reuse in cooling systems at electric power plants. In most case the ash transport slurries are directed into sedimentation ponds in which settling of the ash particles takes place. There is potential to reuse a portion or all of the ash pond effluent, as has been investigated periodically in the past [3].

The amount of ash transport water available at a coal-fired power plant generally can satisfy the cooling water need for the recirculating system in the power plant. The mean value of bottom ash pond overflow is 3,881 GPD/MW [4], which can contribute 27% of the mean value of makeup water needs, in recirculating cooling system, which averages 14,400 GPD/MW [5].

The objective of this study was to investigate the scaling potential of APW under the conditions commonly encountered in recirculating cooling water systems and study the effectiveness of some commonly used scaling inhibitors. Specifically, scale formation of the APW was calculated at different cycles of concentration (CoC) under relevant cooling tower operation conditions using the chemical equilibrium model MINEQL+. The actual APW taken from Reliant Energy Power Plant ash settling pond effluent was tested in a bench-scale water recirculating system to examine its scaling behavior under CoC 1 vs. CoC 4. Synthetic APW was then used to better represent CoC 4 condition. The effectiveness of different antiscaling chemicals were tested using synthetic APW.

5.2   MATERIALS AND METHODS

5.2.1   Ash Pond Water Characterization and Preparation for Laboratory Testing

APW from the Reliant Energy coal-based thermoelectric power plant, located at Cheswick, PA, was used for testing in laboratory experiments, as well as for equilibrium chemical modeling. Water samples were collected on October 2, 2007, and analyzed for a range of water quality constituents [6]. The water samples were collected with a 1-L polyethylene sampler and then transferred to appropriate polyethylene or glass sample containers provided by the commercial laboratory, TestAmerica (Pittsburgh, PA). Appropriate preservatives were added to the sample bottles prior to sampling. Analyses performed are summarized in Table 5.1.

Parallel to the sampling for chemical analysis, a larger amount of the APW was collected for laboratory experiments. The water was concentrated in the laboratory by heat evaporation at 35-40°C to reach 4 cycles of concentration (CoC 4) as determined by 75% water volume reduction. This concentration level is representative of the CoC used in recirculating cooling tower systems operated with impaired waters.

5.2.2   Equilibrium Modeling of APW Scaling Potentials

The chemistry of the APW cooling water at different CoC was modeled using MINEQL+ [7, 8] to gain insight into the effects of CoC on scaling. The primary objective for this effort was to estimate the amount and composition of mineral solids that would precipitate and the water chemical composition that would occur under typical cooling tower operation conditions as a

87

function of CoC. The major constituents and their chemical speciation were assessed and the dominant scale-producing reactions were identified.

Table 5.1 Characteristics of the ash pond water from Reliant Energy coal-fired thermoelectric power plant, Cheswick, PA (sampled on October 2, 2007)

Analyte	Result (mg/L)	Reporting limit
Al	0.588	0.2
Ca	43.4	5
Fe	0.344	0.1
K	2.56 B	5
Mg	9.38	5
Mn	0.0281	0.015
Na	21.6	5
SiO_2	3.29	1.07
pH	8.4	-
Acidity	ND	5.0
NH_3-N	0.068 B,J	0.10
Bicarbonate Alkalinity	56.3	5.0
BOD	ND	2.0
Cl	30.4	1.0
NO_3-N	0.28	0.05
Specific Conductance (mS/cm)	402	1.0
SO_4	92.4	1.0
Total P	0.033 B	0.1
Total Alkalinity	60.4	5.0
TDS	271	10.0
TSS	20.8	4.0
TOC	2.4 J	1.0

Notes: J: Method blank contamination. The associated method blank contains the target analyte at a reportable level. B: Estimated result. Result is less than reporting limit. ND: Not detected.

The following four operational conditions were simulated for the APW water:

1) The aqueous system was open to the atmosphere ($P_{CO2} = 10^{-3.5}$ atm) to allow the alkalinity to be in equilibrium with $CO_2(g)$ and solids were allowed to precipitate.

2) The aqueous system was open to the atmosphere ($P_{CO2} = 10^{-3.5}$ atm) to allow the alkalinity to be in equilibrium with $CO_2(g)$ and solids were not allowed to precipitate (i.e., water can be super-saturated).

3) The aqueous system was closed to the atmosphere with total alkalinity fixed and solids were allowed to precipitate.

4) The aqueous system was closed to the atmosphere with total alkalinity fixed and solids were not allowed to precipitate.

The four conditions represent the extreme effects of atmospheric CO_2 and solution supersaturation. It is reasonable to expect that the actual conditions for field testing would fall within these boundary conditions.

5.2.3   Bench-scale Tests with REAPW

The objective of the bench-scale studies with APW was to test the effectiveness of different scaling inhibition chemicals, added either individually or in proper combinations. The experimental system was depicted in Figure 5.1. Four antiscalants were tested whose selection was based on a literature review and consultation with experts in the cooling industry. The antiscalants were polyacrylic acid (PAA), polymaleic acid (PMA), 2-phosphonobutane-1,2,5-tricarboxylic acid (PBTC), and tetrapotassium pyrophosphate $K_4P_2O_7$ (TKPP). PAA and PMA are short-chain organic polymers, while PBTC and TKPP are phosphorous-based (i.e., phosphates/phosphonates) common antiscalants. At the start of each experiment, an antiscalant

was added to the recirculating water. The combination of PMA and PBTC at a dosing ratio of 2:1, as recommended by cooling experts for better performance, was also tested. In addition, the effect of cycles of concentration (CoC) was examined with an actual ash pond effluent from Reliant Energy power plant.
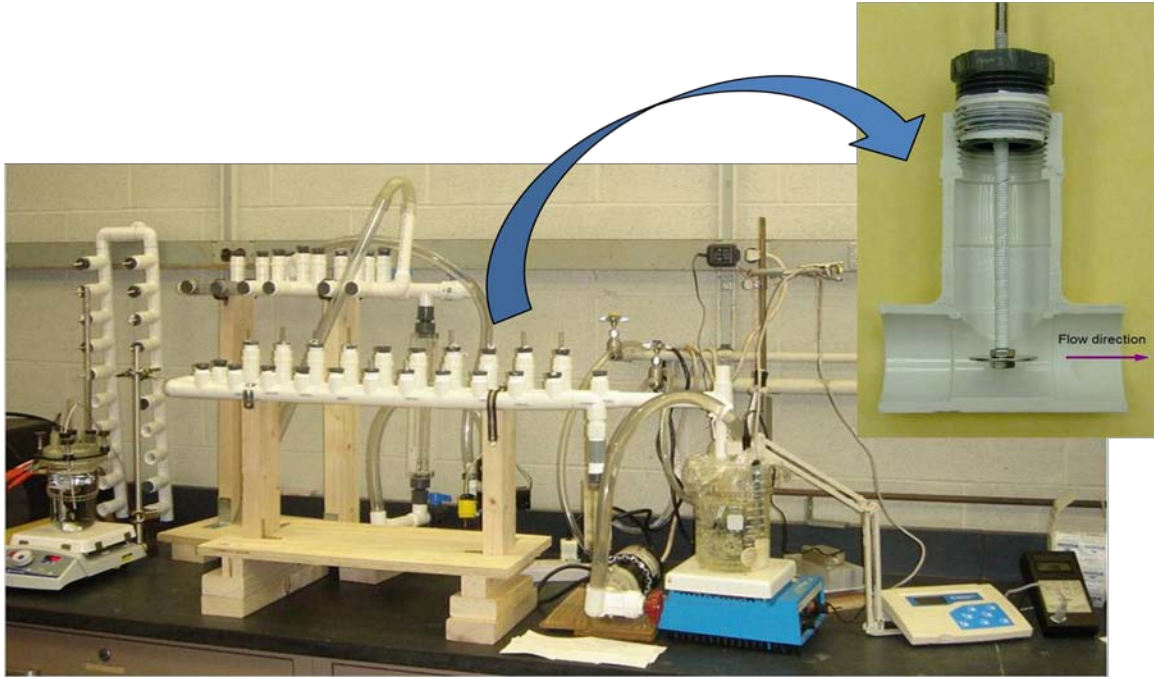
Figure 5.1 Bench-scale water recirculating system with inserted stainless steel circular disc specimens for scale collection and subsequent mass gain measurement.

Inset shows a pipe T-section where stainless steel circular disc specimens were inserted. Both actual and synthetic APW was tested.

5.3   RESULTS AND DISCUSSION

5.3.1   Precipitation Modeling with Equilibrium Calculations

The chemical equilibrium model MINEQL+ (version 4.5) was used in detailed evaluation of the cooling water chemistries. Scaling potentials at different cycles of concentration, as measured by the two most commonly referenced practical saturation indexes and direct predictors of precipitation formation, were analyzed. The pH values with respect to cycles of concentration were also calculated.

Detailed modeling results consist of the following:

The Langelier Saturation Index (LSI) and Ryznar Stability Index (RSI) under open/closed conditions as a function of CoC (Figure 5.2);
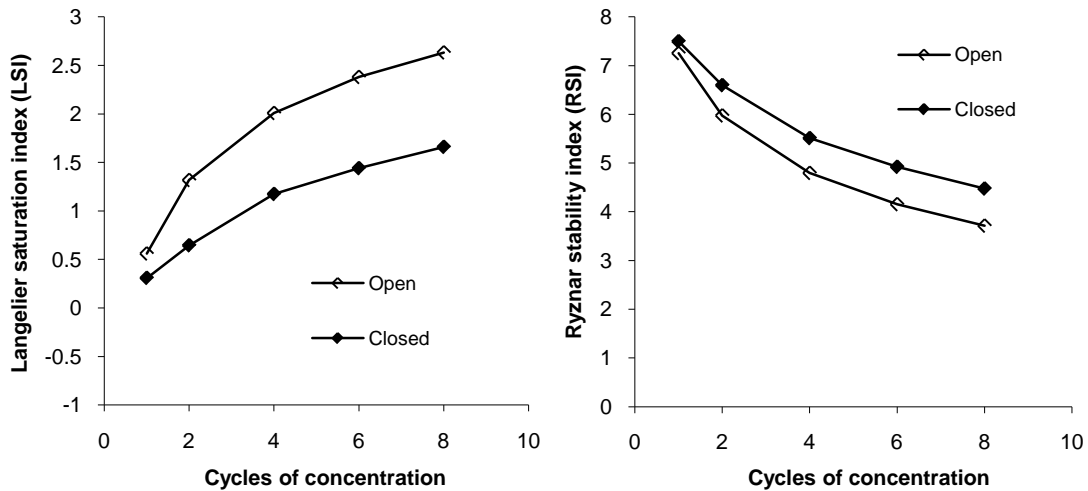
Figure 5.2 Modeling results of LSI (left) and RSI (right) for both open and closed to air cases, Reliant Energy ash pond water.

Amount and form of solid precipitates under open/closed conditions as a function of CoC (Figure 5.3);

Changes of aqueous pH with increasing CoC (Figure 5.4).
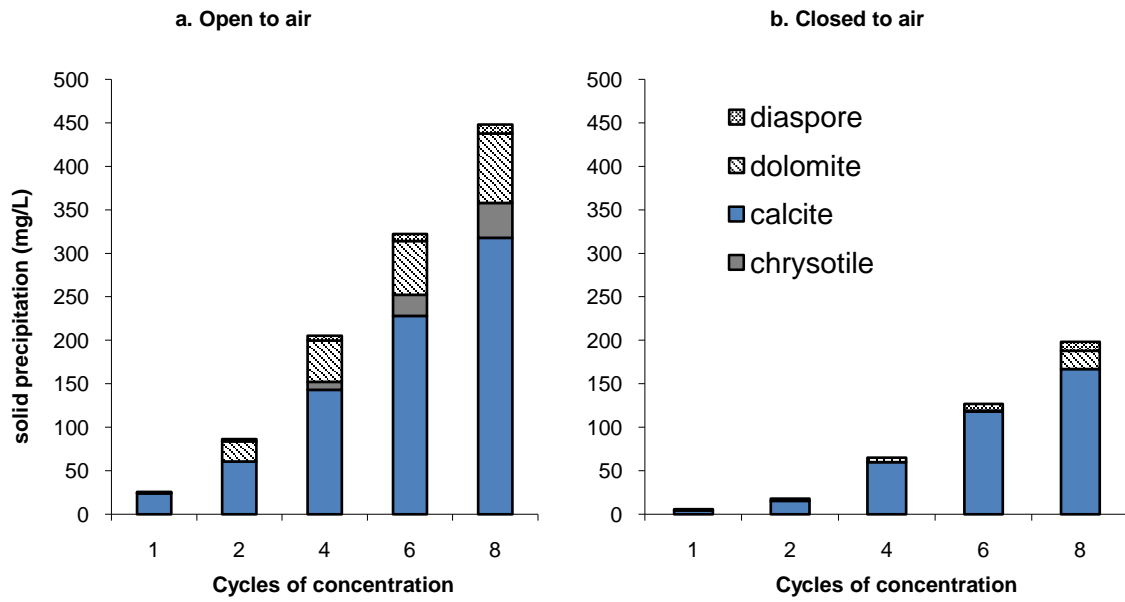
Figure 5.3 Predicted solid precipitation from the Reliant Energy ash pond water, calculated by MINEQL+.
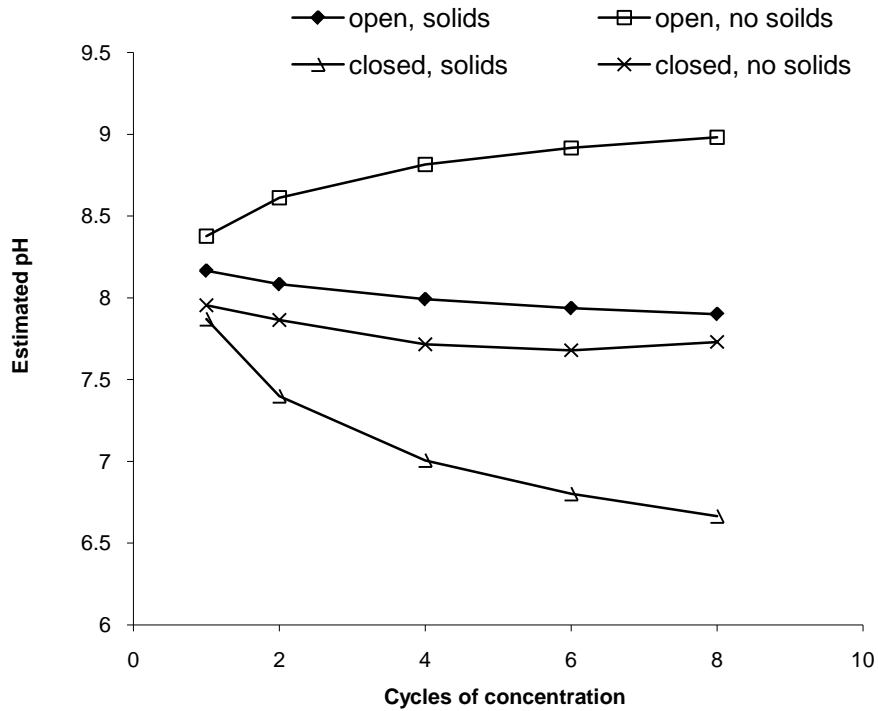
Figure 5.4 Predicted solution pH at different CoC under four different operation scenarios (open or closed to air; solid precipitation is allowed or not), Reliant Energy ash pond water.

The Langelier Saturation Index (LSI) increased with cycles of concentration, so did the scaling potential. For the Ryznar Stability Index (RSI), it was calculated by a different formula and usually exhibited an opposite trend compared to the LSI. The RSI values in Figure 5.2 decreased with the cycles of concentration (as did the corrosion potential). Under all conditions, RSI values were below 8, indicating mild corrosion potentials.

Calcite and dolomite are the major solid precipitates predicted by MINEQL+ to form in the Reliant Energy ash pond water under typical recirculating cooling tower conditions. From Figure 5.3, greater amount of solids precipitated out of solution when operated at an open-to-air condition, because under this condition CO_2 was allowed to be dissolved from the air into solution to provide carbonate species for the formation of calcite and dolomite. Nevertheless,

solids formation from the APW water was very minimal compared to other impaired waters studied in this project.

When the water was open to the atmosphere to allow equilibrium with $CO_2(g)$, the pH values were between 8 and 9. When the water was closed to the atmosphere, the water became acidic. Under open condition, the pH tended to increase with increasing CoC when no solids were allowed to form. This was because of the accumulation of alkalinity with CoC. On the other hand, the pH tended to decrease with increasing CoC when solids formation took place because the alkalinity was consumed by the formation of calcite and dolomite.

5.3.2   Bench-scale Recirculating System Experiments

Tests with actual APW. Interesting scaling behaviors were observed when comparing the amounts of deposit over time in the actual ash pond water at CoC 1 vs. CoC 4 (Figure 5.5). After the water was recirculated in a bench-scale water recirculating system for 120 h (5 d), more deposits were collected from the CoC 1 water. This observation was contrary to expectations because the water at CoC 1 (i.e., un-concentrated raw water) should contain only one quarter of the amounts of mineral solutes than the CoC-4 water, and thus would be much less scale forming. Results depicted in Figure 5.6, which compares the predicted and measured TDS in APW that was being concentrated by evaporation, offered an explanation for this discrepancy. During the concentration process of water evaporation to reach CoC 4, a portion of the mineral solids was precipitated out of solution. As a result, the TDS contained in the CoC-4 water (the CoC was determined by a 75% water volume reduction) was less than four times of the TDS contained in the raw (CoC-1) water. On the same figure, the results from modeling prediction by MINEQL+ provided similar trend.

94
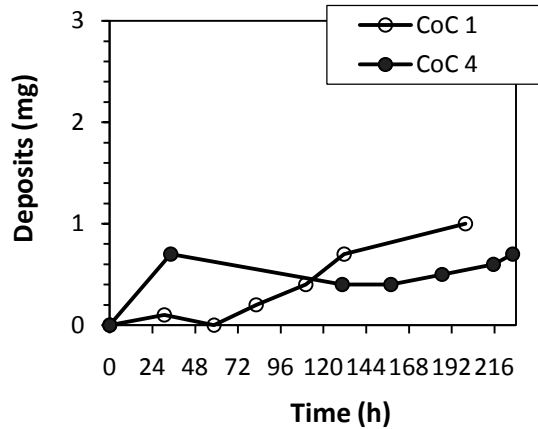
Figure 5.5 Scaling behavior of the Reliant Energy ash pond effluent in bench-scale water recirculating tests: effect of cycles of concentration (CoC).

Experimental conditions: 40°C and 3 GPM. For CoC-4 tests, the water was pre-concentrated by evaporation in a heating bath (40°C) to lose 75% volume before adding to the recirculating system.
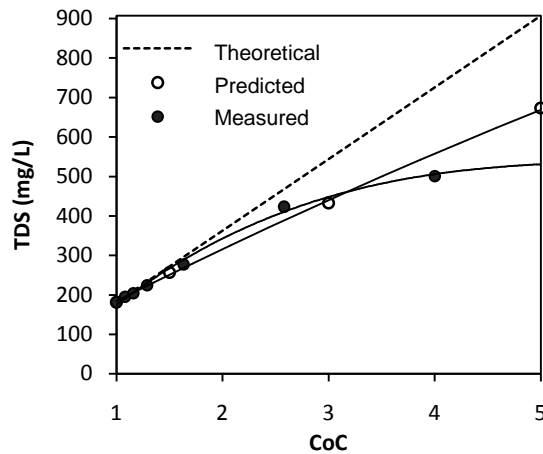
Figure 5.6 Changes in solution TDS as a function of CoC for Reliant Energy ash pond water.

Theoretically, TDS should increase linearly with increasing CoC (dashed line). However, as CoC increases, both MINEQL+ predictions (open circles) and experimental observations (filled circles) deviated from the theoretical curve. The TDS measurements were performed with actual water concentrated by water evaporation.

95

Loss of mineral solids during evaporation did not, however, fully explain the reversal in the scaling of the actual APW at CoC 1 vs. CoC 4. To further explore the causes of this interesting behavior, the chemical composition of the scale collected from both waters was analyzed by energy dispersive X-tray spectrometry (EDS). The analysis revealed a significant amount of iron in the scale produced from the CoC-1 water (data not shown). Given the fact that the actual APW sampled from Reliant Energy contained very little iron (< 1 mg/L), it is inferred that the iron-laden deposit came from the corrosion of mild steel coupons that were inserted for simultaneous corrosion studies in the same recirculating system. This was corroborated by the fact that the average corrosion rate of the mild steel was 105 MPY, which was more than 10 times greater than the corrosion rate observed in the concentrated APW (CoC 4). Three other corrosion-study coupons made of aluminum, copper, and copper-nickel were also present in the recirculating water but their corrosion rates were negligible compared to the mild steel. To remove the complications of mild steel corrosion on scaling determination, other experiments were performed with corrosion coupons removed from the system, unless stated otherwise (corrosion studies were continued using a separate recirculating system).

The significance of corrosion complications to scaling depends on the relative amounts of iron oxidized and released from the mild steel coupons to water. In the bench-scale recirculating system, the amounts of iron corroded and added to the recirculating water were significant in the relatively small volume of water used (i.e., 2-3 L of total water for each experiment). On the other hand, corrosion may not affect scaling as much in the field testing even when both corrosion and scaling coupons are used simultaneously, because the water volume contained in a cooling tower is much greater (e.g., 75 L in our pilot-scale cooling tower). Nevertheless, these findings are indicative in that scaling determination in industrial cooling systems should be

carefully executed to take into account the potential contributions of corrosion products to scale formation.

    Tests with synthetic APW. Based on the observation in the actual APW at CoC 1 vs. CoC 4 as discussed in the previous section, it was decided to use a synthetic APW water that truly simulated the chemical composition of the CoC-4 APW, in the study of APW scaling and its control by different antiscalants. The chemical composition of the synthetic APW used is listed in Table 5.2. The effectiveness of scaling control by PAA, PMA, and PBTC was examined first with individual tests of each agent (Figure 5.7). PAA was less effective than PMA, which was equally effective as PBTC. To further test the synergistic effect of polymer and phosphonate at a 2:1 dosing ratio, which is a widely adopted mix ratio in industrial practices for scaling control in cooling systems [9], PMA and PBTC dosed at 10 ppm and 5 ppm respectively were added to the synthetic ash pond water (CoC 4). It was observed that the addition of 5 ppm of PBTC to 10 ppm of PMA further improved the antiscaling effectiveness but not to a significant degree (the difference in the scale mass was less than 10%).
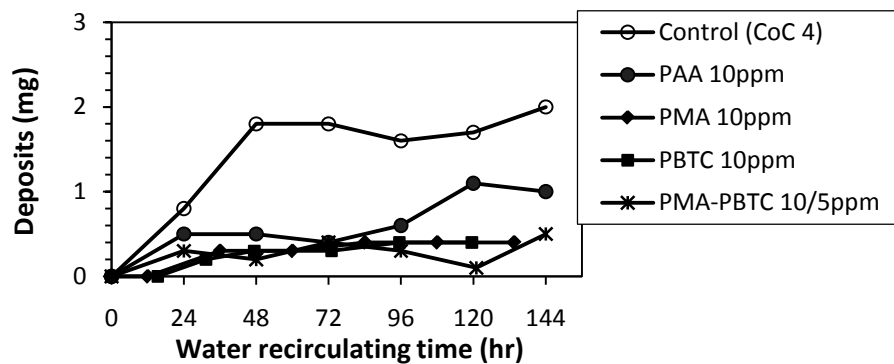
Figure 5.7 Scaling behavior of synthetic ash pond effluent in bench-scale tests: effectiveness of different antiscalants at CoC 4.

Table 5.2 Chemical composition of synthetic ash pond water effluent (representing 4 cycles of concentration)

Cation	Concentration		Anion	Concentration	
	mM	mg/L		mM	mg/L
Ca^{2+}	4.41	177	SO_4^{2-}	4.08	392
Mg^{2+}	1.63	39.6	HCO_3^-	5.12	312
Na^+	9.45	217	Cl^-	8.81	312
Fe^{3+}	0.28	15.6			

Note: The Fe concentration used in the synthetic water represents an average iron concentration level among different ash pond waters (e.g., Reliant Energy: 0.34 mg/L; TVA plants: 0.03-5.29 mg/L). Initial TDS = 449 (cations) + 1016 (anions) = 1465 mg/L. Ionic strength = 32.5 mM.

Changes in the aqueous concentrations of calcium and magnesium were monitored for each experiment with the synthetic ash pond water. The calcium concentration depleted faster and more significantly in the CoC 4 synthetic APW in the absence of any antiscalants than in the presence of PAA (Figure 5.8). In both cases, no substantial magnesium reduction was observed. Since Ca and Mg were the major cationic constituents of the APW synthetic water, it was concluded that calcium depletion in solution was the major contributor to the high level of scaling as depicted in Figure 5.7 ("control" curve). The connection between scale formation and calcium depletion was demonstrated in an experiment with the addition of PAA: the trend in calcium depletion is virtually mirrored in the observed increase in scale deposits in Figure 5.7 ("PAA 10ppm" curve). Ca depletion began to accelerate after 3-4 days of the experimental run, corresponding to the acceleration in scale formation after the same time period. Thereby, both curves pointed to a possible reduction in the effect of scaling inhibition by PAA after 3-4 days.
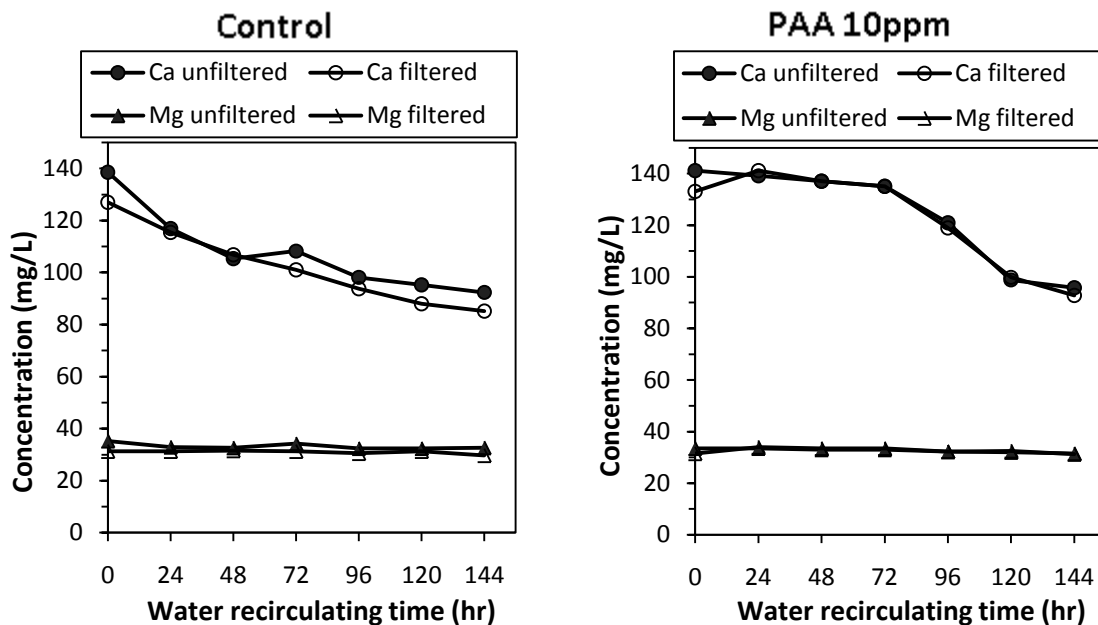
Figure 5.8 Changes in the aqueous concentrations of calcium and magnesium in the synthetic ash pond water in bench-scale tests.

Left: Calcium depletion in the absence of scaling control chemicals. Right: Calcium depletion with PAA treatment. Solid data points represent unfiltered samples while hollow points represent filtered.

Conversely, PMA and PBTC demonstrated a more sustained scaling inhibition capacity over the entire experimental run that lasted 6 days. Solution Ca remained essentially constant during both experiments (Figure 5.9). Figure 5.9 also suggests that PBTC was slightly better in retaining Ca in solution than PMA, although such distinction was not confirmed by the mass gain measurement shown in Figure 5.7.
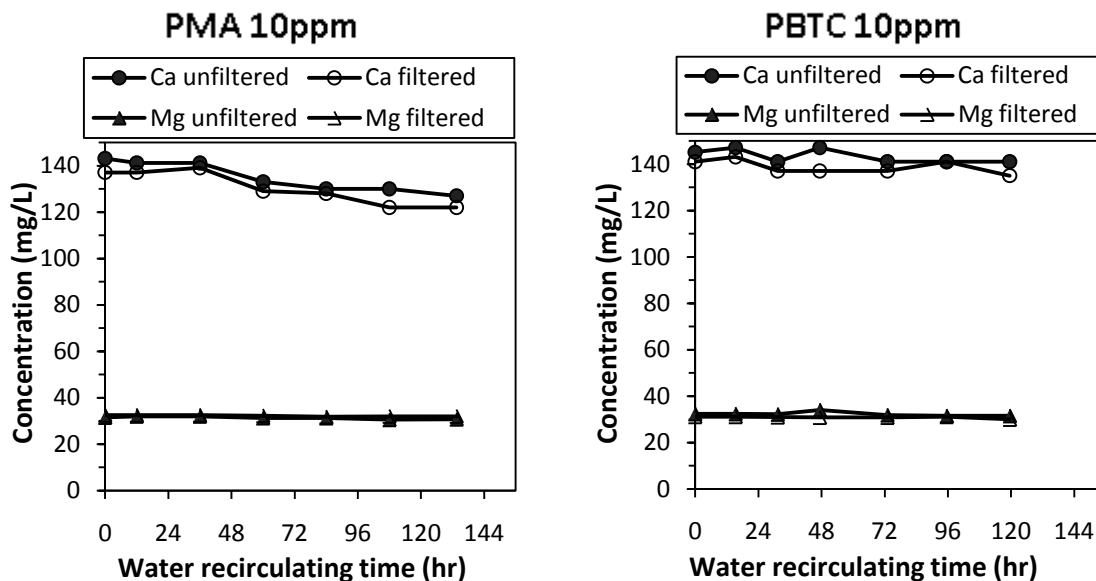
Figure 5.9 Aqueous concentrations of calcium and magnesium in the synthetic ash pond water with antiscaling control by PMA (left) or PBTC (right).

The scaling inhibition by the combination of antiscalants PMA and PBTC produced the most effective results. Ca was completely stabilized in solution over the entire experimental run of 6.5 d (Figure 5.10). Correspondingly, only limited amount of deposits was detected under these conditions (Figure 5.7). Changes in PMA concentration over time was shown in the right pane of Figure 5.10. Most of the polymer antiscalant remained in water over the duration of the experiment.
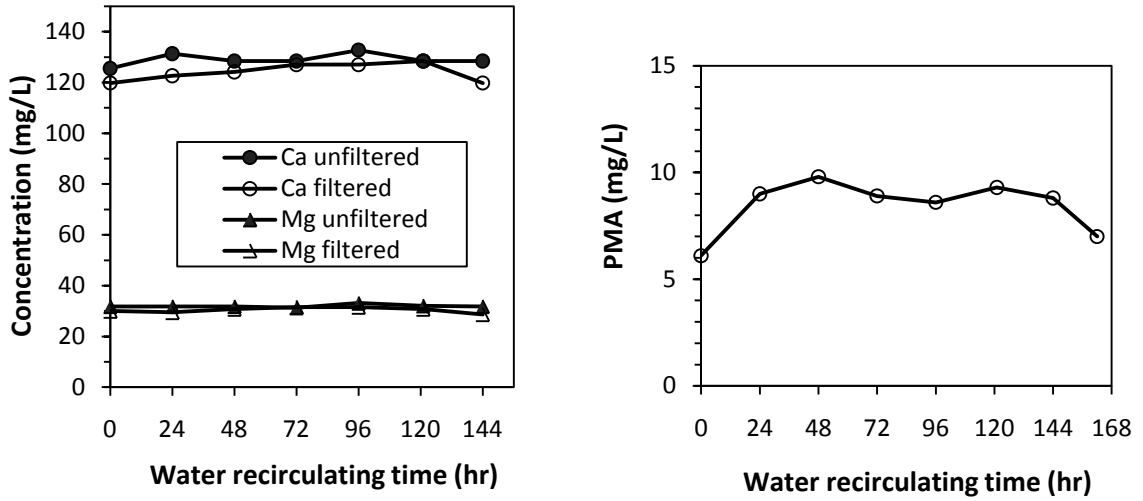
Figure 5.10 The stabilization of aqueous concentrations of calcium and magnesium in the synthetic ash pond water under scaling control by PMA-PBTC (left) is in agreement with the relatively constant PMA concentration in the water (right).

5.4   CONCLUSIONS

Use of synthetic ash pond water with well-controlled solution chemistry allowed testing of the effectiveness of scaling control by different antiscalants. The CoC 4 condition was achieved by preparing the solution chemistry according to the chemical composition listed in Table 5.2.

Both the MINEQL+ model calculations and the experimental results with the ash pond water showed that scaling in this impaired water is less of a problem than with the other two impaired waters previously studied in this project. The major constituents of the scaling solids were calcium minerals. Addition of 10 ppm of PMA or 10 ppm of PBTC proved to be very effective in further suppressing scaling to minimal levels. They both prevented calcium from forming deposits and their effectiveness lasted longer than that of PAA.

6.0   PREDICTING THE PH BEHAVIOR OF RECIRCULATING WATER IN COOLING TOWERS

Reliable prediction of the pH behavior in an open recirculating cooling water system is important for proper operation of the cooling system because the pH changes have significant impact on the scaling potential, corrosion propensity, and bioactivity in the cooling water. Although the water alkalinity is a key factor in pH estimation, existing semiempirical correlations based on the measurements of cooling water alkalinity prove to be not adequately accurate, especially for cooling systems using concentrated water of impaired quality as makeup. Chemical equilibrium modeling with the aid of MINEQL+ software was used to study the influence of solids formation on the cooling water pH, and to simulate CO_2 degassing and ammonia stripping in a recirculating cooling system using secondary-treated municipal wastewater (MWW). Comprehensive modeling was used to estimate the cooling water pH more reliably and was validated by experimental observations. Specifically, the initial sharp increase of water pH from about 7.2 to 8.3, as frequently observed in pilot-scale cooling tower tests using secondary-treated MWW, was well explained by a CO_2 degassing mechanism. A continued pH increase up to 8.7 with increasing cycles of concentration (CoC) was attributable to a combined effect of ammonia stripping and kinetically-limited carbonate precipitation. Both processes were successfully captured by MINEQL+ once relevant modeling conditions (CO_2 exchange, mineral phases, etc.) were adjusted properly. The modeling approach presented in this chapter greatly improves the

ability to forecast the cooling water pH at various CoC, even without knowing the recirculating water alkalinity *a priori*.

6.1 INTRODUCTION

Mineral scale formation, metal pipe corrosion, and biological fouling are major problems that are constantly encountered in industrial cooling systems. These problems can be quite costly and usually demand a great effort to control adequately. Proper management of cooling water systems is essential to maintaining cooling efficiency, stable system operation, and equipment longevity. Water pH is a master parameter that directly impacts mineral scaling, pipe corrosion, and biofouling. Widely used scaling and corrosion indices, such as Langelier, Ryznar, and Puckorius indices, are based on measured and/or calculated pH [1]. Bioactivity is heavily dependent on pH [2]. Understanding the pH behavior of cooling water, therefore, improves the accuracy of estimating the propensities for scaling, corrosion, and biofouling.

In an open recirculating cooling system, water is brought in contact with ambient air to achieve cooling through evaporative water loss. Consequently, the equilibration of CO_2 and other gaseous constituents between water and air is greatly enhanced. As a first approximation, when considering gas exchange reactions, pseudo-equilibrium conditions can be assumed when the cooling system is operated at steady state. On the other hand, mineral precipitation can be a slow process. Under typical operational conditions of recirculating cooling, complete precipitation equilibria may hardly be established.

There are a few empirical relations between water pH and carbonate alkalinity that ware developed based on observations of cooling systems operated using freshwater. With more and

more cooling systems embracing water reuse, non-traditional water sources, many of which are of impaired quality and have more complex chemical composition than freshwater, will become more commonly used [3, 4]. Currently, there is a general lack of knowledge about how the water pH behaves when an impaired water is fed into a cooling system.

The objective of this chapter was to examine the major water constituents that comprise the alkalinity of the water in an open recirculating cooling system using secondary-treated municipal wastewater as a model nontraditional cooling water source. Key operational conditions of the cooling system influencing water pH are discussed. This study presents a more reliable approach to predict the pH behavior of open cooling systems using secondary-treated municipal wastewater as makeup, by considering more thoroughly the factors that contribute to alkalinity as well as mineral solids formation. Ultimately, the proposed approach should be able to forecast the recirculating water pH under designed cycles of concentration (CoC), based on a few parameters of the makeup water quality.

6.2   MATERIALS AND METHODS

Modeling. Equilibrium modeling was performed using MINEQL+ [5, 6] (version 4.6). Temperature was set at 40 °C, which is typical of recirculating water temperature. For open system simulation, it was assumed that P_{CO_2} = -3.50. For closed system, total carbonate was specified based on the measured values of total alkalinity and the pH of makeup water. Non-ideality was considered by incorporating ionic strength corrections. Model calculations of water pH at different CoC were based on solution electroneutrality.

The chemical composition of the modeled municipal wastewater is provided in Table 6.1. Cooling system CoC was simulated by imposing different multipliers to the data in Table 6.1. For each CoC, a variety of modeling conditions were examined.

Table 6.1 Chemical constituents of the modeling water representing secondary-treated municipal wastewater used for equilibrium calculations

Constituent	Total concentration (mM)
Al	0.007
Ca	1.035
Cl	2.986
Fe	0.009
K	0.417
Mg	0.440
Mn	0.006
Na	4.096
NH_4	1.500
NO_3	0.257
PO_4	0.145
SiO_2	0.142
SO_4	0.895
Carbonates	4.040
Measured pH	*7.2*
Ionic Strength	*11.8*

Mineral Precipitation. The compositional analyses of mineral solids collected in pilot-scale cooling tower tests showed that the solids consisted of mainly calcium carbonate and phosphate minerals. Because magnesium was not detected at significant levels, it was assumed that removal of Mg by precipitation can be neglected (Chapter 3). Modeling took into account this limiting factor when evaluating the pH behavior of recirculating water, namely, only calcium carbonate and phosphate precipitation was allowed to take place when appropriate.

Experimentation. During pilot-scale testing, ammonia in the recirculating water had very low concentrations compared to its concentration in the makeup water. Specifically, more than 95% of the ammonia was removed from the recirculating water due to effective stripping. Modeling calculations evaluated the effect of ammonia on pH. To verify ammonia stripping, laboratory aeration tests were performed. Secondary-treated MWW was collected on 11/14/2009 and placed in a series of 1-L beaker reactors that were stirred at 200 RPM. Water temperature was either 23 °C (room temperature) or 40 °C. The water was aerated with fine bubbles of air created by a diffuser stone. Initial pH was 6.8 and ammonia concentration was 19 ppm as N.

Correlation of pH and Alkalinity. In most freshwaters, the acid-base chemistry is dictated by the open carbonate system because non-carbonate acid-base species are comparatively much less significant. The carbonate species are distributed according to the following mass action relationships:

$$CO_2(g) + H_2O = H_2CO_3^* = H^+ + HCO_3^- = 2H^+ + CO_3^{2-} \qquad K_H, K_{a1}, K_{a2} \qquad (1)$$

Or simply,

$$H_2CO_3^* = H^+ + HCO_3^- \qquad K_{a1} = 10^{-6.3} \qquad (2)$$
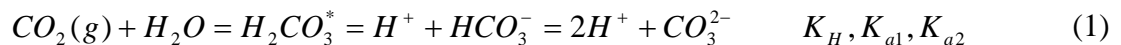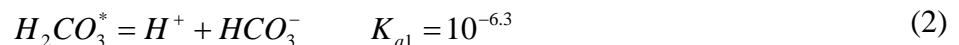
From Eq. (2), one can derive (assuming 25 °C and 1 atm):

$$pH = \log\left[HCO_3^-\right] + 11.3 \tag{3}$$

Under circumneutral pH conditions (pH 6-9), solution alkalinity (ALK) is mainly contributed by bicarbonate:

$$ALK \approx [HCO_3^-] \tag{4}$$

ALK is commonly expressed as mg $CaCO_3$/L. With this unit conversion, Eq. (3) can be written as:

$$pH = \log ALK + 6.6 \tag{5}$$

For fairly simple aqueous systems, Eq. (5) provides a simple equation of estimating pH from ALK, which is readily measurable. However, in actual cooling waters, the correlation between pH and alkalinity may deviate from Eq. (5) due to the existence of other species that can contribute to ALK, e.g., phosphates and organic matter. A more general form to account for complex ALK is used in Eq. (6):

$$pH = a \log ALK + b \tag{6}$$

where the fitting parameters a and b can be determined by least-square linear regression of collected experimental data. A number of empirical values of the fitting parameters have been reported to describe the relationship between pH and ALK in cooling systems [7-9]. They are summarized in Table 6.2.

In a simple carbonate system, ALK can be approximated to bicarbonate concentration with reasonable accuracy. With systems of more complex chemistry, however, a more complete description of ALK should include other species, as listed in Eq. (7).

ALK = OH − H + HCO$_3$ + 2CO$_3$

$$+ HPO_4 + 2PO_4 - H_3PO_4 + NH_3 + HSiO_3 + 2SiO_3 + CaOH + CaHCO_3 + 2NaCO_3 \tag{7}$$

Eq. (7) indicates that phosphates, ammonia, silicates, and calcium complexes can all potentially contribute to ALK.

Table 6.2 The coefficients of Eq. (6) used in empirical relations for pH prediction from alkalinity

Empirical Relation	*a*	*b*	Ref
Puckorius relation	1.47	4.54	[7]
Watertext relation	1.72	4.13	[8]
Kunz relation	1.6	4.4	[9]

CO$_2$ Oversaturation in Makeup Water. In an open carbonate system, carbonate species, besides CO$_2$(g), exist as either dissolved species or carbonate solids. Total dissolved carbonates is expressed as Total Inorganic Carbon (TIC), whose equilibrium values at a given pH can be calculated according to Eq. (1). When the measured TIC is greater than the calculated value, either CO$_2$ degassing or carbonate precipitation will take place to bring the system to equilibrium.

6.3 RESULTS AND DISCUSSION

CO$_2$ Degassing. Based on the information about the chemical composition of the MWW in Table 6.1 and without considering potential exchange with gas phase and solid formation (i.e., a closed system without precipitation), that the water pH predicted by MINEQL+ was 7.2, which was identical to the value measured for actual MWW. Under this "initial" condition, the total carbonates were 4.04 mM (Table 6.3). When the system was allowed to exchange with gas phase

and to form precipitates (i.e., an open system with precipitation), MINEQL+ calculation shows that the water pH would increase to 8.5. This pH increase would be accompanied by the formation of calcite and dolomite, which are two most stable calcium (and magnesium) carbonate crystalline forms. The concentration of total carbonates decreased to 1.42 mM. If there was no $CO_2(g)$ exchange between air and water, the precipitates would account for the difference, which is 2.62 mM. However, the total precipitated carbonate (CO_3^{2-}) associated with the solids was only 0.94 mM. The only possibility for the imbalance is CO_2 degassing where a total of 1.68 mM CO_2 was released to the air when the system was allowed to equilibrate with atmosphere. As shown in Eq. (8), CO_2 degassing resulted from HCO_3^- taking up H^+, and consequently, the water pH increased from 7.2 to about 8.5 due to decrease in H^+ concentration.

Table 6.3 Carbonate speciation at initial (closed system) and equilibrium stages (MINEQL+ modeling of MWW CoC 1). Unit: mM

	pH	CO_3^{2-}	$CaHCO_3^+$	H_2CO_3	HCO_3^-	Ct	Calcite	Dolomite	$CO_2(g)$
Initial (closed)	7.2	0	0.04	0.59	3.39	4.04	-	-	0
Equil. (open)	8.5	0.04	0	0.01	1.36	1.42	0.24	0.35	1.68

Should the precipitation not take place, the pH increase entirely due to CO_2 degassing would be even higher (modeling calculation under this scenario indicates a pH of 8.8). Indeed, carbonate precipitation consumes alkalinity, which leads to a decrease of pH, as indicated by Eq. (8):

$$Ca^{2+} + 2HCO_3^- = CaCO_3(s) + H_2O + CO_2(g) \tag{8}$$

Comparing the pH changes in the opposite direction as initiated by Eq. (1) vs. Eq. (8), one can see that the CO_2 degassing process effected pH more profoundly than precipitation reactions. The result was a net increase in pH (Figure 6.1).
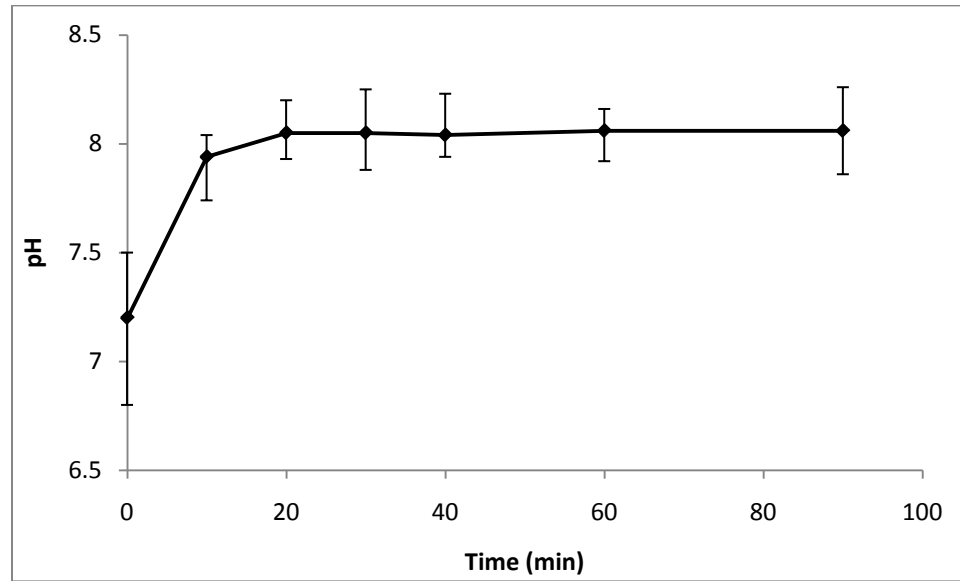
Figure 6.1 pH increase due to CO_2 degassing by aeration experiment using secondary-treated MWW. Error bars indicate the measurement ranges.

Ammonia Stripping. Similar to carbonate precipitation, NH_3 stripping also consumes alkalinity and thus lowers the pH. Because NH_4^+ is the dominant ammonia form in the pH range of interest (i.e., pH 6-9), it will react with HCO_3^- to produce both $NH_3(g)$ and $CO_2(g)$, as shown in Eq. (9).

$$NH_4^+ + HCO_3^- = NH_3(g) + H_2O + CO_2(g) \tag{9}$$

In pilot-scale cooling tower tests, it was found that NH_4^+ was largely removed from cooling water. This observation is confirmed in lab aeration experiments, where ammonia was effectively stripped out when water pH was above 8 and temperature was raised to 40 °C from

about 23 ℃ (room temperature) (Figure 6.2). Note that the 20 ppm of ammonia initially present in MWW could potentially contribute to 1.43 mM alkalinity should all the ammonia be present as NH_3. (However, ammonia does not contribute to M-Alk., or commonly referred as the total Alk.).
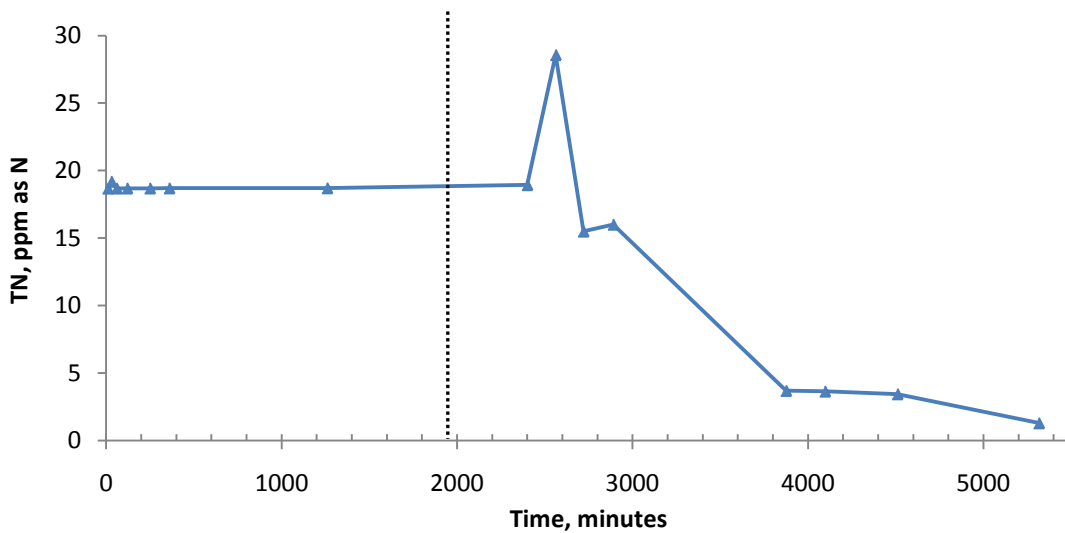
Figure 6.2 Total ammonia concentration in secondary MWW in beaker stripping test in the lab. Water temperature was raised from 23 to 40°C at 2500 min.

pH as a Function of ALK. The correlation between pH and ALK described by Eq. (5), which is *calculated* based on carbonate alkalinity, as well as three empirical relations are shown in Table 6.2 and depicted in Figure 6.3. MINEQL+ modeling results were based on the six possible conditions that may be correlated when the system is "open to atmosphere" (Figure 6.4). Although none of the equations captured our pilot-scale data accurately, they provided reasonable boundaries for the field data. It is important to note that the MINEQL+ modeling data for MWW match Eq. (5) exceptionally well, indicating that the pH-ALK relationship in MWW

can be well described by Eq. (5) under open equilibrium conditions and that ALK is primarily contributed by bicarbonate.
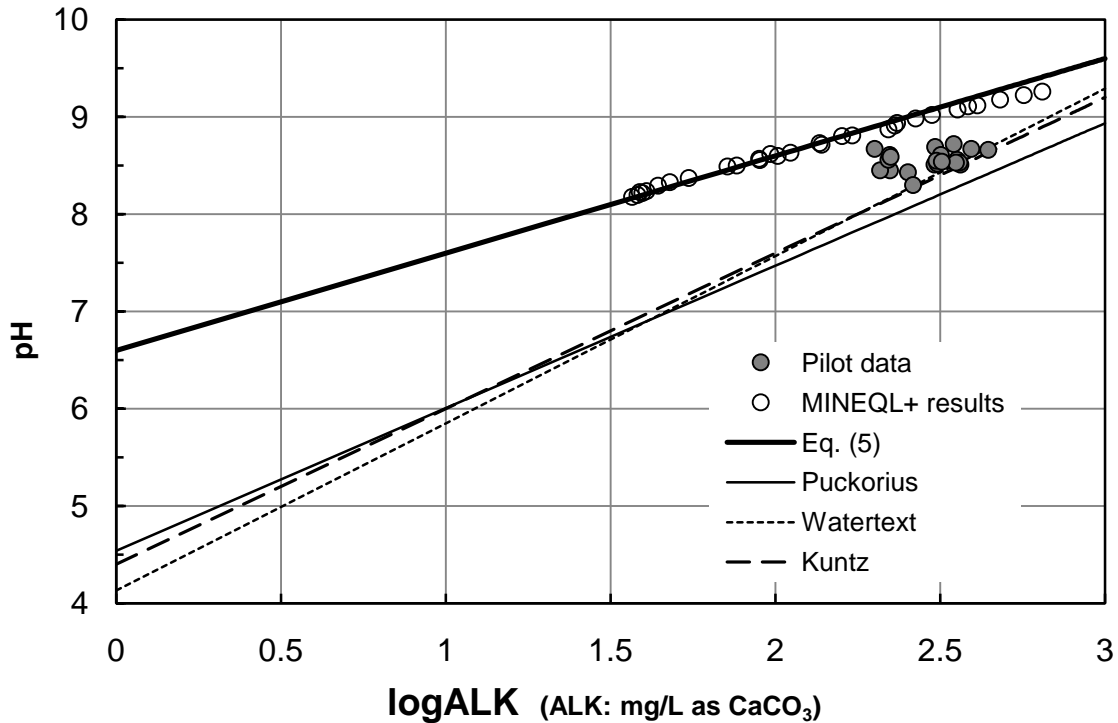
Figure 6.3 Correlation between pH and ALK. The open circles are modeling results of open equilibrium conditions. The conditions included: solid precipitation vs. no solid precipitation; only calcite and hydroxylapatite formation; as well as with or without NH_3 species. The solid circles are field testing results of pH and ALK.

It is clear from Figure 6.3 that the actual ALK in cooling water of high CoC should not be simply the product of makeup ALK and CoC. In actual field testing, the ALK may be contributed not only by soluble ALK but by other substances as well, such as organic matter and carbonates that are embedded in particulate matter and microbial cell membranes. Moreover, alkalinity can be consumed by precipitation reactions. Thus, for secondary-treated MWW as

cooling water of complex water chemistry and operational conditions, the real bicarbonate concentration was lower than the measured ALK. In other words, the ALK used in the empirical relations may be very likely over estimated. One probable way to correct the overestimation is to use bicarbonate concentrations as ALK. In doing so the solid circles should shift to the left hand side and be closer to the straight line representing Eq. (5).

pH Prediction Based on More Complete Consideration. The behavior of water pH at different CoC for eight modeling conditions described in Figure 6.4 is shown in Figure 6.5. Open to the atmosphere and close to the atmosphere conditions resulted in significantly different pH levels. In an open cooling system, the actual condition is closer to open to the atmosphere rather than closed, except for very low cycles of concentration when CO_2 degassing is not of significant influence. Thus, the modeling results for CoC 1 (or makeup water) are better approximated by the closed condition while higher CoCs are more likely approaching an open condition.
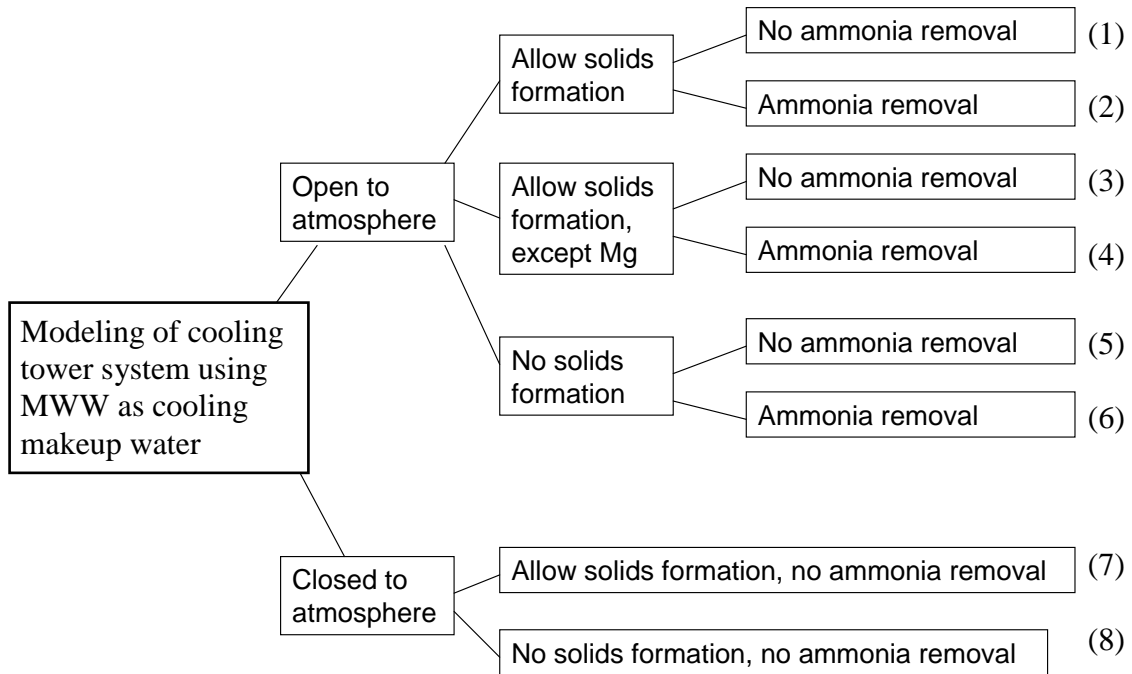
Figure 6.4 MINEQL+ modeling conditions for MWW used as cooling system makeup.

Each condition was examined for CoC 1-6 at 40°C.
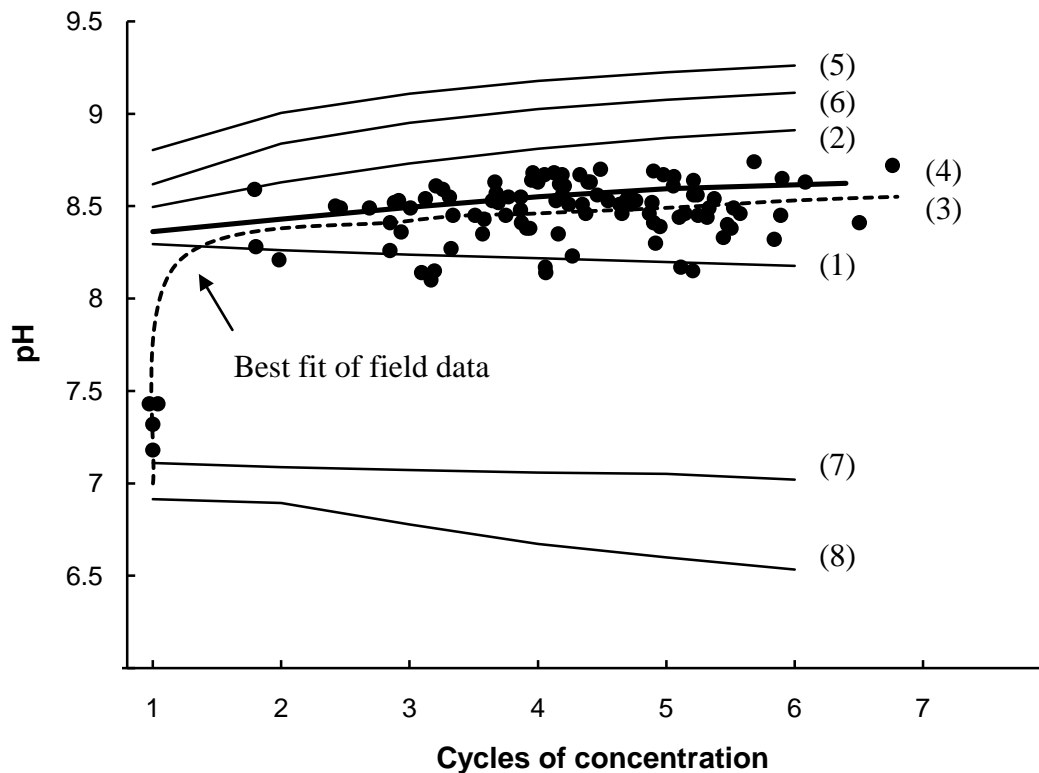
Figure 6.5 Modeling of pH as a function of CoC under different operational conditions.

The dashed line represent a best fit of the experimental data by the least square second order polynomial.

Based on the experimental evidence from both laboratory and field studies, magnesium was stable in the cooling water and the mineral scales were mainly calcium carbonates and phosphates. Also, ammonia had very low concentration (around 98% removal) in the cooling water. As such, the scenario (4) from Figure 6.4 (i.e., "Open, solids, no NH_3, no Mg") should be the most representative modeling condition. Indeed, the results of Figure 6.5 for this scenario fit the field data well, especially at CoC > 2.

For the field data depicted in Figure 6.5, the CoC was determined by the ratio of the specific conductivity of cooling water and makeup water. During field testing, the CoC was determined

116

on daily basis and the targeted CoC was 4. The true CoC should be determined by makeup to blowdown flow ratio. However, since makeup and blowdown flow were not continuous, the exact CoC was difficult to determine at the exact time when pH measurement took place. The conductivity of both makeup and recirculating water was measured at the same time when pH was measured and should thus be more representative.

Figure 6.5 implies that by carefully considering the influence of solid formation and ammonia stripping, the pH of cooling water at various CoC can be estimated with precision using water chemistry equilibrium model such as MINEQL+.

6.4   CONCLUSIONS

The pH behavior of recirculating water in open cooling systems using impaired waters, such as treated municipal wastewater, is not easily predicted by existing simple empirical equations because those equations were established based on data obtained from systems using freshwater as cooling makeup. Carbonate alkalinity, which requires accurate measurements in the recirculating water, is a critical parameter in those pH estimation equations. Unfortunately, alkalinity determination can be extremely difficult in practice, especially with open cooling water systems where a variety of parameters can be ever changing. A more comprehensive modeling approach, as described in this paper, considers the degassing effect due to cooling tower aeration and the solids formation due to the concentration effect of recirculating cooling. This approach is demonstrated to be capable of estimating the cooling water pH behavior more accurately and robust. Using this approach, one can predict the pH changes after the water is recirculated in an open cooling system operated at various CoC, with just the limited knowledge

117

of makeup water quality. This modeling approximation does not need to measure the alkalinity of the recirculating water.

7.0   INSIGHTS INTO MECHANISMS OF MINERAL SCALING INHIBITION BY POLYMALEIC ACID (PMA)

The occurrence of inorganic mineral deposition (scaling) is ubiquitous in water-based industrial processes. It causes system problems, particularly in evaporators, heat exchangers, and membrane desalinators, and can significantly increase operating costs. Research on developing antiscaling chemicals (antiscalants) has been focused on manipulating the water chemistry, most notably raising the solubilities of the precipitating minerals or chemically interrupting mineral crystallization processes to stabilize the mineral suspension and prevent solids formation. Up to date, the assessment of the antiscaling effectiveness of various polymer antiscalants is largely based on empirical tests at either bench or field scale, and lacks theoretically sound systematic investigation. In this study, the antiscaling mechanisms of polymaleic acid (PMA), which had been used in this study for scaling control in different impaired waters, was systematically evaluated using both analytical methods based on bulk solution chemistry and complimentary characterization of the mineral solids formed in solution. It was identified that the antiscaling mechanisms of PMA on mineral precipitation in bulk liquid was fundamentally different from that on mineral deposition on substrate surface. With regard to mineral precipitation in the bulk, PMA delayed the initiation of the mineral precipitation even at very low dosing (< 1 ppm). And at high doses (> 5-10 ppm) PMA completely eliminated the "fast precipitation" phase in the bulk. Also, the precipitation rates were significantly reduced in the presence of PMA. Analysis

119

on the precipitates indicated that magnesium exhibited stronger associations with PMA molecules than calcium, resulting in its incorporation in the amorphous solids. With regard to surface deposition, PMA worked well to prevent deposition of *pre-formed* (existing) suspended mineral solids. Surface adsorption of PMA onto suspended mineral particles increased the negative charges of the solids and rendered them less favorable for deposition onto negatively charged stainless steel surfaces. On the other hand, if the suspended solids were not preformed, PMA tended to incorporate into the mineral particles during the precipitation process to significantly alter the particle morphologies and surface charge distributions to a point that PMA lost much of its effect on deposition mitigation. The finding has significant implications in scaling control practices in that the protocol for PMA addition should be carefully evaluated. Under conditions when mineral precipitation takes place in the bulk, PMA should be better added after the fast precipitation took place to avoid the formation of PMA-incorporated mineral particles.

7.1   INTRODUCTION

Inhibition of mineral scale formation is important in water-based industrial processes because mineral scaling on equipment surfaces incurs significant removal costs [1, 2]. Typical water-based industrial processes where mineral scaling is of primary concern include cooling towers, evaporators, heat exchangers, membrane desalinators, and drinking water distribution networks. Scale inhibition can be achieved through the addition of chemical compounds known as inhibitors or antiscalants. To understand how scale inhibitors work, a detailed assessment of the fundamental processes involved in mineral precipitation and deposition is necessary. As

schematically shown in Figure 7.1, the mineral ions under supersaturation conditions in solution gather through random thermal motion to form clusters. These clusters constantly sample for different configurations until reaching a critical size beyond which nucleation takes place. Once the embryos become nuclei, crystallization proceeds spontaneously to form larger particles. Depending on the surface properties of these particles, they can either stay suspended for long time or aggregate to form even larger particles. Eventually, these particles, as well as the mineral ions, diffuse through the hydraulic boundary layer, and deposit on a solid surface to form scale. To inhibit, or to at least mitigate surface scaling, a chemical added to the suspension needs to disrupt at least one of the processes, and it would be more effective if the disruption occurs in multiple steps.
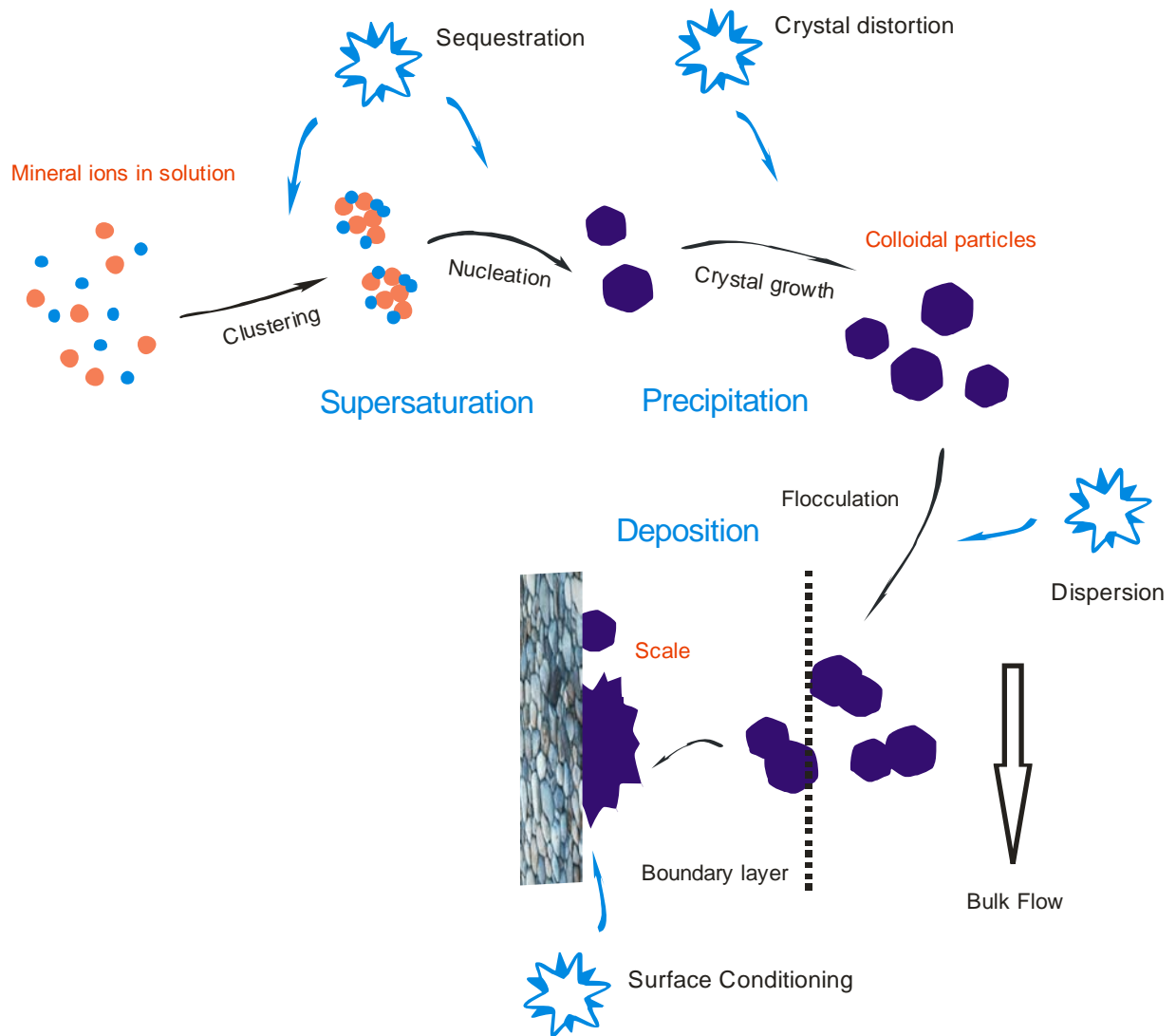
Figure 7.1 Simplified schematic of the physical chemical processes of mineral scaling and scaling control by chemical additives.

An added antiscaling chemical can prevent scaling in various ways. The chemical can work to sequester or complex with scale forming cationic species, thereby raising the operational solubilities of the mineral ions and impeding the processes of clustering and nucleation. The chemical can work as a crystal modifier to alter the crystallization pathways and cease the growth of mineral particles. The chemical can work as a dispersant by providing an electronic and/or steric repellency between the mineral particles, and keeping them from flocculation and aggregation. Finally, the chemical can also work as a surface conditioner to render the surface unfavorable for scale formation. A good inhibitor chemical should work through multiple mechanisms to prevent scaling.

The objective of this chapter is to elucidate the antiscaling mechanisms of polymaleic acid (PMA), which has been used in previous chapters and proved to be effective in mitigating scaling of several impaired waters. The effect of PMA on mineral precipitation in bulk solution and on mineral particle deposition on solid surfaces was examined independently to obtain insights into potentially different mitigation mechanisms of PMA on precipitation and deposition. The influence of PMA on mineral particles was investigated using both pre-formed particles in the absence of PMA and particles formed in the presence of PMA.

7.2   THEORETICAL BACKGROUND

7.2.1   Nucleation

Under supersaturated conditions, mineral ions constantly sample for different configurations for mineral solid formation [3-7]. This random clustering of ions arising from their ionic thermal motion is easily reversible, i.e., the clusters are in a constant state of formation, break-up, and disappearance. The mineral clusters can consist of a broad size range, from dimers, trimers, etc., all the way to i-mers (i > 100, in terms of the number of ions), until a cluster reaches a critical number j, at which state the addition of an extra monomer leads to nucleation. Before the cluster reaches the critical number or critical size, the energy barrier is high, i.e., the cost to create a nano-sized particle of high specific surface area overwhelms the benefit of energy gain through ionic bonding. Nucleation refers to the formation of new clustering centers from which spontaneous crystal growth can proceed (i.e., energy gain from bonding overtakes energy cost for creating the additional surface area). The nucleation process determines the size and size distribution of the crystals produced. Subsequently, monomers (ions) are deposited on these nuclei, and crystallites are being formed.

At the very beginning of nuclei formation, the crystals are sufficiently small (1-10 nm in dimension), and quantum-mechanical effects may alter various physical and chemical properties, and complicate the classical treatment of nucleation and crystallization theories. Nevertheless, a brief review of the classical nucleation theory is given below.

The free energy of formation of a nucleus corresponding to the critical j-mer, consists essentially of the energy gained from making bonds (volume-based free energy) and of the work required to create the nucleus surface [8]:

$$\Delta G_j = \Delta G_{bulk} + \Delta G_{surf} \tag{1}$$

For a nucleus, the bulk energy gain, which is always negative for a supersaturated solution, can be expressed as

$$\Delta G_{bulk} = -jkT \ln S \tag{2}$$

where, j is the number of ionic units (monomers) in the nucleus. When expressed in terms of volume for a spherical nucleus having radius r and ionic volume V_{ion} (m^3), j takes the following form:

$$j = \frac{4\pi r^3 / 3}{V_{ion}} \tag{3}$$

S is the saturation ratio:

$$S = \left(\frac{IAP}{K_{SP}}\right)^{1/n} \tag{4}$$

where, IAP stands for ionic activity product, K_{SP} is solubility product, n is the number of ions in the formula unit of a mineral $A_x B_y$ (i.e., $n = x + y$). Because of the normalization by n, the saturation ratio is independent of the way the formula is written, e.g., $Ca_5(PO_4)_3OH$ or $Ca_{10}(PO_4)_6(OH)_2$.

The energy cost of surface formation can be expressed in terms of the specific interfacial energy or surface tension γ (mJ/m^2), which is assumed to be independent of nucleus size, and a spherical surface area:

$$\Delta G_{surf} = 4\pi r^2 \gamma \tag{5}$$

Hence, the nucleation energy of a spherical crystal can be written as:

$$\Delta G_j = -\frac{4\pi r^3 / 3}{n V_{ion}} kT \ln \left(\frac{IAP}{K_{SP}}\right) + 4\pi r^2 \gamma = f(T, S, r) \tag{6}$$

Table 7.1 Critical cluster formation and associated energy barrier

($V_{ion} = 3 \times 10^{-29} \, m^3$ corresponding to a spherical ion of radius 1.9 Å; T = 25°C; γ = 100 mJ/m²)

S (supersaturation)	4	5	7.5	10	15	20	25	50	100
ΔG_j^* ($10^{-20}J$)	46.4	34.4	21.9	16.8	12.2	9.9	8.6	5.8	4.2
r_j^* (Å)	10.5	9.2	7.3	6.4	5.4	4.9	4.5	3.8	3.2
j^* (#)	162	107	53	36	22	16	13	7	4

It can be seen that the nucleation energy is a function of temperature, saturation ratio, and the nucleus size. Table 7.1 calculated the nucleation energy and the critical size for nucleation as a function of the saturation ratio. In Figure 7.2, ΔG_j is plotted as a function of r (or equivalently, of j) for a series of saturation ratio S values. Obviously, spontaneous nucleation would proceed only when the solution is supersaturated and the size of ion clusters is large enough to overcome the activation energy barrier. Increasing the saturation ratio will not only lower the energy barrier, but also shorten the time needed for spontaneous nucleation by reducing the critical cluster size. From the right pane graphs, it appears that S = 10-20 is needed for favorable and quick nucleation. Also note that the curve for S = 1 depicts the energy cost to create the crystal surface because there is no bulk free energy gain under this equilibrium condition. When $S > 1$, with increasing cluster size the bulk energy gain, which increases with r^3, outweighs the surface energy cost, which increases with r^2. The energy cost for large crystals becomes negligible, and continued crystal growth may only be hindered by other barriers, such as a decrease in S or in ionic diffusion, or an increase in hydraulic shear exerted on the crystals. All of these mechanisms are utilized to a varied extent by antiscaling chemicals added to a supersaturated mineral solution.
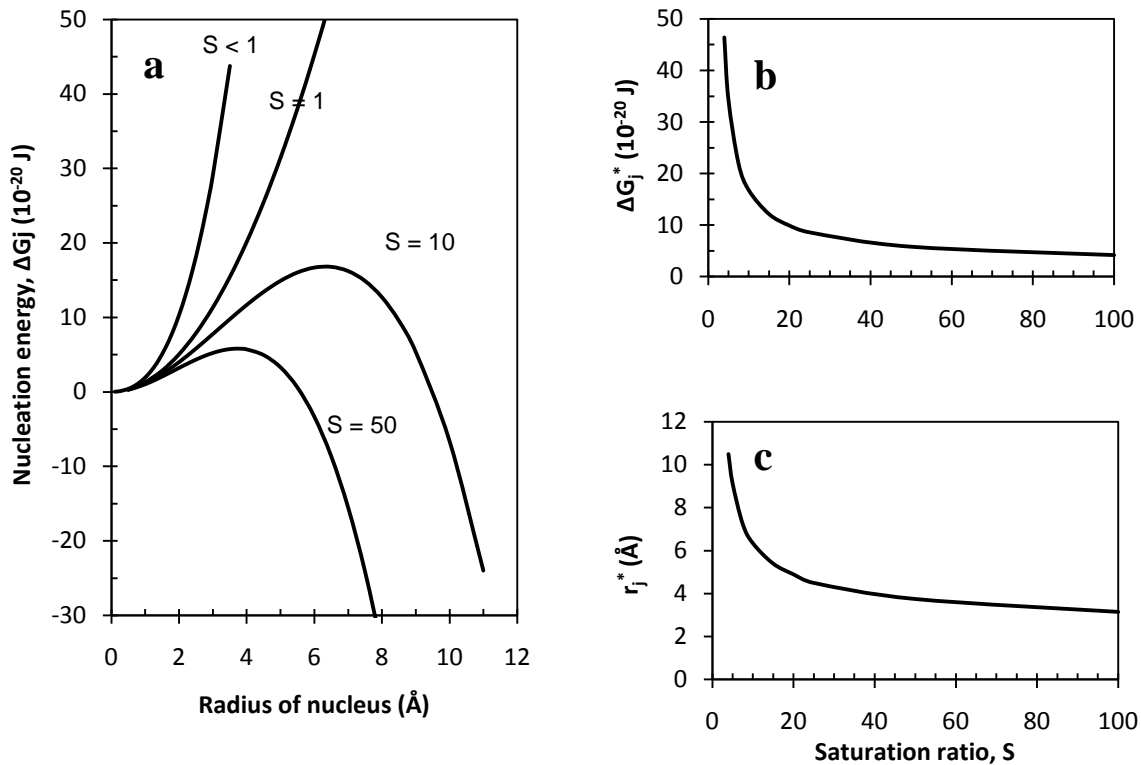
Figure 7.2 Energetics of mineral nucleation.

The energy barrier and the critical size of nucleus depend on the supersaturation (S). a) Free energy of formation of a spherical nucleus as a function of its size, calculated for different saturation ratios. The height of the energy maximum, ΔG_j^*, is the activation barrier to the nucleation process at a saturation level specified by S. b) The activation energy decreases with increasing supersaturation. c) The size of critical nucleus also decreases with increasing supersaturation. The curves were calculated based on the following assumptions: $V_{ion} = 3 \times 10^{-29} m^3$ (corresponding to a spherical ion of radius 1.9 Å); T = 25°C; γ = 100 mJ/m².

To get a better sense of the newly-formed nucleus size, one can ask the question, how many ions have to be incorporated in a cluster before reaching a critical size. When S = 10 for instance, $r_j^* = 6.35$ Å, it is estimated that j = 36. For S = 20, $r_j^* = 4.9$ Å, and j = 16. A list of these parameters is also provided in Table 7.1.

The temperature effect on nucleation is reflected by the kT term, assuming that the surface energy is independent of temperature. Increasing temperature renders nucleation more favorable. For example, at $S = 10$, increasing temperature from 25°C to 40°C leads to a 9% lowering of the energy barrier and 8% reduction in the critical cluster radius.

7.2.2 Nucleation kinetics

Several chemical affinity-based rate models have been developed to describe the nucleation kinetics in terms of free energy changes, ΔG. Two basic types of rate laws are widely used: linear and nonlinear rate laws with respect to ΔG. The linear rate laws have the following general form [9]:

$$r = k_f \left[e^{\frac{n\Delta G}{RT}} - 1 \right] \tag{7}$$

where r is in mole/(time · area), k_f is the nucleation rate constant, R is the ideal gas constant, T is absolute temperature. The parameter n is a constant and has been assumed to contain information about the growth mechanism, e.g., $n = 1$ is indicative of surface adsorption-controlled growth.

The nonlinear rate laws are generally expressed as:

$$r = k_f \left[e^{\frac{\Delta G}{RT}} - 1 \right]^n \tag{8}$$

In both of the rate law expressions, the physical meanings of the parameters are the same. Theoretical models have been used to argue that $n = 2$ (second order) describes growth at screw dislocations on the crystal surface with a spiral mechanism while higher orders can be applied to growth at both screw and edge dislocations.

7.2.3 Nonspherical crystal geometry

For a nonspherical crystal, its surface area can be expressed as

$$A = \alpha \left(\frac{V_M}{nN_A}\right)^{2/3} j^{2/3} \tag{9}$$

where, V_M is the molar volume of the solid phase (volume occupied by one mole of formula units in the solid, $V_M = nV_{ion}N_A$), α is a geometric factor that depends on the shape of the crystal, e.g., for a sphere $\alpha = \sqrt[3]{36\pi} = 4.84$ [8].

The mean ionic radius (typically 1-2 Å) can be written as:

$$r_{ion} = 0.5 \left(\frac{V_M}{nN_A}\right)^{1/3} \tag{10}$$

where the molar volumes are available in CRC Handbook of Chemistry and Physics.

Using this expression, the surface energy term can be written in a more general form:

$$\Delta G_{surf} = \alpha \left(4 \, r_{ion}^2 \, j^{2/3}\right) \gamma \tag{11}$$

7.2.4 Interfacial energy: homogeneous nucleation vs. heterogeneous nucleation

For homogeneous nucleation as discussed above, the interface is between water (W) and a mineral cluster (C):

$$\gamma = \gamma_{CW} \tag{12}$$

Empirical relations exist for a given type of crystals (oxides, sulfates, carbonates, etc.). As a rule of thumb, high γ_{CW} corresponds to low solubility: the mineral particles prefer self-interaction among themselves over interaction with water due to higher energy cost to do the latter. One empirical relationship states [10]:

$$\frac{4\,r_{ion}^2}{kT}\gamma_{CW} = 4.7 - 0.272\ln C_{sat} \tag{13}$$

where C_{sat} is the molar concentration of mineral formula unit in solution at solubility limit (e.g.,

max moles of $CaCO_3$ unit per liter of solution in equilibrium with solid $CaCO_3$); r_{ion} is the mean

ionic radius (in m); and the unit of γ_{CW} is J/m^2. Table 7.2 provides a list of interfacial energies

for common minerals, the solubilities (values were calculated for pH = 7 for oxides and

hydroxides), and values for the mean ionic radius. It should be noted that calculated surface

energies for solids will never serve as more than a guide as to what expect experimentally.

Different preparations of the same substance and widely different experimental methods and

conditions may yield different observations.

In the case of heterogeneous nucleation, γ needs some redefinition because the nucleus is

now formed in part in contact with the solution and in part in contact with the surface of a solid

substrate (S):

$$\Delta G_{surf} = \gamma_{CW}A_{CW} + (\gamma_{CS} - \gamma_{SW})A_{CS} \tag{14}$$

In the case of promoting heterogeneous nucleation, the substrate operates as such that its

interaction with the mineral is energetically favorable (i.e., small, even negative γ_{CS}) and its

interaction with water is no better, or worse than the interaction of minerals with water: $\gamma_{CW} \approx$

γ_{SW}. Under these conditions,

$$\Delta G_{surf} \approx \gamma_{CW}(A_{CW} - A_{CS}) \tag{15}$$

Table 7.2 Surface free energies of minerals

Mineral	Formula	γ_{CW} (mJ/m^2)	C_{sat} (M)	r_{ion} (Å)	Ref
Calcite	$CaCO_3$	94	6×10^{-5}	1.56	Christoffersen et al. (1988)
Witherite	$BaCO_3$	115	1×10^{-4}	1.68	Nielsen and Sohnel (1971)
Gypsum	$CaSO_4 \cdot 2H_2O$	26	1.5×10^{-2}	1.57	Chiang et al. (1988)
Barite	$BaSO_4$	135	1×10^{-5}	1.76	Nielsen and Sohnel (1971)
F-apatite	$Ca_5(PO_4)_3F$	289	6×10^{-9}	1.54	Van Cappellen (1991)
Hydroxyapatite	$Ca_5(PO_4)_3OH$	87	7×10^{-6}	1.54	Arends et al. (1987)
OCPp	$Ca_5(PO_4)_3 \cdot H_2O$	26	2×10^{-4}	1.58	Van Cappellen (1991)
Portlandite	$Ca(OH)_2$	66	6×10^{-5}	1.32	Nielsen and Sohnel (1971)
Brucite	$Mg(OH)_2$	123	1.5×10^{-4}	1.19	Nielsen and Sohnel (1971)
Gibbsite (001)	$Al(OH)_3$	140	7×10^{-8}	1.18	Smith and Hem (1972)
Quartz	SiO_2	350	1×10^{-4}	1.16	Parks (1984)
Amorph. Silica	SiO_2	46	2×10^{-3}	1.16	Alexander et al. (1954)
Kaolinite	$AI_2Si_2O_5(OH)_4$	200	1×10^{-6}	1.17	Steefel and Van Cappellen (1990)

OCPp = Octacalcium phosphate (subscript p = precursor).

7.2.5 Nucleation inhibition

Many organic molecules were reported to display an ability to retard or totally inhibit mineral precipitation from solution when present at very low (ppm) concentrations [10]. Although the precise mechanism of precipitation inhibition is not clearly understood at this time, it is known that in supersaturated solutions of sparingly soluble salts, a significant delay in crystal nucleation

and subsequent growth is observed in response to chemical treatment [11]. This delay is referred to as the "induction time" of the system, which occurs at remarkably low "threshold dosages" of the chemicals added, usually in the order of 1-10 ppm. The scale inhibition capability of antiscaling chemicals is related to chemical structure, molecular weight, active functional groups and solution pH, parameters that have been studied in depth by several investigators [12-15]. In all cases, the effect of precipitation retardation by antiscaling chemicals is equivalent to a reduction in the supersaturation level of the mineral solution.

7.2.6   Inhibition of crystal growth

Broadly speaking, crystal growth inhibition can be achieved through particle stabilization [16]. The stability of mineral colloids can be achieved by maintaining or even increasing interparticle repulsive forces such as electrostatic (charge-based) and steric forces. Surface charging of mineral particles commonly arises from nonspecific ionic adsorption.

Charge stability can be semi-quantitatively measured by the zeta potential of the charged particles. Measured zeta potentials exceeding ±20 mV is regarded to be indicative of good stability whereas within ±10 mV is deemed unstable. With very weak surface potentials, coagulation quickly leads to the formation of bigger particles.

Theoretically, charge stability can be described by the classical DLVO theory that takes into account both electrostatic repulsion and van der Waals attraction [8]. Solution chemistry plays a critical role in the DLVO interactions, with the most important parameters being pH, counter ion concentrations, and solution ionic strength. Near the pH values corresponding to a zero zeta potential (i.e., pH_{iep} or pH_{pzc}), the electrostatic repulsive forces diminish. It is therefore

important to have the knowledge about the specific pH_{pzc} of the aqueous system in order to keep the suspension stable. Practically, it is important to specify the solution pH.

The pH_{pzc} can be determined by potentiometric titration technique, in which HCl or NaOH solution is added to the suspension and resulting pH is recorded. From the titration curve usually two pK values can be identified corresponding to the dissociation of the acid and base functional groups, and the pH_{pzc} is calculated by the following equation:

$$pH_{pzc} = \frac{pK_1 + pK_2}{2} \tag{16}$$

The steric effects between suspended particles are not captured by the DLVO description and the steric forces constitute an important part of non-DLVO interactions, among which the hydration force is most commonly encountered in aqueous suspension. A surface having ions or other surface groups that interact very strongly with water will have a net repulsion with another likely-configured surface due to the energetic cost of removing the bound water layers (opposite to the hydrophobic force that arises from an energetic gain in removing water layers from between two surfaces that repel water in nature). The hydration potential can be superimposed on the DLVO potential. The repulsive hydration force is generally exponential in form with a decay length of 1-2 nm attributed to the adsorption of hydrated ions to the mineral surface. While there is little doubt that the presence of a solid surface significantly perturbs the structure of the water adjacent to the surface (such structurally perturbed water at an interface was even given a term "vicinal" water), there remains a significant controversy in the literature about the correct measurement and theorization of water-induced forces, either hydration (hydrophilic) or hydrophobic in origin.

7.3   MATERIALS AND METHODS

7.3.1   Properties of polymaleic acid (PMA)

The polymaleic acid (PMA) (in 50% active content by weight) was provided by Kroff Chemical Company (Pittsburgh, PA). The molecular weight of this monopolymer was 1000 g/mol (according to the chemical provider). The repeating unit of PMA is illustrated in Figure 7.3. PMA molecules contain the most dense carboxylic groups per backbone carbon atom (one carboxylate per backbone carbon).
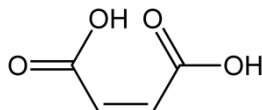
Figure 7.3 Repeating unit of polymaleic acid.

7.3.2   Effect of PMA on Mineral Precipitation

The effect of PMA on mineral precipitation processes over time was investigated in stirred batch reactors. The chemical composition of the working solutions is shown in Table 7.3. The components were added from 1-M stock solutions of $CaCl_2$, $MgCl_2$, $NaHCO_3$, KCl, KH_2PO_4, and Na_2SO_4. The stock solutions were made with reagent grade or better quality chemicals. In the experiments with PMA treatment, predetermined amounts (ppm) of PMA were added from a 5000-ppm stock solution at the start of experiment. For each experiment, 750 mL of mineral solution was prepared in a Pyrex cell reactor. The solution pH (7.5) and initial ionic strength (IS)

134

were maintained the same; variations in pH and IS due to PMA addition were corrected with NaOH, HCl, or NaCl. Temperature was maintained at 40°C and solution/suspension was stirred with a teflon-lined magnetic stirrer at 300 rpm. Solution conductivity was monitored continuously using an on-line conductivity meter (Fisher Scientific) and the suspension turbidity was measured periodically. The effect of PMA on the precipitation kinetics was analyzed based on the changes of the solution conductivity over time.

After a "fast precipitation" took place (cf. Figure 7.4) in the absence of PMA, the mineral suspension was split into two equal volumes (375 mL each) and 5 ppm of PMA was added to one of the suspensions and let equilibrated for 48 hr before the examination of the PMA effect on the deposition of mineral particles.
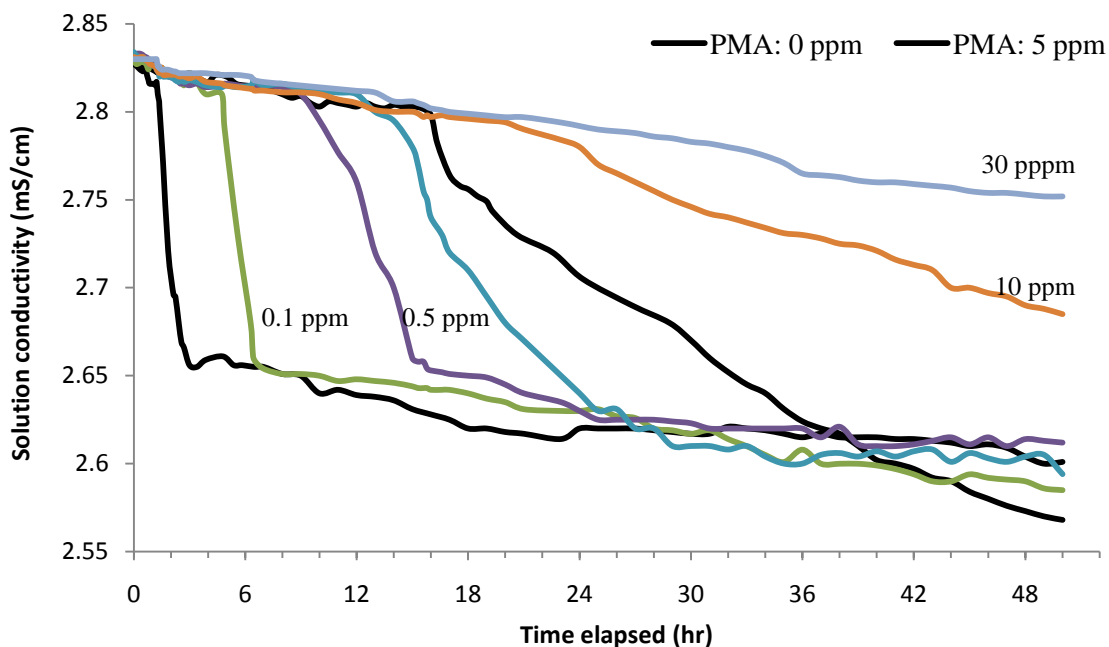
Figure 7.4 Effect of PMA addition on the precipitation reaction as measured by solution conductivity changes over time.

The chemical composition of the supersaturated solution is provided in Table 7.3. Experimental condition: 750-mL solution in a Pyrex cell reactor, pH 7.5, 40°C, and 300 rpm.

Table 7.3 Initial concentrations of the chemical constituents in bulk solutions for mineral precipitation retardation studies with PMA (unit: mM)

Component	Ca	Mg	Na	K	HCO$_3$	PO$_4$	SO$_4$	Cl
Initial Concentration (mM)	4.0	1.6	19.0	4.8	12	4.8	3.5	11.2

7.3.3 Mineral particle characterization

Mineral precipitate was collected from each reactor on a 0.22-µm membrane filter paper to remove residual water, dried, and inspected under a scanning electron microscope (SEM, Philips XL30, FEI Co., Hillsboro, OR) for its morphology. The elemental composition of the precipitate was analyzed using EDS. The particle size distribution was determined using a Microtrac S3500 system (Microtrac Inc., Montgomeryville, PA). A Malvern NanoSeries ZetaSizer (Nano-ZS, Malvern Instruments, Westborough, MA) was used to measure the zeta potentials of the mineral particles in prepared suspension.

7.3.4 Association/complexation of PMA with K$^+$, Ca^{2+}, and Mg^{2+}

In a series of 50-mL volumetric flasks, 5 ppm of PMA was added to each. The concentrations of K$^+$, Ca^{2+}, or Mg^{2+} were varied according to Table 7.4. The solution volume was then adjusted with DI water. After equilibrating for 3 hr, the concentration of free PMA (PMA that is not complexed) in each flask was measured colorimetrically at 505 nm using a commercial test kit (MCI analytical test procedure, Masters Company, Wood Dale, IL). Standard calibration curves of absorbance vs. PMA concentration were developed in DI water with known concentrations of PMA, which was added from a stock solution (5000 ppm PMA). A selected subset of samples were measured again after 12 hr, the changes in PMA concentration between 3 hr and 12 hr were

minimal. The free PMA measurement is based on complexation of the available carboxylate groups of PMA with the test reagent (a weak complexing agent) and subsequent colorization of the solution with the addition of a second reagent [17].

Table 7.4 Concentrations of cations tested for their association/complexation with PMA

Electrolyte	Concentration (mM)				
KCl	0	6	12	18	30
CaCl$_2$	0	2	4	6	10
MgCl$_2$	0	2	4	6	10
Solution IS (*I*)	0	6	12	18	30

7.3.5 Adsorption isotherm of PMA on SS surface

Intertwined strands of stainless steel (SS) wire in the form of a sponge-like structure were used to provide the surface for PMA adsorption. The SS surface was cleaned before use with an acetone/ethanol mixture (1:1 volume ratio) and then with DI water. Known amounts of the SS wire (pre-weighed) were put into a Nalgene plastic (PE) bottle of 240 mL total volume (Table 7.5). 230 mL of PMA solution was poured to the bottle. The solution pH was then adjusted to 7.5 with NaOH or HCl. A series of bottles containing solutions of varied PMA initial concentrations were continuously agitated on a wrist-action shaker (Model 75, Burrell Scientific, Pittsburgh, PA). Samples were taken from each bottle at predetermined times to measure the concentrations of PMA remaining in the aqueous phase.

Table 7.5 Amount (weight) of stainless steel wire used in each adsorption isotherm test with different amount of PMA

Test #	1	2	3	4	5	6
Initial PMA concentration C_0 (ppm)	0	4	8	12	16	20
Stainless steel wire (g/L)	110.4	106.7	108.7	109.2	107.5	134.1

7.4 RESULTS AND DISCUSSION

7.4.1 Retardation of mineral precipitation by PMA

Figure 7.4 shows the different patterns of mineral precipitation as measured by the changes in solution conductivity with different doses of PMA addition. Without PMA, precipitation started at about 1.5 hr, and was essentially completed within a few minutes. With PMA addition, the onset of precipitation was delayed. Even with just 0.1 ppm of PMA, the precipitation started after 4.8 hr, which is delayed by 3.3 hr compared to the case without PMA. With greater amounts of PMA added to the solution (0.5 ppm, 1 ppm, and 5 ppm), the induction times were delayed even further; with 5 ppm of PMA, precipitation started after 15.6 hr. Not only were the induction times delayed with PMA, but the precipitation rates (the slopes of the conductivity change with time) were also slower with greater PMA addition. When the PMA concentration was increased to 10 ppm, no "fast precipitation" was identified over the entire experimental period (50 hr).

The effect of PMA on the delay of the onset of mineral precipitation can be explained by the reduction of the mineral solution supersaturation level in the presence of this organic polymer. PMA molecules dissolved in solution may effectively interfere with the diffusivity of

138

the mineral ions, thereby reducing the driving force and chances of clustering and nucleation. Also, the interactions between PMA molecules and newly-formed mineral surfaces may reduce the magnitude of coefficient n in Equation (7) or (8), thus decreases the precipitation reaction rates.

7.4.2   Solid characteristics and chemical composition of the precipitate

For a more detailed evaluation of the retardation effect by PMA, the mineral precipitate from the experiments with no PMA and 5 ppm of PMA (Figure 7.5) was collected and analyzed. In addition, the mineral suspension without PMA addition at time zero was split into two equal volumes and 5 ppm of PMA was added to one of the suspensions for further examination of the PMA effect on pre-formed suspended particles. The SEM images of the mineral particles collected from the three suspensions (at 48 hr) are shown in Figure 7.6. In the absence of PMA (Figure 7.6-Left), the precipitate is comprised of multidispersed crystal pieces with highly irregular shapes. With PMA added after the precipitate had formed, the crystal solids tend to stick together to form clusters (Figure 7.6-Middle). In the case where PMA was added at the beginning of experiment (before any precipitation took place), two distinct morphologies can be identified, crystal and amorphous (Figure 7.6-Right).
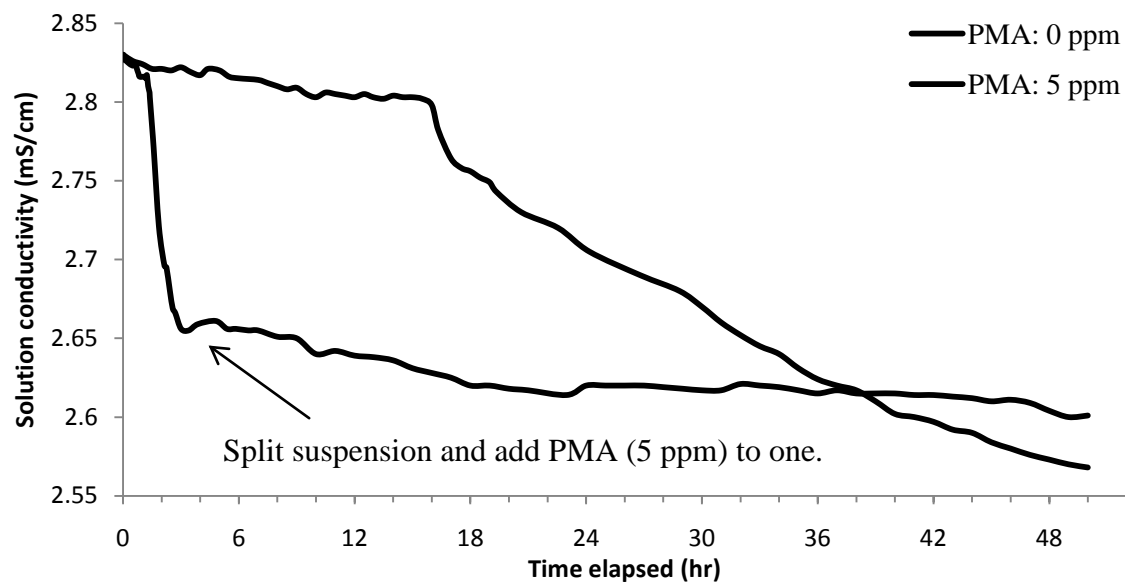
Figure 7.5 Solution conductivity changes over time in the absence and presence of PMA (5 ppm, added at time 0). Experimental condition: 750-mL solution in a Pyrex cell reactor, pH 7.5, 40°C, and 300 rpm. After precipitation took place without PMA, the mineral suspension was split into two equal volumes (375 mL each) and 5 ppm of PMA was added to one of the suspensions for the examination of the PMA effect on the deposition of mineral particles.

PMA: 0 ppm

PMA: 5 ppm added post precipitation

PMA: 5 ppm added at time zero (prior to precipitation)
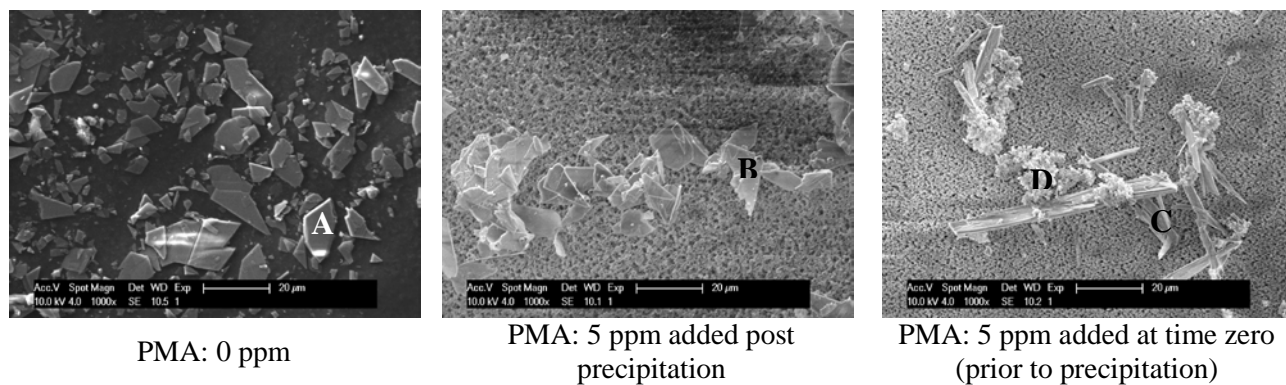
Figure 7.6 SEM images of the precipitated mineral particles collected under different PMA treatment.

Capital letters on images indicate the spots (areas) for EDS analysis.

To further reveal the effect of PMA on mineral precipitation, the elemental compositions of the precipitate were determined by Energy Dispersive X-ray Spectroscopy (EDS, EDAX Inc., Mahwah, NJ). The relative signal intensities of the elements making up the precipitate are shown in Figure 7.7. The precipitate appears to be a mixture of calcium phosphates and carbonates. Surface adsorption of PMA that was added after bulk precipitation was evidenced by the elevated peak intensities of C and O in Figure 7.7 upper panel. In the case where PMA was added prior to bulk precipitation (Figure 7.7 lower panel), the elemental composition of the two distinct morphologies (Figure 7.6-Right) was different. In the amorphous solids, more PMA was incorporated than in the crystal structures. More importantly, with the amorphous formation, appreciable amounts of Mg were also incorporated, which was not observed in other cases. When curves (A) and (C) are compared in Figure 7.7, calcium carbonate formation is suppressed by PMA, suggesting that calcium phosphate is more dominant in the presence of PMA.
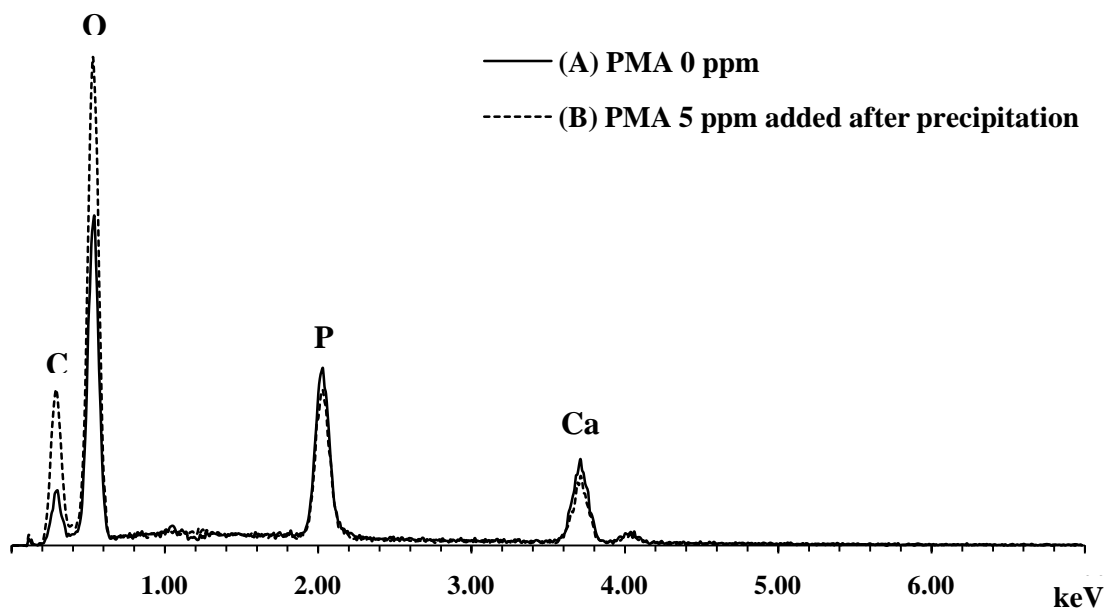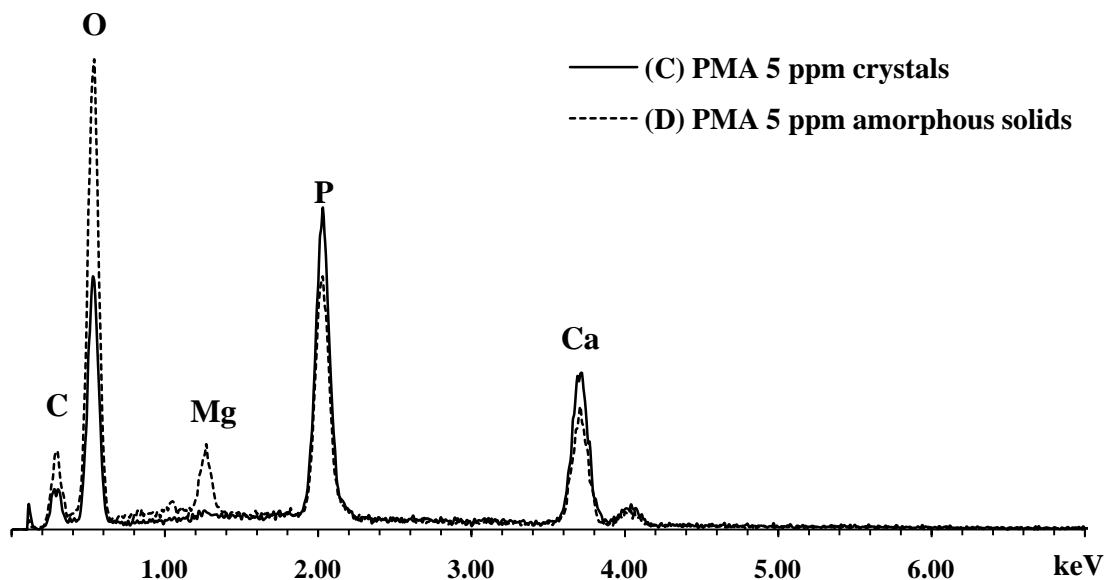
Figure 7.7 Elemental composition of the precipitated mineral particles collected after different PMA treatment. Capital letters for each curve correspond to the scanning spots (areas) indicated in Figure 7.5.

7.4.3 Association/complexation of PMA with Mg^{2+}, Ca^{2+}, and K^+

Figure 7.8 shows the concentrations of PMA that was free in solution, i.e., PMA not complexed with the cationic species present in solution at different concentration levels. PMA exhibited strong affinity toward Mg^{2+}. At $[Mg^{2+}]_0 = 10$ mM (corresponding to solution $I = 30$ mM), more than 50% of the PMA (2.6 ppm) was in complexed form, whereas with Ca^{2+} only 30% of the PMA (1.6 ppm) was complexed. The strong affinity between Mg^{2+} and PMA was responsible for Mg incorporation into the mineral precipitates (Figure 7.7), which was not detected in the absence of PMA.

It is known that ligands such as CO_3^{2-} and PO_4^{3-} exhibit different affinities for Ca^{2+} and Mg^{2+}. Compared to Ca^{2+}, Mg^{2+} has less affinity for inorganic ligands, as evidenced by the

142

smaller values of K_{sp} (the first two columns of Table 7.6). With regard to organic ligands that bear primarily carboxylate groups, Mg^{2+} cations tend to be more strongly associated with them than Ca^{2+} cations do, forming more stable complexes (the last three columns of Table 7.6). Furthermore, the carboxylate groups in humic acids (HAs) were confirmed to be responsible for HA complexation with divalent cations [18]. The HA fractions rich in carboxyl carbon may become smaller in size thus more diffusive when complexed with Mg^{2+} or Ca^{2+} as revealed by NMR studies [18]. The improved diffusivity contributes to the easier incorporation of the complexes into the mineral precipitates, effectively distorting the crystallization process.

On the other hand, the amount of calcium or magnesium complexed with PMA was minimal compared to the total concentrations of the cations present in the bulk solution. The repeating unit (base unit) of PMA is -CH(COOH)-, which has a "molecular weight" of 58 g/mol. Accordingly, 1 ppm of PMA corresponds to 17.24 µM of the PMA base unit. In the test solution containing 5 ppm of PMA, there were 86.21 µM of the PMA unit. Assuming two units complex with one Ca^{2+} ion, only 1% of the Ca^{2+} present in solution will be complexed ($[Ca^{2+}]_0 = 4.0$ mM) even under a maximum complexation capacity of the PMA. This calculation suggests that the changes of calcium concentration due to PMA complexation were insignificant, and would not contribute significantly to the inhibition of calcium precipitation.
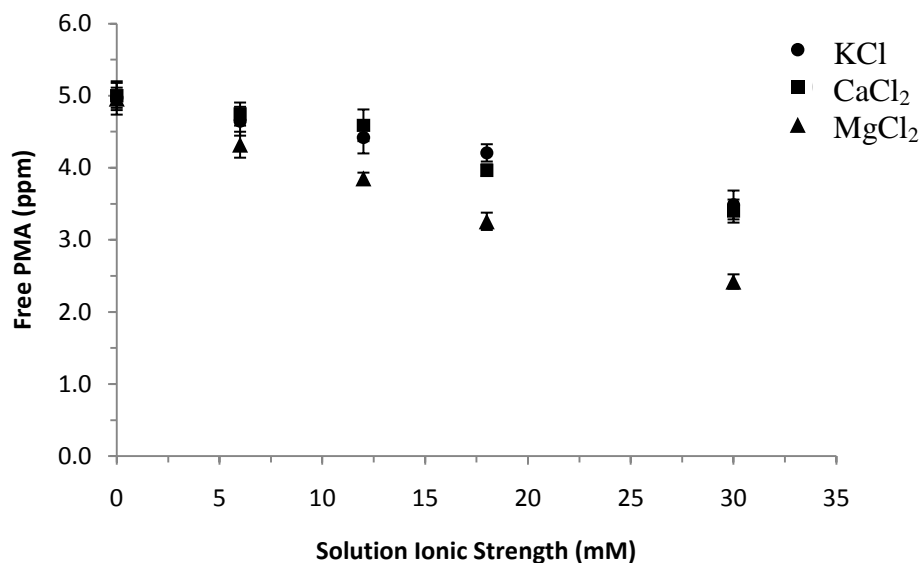
Figure 7.8 Solution concentrations of free PMA that was not complexed with cationic species.

Initial PMA added: 5 ppm, solvent: DI water. Solution was equilibrated for 3 hr before PMA measurements. Error

bars indicate triplicate preparation of test solutions.

Table 7.6 Stability constants (complexation constants or solubility product constants) of ligands with calcium and

magnesium (usually measured at 25°C, 1 atm, and $I = 0$)

pK	Ligand		
	CO_3^{2-}	PO_4^{3-}	CH_3COO^-
	Carbonate	Phosphate	Acetate
Ca^{2+}	8.3^1	$44.2\text{-}55.6^3$	1.2^5
Mg^{2+}	5.0^2	25.2^4	1.3^5

[1] 8.48 for calcite and 8.36 for aragonite in Mark Benjamin[2]; 8.34 for calcite and 8.22 for aragonite in Snoeyink[3].
[2] Sneoyink[3]; 4.67 for $MgCO_3 \cdot 3H_2O$ in Morel and Hering[4].
[3] Hydroxylapatite in Mark Benjamin[2] and Morel and Hering[4].
[4] Bobierrite $Mg_3(PO_4)_2 \cdot 8H_2O$ in Morel and Hering[4].
[5] 1:1 complex in Morel and Hering[4].

7.4.4 Adsorption isotherm of PMA on SS surface

The data shown in Figure 7.9 reveal an interesting phenomenon where the suspended particles formed in the presence of PMA (5 ppm) appear to be "sticky" to the reactor wall. When PMA was not added to the solution, turbidity increased after just one hour due to the formation of suspended solids in the bulk phase. Addition of 5 ppm of PMA from the start of the experiment delayed solids formation by 16 hr. However, a steady decrease in turbidity was observed after 20 hr of contact to the point that the turbidity decreased to about 40% of the initial value observed after 20 hr. The turbidity was only recovered when the suspension was vigorously stirred to re-suspend the mineral particles that had accumulated on the reactor wall. This raises a question, how did PMA increase mineral deposition on the reactor wall? Data from previous studies demonstrate that PMA addition to supersaturated solution helped mitigate mineral scaling on stainless steel disc specimens (Chapters 3-5). How does the stainless steel surface differ from the reactor wall (Pyrex glass) with regard to PMA adsorption, if any? To answer these questions, batch reactors of similar volume but made of different materials (i.e., stainless steel, Pyrex glass, and PE plastic) were used to study the potential adsorption of PMA to the reactor walls.Figure 7.10 shows that within 12 hr of equilibration with 5 ppm of PMA initial concentration, PMA did not adsorb onto any of the reactors significantly.
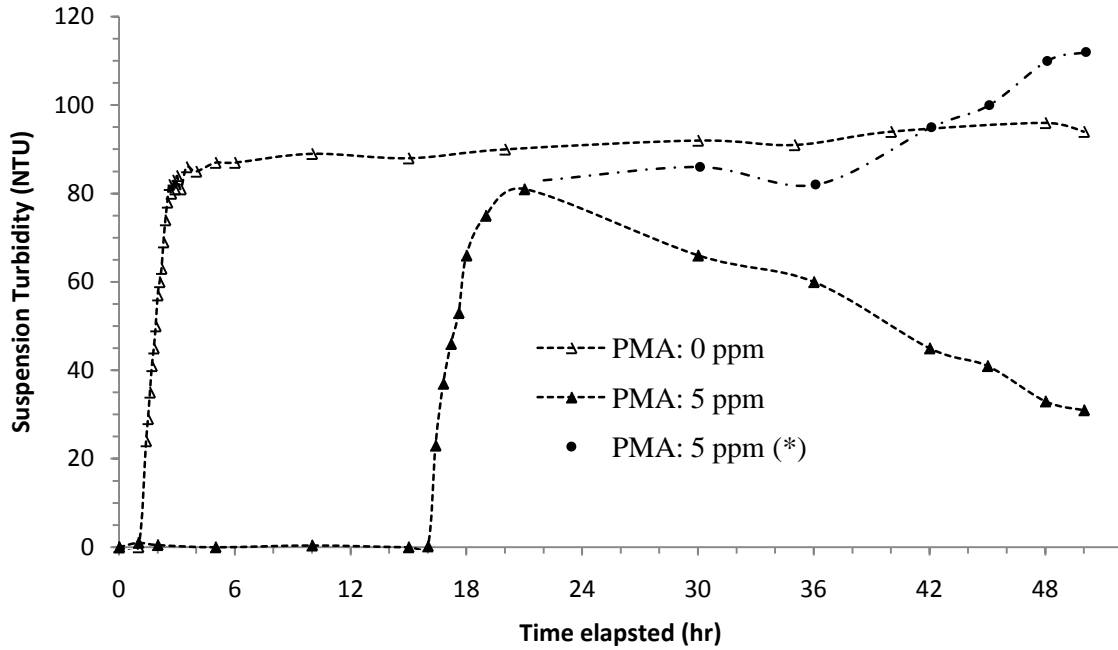
Figure 7.9 Suspension turbidity changes over time in the presence and absence of PMA (5 ppm, added at time 0). Experimental condition: 750-mL solution in a Pyrex cell reactor, pH 7.5, 40 °C, and 300 rpm. * Solid circles show measurements after the suspension was vigorously stirred to re-suspend the mineral precipitates that had accumulated on the reactor wall.
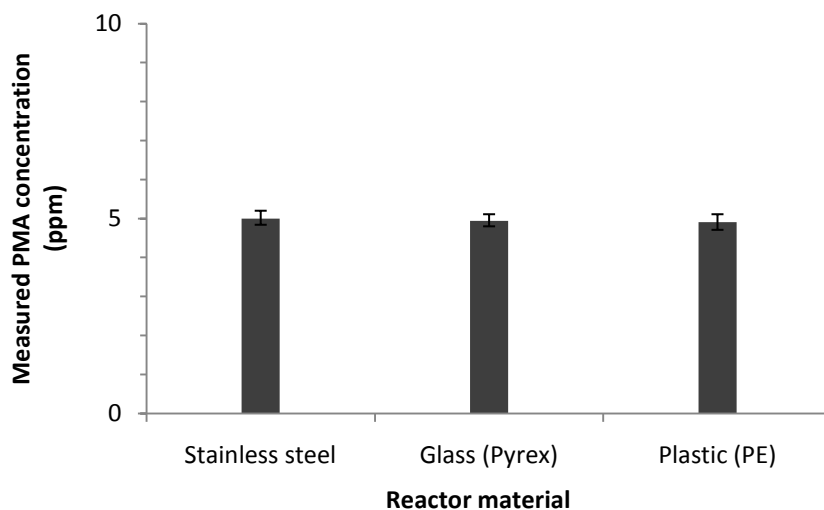
Figure 7.10 Solution PMA concentration in batch reactors made of different materials.

PMA added: 5 ppm, solvent: DI water, pH = 7.5 (adjusted with NaOH). Solution was equilibrated for 12 hr before taking measurements. Error bars indicate triplicate preparation of the test solutions. This Figure shows that PMA did not adsorb onto the reactor wall significantly.

Moreover, the experimental data in Figure 7.11 show that no PMA adsorption to the stainless steel surface was observed after 60 hr of equilibration in an aqueous solution containing an initial PMA concentration of 12 ppm at pH 7.5.Figure 7.12 shows that no PMA adsorption to the stainless steel surface was observed when the initial PMA concentration ranged from 0-20 ppm and the solution pH varied from 8.5 and 7.0.

Table 7.7 Amount (weight) of stainless steel wire used in each adsorption isotherm test with different amount of PMA

Test #	1	2	3	4	5	6
Initial PMA concentration C_0 (ppm)	0	4	8	12	16	20
Stainless steel wire (g/L)	110.4	106.7	108.7	109.2	107.5	134.1
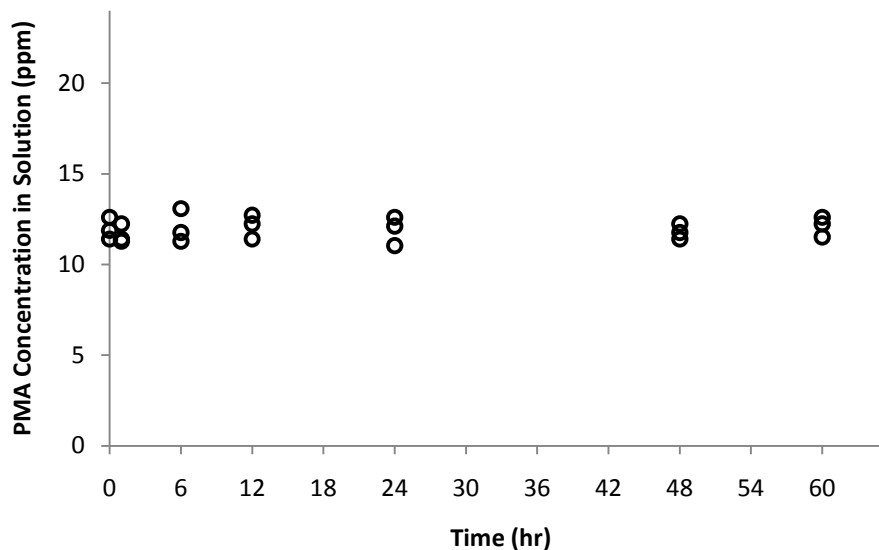
Figure 7.11 PMA concentration in aqueous solution (I = 5 mM KCl) with 109.2 g/L of stainless steel wire immersed.

PMA initial concentration = 12 ppm, solution pH = 7.5, room temperature (23 ± 1°C). Data points are triplicate measurements at each time.

The pK_a values of acrylic acid (AA) and maleic acid (MA) were reported to be 4.25 and 1.83, respectively [19]. Another group reported a pK_a value of acrylic acid to be 4.5 [20]. Wang et al. [21] reported a pK_a value of 5.12 for PMA, which was determined by a Gaussian distribution model in the simulation of the protonation/deprotonation behavior of the multiligand system of PMA. Using a Langmuir isotherm equation, the authors also observed a fairly low qm value of 0.369 mg C/m^2 for PMA adsorption on goethite at pH 5.8.

As for the charge properties of the stainless steel surface, literature information is rather limited. Although the deposition of self-assembled monolayers (SAMs) on solid supports and particularly metal surfaces has been extensively studied, only a few reports are available dealing with SAMs on stainless steel. It is generally proposed in these reports that the innate SS surface is of oxide nature with Me-O-Me and Me-OH groups covering the surface [22-24]. However, no

148

quantitative characterization of the SS surface in terms of its charge behavior as a function of pH is available in the literature. One study measured the PZC value of nanoscale zerovalent iron (NZVI) to be 7.7 [25] but its relevance to a smooth surface of stainless steel may be limited despite the fact that both surfaces contain predominantly iron atoms. A study measured the zeta potential of stainless steel surfaces over the water pH of 8-11 [26] and found that the zeta potential of the SS surfaces varied from -15 mV to -35 mV.

Based on the literature values it suggests that, in circumneutral pH ranges of our interests, PMA adsorption to steel surfaces can be minimal due to the electrostatic repulsion between the negatively charged PMA molecules and the negatively charged metal surface.
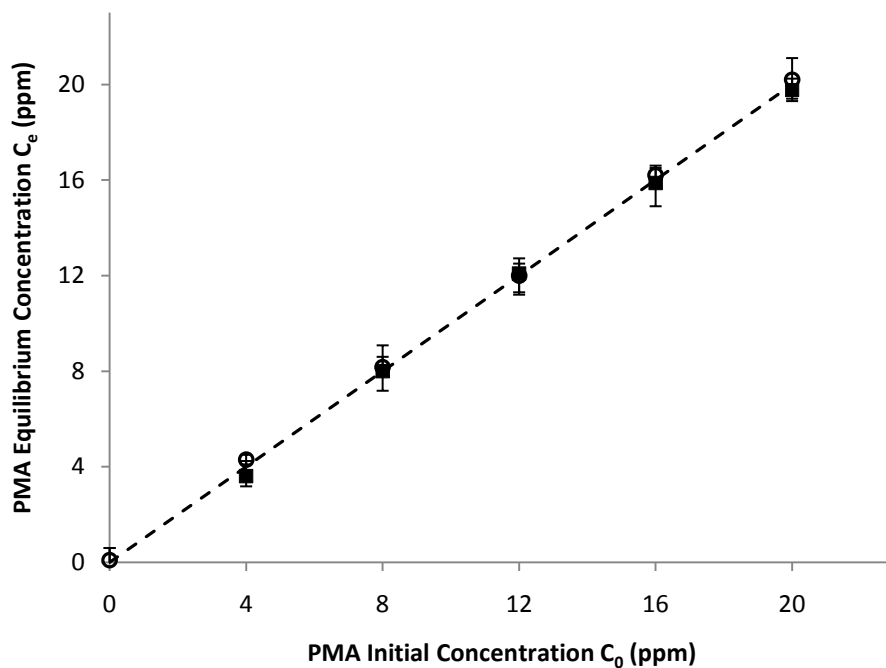
Figure 7.12 PMA equilibrium concentration as a function of initial concentration in aqueous solution (I = 5 mM KCl) containing stainless steel wire (Table 7.7).

Solution pH = 8.5○(and 7.0 (■), room temperature (23 ± 1°C). Measurements were made after 48 hr of equilibration. Error bars show the range of triplicate measurements. Dashed line indicates the 1:1 slope.

7.4.5 Size distribution and zeta potential of the precipitate

The particle size distribution (PSD) of suspensions with and without PMA was measured with a laser scattering particle size analyzer (Microtrac S3500 system, Montgomeryville, PA) and the data are shown in Figure 7.13. Without PMA, the peak size (in terms of particle volume fraction) appears at 28 µm. When PMA was added post precipitation, the peak size was shifted to about 40 µm, which was probably due to the inter-particle bridging effect of PMA molecules resulting in particle aggregation. In the case where PMA was added at time zero, the PSD curve is more dispersed, with two distinct peaks appearing at 12 µm and 44 µm. The peak at 44 µm very likely indicates the crystal structures depicted in Figure 7.6-Right and the peak at 12 µm corresponds to the amorphous solids.
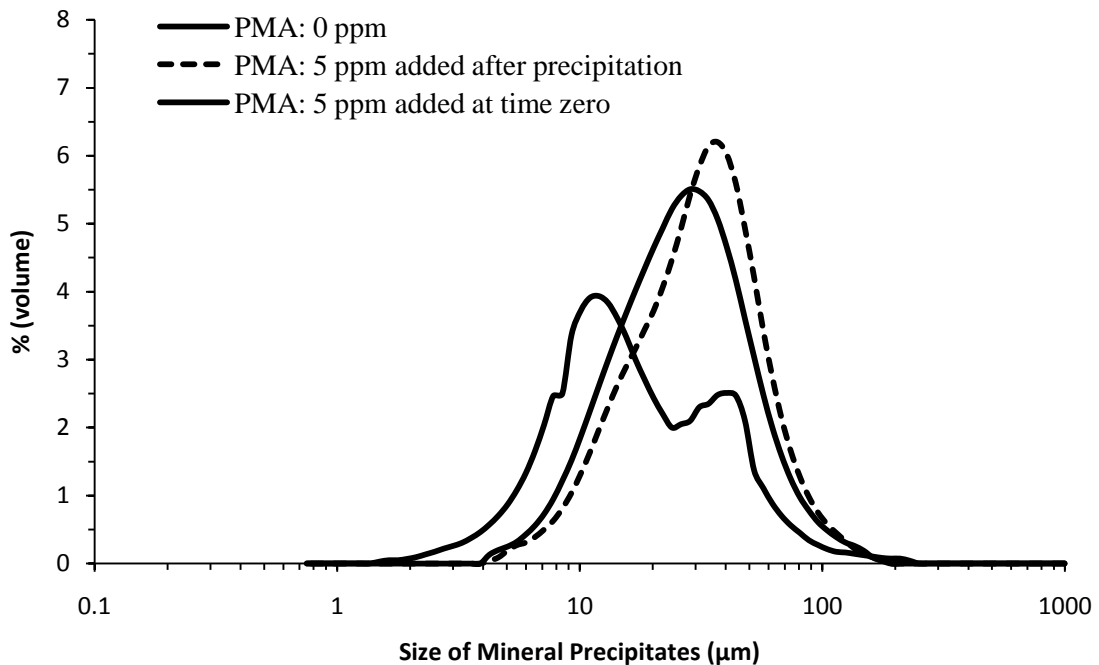
Figure 7.13 Variation in particle size distribution of the mineral suspension with different PMA treatment. Initial chemical composition of the supersaturated solution is provided in Table 7.3.

150

The zeta potential of the precipitate exhibited distinct values with different PMA treatment (Figure 7.14). Without PMA, the particle zeta potential was neutral to slightly negative, -2.92 ± 8.61 mV (peak ± deviation, calculated by the Zetasizer program). When PMA was added post precipitation, the particles were more negatively charged, -14.3 ± 6.17 mV, confirming the particle association with negatively charged PMA molecules. In the case where PMA was added at time zero, the zeta potential is more dispersed, with two distinct peaks appearing at -15.91 mV and -3.21 mV. The more negative peak indicates stronger association of PMA with the mineral particles, corresponding to the more amorphous solids that contain more PMA than the crystalline solids (Figure 7.6-Right).
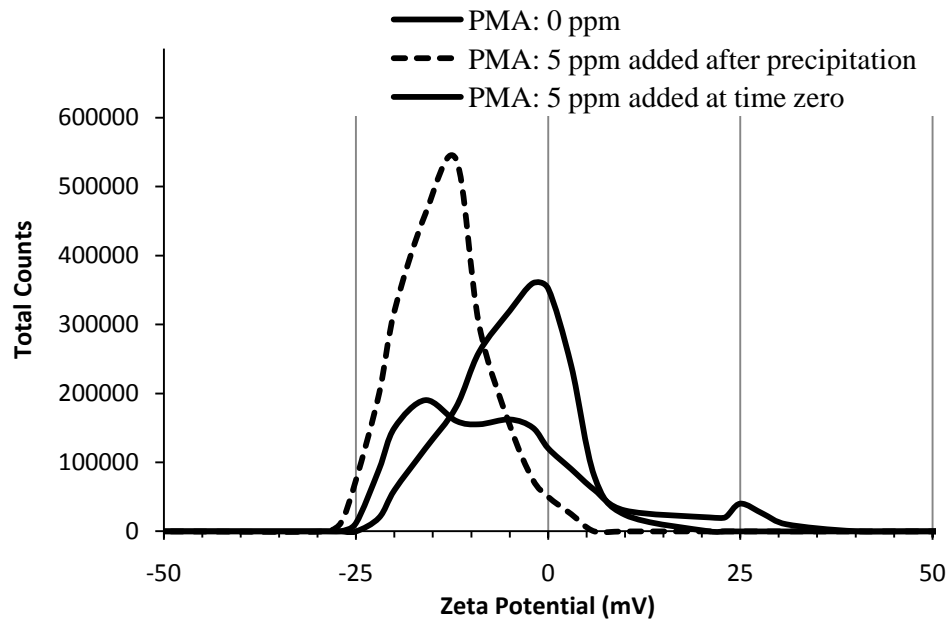
Figure 7.14 Changes in zeta potential of the mineral particles obtained from the mineral suspension with different PMA treatment.

The electrical repellency between particles affected by PMA surface adsorption is manifest in the data shown on Figure 7.15. It is clear that much less deposition on stainless steel specimens was observed in the suspension treated with PMA (5 ppm) after bulk precipitation. In the other case where 5 ppm of PMA was added at time zero, more deposits were collected on the specimen surface, which was consistent with the observation of reactor wall accumulation of mineral solids (Figure 7.9). Although PMA addition at time zero effectively retarded mineral precipitation, the precipitate formed in the presence of PMA became more "sticky" toward surfaces in contact with the suspension, which is undesirable for scaling control. The phenomenon was likely due to the formation of amorphous solids (smaller particle sizes in Figure 7.13) in the presence of PMA and the broadening of the zeta potential into both the positive and negative charge ranges (Figure 7.14). Both of these processes favored solid deposition on surfaces. Overall, adding PMA after mineral precipitation has occurred a better approach to prevent scaling.
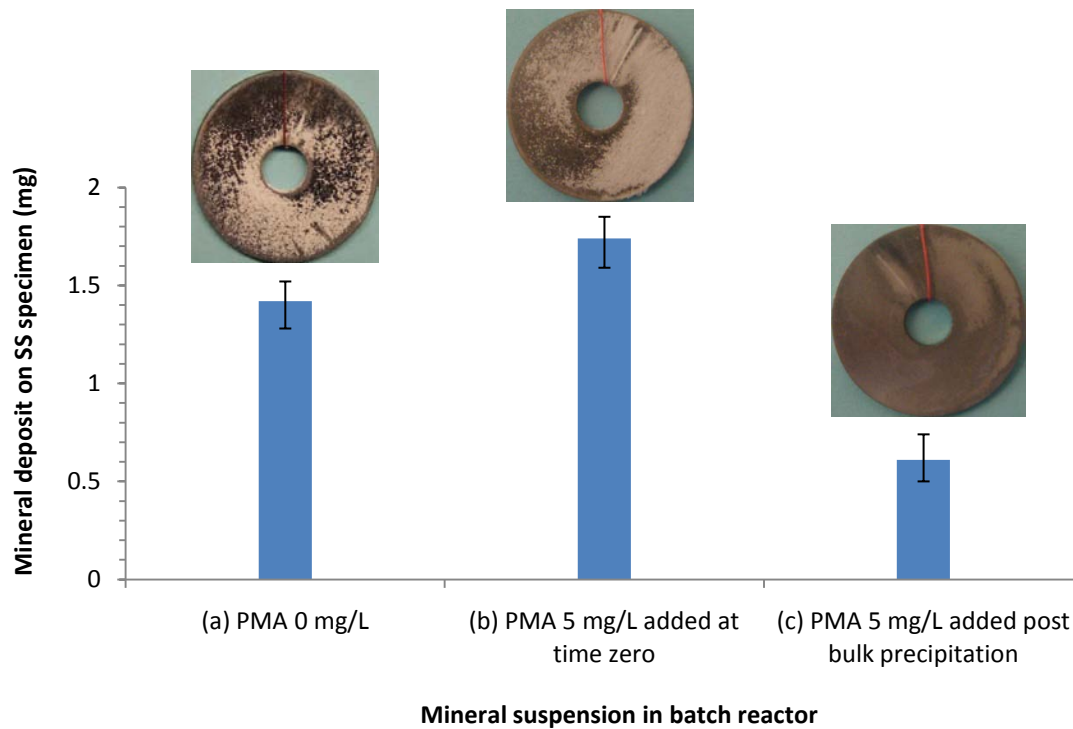
Figure 7.15 Mineral deposition on stainless steel specimens with different PMA treatment.

In case (a) and (b) the specimens were immersed at time zero and withdrawn at 48 hr; in case (c) the specimens were immersed immediately after the PMA (5 ppm) was added after bulk precipitation and kept in the suspension for 48 hr. Error bars indicate the measurement ranges of triplicate specimens.

7.5   CONCLUSIONS

The addition of PMA to a supersaturated mineral solution mitigated the mineral precipitation and deposition via several mechanisms. PMA delayed the onset of the mineral precipitation even at very low dosage (less than 1 ppm). At high doses (> 5-10 ppm) of PMA, not only did the "fast precipitation" phase become gradually less and less pronounced, but the precipitation rates were

also significantly reduced. The effect of PMA on mineral precipitation was similar to lowering the supersaturation of the mineral solution, which not only prolongs the induction time for precipitation, but also reduces the precipitation rates.

Magnesium exhibited stronger associations with PMA molecules than calcium, resulting in its incorporation in the amorphous solids in the presence of PMA. The interactions between Mg/Ca and PMA suppressed the formation of calcium carbonate. Consequently, calcium phosphate was more abundant in the precipitate formed in the presence of PMA.

The antideposition effect of PMA worked well with pre-formed suspended solids. Surface adsorption of PMA onto mineral particles increased the negative charge of the solids and rendered them less favorable for deposition on likely-charged substrate surfaces made of stainless steel. On the other hand, if the suspended solids were not preformed, PMA tended to incorporate into the mineral particles during the precipitation process to significantly alter the particle morphologies and surface charge distributions to the point that it appeared to lose much of its effect on deposition mitigation. The finding has significant implications in scaling control practices in that the protocol for PMA addition should be carefully evaluated. Under conditions when mineral precipitation takes place in the bulk, PMA should be better added after the fast precipitation took place to avoid the formation of PMA-incorporated mineral particles.

8.0 ELECTROCHEMICAL IMPEDANCE SPECTROSCOPY (EIS) BASED CHARACTERIZATION OF MINERAL DEPOSITION FROM PRECIPITATION REACTIONS

The study of mineral deposition on surfaces, such as that in cooling systems, has often relied on chemical equilibrium-based precipitation calculations, and simple measurements of mass gain from mineral accumulation on conducting surfaces. While these methods generally provide an initial estimate of the deposition potential or a gross measure of deposit formation, measurement of instantaneous rate of deposition would be useful for many kinds of scientific analyses and practical applications. An accurate and convenient approach for monitoring the rate of mineral deposition on metals in real time was developed and involves use of an electrochemical cell employing the metallic collecting surface as a working electrode. In this configuration, the working electrode serves as both the surface for mineral deposition and a sensor for probing subtle changes attributable to the growth of mineral deposits in the metal-mineral-water interface. The electrical impedance of the interface was measured by Electrochemical Impedance Spectroscopy (EIS). The interfacial capacitance obtained from the EIS data was used as a measure of surface coverage by mineral scale. An equivalent-circuit approximation was adopted to evaluate the distributed dielectric permittivity of minerals, which was reported as the capacitance of constant-phase element (CPE). The results show that the CPE capacitance correlated very well with the mass of mineral deposits accumulated on the metal surface.

Moreover, the characteristics of different minerals evaluated in this study, i.e., calcium carbonate, calcium sulfate, and calcium phosphate, did not affect the measurements of the CPE capacitance significantly. Rather, the CPE capacitance was sensitive to small changes in the mineral mass deposited on the electrode (< 0.1 mg). Unlike traditional methods for measurement of mineral deposition, the EIS allows in situ semi-continuous measurements of overall mineral deposition, and its sensitivity provides a means of early detection of mineral deposition. This study also showed that it is possible to use much narrower ranges (0.1 Hz or 1 Hz ± 10% of the frequency specified) of AC scanning frequencies, as opposed to using the entire six decades of frequencies (10 mHz to 10 kHz) to save measurement time and EIS device cost, without sacrificing measurement sensitivity.

8.1   INTRODUCTION

Predicting and monitoring mineral formation in water is a long-standing challenge in municipal and industrial water and wastewater systems. Deposition (scaling) of the minerals on heat exchanger, pipe and reactor surfaces can lead to myriad serious problems, including loss of heat transfer efficiency, clogging of filters, obstruction of flow, localized corrosion attacks, excessive wear of metal parts, unscheduled shutdowns, and ultimately, system failures. Over the last century, saturation and scaling indices, from the Langelier Saturation Index [1] to the Puckorius Scaling Index [2], were developed and constantly modified to predict the behavior of calcium carbonates (in some cases, calcium phosphates as well), in an effort to protect water distribution systems from mineral scaling and corrosion [1-4]. However, these equilibrium-based indices have been demonstrated to be of limited utility due to the inherent lack of kinetic considerations

and unable to account for variations in water quality [6-8]. The ability of equilibrium-based indices to predict precipitation accurately for actual water systems is limited and often not validated through experimental observations.

Despite significant research progress, there remains a great need for improved measurements and models of the kinetics of mineral deposition at solid surfaces under conditions of complex water chemistry. Often, large anomalies exist between actually observed deposition intensities and rates estimated by predictive models based on scaling indices or bulk precipitation reactions [4, 9]. The existence of these anomalies is partly due to the limited availability of methods that can be used to describe and monitor the deposition processes. Existing methods that rely on measurements of mineral mass gain [10, 11] or heat transfer loss [12, 13] arising from mineral surface accumulation are generally insensitive to small changes in scale deposition.

The Electrochemical Impedance Spectroscopy (EIS) technique has gained remarkable interest and application in a broad array of fields, including coatings and paintings [14, 15], corrosion [16-18], batteries [19-21], fuel cells [22-24], self-assembled layers [26-29], polymer degradation [30, 31], and membrane fouling [32, 33]. EIS has also been used in mineral deposition studies [34-41]. However, nearly all of the reported studies interpreted the EIS data based on the construction of distinctive, often complex electrical circuit analogies, many of which are difficult to connect to meaningful physicochemical properties of deposits. In addition, corrosive metals (e.g., mild steel) were sometimes used as the working electrode, which complicates the analysis of the EIS signals because of corrosion interference [37, 41]. Moreover, mineral deposition in these systems was often influenced by applied potentials which induced local pH changes at the solid-liquid interface [21, 36, 38-41].

The objective of this study was to evaluate the use of EIS as a technique for in situ monitoring of the rate of mineral deposition in aqueous systems. Stainless Steel (SS) materials were used to preclude corrosion influence on EIS measurements. Sufficiently low electrical potentials were applied to minimize the probability of inducing redox reactions that may cause local pH changes. Capacitance values of a single constant-phase element (CPE) parameter based on a simple electrical circuit equivalence were obtained from mineral deposition experiments. The changes of the CPE capacitance over time were correlated to the mineral mass deposited, thereby establishing the physical meaning of the CPE parameter. This technique not only enables rapid and convenient tracking of mineral deposition processes, but also holds potential for in situ study of fundamental aspects of mineral deposition on metal surfaces.

8.2   THEORETICAL BACKGROUND

At the metal-solution interface, an electrical double layer usually forms owing to the differential of chemical energies between the metal surface and the solution. The chemical energy differential is commonly measured as electrochemical potentials (Figure 8.1a). When an electric signal (e.g., a sinusoidal potential wave) is applied to the interface, the response signal (e.g., a varying current) can exhibit a capacitive character. The behavior of the double layer, by analogy, can thus be approximated by that of a simple capacitor [42].
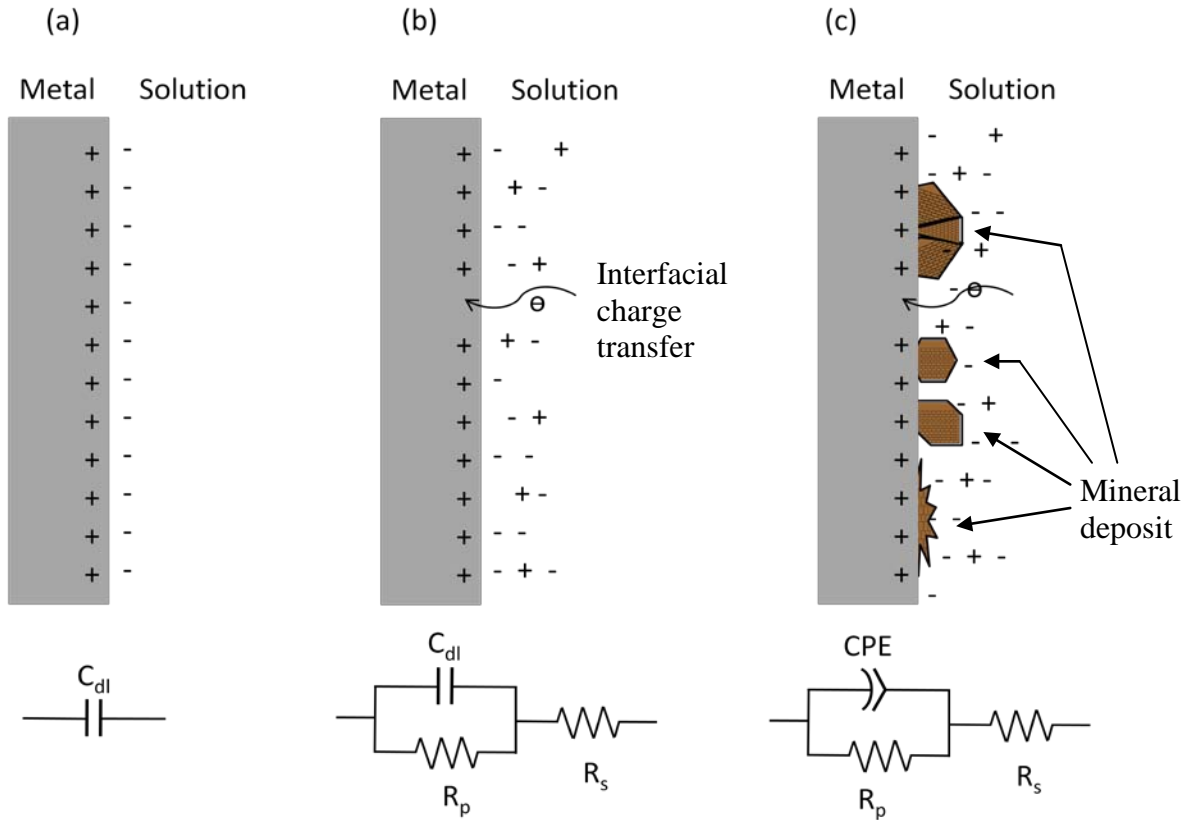
Figure 8.1 Schematic representations of the electrical double layer at the metal-solution interface and their corresponding equivalent circuit diagrams.

Charges on metal surface are depicted as positive, but negative charges are also possible (with corresponding counter charges in the solution side). C_{dl} = double-layer capacitance, R_p = polarization (charge transfer) resistance, R_s = solution resistance due to ionic diffusion, CPE = constant-phase element (non-ideal) capacitance.

For an alternating current (AC) signal, like a sine waveform, Ohm's law takes the following form:

$$V(\omega) = I(\omega) \times Z(\omega) \qquad (1)$$

where V, I, and Z are frequency-dependent potential (volt), current (amp), and impedance (Ω), respectively. The angular velocity, ω (rad/sec), is given by

$$\omega = 2\pi f \qquad (2)$$

where f is the signal frequency in Hz.

In principle, the impedance, Z, may originate from a system element that is resistive, capacitive, or inductive in nature, with an inductive impedance rarely encountered in solution-based electrochemical systems [42]. Resistive impedance, Z_R, is independent of the frequency and thus equivalent to the resistance in the direct current (DC) mode. In a resistance-only system, the response signal is always in phase with the excitation signal, and the resistance (or, the *real* component of the impedance) constitutes the entire impedance.

Capacitive impedance, Z_C, can be expressed as [43]:

$$Z_C = \frac{1}{i\omega C} \tag{3}$$

where, the imaginary unit $i = \sqrt{-1}$ indicates a 90° phase angle shift between the excitation and response signals, and the impedance is constituted entirely of the *imaginary* component of the impedance (e.g., the impedance of an ideal capacitor). The capacitance, C (farad), can be evaluated from the relation

$$I = C\frac{\partial V}{\partial t} \tag{4}$$

Eq (3) indicates that, unlike the resistive impedance, the magnitude of the capacitive impedance depends on the frequency.

The capacitive impedance of the electrical double layer can be determined by EIS measurements. In EIS, measurements of electrical current are carried out on a system in which a periodic AC potential is applied over a broad range of frequencies—hence the name impedance spectroscopy.

Analysis of the EIS data yields insightful information about the metal-solution interface with regard to its structural features [34] and possible chemical reactions taking place near the

metal electrode [21, 36, 38-41]. The electrode interface undergoing electrochemical reactions is analogous to an electric circuit comprising a certain combination of resistors, capacitors, and inductors. By using established AC circuit theories, one can take advantage of this analogy to probe property changes at the interface. One example is represented on Figure 8.1b, which is a more realistic depiction of Figure 8.1a. In this example, the solid surface is smooth but the electrical layer on the solution side has to be modified to reflect the ionic diffusion and interfacial charge transfer, which are approximated by a solution resistance, R_S (Ω), and a polarization resistance, R_P (Ω), respectively. This particular type of equivalent electrical circuit (EEC) is called a simplified Randles model [42]. Experimental EIS data can be fitted to EEC models such as the Randles model in a fairly straightforward manner. However, a challenging task is to establish physical meanings from the fitted model parameters. This requires knowledge of the electrochemical cell under study and the reaction mechanisms involved, both built on a fundamental understanding of the behavior of the cell elements.

With surface deposition (Figure 8.1c), the electrochemical picture becomes more complicated and the Randle's model no longer describes the system adequately. Impedance results obtained from surfaces covered by a deposit layer often exhibit frequency dispersions. The frequency dispersion can be attributed to a capacitance dispersion expressed in terms of a constant-phase element (CPE), which replaces the ideal capacitor in the Randle's model [42, 44, 45]. The impedance of a CPE is given by:

$$Z_{CPE} = \frac{1}{Y_0 (i\omega)^\alpha}$$

(5)

where, Y_0 is the CPE constant, referred to as the CPE capacitance (with units that depend on the power law relationship) and the exponent α is generally used to represent the degree of capacitive dispersion (i.e., values further away from unity indicate more dispersive capacitance).

In addition, the phase angle shift, represented as i^{α}, is between 0° and 90°. The inclusion of CPE for modeling is often intended to account for distributed time constants which originate from several physicochemical processes taking place at the interface [44, 46, 47]. The processes most relevant to mineral deposition include surface roughening and chemical heterogenization due to the mineral deposit coating. Similar to the quantification of simple capacitance [42, 44, 45], the CPE capacitance can be related to several coating properties, including the dielectric constant, ε_r (unitless), of the coating material, the surface area, A (m^2), and the coating thickness, d (m):

$$Y_0 \propto \varepsilon_r \frac{A}{d} \qquad (6)$$

The EIS methods have been employed previously to characterize properties of coatings on metal surfaces [14, 15]. The method was employed in this work in a similar way as a sensitive and in situ method to characterize the surface coating by mineral deposition. The presence of a mineral deposit coating alters the electrical properties of the working electrode-solution interface, which is detected by EIS and reflected in the changes of the CPE capacitance.

8.3   EXPERIMENTAL

8.3.1   Materials and Methods

Solutions were made in deionized (DI) water (resistivity > 18 MΩ-cm) with the addition of chemical constituents (reagent grade or better). Calcium was provided as CaCl$_2$, phosphate as Na$_2$HPO$_4$, carbonate as Na$_2$CO$_3$, sulfate as Na$_2$SO$_4$, and nitrate as NaNO$_3$. Solution pH was

adjusted to 7.5 with 0.1 M HCl or NaOH. The initial concentrations of the mineral ions employed in the various experiments are listed in Table 8.1.

Table 8.1 Test solutions used in both EIS and mineral mass measurements at pH 7.5 and 40°C

The amounts of equilibrium precipitation were calculated by MINEQL+. Solutions with the same potential production of mineral solids were used. However, different amounts of deposit for different minerals were collected under the experimental conditions employed.

Test Solution #	Mineral	$[Ca]_T$* mM	$[Anion]_T$* mM	Expected Precipitate Mass Concentration mg/L
1	$Ca(NO_3)_2$	11.4	400	--
2	$CaSO_4$	11.4	225	385
3	$CaCO_3$	11.4	4.3	386
4	$Ca_5(PO_4)_3(OH)$	11.4	2.3	386

* Total concentrations added.

The cell configuration for mineral deposition experiments in a stirred batch reactor with accompanying EIS measurements is depicted in Table 8.2. The system components were selected such that they were chemically inert to avoid unnecessary reactions that may complicate the electrochemical measurements. The materials that were put in contact with a test solution were limited to Pyrex, PVC, teflon, graphitic carbon, or stainless steel (SS). UNS 316 type stainless steel (Metal Samples, Munford, AL) was used as the working electrode (WE) material because of its high corrosion resistivity. Deposition was measured on the surface of a stainless steel cylinder WE with a surface area of 4.32 cm^2 (excluding the blocked area under the teflon gasket). A saturated calomel electrode (SCE) was used as a reference electrode (RE) and was placed inside a Luggin Capillary to minimize solution interference. A high-density graphite rod was

used as the counter electrode (CE). A temperature probe immersed in the working solution was used to maintain solution temperature by adjusting a thermostat on a heated stir plate. The solution was kept at 40 °C and stirred at 300 rpm with a teflon-lined magnetic stir bar. An extra port (not shown on Figure 8.2) on the Pyrex lid of the reactor cell of the system was used for solution pH and conductivity measurements.

Table 8.2 CPE model parameters evaluated as calcium phosphate deposition took place from 1 hr to 52 hr in batch reactor experiments (cf. Figure 8.5).

CPE model Parameter	1 hr	52 hr
GOF	3.9×10^{-4}	2.6×10^{-4}
R_p	1×10^{35} kΩ	1×10^{35} kΩ
R_s	9.7 Ω	10.3 Ω
Y_0	4.1×10^{-4}	2.7×10^{-4}
α	0.885	0.857
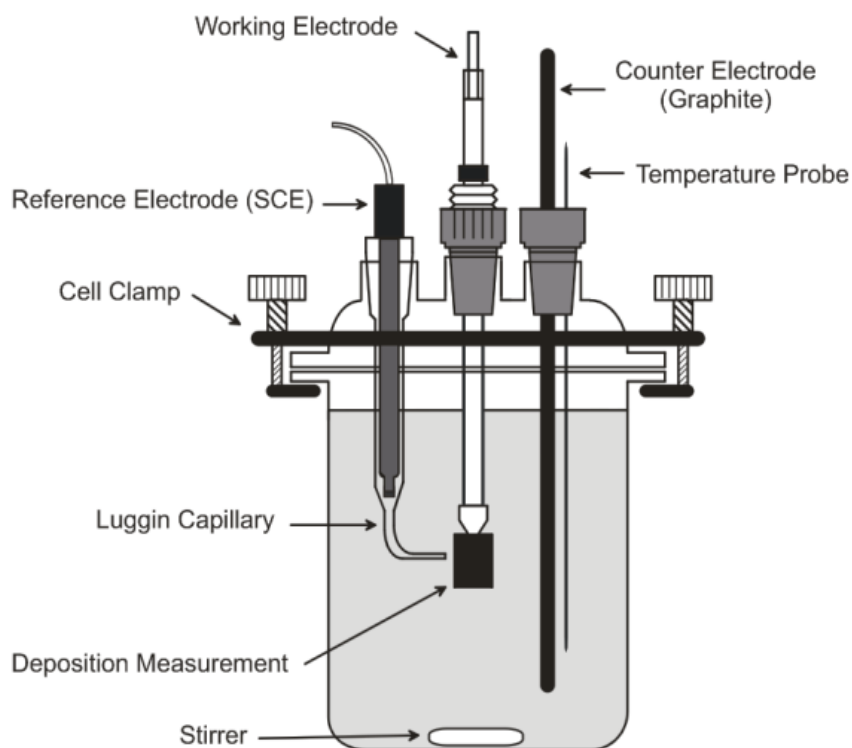
Figure 8.2 Configuration of the experimental system for mineral deposition studies by EIS in batch reactor experiments.

The electrodes were connected to a potentiostat (Series G300, Gamry, Warminster, PA) capable of producing AC signals in the frequency range of 10 µHz to 300 kHz. The associated EIS300 software (Echem Analyst, version 6.0) was used for data acquisition, processing, and equivalent circuit model fitting.

For concomitant EIS and mineral mass deposition measurements in a flow-through system, a bench-scale recirculation system was developed (Figure 8.3) in which pipe sections were modified to accommodate the three-electrode configuration for EIS measurements, and SS circular disc specimens (surface area 5.61 cm2) for mass gain measurements (see inset of Figure 8.3b). The solution was circulated through the PVC pipe at a flow velocity of 0.57 m/s and SS

disc specimens were periodically removed to measure the mass of accumulated mineral deposit with time.
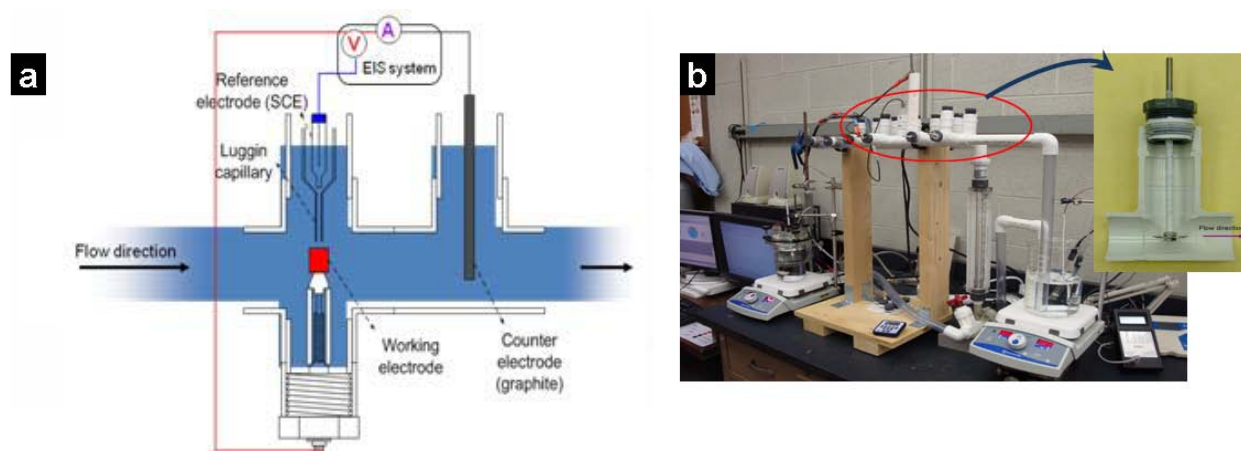
Figure 8.3 Customized bench-scale water recirculation system for simultaneous measurements of EIS and mineral mass deposited.

a) Schematic of the three electrode system for EIS measurements in bench recirculating experiments. b) Photograph of the water recirculating system. Inset shows circular stainless steel disc specimen used to collect mineral deposits.

The chemical equilibrium model MINEQL+ [48] was used to predict the total mass concentration of precipitate that will form at equilibrium under the experimental conditions employed.

8.3.2 EIS Experiments

The volume of the Pyrex cell shown in Figure 8.2 was 900 mL, in which 700 mL of working solution was maintained at 40 °C and stirred at 300 rpm. DI water was added to the cell before chemical addition. The electrodes were then immersed in the DI water to allow temperature

equilibration and the removal of gas bubbles formed on the WE surface. Chemicals were introduced sequentially from 10× concentrated stock solutions. To avoid possible pre-experiment chemical reactions, the $CaCl_2$ stock solution was added last. While other chemicals were added all at once with a 26-mL glass pipette, the Ca solution was added more slowly using a syringe pump to avoid potential local precipitation at the point of addition. When the addition of chemicals was completed and the solution pH was adjusted to 7.5 with HCl or NaOH, all the ports of the cell lid were sealed with Parafilm to prevent airborne particles and atmospheric CO_2 from entering the system. Solution conductivity was continuously monitored until bulk precipitation took place, as indicated by a fast decrease in conductivity measurements. EIS measurements were started when the bulk precipitation was occurring. Triplicate experiments were carried out for each precipitation condition with different minerals.

For each EIS measurement, the intrinsic electric potential of the WE-solution interface (or the open circuit potential, OCP) was determined first and then the AC potential was set at ± 10 mV (rms) around the OCP. Excessive AC perturbations were avoided to minimize the electric current generated at the WE surface that may cause surface reactions. A frequency range of 10 mHz to 10 kHz was used to ensure data quality for subsequent model fitting. The low end of frequency measurements was set at 10 mHz so that the total measurement time was less than 3 min. The electrochemical system was a dynamic sample and it was important to make real-time measurement quickly. The measurement time of 3 min was comparatively very short during the mineral deposition process, which usually took hours and days.

For the experiments involving concomitant mineral mass determination, the SS disc specimens were cleaned before use by ultrasonic wash in an acetone/ethanol solution (1:1 volume ratio) for 5 min, rinsed with DI water and air-dried in a laminar flow hood. At

predetermined time intervals during an experiment, the specimens were removed from the circulating water through the sampling ports. The bulk water remaining on the disc surface was carefully removed by paper tissue without disturbing the solid deposit on the surface. The discs were then air-dried under laminar airflow for at least 48 hr and the mass of each disc was measured using an analytical balance (Mettler AE163, detection limit 0.01 mg). Final weighing was performed only when a constant mass was achieved (mass measurement variation < 0.05 mg/hr). Three measurements were taken for each disc specimen and the average was used as the reported mineral mass on the disc.

8.4   RESULTS AND DISCUSSION

8.4.1   Changes of CPE Capacitance over Time due to Mineral Deposition

The batch reactor experimental system depicted on Figure 8.2 was used to obtain EIS data at predetermined times while mineral deposition took place on the surface of the stainless steel (SS) working electrode (WE). Figure 8.4 shows representative EIS measurements after 1 hr of mineral deposition in the batch reactor system containing calcium and phosphate (i.e., test solution #4 in Table 8.1). For illustration, the following detailed discussion of EIS modeling is based on the data collected from the test solution #4.
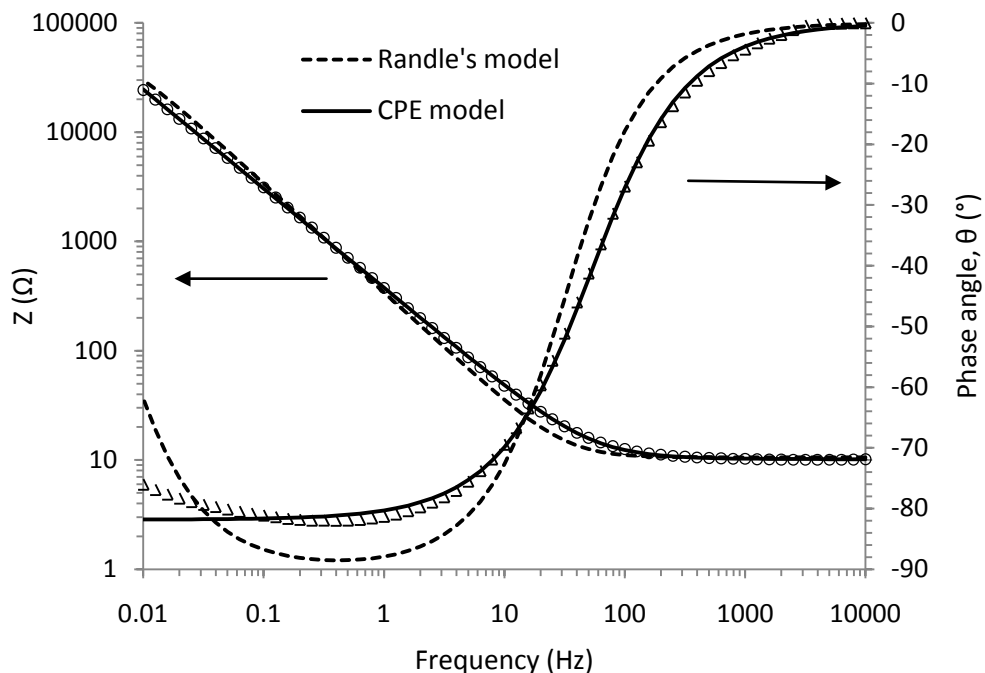
Figure 8.4 Representative EIS measurement on the stainless steel WE surface in the batch reactor system when the Ca-P deposition took place for 1 hr.

This measurement corresponds to the number 4 experiment with Ca-P in Table 8.1. Data points represent EIS measurement results. Dashed lines are model fitting with the Randle's circuit (cf. Figure 8.1b) and solid lines are model fitting with the CPE model (cf. Figure 8.1c). EIS experimental conditions: AC potential perturbation ±10 mV biased at the system's open circuit potential (OCP); frequency scan from 10^{-2} to 10^{4} Hz; data sampling at 10 points/decade.

Before model fitting, the quality of the EIS data was evaluated with the Kramers-Kronig module in the Echem Analyst software (Gamry, Warminster, PA). Only the data that were K-K compliant, i.e., linear, causal, and stable, were used for model fitting. The equivalent circuit was fit to the data using the Simplex algorithm. The EIS300 overlays the fit onto the data and generates a goodness-of-fit (GOF) coefficient that related to the residual errors after the model fitting. To obtain useful information from the EIS data, different equivalent-circuit models were applied to the data. With the Randle's model, the fit was unsatisfactory as evidenced by a calculated GOF coefficient of 4% (a smaller value of GOF coefficient is desirable for a better fit). On the other hand, the CPE model fitted the data better (solid lines on Figure 8.4), which was also evidenced by a much smaller GOF coefficient, 0.04%. Several CPE model parameters were obtained from the fit. An enormous magnitude of the polarization resistance ($R_P = 1 \times 10^{35}$ kΩ) agreed with the stainless steel used as the electrode material (i.e., extremely high polarization resistance); the capacitance (Y_o) was around 4×10^{-4} F/cm^2, which is reasonable in that values in the range of 10^{-4}–10^{-3} F/cm^2 are often reported in the literature [42].

To detect changes at the electrode surface during mineral deposition, EIS data were obtained at different times and corresponding CPE capacitance values were calculated using the CPE model. Figure 8.5 shows the changes of EIS at two representative times of 1 hr and 52 hr for the batch reactor experiments with test solution #4. The corresponding CPE model parameters are provided in Table 8.2. The GOF coefficients are satisfactorily small, indicating good model fitting with the CPE model. A slight increase in solution resistance, R_s, is expected because of the decrease of solution conductivity due to mineral precipitation. Changes in the CPE capacitance (Y_o) reflect changes incurred by mineral deposition at the electrode surface. Figure 8.6 shows the entire time course of changes in Y_o for calcium phosphate deposition.
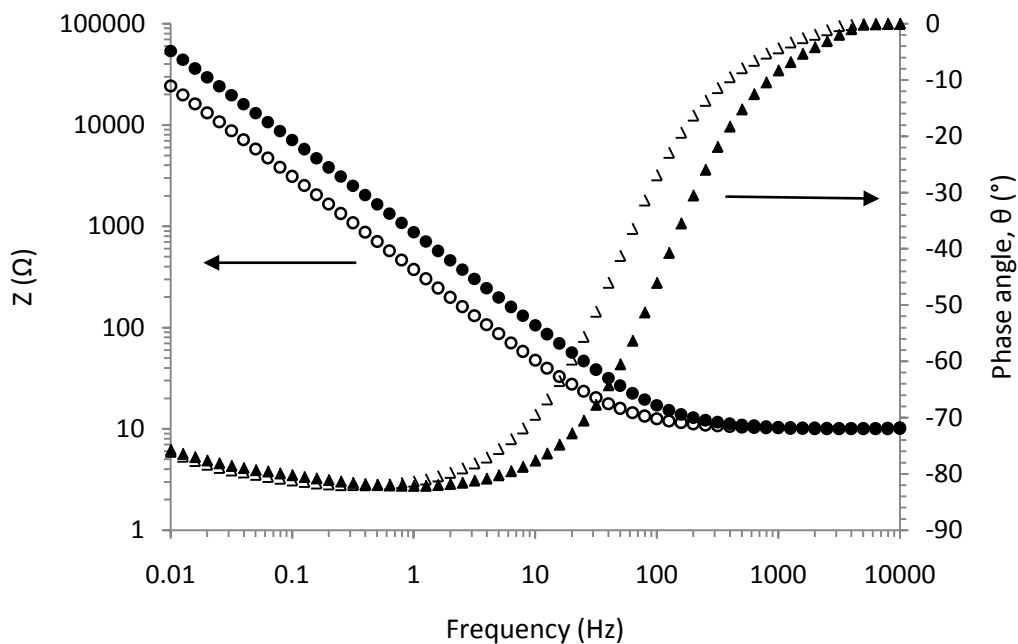
Figure 8.5 EIS measurements in batch reactor tests with test solution #4 at two different times.

Unfilled symbols are results of measurements made at 1 hr, while filled symbols are measurements made at 52 hr.

Similarly, in the batch reactor experiments with other test solutions (test solutions #2 and #3), the EIS measurements were able to track the progress of mineral deposition with time (test solution #1 was used as a control experiment). It is not clear, however, whether the EIS is sensitive to the characteristics of different mineral deposits. This question cannot be answered without a connection of the model parameter with the physical properties of the mineral layer deposited, such as the surface area exposed to solution, or the deposit layer thickness. Unfortunately, neither the thickness nor the exposed area of the layer is well defined for the mineral deposits, particularly during early stages of deposition when trace amounts are deposited to only form a rough, nonuniform, and porous layer. This makes both the layer thickness and the cover ill defined and difficult to measure experimentally. For this reason, we measured instead

171

the cumulative mineral mass deposited when the EIS data were collected, and correlated the changes of CPE capacitance to the mineral mass deposited. Details of the correlation are discussed in the next section.
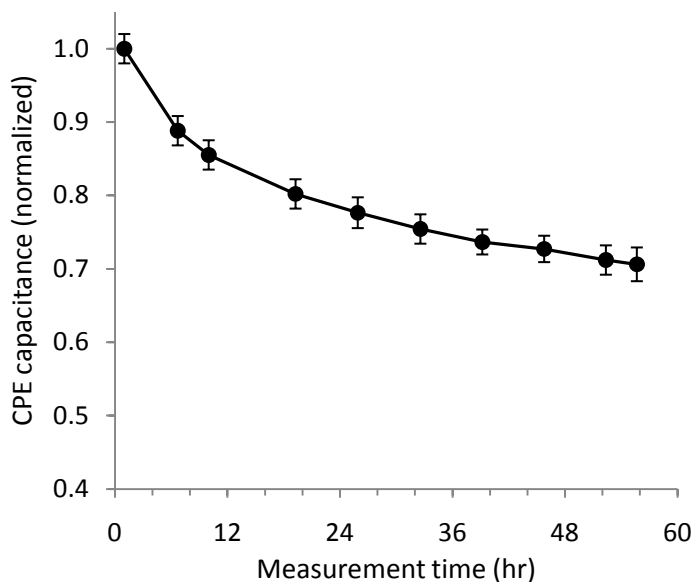
Figure 8.6 Decrease of CPE capacitance Y_0 due to calcium phosphate deposition on the stainless steel working electrode in batch reactor tests with test solution #4.

Error bars indicate the standard deviation of triplicate experiments.

8.4.2   Correlation of CPE Capacitance and Mineral Mass Deposited

A water recirculating system (Figure 8.3) was used to obtain simultaneous measurements of (a) capacitive characteristics of the mineral layer on the SS working electrode using EIS and (b) the mass accumulation due to mineral deposition. Mineral mass deposited was determined using a series of SS circular disc specimens that were immersed in a supersaturated solution of test

mineral. For each individual experiment, six disc specimens were used to provide substrate surface for mineral deposition. Each experiment was repeated three times. At predetermined time intervals when the EIS measurements were taken, the pre-weighed SS circular discs were withdrawn from the test solution for final weighing, which was conducted in triplicate. In parallel to the mineral mass measurements, an extra disc immersed in DI water (batch mode only) was subjected to the same cleaning, drying, and weighing procedure to check for potential artifacts due to specimen processing. No substantial mass changes were detected on this control disc before and after each experiment, ensuring that air-borne deposits and the cleaning steps did not interfere with the mineral mass determination.

Figure 8.7 shows the data collected from the recirculating system experiments with test solution #4 (calcium phosphate)—loss of CPE capacitance vs. mineral mass deposited. A linear regression of the data was applied. An analysis of residual errors (not shown) of the regression indicated that the distribution of errors was random around zero, not skewed to either direction, thereby indicating that a normal distribution of the EIS parameter (i.e., loss of the CPE capacitance) with respect to the mineral mass accumulation is statistically reasonable.
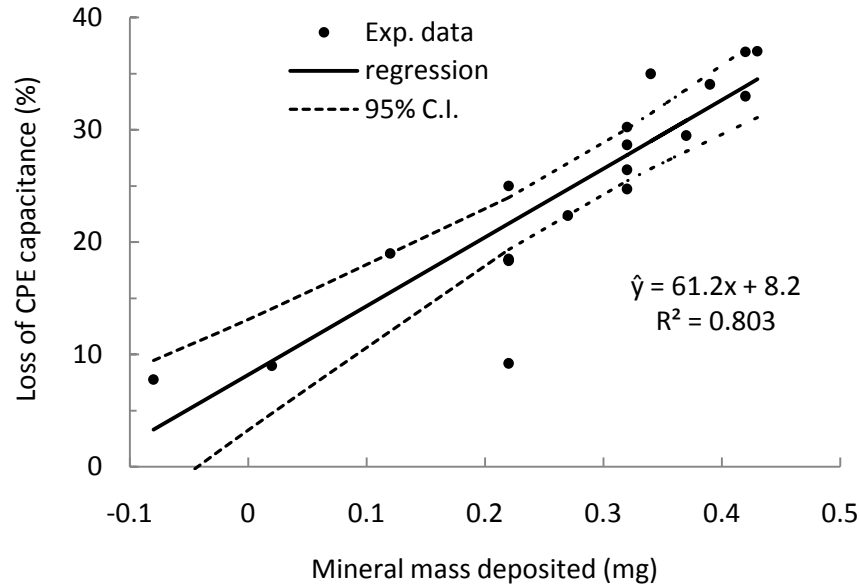
Figure 8.7 Loss of CPE capacitance (%) vs. mineral mass deposited (mg) for test solution #4.
Data were collected for Ca-P deposition on the stainless steel surface in a water recirculating system (40 °C, pH 7.5, 3 gpm of flowrate or 0.57 m/s flow velocity).

The linear regression model was used to develop a relationship between the loss of the CPE capacitance due to mineral deposition and the mass of the mineral deposits accumulated on the SS surface over time. For example, the loss of CPE capacitance due to Ca-P accumulation is given by

$$\text{Loss of CPE capacitance } (\%) = 61.2 \times \text{mineral mass deposited} + 8.2 \qquad (7)$$

where the capacitance loss is expressed as percentage and the mineral mass is in mg on the total area of a disc specimen (5.61 cm^2). The relatively large ratio of capacitance loss to mineral mass deposited (the slope) indicates that EIS measurement can be a sensitive technique to detect small changes in surface mass deposition.

To assess the statistical significance of the responses of the CPE capacitance to changes in deposition, the mean ± 95% confidence interval for the CPE capacitance loss as a function of mineral mass deposited is also presented in Figure 8.7. Sixteen out of the 18 data points fall closely "within" the 95% confidence interval, suggesting that the linear regression is a reasonable model for the relationship between the mineral mass measurements and the EIS measurements of the CPE capacitance loss. Furthermore, the significance of the slope obtained by the linear regression was evaluated by an *F* test based on the analysis of variance (Table 8.3). The small *p*-value (much smaller than 0.05) indicates that the regression is robust, meaning that the linear relation between the CPE capacitance loss and the mineral mass deposited is statistically strong.

Table 8.3 Analysis of Variance (ANOVA) for linear regression of the the EIS parameter, loss of CPE capacitance, and the mineral mass deposited ǂ. Data given in Figure 8.7

Source	Degree of Freedom	Sum of Squares*	Mean Squares	*F* value	p-value
Regression	1	1225.7	1225.7	65.2	4.92E-07
Residual	16	300.8	18.8		
Total	17	1526.5			

ǂ *F*-test follows standard procedures outlined in *Introduction to the Practices of Statistics* by Moore and McCabe, W. H. Freeman and Company, New York, 1998.

* $R^2 = 1225.7/1526.5 = 0.8029$ and adjusted $R^2 = 0.7906$.

8.4.3 Effects of Mineral Deposit Composition on CPE Capacitance

Following the same experimental procedures as described with the calcium phosphate solutions, the changes in CPE capacitance, Y_o, during the deposition of different calcium minerals, and the mineral mass deposited, were measured under identical experimental conditions in the recirculating system tests. Starting with supersaturated solutions, the precipitation reactions of calcium sulfate, calcium carbonate, and calcium phosphate were expected to generate comparable amounts of mineral solids, as calculated by the chemical equilibrium model MINEQL+. The tests with solutions of calcium nitrate, which is highly soluble, served as a control. The EIS measurements and mineral mass deposition data for calcium carbonate and calcium sulfate were then subjected to similar statistical analyses. The impact of mineral deposition on the CPE capacitance reduction, i.e., the linear regression between CPE capacitance and mineral mass, is summarized on Figure 8.8 for different mineral scales evaluated in this study. The p-values for the F tests, obtained for the linear relationship between CPE capacitance loss and mineral mass deposited, were 3.36×10^{-7} and 5.02×10^{-7} for calcium carbonates and calcium sulfate, respectively.

Interestingly, the chemical properties of the mineral scale did not appear to impact the EIS measurements significantly. The relatively constant b values across the three different minerals suggest that the characteristics of each individual mineral did not influence the EIS measurements significantly. This finding reinforces the direct relationship between the CPE capacitance and the mass of mineral deposits. We note that the supersaturated mineral solutions used in this study were designed to produce the same amount of precipitates at equilibrium (Table 8.1). However, different amounts of mineral deposits were collected on the SS disc

specimens within similar experimental periods (less than 60 hr), which produced different CPE behavior in EIS. Even so, the correlation between the CPE capacitance and the mineral mass deposited was essentially constant for the different minerals tested. Hence, the EIS method can be used to replace the traditional gravimetric method to detect mineral deposition on a surface with more sensitivity for mineral mass but with indiscrimination toward different minerals, at least for common calcium minerals, which is convenient if one cares primarily about the total amount of deposits on a surface.

$$b = \frac{\text{reduction of CPE capacitance (\%)}}{\text{mineral mass deposited (mg/cm}^2)}$$
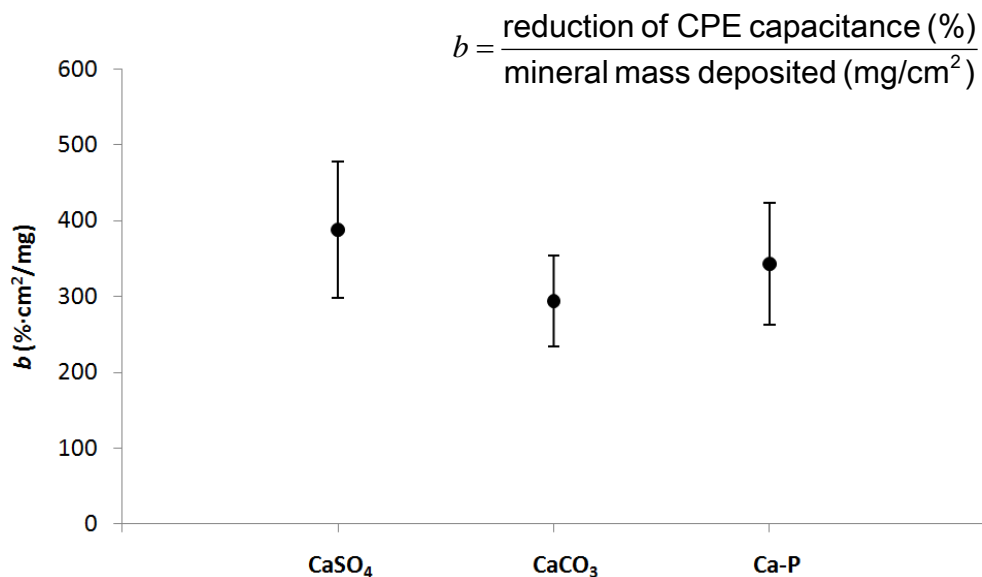
Figure 8.8 Reduction of CPE capacitance normalized to mineral mass deposited per unit surface area for different mineral deposits studied.

Error bars indicate ± 95% Confidence Interval (C.I.).

8.4.4 Frequency Range Analysis

The EIS data obtained in this study were based on the impedance measurements across a broad range of frequency, i.e., 10 mHz to 10 kHz, which can only be accomplished with an EIS system capable of producing AC signals in such a wide range. However, the EIS method for mineral deposition detection may still be viable when the impedance measurements are performed for narrower ranges of frequency, and perhaps even at a single AC frequency. Thus, simpler EIS instruments that produce a narrow range of AC frequency may be used for mineral mass detection, thereby saving both measurement time and equipment cost.
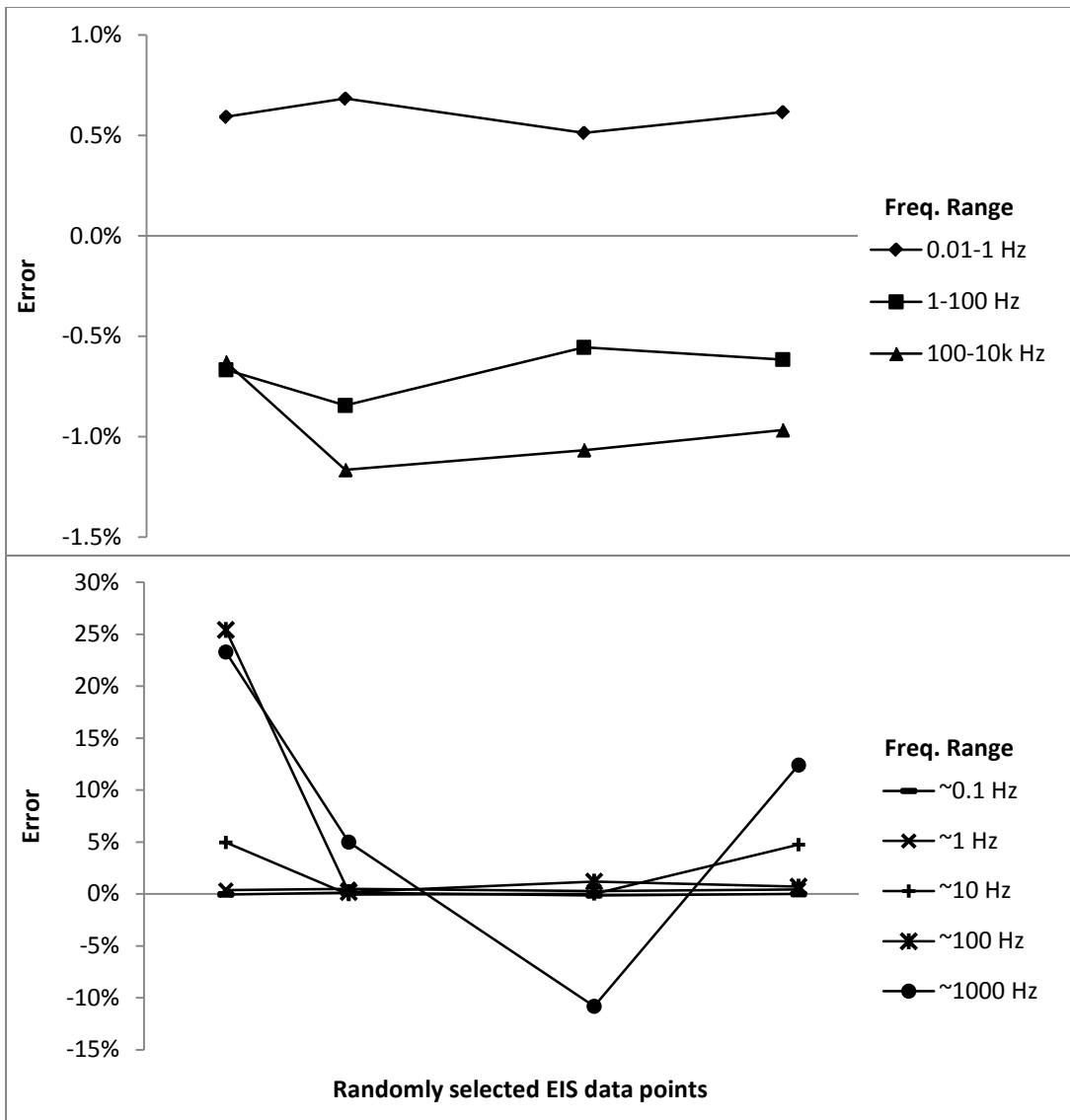
Figure 8.9 Analysis of the frequency-dependent accuracies of EIS measurements.

The data points for analysis were randomly selected from the entire experimental range for calcium carbonate bench-scale recirculating experiments. For each data point, the CPE model was fitted to the selected frequency ranges and the Y_0 values were obtained and compared to the Y_0 value obtained based on the entire frequency range (10 mHz to 10 kHz). In the lower panel, the frequency ranges used for the re-fitting are $\pm 10\%$ of the specific frequencies listed.
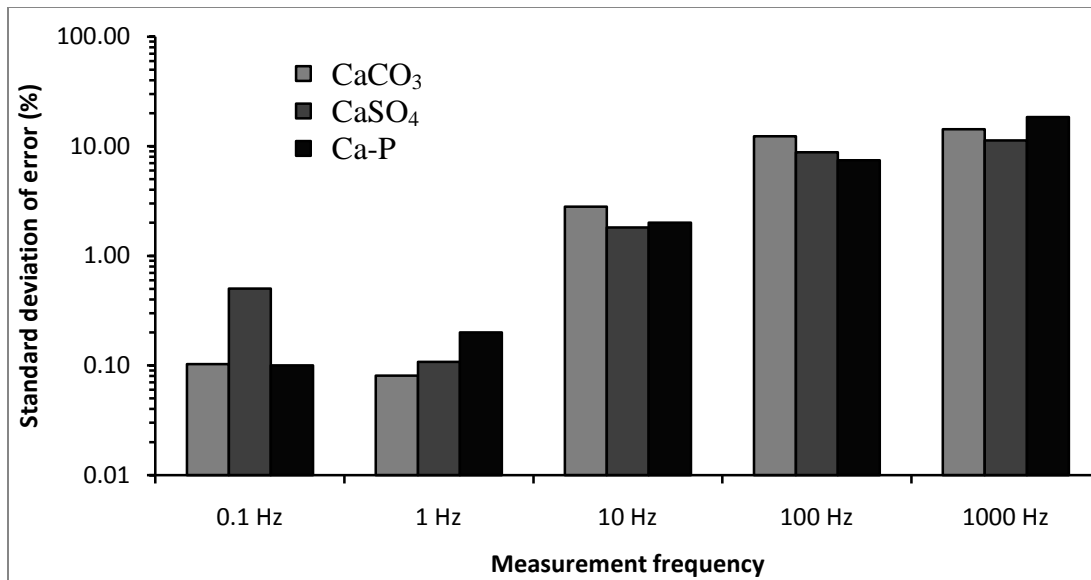
Figure 8.10 Standard deviation of the errors of the Y_0 values obtained for $CaCO_3$ system EIS measurements. The data were according to Figure 8.9 at the specific frequencies ($\pm 10\%$) as compared to the Y_0 value obtained based on the entire frequency range (10 mHz to 10 kHz).

To examine this proposition, the EIS data for $CaCO_3$ deposition were examined as an example. The CPE capacitance of four randomly selected measurements out of the total of 18 measurements over the full frequency range (i.e., 6 decades from 10 mHz to 10k Hz) were re-evaluated based on narrower frequencies. Figure 8.9 (upper panel) shows that the Y_0 values obtained using 2-decade frequency ranges (10 mHz – 1 Hz, 1 Hz – 100 Hz, and 100 Hz – 10 kHz) were very similar to Y_0 values obtained from fitting the entire data range. However, when the model fitting frequencies were further narrowed to near single-frequencies (Figure 8.9 lower panel), the errors of Y_0 values were significantly larger, especially for the higher frequencies. Indeed, at higher frequencies, capacitive properties of the deposit layer, such as Y_0, become more responsive to frequency shifts [42]. Figure 8.10 summarizes the errors for all the three minerals tested under single frequency measurements at indicated frequencies $\pm$ 10%. The data indicate that EIS measurements at 0.1 Hz or 1 Hz frequency range would produce Y_0 values only slightly different from those measured based on the entire six decades of frequencies. These much narrower frequency ranges can be potentially used with a customized simple EIS device for the detection of mineral mass deposition, without sacrificing measurement accuracy.

8.5   CONCLUSIONS

The Electrochemical Impedance Spectroscopy (EIS) method was applied to study mineral deposition from precipitation reactions in aqueous solutions. The values of constant-phase element (CPE) capacitance were obtained from the EIS data for three calcium minerals: calcium carbonate, calcium sulfate, and calcium phosphate—the most commonly occurring mineral solids in municipal and industrial water processes, such as cooling water systems and water

distribution networks. The CPE parameter was successfully correlated, with statistical verification, to the amount of the mineral mass deposited. Furthermore, the correlation proved to be constant across the three minerals tested, indicating the usefulness of this EIS technique as a new, more sensitive, in situ detection method to replace the traditional gravimetric measurements of mineral mass deposited on surfaces in water systems, even for systems with multiple mineral deposits. In addition, the possibility of conducting the EIS measurements within narrow frequency ranges was examined, and it was found that narrow frequency ranges can be used to obtain CPE capacitance values without losing measurement accuracy.

9.0   EXPANDED APPLICABILITY OF ELECTROCHEMICAL IMPEDANCE SPECTROSCOPY (EIS) FOR MINERAL DEPOSITION MONITORING UNDER BROAD WATER CHEMISTRIES

An EIS method for the detection and quantification of mineral deposition has been established in Chapter 8. Different minerals of common interests have been tested in simple aqueous solutions containing solely the involved mineral constituents. In this chapter, the applicability of the EIS method for mineral deposition detection is expanded under broad water chemistries in solutions containing multiple minerals. With a two-mineral system of calcium carbonate and phosphate, the linear relationship between the changes of the CPE capacitance obtained from EIS and the mineral mass deposited on the surface of disc specimens was proved to be valid. This linear relationship still held even with a synthetic municipal wastewater (MWW) containing a variety of dissolved species. Besides the validation of the EIS method with multiple minerals, the method was also evaluated under the influence of polymaleic acid (PMA), one of the most effective antiscaling chemicals tested in cooling systems using treated MWW. The presence of PMA in solution did not show significant impacts on the EIS method. However, chlorine-based biocides substantially altered the impedance signals collected using EIS and made the subsequent data processing for the evaluation of the CPE capacitance difficult. Monochloramine was less detrimental than free chlorine thanks to its less aggressive oxidation power. To obtain reliable

modeling outputs from the EIS data collected in the presence of chlorine biocides, narrower scan ranges around 1-10 Hz should be used.

9.1   INTRODUCTION

In Chapter 8, an accurate and convenient approach for monitoring the rate of mineral deposition on metals in real time has been developed by means of an electrochemical cell employing the same metal material as a working electrode. The electrical impedance of the metal-solution interface was measured by Electrochemical Impedance Spectroscopy (EIS). The interfacial capacitance obtained from the EIS data was used as a measure of surface coverage by mineral scale. An equivalent-circuit approximation was adopted to evaluate the distributed dielectric permittivity of minerals, which was reported as the capacitance of constant-phase element (CPE). The results show that the CPE capacitance correlated very well with the mass of mineral deposits accumulated on the metal surface immersed in simple solutions containing single minerals. Moreover, the characteristics of different minerals evaluated in this study, i.e., calcium carbonate, sulfate, and phosphate, did not significantly affect the measurements of the CPE capacitance. Rather, the CPE capacitance was sensitive to small changes in the mineral mass deposited on the electrode (< 0.1 mg). It is established that the EIS, unlike traditional methods, is a nondestructive method that allows in situ semi-continuous measurements of overall mineral deposition.

The objective of this chapter was to expand the applicability of the EIS method for mineral deposition under broad water chemistries and in solutions containing multiple minerals. First, a two-mineral system of calcium carbonates and phosphates was tested for the linear

relationship between the changes of CPE capacitance and the mineral mass deposited on the surface of disc specimens. Similar experiments were then carried out in a synthetic municipal wastewater (MWW) containing a variety of dissolved solids. Besides the validation of the EIS method with multiple minerals, the method was also evaluated under the influence of polymaleic acid (PMA), one of the most promising antiscaling chemicals tested in cooling systems using treated MWW. The primary concern with PMA is that some of the PMA added in solution may adsorb onto the surface of the working electrode and thus interfere with the EIS data collection. Besides PMA, chlorine-based biocides were also tested to check for their potential interferences with the electrode. Both free chlorine and monochloramine were tested.

9.2 EXPERIMENTAL SECTION

Materials and Methods. Solutions were made in DI water (resistivity > 18 MΩ-cm) with the addition of chemical constituents (reagent grade or better). Calcium was provided as $CaCl_2$, magnesium as $MgCl_2$, phosphate as Na_2HPO_4, carbonate as Na_2CO_3, sulfate as Na_2SO_4, nitrate as $NaNO_3$. Solution pH was adjusted to 7.5 with 0.1 M HNO_3 or NaOH. For the two-mineral system, the initial concentrations of the mineral ions are listed in Table 9.1. For the synthetic municipal wastewater, the chemical recipe is provided in Table 9.2.

The cell configuration for EIS measurements of mineral deposition is depicted in Figure 8.2a. The experimental conditions employed in this chapter were exactly the same as those described in Chapter 8.

Table 9.1 The 2-Mineral Test Solution Used in Both EIS and Mineral Mass Measurements at pH 7.5 and 40°C. The Amount of Equilibrium Precipitation Was Calculated by MINEQL+ (version 4.6)

#	Mineral	$[Ca]_T^*$ mM	$[Anion]_T$ mM	Expected Precipitates mg/L
1	$CaCO_3$	5.7	2.2	193
2	$Ca_5(PO_4)_3(OH)$	5.7	1.2	193

* Total concentrations added.

Table 9.2 Chemical Recipe for Synthetic Municipal Wastewater

Component	Ca	Mg	Na	K	HCO_3	PO_4	SO_4	Cl	NH_4 (as N)
Total Concentration (mM)	7.6	7.2	26.9	0.7	13.4	0.2	2.8	31.1	7.0

Note: The recipe reflects average values of secondary MWW quality from several sources.

For concomitant EIS and mineral mass measurements, the batch reactor system modified based on the batch setup is shown in Figure 8.3. Detailed experimental conditions are described in Chapter 8.

EIS Experiments. The volume of the Pyrex cell used for batch tests was 900 mL, in which 700 mL of working solution was maintained at 40 °C and stirred at 300 rpm. DI water was added to the cell before chemical addition. The electrodes were then immersed in the DI water to allow temperature equilibration and the removal of gas bubbles formed on the WE surface. Chemicals were introduced sequentially from 10× concentrated stock solutions. To avoid possible preemptive chemical reactions, the $CaCl_2$ stock solution was added last. While other chemicals were added with a 25-mL glass pipette, the Ca solution was added more slowly using a syringe pump to avoid potential local precipitation at the point of addition. When the addition of chemicals was completed and the solution pH was adjusted to 7.5 with HNO_3 or NaOH, all

the ports of the cell lid were sealed with Parafilm to prevent airborne particles and atmospheric CO_2 from entering the system. Solution conductivity was continuously monitored until bulk precipitation took place, as indicated by a fast decrease in conductivity. EIS measurements were started when the bulk precipitation was occurring. Triplicate experiments were carried out for each precipitation condition with different minerals.

For each EIS measurement, the intrinsic electric potential of the WE-solution interface (or, the open circuit potential, OCP) was determined first and then the AC potential was set at ± 10 mV (rms) around the OCP. Excessive AC perturbations were avoided to minimize the electric current generated at the WE surface that may cause surface redox reactions and change the local pH. A frequency range of 10 mHz to 10 kHz was used to ensure data quality for subsequent model fitting. The low end of frequency measurements was set at 10 mHz so that the total measurement time was less than 3 min [1].

For the experiments involving concomitant mineral mass determination, the SS disc specimens were cleaned before use by ultrasonic wash in an acetone/ethanol solution (1:1 volume ratio) for 5 min, rinsed with DI water and air-dried in a laminar flow hood. At predetermined time intervals during an experiment, the specimens were taken out of the circulating water through the sampling ports. The water remaining on the disc surface was carefully removed with paper tissue, without disturbing the solid deposit on the surface. The discs were then air-dried for at least 48 hr and the mass of each disc was measured using an analytical balance (Mettler AE163, detection limit 0.01 mg). Final weighing was performed only after a constant mass was achieved (variations between mass measurements < 0.05 mg/hr). Three measurements were taken for each specimen and their average was used as the mineral mass on the disc.

Influence of Antiscalants and Chlorine Biocides on EIS. The potential influence of antiscalants on the EIS results was studied by adding polymaleic acid (PMA) to the Pyrex cell batch reactor containing 10 mM of KCl solution at pH 7.5. The standard 3-electrode setup (Figure 8.2) was used. The reference electrode (RE) was a standard Ag/AgCl electrode. Chlorine biocides, in the form of free chlorine (HOCl/OCl$^-$) or monochloramine (NH$_2$Cl), were also tested with the same batch reactor setup. Solution temperature was maintained at 40°C. The electrochemical measurements were performed after 10 min and 5 hr of the addition of either PMA or a biocide. The solution was stirred with a teflon-lined magnetic stirrer at 300 rpm. The EIS signals collected in the presence of the additives were compared with the signals collected in the absence of the additives. The influence of the chemical additives on EIS is determined by the extent of data distortion incurred due to the addition of the chemicals.

9.3   RESULTS AND DISCUSSION

EIS Applicability in Two-Mineral Systems. In Chapter 8, calcium carbonate, calcium phosphate, and calcium sulfate were tested individually to establish the EIS method as a new approach to detecting mineral deposition. Figure 9.1 shows the linear relationship between the mineral mass deposited and the changes of CPE capacitance evaluated from the EIS data for aqueous systems supersaturated with both calcium carbonate and calcium phosphate. The linear regression line fits the experimental data reasonably well. Ten of the sixteen data points collected from repeating experiments fall within the 95% confidence interval. Also, the regression residuals are reasonably random around zero, not skewed to either direction, indicating that the linear relationship between the two variables is statistically sound.
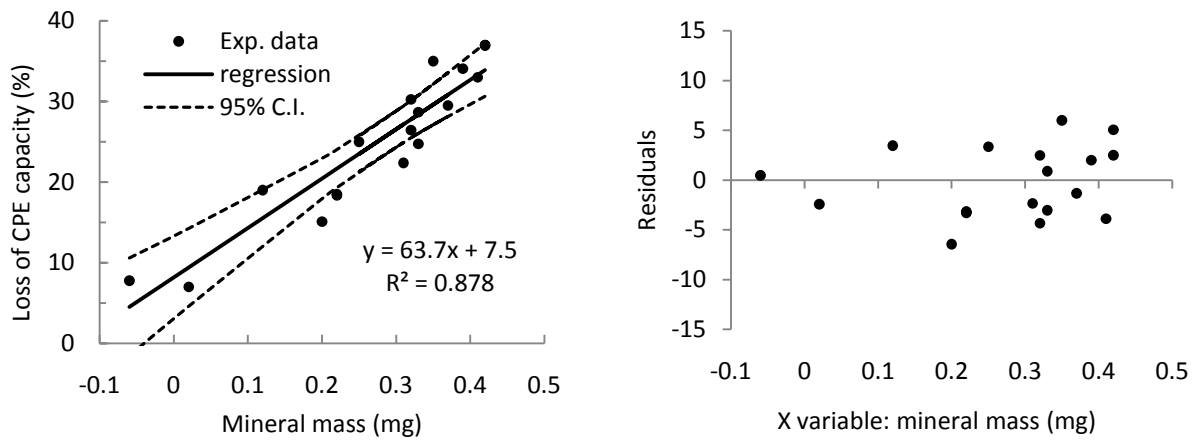
Figure 9.1 Scatter plot (left) and residuals plot (right) of the data from simultaneous EIS and mineral mass measurements ($CaCO_3$ + CaP).

Data were collected for $CaCO_3$ + CaP deposition on the stainless steel surface in a water recirculating system (40 °C, pH 7.5, 3 gpm of flowrate or 0.57 m/s flow velocity).

EIS Applicability in Synthetic Municipal Wastewater. Figure 9.2 shows the linear relationship between the mineral mass deposited and the changes of CPE capacitance evaluated from the EIS data for a synthetic municipal wastewater pre-concentrated four times. Following a similar statistical analysis procedure as that used in Figure 9.1, the linear regression appears to be reasonably strong in the case of synthetic municipal wastewater.
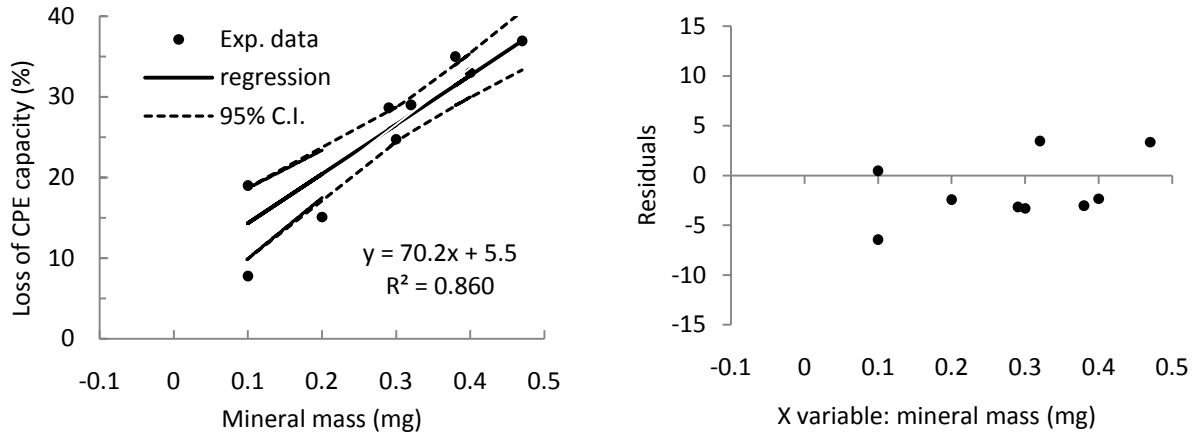
Figure 9.2 Scatter plot (left) and residuals plot (right) of the data from simultaneous EIS and mineral mass measurements (MWW).

Data were collected for mineral deposition on the stainless steel surface in a water recirculating system using a synthetic municipal wastewater (40 °C, pH 7.5, 3 gpm of flowrate or 0.57 m/s flow velocity).

Figure 9.3 summarizes the linear relationship between the EIS parameter (i.e., the CPE capacitance) and mineral mass for the five mineral aqueous systems tested in Chapters 8 and 9. The *b* value, which is the ratio of the reduction in CPE capacitance (in %) and the mineral mass deposited on specimen discs (in mg/cm^2), corresponds to the slope of the regression line in data plots such as those depicted in Figure 9.1 andFigure 9.2. The relatively constant *b* values across different mineral solids suggest that the chemical characteristics of the deposit layer do not actually play an important role in determining the EIS signal. The EIS signal correlated very well with the amount of mineral solids deposited on the surface of the electrode. As a result, the EIS method can be used to replace the traditional gravimetric method with regard to mineral scale detection.

$$b = \frac{\text{reduction of CPE capacitance (\%)}}{\text{mineral mass deposited (mg/cm}^2)}$$
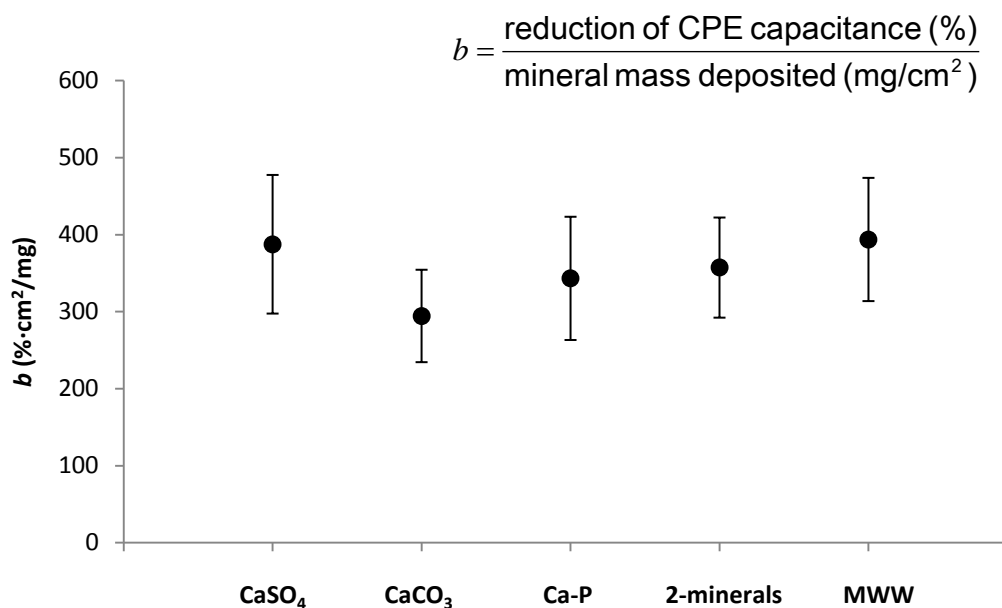
Figure 9.3 CPE capacitance vs. mineral mass deposited: the ratio (*b* value) of reduction of the CPE capacitance and the mineral mass deposited per surface area for different minerals.

Error bars indicate ± 95% Confidence Interval (C.I.).

Influence of PMA on EIS. Figure 9.4 shows the EIS at the stainless steel working electrode (WE) surface before and after PMA addition (5 ppm) in a 10 mM of KCl solution. Compared to the EIS collected without PMA, the addition of PMA (5 ppm) did not effect any significant changes in EIS, even after 5 hr of contact with PMA. The capacitive impedance became slightly greater in the presence of PMA only toward the end of the low AC frequencies (the Nyquist plot of Figure 9.4). This slight increase of the capacitive impedance is expected in that the PMA molecules present near the electrode surface in solution can serve as a diffusional barrier that increases charge transfer resistance, which is a major contributor to the capacitive impedance [2]. However, this influence did not impact the CPE evaluation in the Bode plot (Figure 9.4), which produced CPE capacitance values in the range of 40.26 ± 0.12 $\mu F/cm^2$ in the three cases tested.
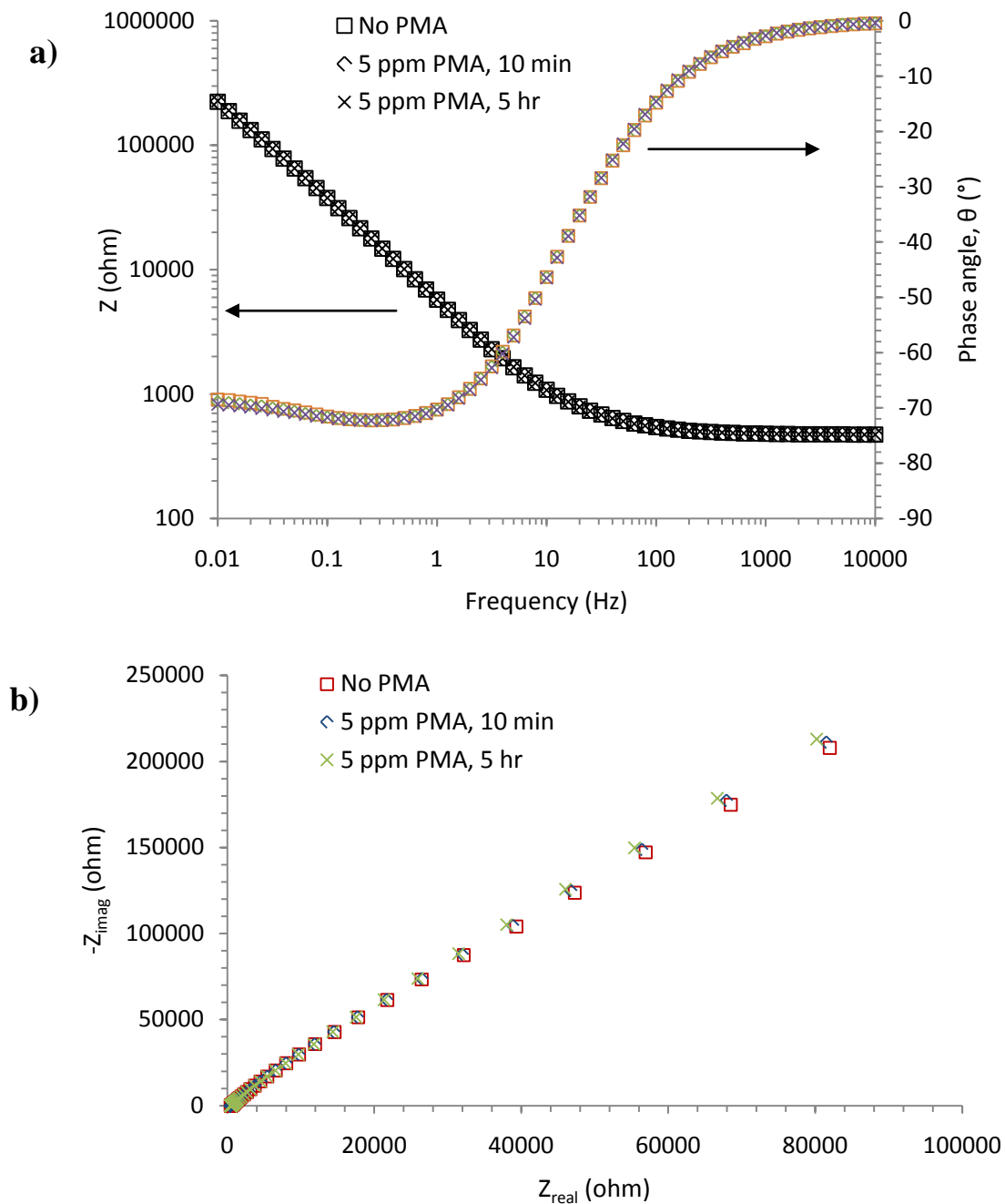
Figure 9.4 EIS at the stainless steel WE surface before and after PMA addition (5 ppm) in aqueous solution.

Solution IS I = 10 mM KCl at pH 7.5, 40 °C, and 300 rpm. EIS experimental conditions: AC potential perturbation ±10 mV biased at the system's open circuit potential (OCP); frequency scan from 10^{-2} to 10^4 Hz; data sampling at 10 points/decade. a) Bode plot, and b) Nyquist plot.

Influence of Chlorine Biocides on EIS. Figure 9.5 shows the EIS at the stainless steel working electrode (WE) surface with different chlorine biocide additions in a 10 mM KCl solution. Compared to the EIS collected without chlorine, the addition of either 1 ppm of free chlorine or 2 ppm of monochloramine substantially altered the EIS response curves. The alteration is apparent toward both ends of the AC scanning frequencies, i.e., < 0.1 Hz or > 1 kHz. The EIS in the presence of free chlorine deviated from the reference EIS (i.e., EIS collected in the absence of chlorine) to a greater extent than in the presence of monochloramine. This deviation pattern suggests that the interference of the chlorines on EIS is related to the oxidation power of the biocide, with free chlorine being more powerful than monochloramine. The standard oxidation potential of $HOCl/Cl^-$ (or OCl^-/Cl^-) is greater than that of NH_2Cl/Cl^-, i.e., E_H^0(free chlorine) = 1.5~1.6 V [3, 4] vs. E_H^0(monochloramine) = ~1.4 V [5, 6], and the measured Oxidation Reduction Potential (ORP) values of water solutions containing free chlorine can be 0.25~0.30 V greater than those containing monochloramine [7].
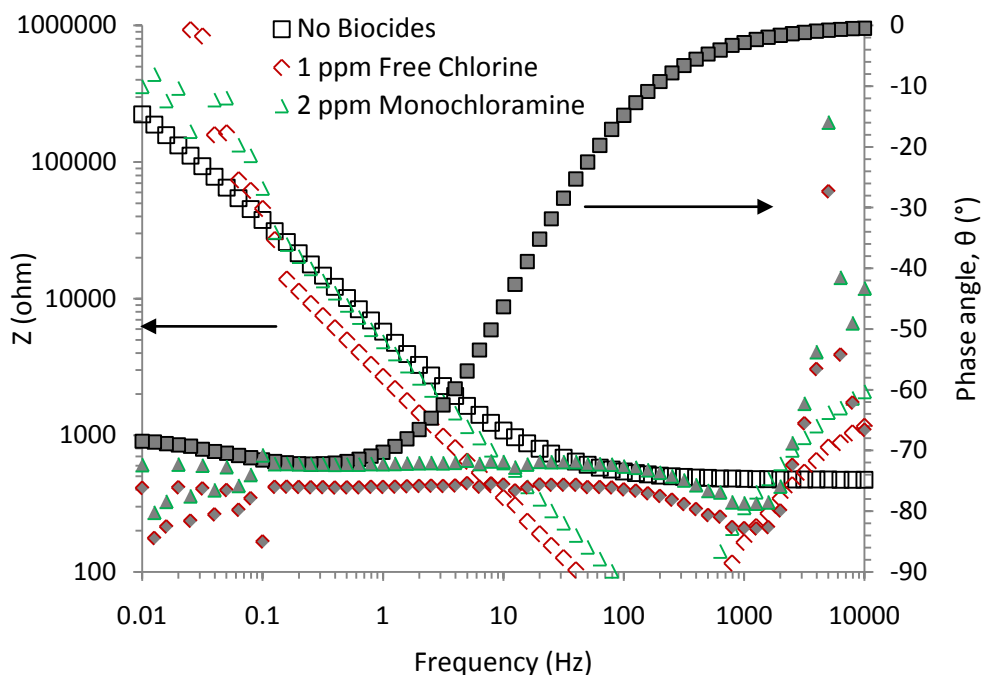
Figure 9.5 EIS at the stainless steel WE surface with or without chlorine biocides.

I = 10 mM KCl at pH 7.5, 40 °C, and 300 rpm. EIS experimental conditions: AC potential perturbation ±10 mV biased at the system's open circuit potential (OCP); frequency scan from 10^{-2} to 10^{4} Hz; data sampling at 10 points/decade. Unfilled data are impedance (vertical axis on the left) and filled data are phase angle (vertical axis on the right). Measurements were taken after 10 min of biocide addition.

In either case, the addition of the oxidative biocides significantly changed the redox potential of the aqueous solution, which translated to the fluctuations in the electrochemical properties of the electrode-water interface. Moreover, the concentrations of the chlorine was observed to be unstable in the aqueous solutions and decayed quickly (i.e., more than 40% decay in 5 hr for free chlorine and about 20% decay for monochloramine under the experimental conditions employed in this study) further adding to the rather erratic signal of EIS toward the ends of the AC frequency scan for both free and combined chlorine.

Although the EIS data obtained from the AC scan over the entire frequency range of 10 mHz-10kHz with the addition of chlorine biocides became unreliable, it was observed that the EIS over narrower ranges, around 1-10 Hz particularly, appeared to be still consistent with the EIS measured in the absence of biocides. Chapter 8 has already established that EIS in the narrow AC frequency range does not affect the accuracies of the evaluation of the CPE capacitance for the purpose of mineral deposition detection. As such, narrower scan ranges around 1-10 Hz are recommended in order to obtain reliable modeling outputs from the EIS data collected in the presence of chlorine biocides.

9.4   CONCLUSIONS

In a two-mineral aqueous system of calcium carbonate and phosphate, the linear relationship between the changes of the CPE capacitance in EIS and the mineral mass deposited on the surface of stainless steel disc specimens was proved to be valid. This linear relationship still held even in water representative of municipal wastewater (MWW) containing a variety of dissolved mineral solids and other common species (e.g., NH_4^+). Moreover, the EIS parameter (the CPE capacitance) responded primarily to the amounts of mineral solids deposited, rather than to any specific chemical properties of the individual minerals. This indiscriminating correlation between CPE and mineral mass is a valuable trait of the EIS method for mineral scaling detection.

Besides the validation of the EIS method in aqueous systems producing multiple mineral deposits, the method was further evaluated under the influence of polymaleic acid (PMA) or chlorine. PMA has shown its effective antiscaling properties tested in cooling systems using

different impaired waters, including secondary-treated MWW, passively-treated abandoned mine drainage, and coal-fired power plant ash sluicing pond effluent. The presence of PMA in solution did not show any significant impacts on EIS. However, chlorine-based biocides substantially altered the impedance signals collected using EIS and made the subsequent data processing for the evaluation of CPE capacitance difficult. EIS data processing over the entire AC frequency range became impossible in the case of free chlorine due to signal fluctuations at both ends of the scanning frequencies, i.e., < 0.1 Hz or > 1 kHz. The presence of monochloramine in solution was less detrimental to steady EIS data collection than free chlorine, but still led to significant challenges in obtaining the CPE capacitance based on the overall frequencies. To obtain reliable modeling outputs from the EIS data collected in the presence of chlorine biocides, narrower scan ranges around 1-10 Hz should be used instead.

10.0   SUMMARY AND KEY CONTRIBUTIONS

10.1   SUMMARY

The US total water withdrawal for human use reached 410 billion gallons a day in 2005, of which 85% was freshwater. Since then, thermoelectric power generation has become the single largest use of freshwater, surpassing agriculture. Given the increasing water shortage and growing energy demand, fierce competition for water for cooling in thermoelectric power plants is inevitable. To replace freshwater, alternative water sources, if abundant and reliable, can be used for cooling to help sustain power production in the future. However, complicated chemistries of many alternative waters and changing operating conditions in open recirculating cooling pose challenges for the use of traditional chemical approaches to simultaneously control mineral scaling, corrosion, and biofouling. This dissertation work evaluated three nontraditional water sources for use in power plant cooling systems, with a focus on understanding the mechanisms, kinetics, and inhibition of mineral precipitation and deposition (scaling).

Secondary-treated municipal wastewater (MWW) is a promising alternative as power plant cooling-system makeup water because of its wide availability, fairly consistent quality, and geographical proximity to power plants. Polymaleic acid (PMA), when dosed at 10 mg/L, effectively reduced scaling in this water by more than 90%, even at four cycles of concentration (CoC 4). However, when biofouling was not well controlled, scaling was accelerated due to

mineral incorporation into biofilm. PMA was compromised by free chlorine added for biofouling control. Monochloramine was less reactive with PMA than free chlorine. Phosphorous-based corrosion inhibitors were not appropriate as they precipitated with calcium. Chemical equilibrium modeling for scaling prediction was challenging in recirculating cooling systems using MWW because of kinetic limitations and complex water chemistries involved.

Two other alternative waters of impaired quality, passively-treated abandoned mine drainage (AMD) and clarified ash pond water (APW), were also evaluated for their feasibility as cooling system makeup water. PMA was effective in suppressing scaling in both waters. In clarified APW, which is available in many coal-fired power plants, mineral scaling was much less severe than in the mine drainage or MWW without scaling control. The addition of 10 mg/L of PMA helped to reduce scaling by 80% in laboratory water recirculating systems. In passively-treated (to remove Fe/Mn) AMD, PMA decreased the settling of suspended solids in the pipe flow sections of pilot-scale cooling towers. In the absence of PMA, significant amounts of solids settled in cooling tower sumps where flow velocity was minimal. Besides the flow effect, different surface materials accumulated different amounts of scale. PVC surfaces yielded more deposition than stainless steel. This observation implies that the severity of scaling problems can vary in different sections of a cooling system because of the varied flow patterns and surface materials.

For reliable predictions of the pH behavior of recirculating cooling water, which is important for proper cooling system operations, MINEQL+ based chemical modeling that considered the processes of degassing and kinetically-limited solids formation was able to capture the underlying mechanisms influencing the pH changes observed in pilot-scale cooling towers. The initial sharp increase of water pH from about 7.2 to 8.3 was well explained by the

CO$_2$ degassing mechanism. Continued pH increase up to 8.7 with increasing CoC was attributable to a combined effect of ammonia stripping and kinetically-limited carbonate precipitation. By using the knowledge of the makeup water quality and potential gas exchange, as well as mineral precipitation constraints, the new modeling approach greatly improves the ability to forecast the cooling water pH at various CoC, without measuring the alkalinity of the recirculating water.

In light of the effective scaling control by PMA in all the impaired waters studied, the antiscaling mechanisms of PMA were systematically investigated. Results show that the antiscaling mechanisms of PMA for mineral precipitation in bulk liquid were fundamentally different from those employed to control mineral deposition on substrate surface. Mineral precipitation in the bulk liquid was significantly delayed by PMA, even at very low dosing (< 1 ppm). Addition of PMA at high doses (> 5-10 ppm) completely eliminated a "fast precipitation" phase. Also, the rates of the "fast precipitation" were significantly reduced in the presence of PMA. Chemical analysis of the precipitates indicated that magnesium exhibited strong associations with PMA molecules, resulting in its incorporation in the newly-formed amorphous solids. The antideposition effect of PMA worked well to control surface deposition of pre-formed mineral solids in suspension. Surface adsorption of PMA onto those suspended particles increased the negative charges of the solids and rendered them less prone to deposition on negatively-charged surfaces. If the mineral solids were not pre-formed, PMA would participate in the precipitation process to alter the particle morphologies and surface charge distributions. However, these alterations appeared to cause losses of the antideposition ability of PMA.

As demonstrated in the studies with the three impaired waters, simple measurements of mineral mass gain on scaled surfaces can be crude, inconvenient, and time-consuming. Also, the

mineral mass gain measurements cannot be performed in real time. A more accurate and convenient approach for monitoring mineral deposition rates in real time was developed in this study. The electrical impedance of the metal-mineral-water interface was measured by Electrochemical Impedance Spectroscopy (EIS). The CPE capacitance obtained from the EIS measurements correlated very well with the mass of mineral deposits and was sensitive to small changes in the mineral mass deposited on the electrode (< 0.1 mg). The sensitivity of the EIS provides a new method for early detection of mineral deposition. Further analysis showed that narrower ranges (0.1 Hz or 1 Hz ± 10% of the frequency specified) of AC scanning frequencies can be used without sacrificing measurement sensitivity. This trait not only saves the measurement time and the EIS device cost, but proves to be particularly useful when the water contained chlorine biocides, which caused unstable EIS readings at frequencies < 0.1 Hz or > 1 kHz. To obtain reliable modeling outputs from the EIS data collected in the presence of chlorine biocides, narrower scan ranges around 1-10 Hz can be used.

The applicability of the EIS method for mineral deposition detection was further expanded to broader water chemistries and in solutions containing multiple minerals. The linear relationship between the changes of the CPE capacitance and the mineral mass deposited was proved to be valid in two-mineral systems (calcium carbonate and phosphate) and synthetic municipal wastewater containing a variety of dissolved species. Moreover, the presence of PMA, added in the solution as an antiscaling agent to mitigate scale formation, did not show significant interference with the EIS approach. This electrochemical method is, therefore, potentially very useful for convenient and sensitive scaling detection under practically-relevant cooling water conditions.

10.2 KEY CONTRIBUTIONS

This dissertation work contributes to our improved understanding of the kinetics, mechanisms, and inhibition of mineral precipitation and deposition in the context of wastewater reuse in industrial cooling systems. The results presented here enable a better prediction of the behavior of key water chemical parameters that influence mineral precipitation and deposition in recirculating cooling systems, and provide a new convenient and sensitive method for in situ scaling detection and rate monitoring. The results also help to guide the selection of antiscaling chemicals for effective control of mineral scaling in wastewater reuse. The specific contributions of this dissertation are summarized below:

- **Assembled an overview of the challenges of escalating water demands for energy production and the opportunities of using pre-treated wastewater in power plant cooling systems.**

- **Provided scientific evidence and understanding, through theoretical, laboratory, and pilot-scale studies, of the mineral scaling behaviors in three promising sources of impaired water as alternative makeup water for power plant cooling.** Scale formation in secondary-treated municipal wastewater under typical cooling tower operation was mainly due to high pH and high levels of suspended solids that were not sufficiently removed after secondary clarification. Good control of biofouling, which accelerated scaling through adsorption of minerals onto biofilm and co-precipitation of minerals with biosolids, was a critical issue. Scale formation in passively-treated abandoned mine drainage revealed the influence of flow patterns and surface materials, which resulted in varied degrees of scaling severity in different sections of a cooling tower system. Scale formation in clarified ash pond water, which represents an internally

available cooling water source in many coal-fired power plants, was the least among the three waters tested. Polymaleic acid worked effectively in mitigating scaling in all three impaired waters.

- **Proposed and validated a new approach for reliable pH prediction that accounts for complicated cooling water chemistries and kinetic limitations.** The approach built on the computation power of the chemical equilibrium model MINEQL+ and extended its utility for accurate pH prediction in cooling water systems.

- **Investigated the antiscaling mechanisms of polymaleic acid and obtained important insights.** Scaling mitigation by polymaleic acid was achieved through two distinct mechanisms: the retardation of mineral precipitation via competitive interactions with crystallizing species and the stabilization of suspended mineral particles via surface adsorption of the charged polymer molecules. An inadvertent effect of PMA, as revealed in this study, was that the amorphous mineral solids that incorporated PMA during precipitation appeared to favor surface deposition.

- **Developed a new electrochemical method for convenient and sensitive detection of mineral scaling and in situ measurements of scaling rates.** This method is based on Electrochemical Impedance Spectroscopy to replace a traditional gravimetric method for mineral mass determination. Its broad applicability was established under practically-relevant cooling water chemistries and cooling system operations.

11.0   FUTURE DIRECTIONS

Given the largely exploratory nature of the dissertation work and the encouraging results obtained, exciting and promising opportunities for future research are many. To broaden the scope of the exploration in the areas of mineral deposition monitoring and control, the future work in the following three principle directions should be the most fruitful:

- **Development of EIS-based sensor technologies for mineral scaling monitoring**

- **Elucidation of mineral-polymer interactions for improved scaling mitigation**

- **Engineering of substrate surfaces for mineral deposition inhibition**

Along the first direction, it will be practically meaningful to further explore the use of the electrochemical techniques in characterizing processes at solid-solution interfaces, which can be built on the electrochemical sensor that was developed for in situ detection of mineral deposition in cooling water systems.

- Combine the EIS data with other electrochemical measurements using the same experimental setup to obtain other information about mineral scaling process, such as the porosity and chemical heterogeneity, thereby to broaden the utility of the EIS method.

- Test the robustness of the EIS method under other practically relevant conditions and water chemistries, such as in the presence of non-oxidizing biocides and surface-coating based corrosion control chemicals.

– Identify the most widely applicable AC scanning frequencies to minimize interferences of chemical additives, and design portable EIS systems that measure mineral scaling over those frequencies.

– Reconfigure the EIS electrode setup to measure scaling/fouling across membrane filters.

Along the second direction, mineral interactions with organic polymers, either artificial polymers with well-defined structures and molecular sizes or natural organic matter, are ubiquitously important phenomena that influence many processes in both natural and engineering systems, processes that have been observed but not fully understood. To further study these interactions, specifically, future work may focus on the following:

– Formulate a theoretical framework based on classical nucleation theories or molecular dynamics to explain the experimentally observed precipitation retardation effects of PMA or other polymer antiscalants.

– In membrane filtration, investigate the interactions between mineral and organic constituents in feed solutions and on membrane surfaces or inside the pore structures to improve the understanding of the role of such interactions in the sorption and separation capacities of membranes.

– Investigate the role of minerals present in the extracellular polymeric substances in bio-adhesion. The underlying hypothesis is that the attractive forces between a cell and a surface may be derived primarily (or at least partially) from the mineral properties of both the cell membrane and its substrate.

Along the third direction, although a substantial amount of research has been devoted to the thermodynamics and kinetics of mineral precipitation and dissolution in bulk solutions, mineral precipitation in the bulk is different from surface deposition with respect to both reaction rates and crystal characteristics. It is generally accepted that there is much to be desired in our understanding of the interactions between mineral species (either ions or particles) and substrate surfaces. However, current practice in scale deposition control is still primarily focused on solution chemistry adjustment through chemical addition. In contrast, novel modification of substrate surfaces as an alternative scale deposition control strategy needs to be explored. Surface engineering-based scale inhibition can be a more sustainable approach because it does not involve bulk addition of chemicals, many of which may bear environmental and health consequences. Preliminary investigation (data reported elsewhere) demonstrated that the scale deposition process can be preferentially initiated with heterogeneous precipitation over homogeneous nucleation in the presence of a stainless steel surface in a synthetic MWW solution that is supersaturated with respect to calcium carbonate and phosphate. This finding supports the hypothesis that the surface properties play a significant role in the precipitation behavior of aqueous systems.

Because scale deposition is ultimately a surface phenomenon, a more accurate description of it would rely on a more fundamental understanding of the properties of surfaces that serve as deposition substrates. Such an improved understanding can very well lead to the novel engineering of surfaces to achieve surface properties that offer more effective and robust inhibition mechanisms against scale deposition.

- Alter the hydrophobicity of substrate samples by varying their surface chemical composition and investigate effects of surface hydrophobicity on scaling process.

- Tune the polarity and density of surface charges on substrate samples and investigate their effects on scaling process.

- Tailor the surface morphology of samples in both micrometer and nanometer scales and investigate effects of surface morphology on scaling process.

Other areas of interest for future work are more closely geared toward practical applications pertaining to scaling control in cooling systems. They include:

- Compare the differences in mineral scaling behavior on heated vs. unheated surfaces to obtain the temperature effect on scaling.

- Evaluate scale-caused losses of heat transfer efficiencies in heat exchangers to establish guidelines or "action criteria" for proper scaling control in heat exchangers.

- Place the scale collecting specimens at different locations within the recirculating water to test effects of flow patterns/hydrodynamics on scaling process.

BIBLIOGRAPHY

Chapter 1

1.   Gleick, P. H., Global freshwater resources: Soft-path solutions for the 21st century. *Science* **2003,** *302*, (5650), 1524-1528.

2.   Khuda, Z. R. M. M., Environmental degradation: Challenges of the 21st century. Environmental Survey and Research Unit, Dhaka, Bangladesh, **2001**.

3.   Bouwer, H., Integrated water management for the 21st century: Problems and solutions. *Journal of Irrigation and Drainage Engineering-ASCE* **2002,** *128*, (4), 193-202.

4.   Broome, J., The ethics of climate change. *Sci Am* **2008,** *298*, (6), 96-102.

5.   McCabe, G. J. and Wolock, D. M., Warming may create substantial water supply shortages in the Colorado River Basin. *Geophys Res Lett* **2007,** *34*, (22), p. L22708.

6.   Metcalf & Eddy (AECOM), Water reuse: issues, technologies, and applications. McGraw-Hill: New York, NY, **2007**.

7.   Vidic, R. D. and Dzombak, D. A., Reuse of treated internal or external wastewaters in the cooling systems of coal-based thermoelectric power plants. Final Technical Report to U.S. DOE/NETL, project number DE-FC26-06NT42722, **2009**.

8.   USGS, Estimated Use of Water in the United States in 2000. U.S. Geological Survey Circular 1268, Reston, VA, **2004**.

9.   USGS, Estimated Use of Water in the United States in 2005. U.S. Geological Survey Circular 1344, Reston, VA, **2009**.

10.   Tchobanoglous, G.; Burton, F. L.; Stensel, H. D., Wastewater engineering: treatment and reuse (4th ed.). McGraw-Hill: Boston, MA, **2003**.

11.   Muller-Steinhagen, H.; Malayeri, M. R.; Watkinson, A. P., Recent advances in heat exchanger fouling research, mitigation, and cleaning techniques. *Heat Transfer Engineering* **2007,** *28*, (3), 173-176.

12.   Wang, L. K. and Hung, Y.-T., Advanced physicochemical treatment technologies, Vol. 5 series: Handbook of Environmental Engineering, **2007**.

13. Rafferty, K., Scaling in geothermal heat pump systems. Technical report to U.S. DOE, Oregon Institute of Technology, Klamath Falls, OR, **1999**.

Chapter 2

1. Kenny, J.F., et al., *Estimated use of water in the United States in 2005: U.S. Geological Survey Circular 1344, 52 p.* 2009.

2. Hinrichsen, D. and B. Robey, *Solutions for a water-short world*. 1997: Baltimore, Johns Hopkins School of Public Health, Population Information Program.

3. Gerdes, K. and Nichols, C. *Water requirements for existing and emerging thermoelectric plant technologies*. DOE/NETL-402/080108, U.S. Department of Energy, National Energy Technology Laboratory, Pittsburgh, PA, 2008.

4. OECD/IEA, *Key world energy statistics*. 2007.

5. DOE-NETL, *Use of nontraditional water for power plant applications*. 2009: Oak Ridge, TN.

6. Feeley, T.J. and M. Ramezan. *Electric utilities and water: emerging issues and R&D needs*. in *9th Annual Industrial Wastes Technical and Regulatory Conference*. 2003. San Antonio, TX, Water Environment Federation.

7. Dishneau, D., *Frederick County denies cooling water to proposed power plant*, in *The Baltimore Examiner*. 2007.

8. EPRI, *Use of alternate water sources for power plant cooling*. 2008: Palo Alto, CA.

9. Roy, S.B., K.V. Summers, and R.A. Goldstein, *Water sustainability in the United States and cooling water requirements for power generation.* Universities Council on Water Resources / Water Resources Update, 2003(126): p. 94-99.

10. Nemerow, N.L. and F.J. Agardy, *Strategies of Industrial and Hazardous Waste Management*. 1998: New York, NY, John Wiley & Sons, Inc.

11. DOE-NETL, *Use of reclaimed water for power plant cooling*. 2007: Oak Ridge, TN. ANL/EVS/R-07/3.

12. DOE-NETL, *Power plant water usage and loss study*. 2005: http://www.netl.doe.gov/technologies/coalpower/gasification/pubs/pdf/WaterReport_IGCC_Final_August2005.pdf.

13. Vidic, R.D. and D.A. Dzombak, *Reuse of Treated Internal or External Wastewaters in the Cooling Systems of Coal-based Thermoelectric Power Plants*. 2009: Final Technical Report to US DOE/NETL, project number DE-FC26-06NT42722.

14.   USEPA, *Clean Watersheds Needs Survey: CWNS 2000 Report to Congress*. 2003, U.S. Environmental Protection Agency, Research Triangle Park, NC, EPA-832-R-03-001.

15.   USEPA, *Guidelines of Water Reuse, U.S. Agency for International Development, Washington, D.C.* 2004.

16.   Metcalf&Eddy(AECOM), *Water reuse: issues, technologies, and applications*, T. Asano and I. ebrary, Editors. 2007, McGraw-Hill: New York.

17.   Zdaniuk, G.J., L.M. Chamra, and P.J. Mago, *A survey of cooling tower water quality for condenser tube fouling potential.* Proceedings of the Institution of Mechanical Engineers Part a-Journal of Power and Energy, 2008. 222(A1): p. 111-122.

18.   Liu, X. Y., *A new kinetic model for three-dimensional heterogeneous nucleation*. J Chem Phys 1999. 111(4): p. 1628-1635.

19.   Liu, X. Y. and Lim, S. W., *Templating and supersaturation-driven anti-templating: Principles of biomineral architecture*. J Am Chem Soc 2003. 125(4): p. 888-895.

20.   Morse, J.W. and R.S. Arvidson, *The dissolution kinetics of major sedimentary carbonate minerals.* Earth-Science Reviews, 2002. 58(1-2): p. 51-84.

21.   Morse, J.W., R.S. Arvidson, and A. Luttge, *Calcium Carbonate Formation and Dissolution.* Chemical Reviews, 2007. 107(2): p. 342-381.

22.   Ferguson, J.F. and P.L. McCarty, *Effects of carbonate and magnesium on calcium phosphate precipitation.* Environmental Science & Technology, 1971. 5(6): p. 534-540.

23.   Walter, L.M., *Magnesian calcite stabilities: A reevaluation.* Geochimica et Cosmochimica Acta, 1984. 48(5): p. 1059-1069.

24.   Deleuze, M. and S.L. Brantley, *Inhibition of calcite crystal growth by Mg2+ at 100 C and 100 bars: Influence of growth regime.* Geochimica et Cosmochimica Acta, 1997. 61(7): p. 1475-1485.

25.   Nishino, Y., Y. Oaki, and H. Imai, *Magnesium-Mediated Nanocrystalline Mosaics of Calcite.* Crystal Growth & Design, 2009. 9(1): p. 223-226.

26.   Chen, C.W., et al., *Mechanochemical-hydrothermal synthesis of magnesium-substituted hydroxyapatite nanocrystals.* Abstracts of Papers of the American Chemical Society, 2003. 225: p. U48-U48.

27.   Suchanek, W.L., et al., *Mechanochemical-hydrothermal synthesis of calcium phosphate powders with coupled magnesium and carbonate substitution.* Journal of Solid State Chemistry, 2004. 177(3): p. 793-799.

28. Brecevic, L., A. Sendijarevic, and H. Fedi-Milhofer, *Precipitation of calcium phosphates from electrolyte solutions. VII. The influence of di- and tricarboxylic acids.* Colloids and Surfaces, 1984. 11: p. 55-68.

29. Inskeep, W.P. and J.C. Silvertooth, *Inhibition of Hydroxyapatite Precipitation in the Presence of Fulvic, Humic, and Tannic Acids.* Soil Sci Soc Am J, 1988. 52(4): p. 941-946.

30. Amjad, Z., *Influence of polyelectrolytes on the precipitation of amorphous calcium phosphate.* Colloids and Surfaces, 1990. 48: p. 95-106.

31. Grossl, P.R. and W.P. Inskeep, *Precipitation of Dicalcium Phosphate Dihydrate in the Presence of Organic Acids.* Soil Sci Soc Am J, 1991. 55(3): p. 670-675.

32. van der Houwen, J.A.M., et al., *The effect of organic ligands on the crystallinity of calcium phosphate.* Journal of Crystal Growth, 2003. 249(3-4): p. 572-583.

33. Alvarez, R., et al., *Effects of humic material on the precipitation of calcium phosphate.* Geoderma, 2004. 118(3-4): p. 245-260.

34. Cao, X., et al., *Inhibition of calcium phosphate precipitation under environmentally-relevant conditions.* Science of the Total Environment, 2007. 383(1-3): p. 205-215.

35. Shih, W.Y., et al., *A dual-probe approach for evaluation of gypsum crystallization in response to antiscalant treatment.* Desalination, 2003. 169: p. 213-221.

36. Frayne, C., *Cooling water treatment- principles and practices.* 1999, New York, NY: Chemical Publishing Co.

37. Rossmoore, H.W., *Handbook of biocide and preservative use.* 1995: Blackie Academic & Pro Professional, Chapter 3, page 50-77.

38. Ludensky, M., *Microbiological control in cooling water systems and directory of microbiocides for the protection of materials: a handbook, pp. 121-139.* 2005.

39. USEPA, *Alternative disinfectants and oxidants guidance manual.* 1999: United States Environmental Protection Agency, EPA 815-R-99-014.

40. Rao, T.S., Y.V. Nancharaiah, and K.V.K. Nair, *Biocidal efficacy of monochloramine against biofilm bacteria.* Biofouling, 1998. 12(4): p. 321-332.

41. Turetgen, I., *Comparison of the efficacy of free residual chlorine and monochloramine against biofilms in model and full scale cooling towers.* Biofouling, 2004. 20(2): p. 81-85.

42. Jolley, R., et al., *Water chlorination: environmental impact and health effects, Volume 4, Book 1.* 1983, Chemistry and Water Treatment, Ann Arbor Science, pp. 33.

43.   Wolfe, R.L., N.R. Ward, and B.H. Olson, *Inorganic chloramines as drinking water disinfectants: a review*. Journal of the American Water Works Association, 1984. 75: p. 74-88.

44.   Stumm, W. and J.J. Morgan, *Aquatic chemistry : chemical equilibria and rates in natural waters (2nd ed.)*. Environmental science and technology. 1996, New York: Wiley.

45.   EPRI, *Use of degraded water sources as cooling water in power plants (1005359)*. 2003: Energy Commisssion, Public Interest Energy Research Program, Sacramento, CA.

46.   Goldstein, D., J. Casana, and I. Wei. *Municipal wastewater reuse as makeup to cooling towers*. in *Proceedings of the Water Reuse Symposium II, AWWA Research Foundation*. 1981. Denver, CO.

47.   Schumerth, D.J., *Gray and impaired water cooling in surface condensers and heat exchangers*, in *Proceedings of PWR2006, ASME Power*. 2006: Atlanta, GA, USA.

48.   Rebhun, M. and G. Engel, *Reuse of wastewater for industrial cooling systems*. Journal of Water Pollution Control Federation, 1988. 60: p. 237-241.

49.   Nowack, B., *Environmental chemistry of phosphonates*. Water Research, 2003. 37(11): p. 2533-2546.

50.   *U.S. Energy Information Administration / International Energy Outlook 2010*. Cited July 5, 2010; Available from: http://www.eia.doe.gov/oiaf/ieo/electricity.html.

Chapter 3

1.   Miller, W. G. (2006). "Integrated concepts in water reuse: managing global water needs." Desalination **187**(1-3): 65-75.

2.   Metcalf & Eddy (2007). Water Reuse: issues, technologies, and applications, McGraw-Hill.

3.   Vidic, R. D. and D. A. Dzombak (2009). Reuse of treated internal or external wastewaters in the cooling systems of coal-based thermoelectric power plants, Final Technical Report to US DOE/NETL, project number DE-FC26-06NT42722.

4.   Ehrhardt, R. F. et al. (1986). Analysis of Alternate Sources of Cooling Water (EPRI-EA-4732). Palo Alto, CA, Electric Power Research Institute.

5.   EPRI (2008). Use of alternate water sources for power plant cooling. Palo Alto, CA.

6.   Weinberger, L. W. et al. (1966). "Solving our water problems- water renovation and reuse." Annals of the New York Academy of Sciences **136**: 131-154.

7.   Williams, R. B. and E. J. Middlebrooks (1982). Wastewater reuse- an assessment of the potential and technology. <u>Water Reuse</u>. Ann Arbor, MI, Ann Arbor Science Publishers.

8.   EPRI (2003). Use of degraded water sources as cooling water in power plants (1005359). Energy Commisssion, Public Interest Energy Research Program, Sacramento, CA.

9.   Shakkthivel, P. and T. Vasudevan (2006). "Acrylic acid-diphenylamine sulphonic acid copolymer threshold inhibitor for sulphate and carbonate scales in cooling water systems." <u>Desalination</u> **197**(1-3): 179-189.

10. Du, K. et al. (2009). "Fluorescent-Tagged No Phosphate and Nitrogen Free Calcium Phosphate Scale Inhibitor for Cooling Water Systems." <u>Journal of Applied Polymer Science</u> **113**(3): 1966-1974.

11. Eriksson, R. et al. (2007). "The calcite/water interface: I. Surface charge in indifferent electrolyte media and the influence of low-molecular-weight polyelectrolyte." <u>Journal of Colloid and Interface Science</u> **313**(1): 184-193.

12. Frayne, C. (1999). <u>Cooling water treatment- principles and practices</u>. New York, NY, Chemical Publishing Co.

13. Nowack, B. (2003). "Environmental chemistry of phosphonates." <u>Water Research</u> **37**(11): 2533-2546.

14. Kielemoes, J. et al. (2000). "Influence of Denitrification on the Corrosion of Iron and Stainless Steel Powder." <u>Environmental Science & Technology</u> **34**(4): 663-671.

15. Snoeyink, V. L. and D. Jenkins (1980). <u>Water chemistry</u>. New York, Wiley.

16. Scandolari, L. (03/12/2008). Common antiscalants used in cooling industry. Pittsburgh, PA (Kroft Chemical Co.), personal communication.

17. Beardwood, T. (12/17/2009). Common antiscalants used in cooling industry. Tuscon, AZ (Ashland Chemical Co./Drew Industrial), personal communication.

18. Christophersen, D. (12/19/2007). Common antiscalants used in cooling industry. Vandalia, OH (Crown Solutions/Veolia Water), personal communication.

19. Stumm, W. and J. J. Morgan (1996). <u>Aquatic chemistry : chemical equilibria and rates in natural waters (2nd ed.)</u>. New York, Wiley.

20. Nalepa, C. J. et al. (1999). "A comparison of bromine-based biocides in a medium-size cooling tower." <u>Journal of Cooling Tower Institute</u> **20**: 43-60.

21. Zhang, Y. et al. (2008). "Nitrification in Premise Plumbing: Role of Phosphate, pH and Pipe Corrosion." <u>Environmental Science & Technology</u> **42**(12): 4280-4284.

22. Chien, S.-H. et al. (2010). "Chloramination as biofouling control strategy when using secondary-treated municipal wastewater as power plant cooling system makeup." submitted.

23. Hsieh, M.-K. et al. (2010). "Corrosion control when using secondary-treated municipal wastewater as alternative makeup water for cooling tower systems." Submitted.

24. Gehrke, N. et al. (2005). "Superstructures of Calcium Carbonate Crystals by Oriented Attachment." Crystal Growth & Design **5**(4): 1317-1319.

25. Anderson, H. A. and J. D. Russell (1976). "Possible relationship between soil fulvic acid and polymaleic acid." Nature **260**(5552): 597.

26. Hess, A. N. and Y.-P. Chin (1996). "Physical and chemical characteristics of poly(maleic acid), a synthetic organic colloid analog." Colloids and Surfaces A: Physicochemical and Engineering Aspects **107**: 141-154.

27. Wang, L. L. et al. (1997). "Adsorption of (poly)maleic acid and an aquatic fulvic acid by goethite." Geochimica Et Cosmochimica Acta **61**(24): 5313-5324.

28. Li, C. W. et al. (2000). "Use of UV spectroscopy to characterize the reaction between NOM and free chlorine." Environmental Science & Technology **34**(12): 2570-2575.

29. Kitis, M. et al. (2001). "The reactivity of natural organic matter to disinfection byproducts formation and its relation to specific ultraviolet absorbance." Water Science and Technology **43**(2): 9-16.

30. Hassan, K. Z. A. et al. (2006). "Iron oxide enhanced chlorine decay and disinfection by-product formation." Journal of Environmental Engineering-Asce **132**(12): 1609-1616.

31. Roccaro, P. et al. (2008). "Differential absorbance study of effects of temperature on chlorine consumption and formation of disinfection by-products in chlorinated water." Water Research **42**(8-9): 1879-1888.

32. Chowdhury, S. et al. (2009). "Models for predicting disinfection byproduct (DBP) formation in drinking waters: A chronological review." Science of the Total Environment **407**(14): 4189-4206.

33. Johnstone, D. W. and C. M. Miller (2009). "Fluorescence Excitation-Emission Matrix Regional Transformation and Chlorine Consumption to Predict Trihalomethane and Haloacetic Acid Formation." Environmental Engineering Science **26**(7): 1163-1170.

34. Sperandio, M. and E. Paul (1997). "Determination of carbon dioxide evolution rate using on-line gas analysis during dynamic biodegradation experiments." Biotechnology and Bioengineering **53**(3): 243-252.

35. Ficara, E. and A. Rozzi (2004). "Coupling pH-stat and DO-stat titration to monitor degradation of organic substrates." Water Science and Technology **49**(1): 69-77.

36. Weissenbacher, N. et al. (2007). "Determination of activated sludge biological activity using model correct CO2 off-gas data." Water Research **41**(7): 1587-1595.

37. Zhang, P. et al. (2009). "Waste activated sludge hydrolysis and short-chain fatty acids accumulation under mesophilic and thermophilic conditions: Effect of pH." Water Research **43**(15): 3735-3742.

38. Shakkthivel, P. et al. (2005). "Water soluble copolymers for calcium carbonate and calcium sulphate scale control in cooling water systems." Journal of Applied Polymer Science **96**(4): 1451-1459.

39. Sonnenberg, L. et al. (2007). "Quantitative Single Molecule Measurements on the Interaction Forces of Poly(l-glutamic acid) with Calcite Crystals." Journal of the American Chemical Society **129**(49): 15364-15371.

40. d'Abzac, P. et al. (2010). "Characterization of the Mineral Fraction Associated to Extracellular Polymeric Substances (EPS) in Anaerobic Granular Sludges." Environmental Science & Technology **44**(1): 413-418.

41. Schecher, W. D. and D. C. McAvoy (1992). "MINEQL+: A software environment for chemical equilibrium modeling." Computers, Environment and Urban Systems **16**(1): 65-76.

42. Schecher, W. D. and D. C. McAvoy (1999). MINEQL+ Chemical Equilibrium Modeling System, Version 4 for Windows. Hallowell, ME, Environmental Research Software.

43. Ogino, T. et al. (1990). "The rate and mechanism of polymorphic transformation of calcium carbonate in water." Journal of Crystal Growth **100**(1-2): 159-167.

44. Gutjahr, A. et al. (1996). "Studies of the growth and dissolution kinetics of the CaCO3 polymorphs calcite and aragonite I. Growth and dissolution rates in water." Journal of Crystal Growth **158**(3): 296-309.

45. Alvarez et al. (2004). "Effects of humic material on the precipitation of calcium phosphate." Geoderma **118**(3-4): 245-260.

46. Kjellin, P. et al. (2001). "A new method for the study of calcium carbonate growth on steel surfaces." Colloids and Surfaces A: Physicochemical and Engineering Aspects **194**(1-3): 49-55.

47. Kjellin, P. (2003). "X-ray diffraction and scanning electron microscopy studies of calcium carbonate electrodeposited on a steel surface." Colloids and Surfaces A: Physicochemical and Engineering Aspects **212**(1): 19-26.

48. Wei, H. et al. (2004). "Crystallization habit of calcium carbonate in presence of sodium dodecyl sulfate and/or polypyrrolidone." Journal of Crystal Growth **260**(3-4): 545-550.

49.   Wei, H. et al. (2005). "On the crystallization of calcium carbonate modulated by anionic surfactants." <u>Journal of Crystal Growth</u> **279**(3-4): 439-446.

Chapter 4

1.   Akcil, A. and Koldas, S. (2006) Acid mine drainage (AMD): causes, treatment and case studies. *Journal of Cleaner Production*, 14(12-13): 1139-1145.

2.   Rios, C.A., Williams, C.D., and Roberts, C.L. (2008) Removal of heavy metals from acid mine drainage (AMD) using coal fly ash, natural clinker and synthetic zeolites. *Journal of Hazardous Materials*, 156(1-3): 23-35.

3.   Hustwit, C.C., Ackman, T.E., and Erickson, P.E. (1992) The role of oxygen-transfer in acid-mine drainage (AMD) treatment. *Water Environment Research*, 64(6): 817-823.

4.   USGS, Coal-Mine-Drainage Projects in Pennsylvania, USGS, 2008. Accessed: May 7, 2009. http://pa.water.usgs.gov/projects/amd/.

5.   U.S. Environmental Protection Agency (EPA) (1995) Streams with fisheries impacted by acid mine drainage in Maryland, Ohio, Pennsylvania, Virginia, and West Virginia. Philadelphia, PA.

6.   USGAO, Freshwater Supply—States' Views of How Federal Agencies Could Help Them Meet the Challenges of Expected Shortages, GAO-03-514, U.S. General Accounting Office, Washington, DC, 2003.

7.   Roy, S.; Summers, K.; Chung, C.; and Radde, J. (2003) A Survey of water use and sustainability in the United States with a focus on power generation. 1005474, Electric Power Research Institute, Palo Alto, CA.

8.   USGS, Estimated Use of Water in the United States in 1995, USGS Circular 1200, U.S. Geological Survey, Reston, VA, 1998.

9.   Veil, J.A.; Kupar, J.M.; Puder, M.G.; Feeley, T.K. "Beneficial use of mine pool water for power generation," Ground Water Protection Council Annual Forum, Niagara Falls, NY, September 13-17, 2003a.

10.   Veil, J.A.; Kupar, J.M.; Puder, M.G., Use of Mine Pool Water for Power Plant Cooling, W-31-109-Eng-38, U.S. Department of Energy, National Energy Technology Laboratory, Pittsburgh, PA, 2003b.

11.   Hedin, R.S.; Narin, R.W.; Kleinmann, R.L.P., Passive Treatment of Coal Mine Drainage, IC 9389, Bureau of Mines, U.S. Department of Interior, 1994.

12.   Fish, C.L. and Fish, D.H., "Remediation of abandoned mine discharges in the Loyalhanna Creek Watershed", 16th Annual International Pittsburgh Coal Conference, Pittsburgh, PA, 1999.

13.   Lambert, D.C.; McDonough, K.M., Dzombak, D.A. "Long-term changes in quality of discharge water from abandoned underground coal mines in Uniontown Syncline, Fayette County, PA, USA". Water Research, 38, 277-288, 2004.

14.   Veil, J.A. and Puder, M.G., Update on Use of Mine Pool Water for Power Generation, ANL/EVS/R-06/6, U.S. Department of Energy, National Energy Technology Laboratory, Pittsburgh, PA, 2006.

15.   Schecher, W. D. & McAvoy, D. C. (1992) MINEQL+: a software environment for chemical equilibrium modeling. Computers, Environment and Urban Systems 16(1): 65-76.

16.   Schecher, W. D. & McAvoy, D. C. (1999) MINEQL+ chemical equilibrium modeling system, version 4 for Windows. Environmental Research Software, Hallowell, ME.

17.   APHA/AWWA/WEF, Standard Methods for The Examination of Water & Wastewater: Centennial Edition, 21st edition, APHA, 2005.

18.   ASTM (2000) Standard Guide for Selecting Test Methods to Determine the Effectiveness of Antimicrobial Agents and Other Chemicals for the Prevention, Inactivation and Removal of Biofilm, ASTM E1427-00, American Society for Testing and Materials, West Conshohocken, PA.

19.   ASTM "Standard practice for preparing, cleaning, and evaluating corrosion test specimens," ASTM Standard G1-03, Annual Book of ASTM Standards, Philadelphia, PA, 2005.

Chapter 5

1.   Suloway, J.J., Skelly, T.M., Roy, W.R., Dickerson, D.R., Schuller, R.M., Griffin, R.A., "Chemical and toxicological properties of coal fly ash", *Environmental Geology Notes*, Illinois State Geological Survey, No. 105, 1983.

2.   Roy, W.R.; Griffin, R.A., Dickerson, D.R., Schuller, R.M., Illinois Basin coal fly ashes. 1. Chemical characterization and solubility, *Environmental Science & Technology*, 18(10), 734-739, 1984.

3.   Litherland, S.T., Nassos, P.A., Owen, M.L., Winton, S.L., *Pilot Scale Investigations of Closed Loop Ash Sluicing*, DCN-83-211-004-35, Radian Corp., Austin, TX, 1983.

4.   Nemerow, N.L. and Agardy, F.J., *Strategies of Industrial and Hazardous Waste Management*, 2nd edition, John Wiley & Sons, Inc., New York, NY, 1998.

5.   NETL, Power plant Water Usage and Loss, DOE/NETL-401/08012005, U.S. Department of Energy, National Energy Technology Laboratory, Pittsburgh, PA, 2005 (May 2007 updated).

6.   APHA, AWWA and WEF (1998), Standard Methods for the Examination of Water and Wastewater, 20 ed., American Public Health Association, American Water Works Association, Water Environment Federation, Washington, DC, 20005-2605.

7.   Schecher, W. D. & McAvoy, D. C. (1992) MINEQL+: a software environment for chemical equilibrium modeling. Computers, Environment and Urban Systems 16(1): 65-76.

8.   Schecher, W. D. & McAvoy, D. C. (1999) MINEQL+ chemical equilibrium modeling system, version 4 for Windows. Environmental Research Software, Hallowell, ME.

9.   Christophersen, D. (2007) Common antiscalants used in cooling industry. Vandalia, OH (Crown Solutions/Veolia Water), Personal communication.

Chapter 6

1.   Sheikholeslami, R., Scaling potential index (SPI) for CaCO3 based on Gibbs free energies. *AICHE Journal* 2005, *51*, (6), 1782-1789.

2.   Mattilasandholm, T.; Wirtanen, G., Biofilm Formation in the Industry - a Review. *Food Reviews International* 1992, *8*, (4), 574-603.

3.   TetraTech, Use of Alternate Water Sources for Power Plant Cooling; 1014935; EPRI, Palo Alto, CA, 2008.

4.   Vidic, R. D. and Dzombak, D. A., *Reuse of treated internal or external wastewaters in the cooling systems of coal-based thermoelectric power plants*; Final Technical Report to US DOE/NETL, project number DE-FC26-06NT42722.: 2009.

5.   Schecher, W. D.; McAvoy, D. C., MINEQL+: A software environment for chemical equilibrium modeling. *Computers, Environment and Urban Systems* 1992, *16*, (1), 65-76.

6.   Schecher, W. D.; McAvoy, D. C., MINEQL+ Chemical Equilibrium Modeling System, Version 4 for Windows. In Environmental Research Software: Hallowell, ME, 1999.

7.   Puckorius, P. R., Get a better reading on scaling tendency of cooling waters. *Power Journal* 1993, 79-81.

8.   Caplan, G., WaterText. In Personal communication with Crown Solutions/Veolia Water, 2008.

9.   Kunz, R. G., Environmental Calculations: A Multimedia Approach. Wiley-AIChE: p.570, 2009.

Chapter 7

1.   Muller-Steinhagen, H.; Malayeri, M. R.; Watkinson, A. P., Recent advances in heat exchanger fouling research, mitigation, and cleaning techniques. *Heat Transfer Eng* **2007,** *28*, (3), 173-176.

2.   Steinhagen, R.; Mullersteinhagen, H.; Maani, K., Problems and Costs Due to Heat-Exchanger Fouling in New-Zealand Industries. *Heat Transfer Eng* **1993,** *14*, (1), 19-30.

3.   Yang, Q.; Liu, Y.; Gu, A.; Ding, J.; Shen, Z., Investigation of induction period and morphology of CaCO3 fouling on heated surface. *Chemical Engineering Science* **2002,** *57*, (6), 921-931.

4.   Sear, R. P., Statistical theory of nucleation in the presence of uncharacterized impurities. *Physical Review E* **2004,** *70*, (2), 021605.

5.   Nielsen, A. E.; Toft, J. M., Electrolyte crystal growth kinetics. *Journal of Crystal Growth* **1984,** *67*, (2), 278-288.

6.   Nielsen, A. E., Electrolyte crystal growth mechanisms. *Journal of Crystal Growth* **1984,** *67*, (2), 289-310.

7.   D. Kashchiev, G. M. v. R., Review: Nucleation in solutions revisited. *Crystal Research and Technology* **2003,** *38*, (7-8), 555-574.

8.   Stumm, W.; Sigg, L.; Sulzberger, B., *Chemistry of the solid-water interface : processes at the mineral-water and particle-water interface in natural systems*. Wiley: New York, 1992.

9.   Liu, X. Y., A new kinetic model for three-dimensional heterogeneous nucleation. *The Journal of Chemical Physics* **1999,** *111*, (4), 1628-1635.

10.   Anklam, M. R.; Firoozabadi, A., An interfacial energy mechanism for the complete inhibition of crystal growth by inhibitor adsorption. *The Journal of Chemical Physics* **2005,** *123*, (14), 144708.

11.   Smith, B. R., Scale prevention by addition of polyelectrolytes. *Desalination* **1967,** *3*, (3), 263-268.

12.   Weijnen, M. P. C.; van Rosmalen, G. M., The influence of various polyelectrolytes on the precipitation of gypsum. *Desalination* **1985,** *54*, 239-261.

13. Oner, M.; O Dog an; Oner, G., The influence of polyelectrolytes architecture on calcium sulfate dihydrate growth retardation. *J Cryst Growth* **1998,** *186*, (3), 427-437.

14. Tadros, M. E.; Mayes, I., Linear growth rates of calcium sulfate dihydrate crystals in the presence of additives. *Journal of Colloid and Interface Science* **1979,** *72*, (2), 245-254.

15. Austin, A. E.; Miller, J. F.; Vaughan, D. A.; Kircher, J. F., Chemical additives for calcium sulfate scale control. *Desalination* **1975,** *16*, (3), 345-357.

16. Amjad, Z., Advances in crystal growth inhibition technologies. In ebrary, I., Ed. Kluwer Academic/Plenum Publishers: New York, 2000.

17. Christian, G. D., MCI Analytical Test Procedure: 9437 photometric enhanced polymer reagent system. Personal communication with the technical support at MCI, 04/20/2010. In 2010.

18. Nebbioso, A.; Piccolo, A., Molecular Rigidity and Diffusivity of Al3+ And Ca2+ Humates As Revealed by NMR Spectroscopy. *Environmental Science & Technology* **2009,** *43*, (7), 2417-2424.

19. Mao, Y.; Fung, B. M., A Study of the Adsorption of Acrylic Acid and Maleic Acid from Aqueous Solutions onto Alumina. *Journal of Colloid and Interface Science* **1997,** *191*, (1), 216-221.

20. Zhang, F.; Hou, Z.; Sheng, K.; Deng, B.; Xie, L., Crystallization of calcium carbonate on polyethylene [gamma]-radiation-grafted with acrylic acid. *Journal of Materials Chemistry* **2006,** *16*, (13), 1215-1221.

21. Wang, L.; Chin, Y.-P.; Traina, S. J., Adsorption of (poly)maleic acid and an aquatic fulvic acid by geothite. *Geochimica et Cosmochimica Acta* **1997,** *61*, (24), 5313-5324.

22. Shustak, G.; Domb, A. J.; Mandler, D., Preparation and Characterization of n-Alkanoic Acid Self-Assembled Monolayers Adsorbed on 316L Stainless Steel. *Langmuir* **2004,** *20*, (18), 7499-7506.

23. Raman, A.; Gawalt, E. S., Self-Assembled Monolayers of Alkanoic Acids on the Native Oxide Surface of SS316L by Solution Deposition. *Langmuir* **2007,** *23*, (5), 2284-2288.

24. Raman, A.; Quinones, R.; Barriger, L.; Eastman, R.; Parsi, A.; Gawalt, E. S., Understanding Organic Film Behavior on Alloy and Metal Oxides. *Langmuir* **2009,** *26*, (3), 1747-1754.

25. Giasuddin, A. B. M.; Kanel, S. R.; Choi, H., Adsorption of Humic Acid onto Nanoscale Zerovalent Iron and Its Effect on Arsenic Removal. *Environmental Science & Technology* **2007,** *41*, (6), 2022-2027.

26. Pereira, M. O.; Vieira, M. J.; and Beleza, V. M., Retention of bacteria by cellulose fibres as a means of reducing biofouling in paper pulp production processes. *Biofouling* **1998**, 13, (1), 1-18.

Chapter 8

1. Langelier, W.F., *The analytical control of anti-corrosion water treatment.* J Am Water Works Assoc., 1936. **28**: p. 1500-1521.

2. Puckorius, P.R. and J.M. Brooke, *A new practical index for calcium carbonate scale prediction in cooling tower systems.* Corrosion, 1991. **47**(4): p. 280-284.

3. Azaroual, M., Ch. Kervévana, M.N. Durance, and P. Durst, *SCALE2000: reaction-transport software dedicated to thermo-kinetic prediction and quantification of scales - Applicability to desalination problems.* Desalination, 2004. **165**(1-3): p. 409-419.

4. Sheikholeslami, R., *Scaling potential index (SPI) for $CaCO_3$ based on Gibbs free energies.* AICHE Journal, 2005. **51**(6): p. 1782-1789.

5. Sheikholeslami, R., *Scaling of process equipment by saline streams - challenges ahead.* Water Science and Technology, 2004. **49**(2): p. 201-210.

6. McGaughey, L.M. and J.V. Matson, *Prediction of the calcium carbonate saturation pH in cooling water.* Water Research, 1980. **14**(12): p. 1729-1735.

7. Koutsoukos, P.G., A.N. Kofina, and D.G. Kanellopoulou, *Solubility of salts in water: Key issue for crystal growth and dissolution processes.* Pure and Applied Chemistry, 2007. **79**(5): p. 826-850.

8. Elfil, H. and H. Roques, *Prediction of the limit of the metastable zone in the $CaCO_3$-CO_2-H_2O system.* AIChE Journal, 2004. **50**(8): p. 1908-1916.

9. Elfil, H. and A. Hannachi, *Reconsidering water scaling tendency assessment.* Aiche Journal, 2006. **52**(10): p. 3583-3591.

10. Quddus, A. and L.M. Al-Hadhrami, *Hydrodynamically deposited $CaCO_3$ and $CaSO_4$ scales.* Desalination, 2009. **246**(1-3): p. 526-533.

11. Wu, Z., J.H. Davidson, and L.F. Francis, *Effect of water chemistry on calcium carbonate deposition on metal and polymer surfaces.* Journal of Colloid and Interface Science, 2010. **343**(1): p. 176-187.

12. Kameli, M., N. Esmaeili, and H. Rahimi Mofrad, *Diagnosis of heat exchanger scales in cooling water systems.* Iranian Journal of Chemistry and Chemical Engineering, 2008. **27**(1): p. 66-71.

13.   Rosmaninho, R., G. Rizzob, H. Müller-Steinhagen, and L.F. Melo, *Deposition from a milk mineral solution on novel heat transfer surfaces under turbulent flow conditions.* Journal of Food Engineering, 2008. **85**(1): p. 29-41.

14.   Hinderliter, B.R., S.G. Croll, D.E. Tallman, Q. Su, and G.P. Bierwagen, *Interpretation of EIS data from accelerated exposure of coated metals based on modeling of coating physical properties.* Electrochimica Acta, 2006. **51**(21): p. 4506-4515.

15.   Akbarinezhad, E., M. Bahremandic, H.R. Faridia, and F. Rezaei, *Another approach for ranking and evaluating organic paint coatings via electrochemical impedance spectroscopy.* Corrosion Science, 2009. **51**(2): p. 356-363.

16.   Liu, C., Q. Bi, and A. Matthews, *EIS comparison on corrosion performance of PVD TiN and CrN coated mild steel in 0.5 N NaCl aqueous solution.* Corrosion Science, 2001. **43**(10): p. 1953-1961.

17.   Liu, C., Q. Bi, A. Leylanda, and A. Matthewsaet, *An electrochemical impedance spectroscopy study of the corrosion behaviour of PVD coated steels in 0.5 N NaCl aqueous solution: Part I. Establishment of equivalent circuits for EIS data modelling.* Corrosion Science, 2003. **45**(6): p. 1243-1256.

18.   Liu, C., Q. Bi, A. Leylanda, and A. Matthewsa, *An electrochemical impedance spectroscopy study of the corrosion behaviour of PVD coated steels in 0.5 N NaCl aqueous solution: Part II.: EIS interpretation of corrosion behaviour.* Corrosion Science, 2003. **45**(6): p. 1257-1273.

19.   Diard, J.P., B. Le Gorrec, and C. Montella, *EIS study of electrochemical battery discharge on constant load.* Journal of Power Sources, 1998. **70**(1): p. 78-84.

20.   Diard, J.-P., B. Le Gorrec, C. Montella, and P. Landaud, *Constant load vs constant current EIS study of electrochemical battery discharge.* Electrochimica Acta, 1997. **42**(23-24): p. 3417-3420.

21.   Bouchet, R., S. Lascaud, and M. Rosso, *An EIS study of the anode Li/PEO-LiTFSI of a Li polymer battery.* Journal of the Electrochemical Society, 2003. **150**(10): p. A1386-A1389.

22.   Wagner, N. and E. Gulzow, *Change of electrochemical impedance spectra (EIS) with time during CO-poisoning of the Pt-anode in a membrane fuel cell.* Journal of Power Sources, 2004. **127**(1-2): p. 341-347.

23.   Manohar, A.K., O. Bretschger, K.H. Nealson, and F. Mansfeld, *The use of electrochemical impedance spectroscopy (EIS) in the evaluation of the electrochemical properties of a microbial fuel cell.* Bioelectrochemistry, 2008. **72**(2): p. 149-154.

24.   He, Z. and F. Mansfeld, *Exploring the use of electrochemical impedance spectroscopy (EIS) in microbial fuel cell studies.* Energy & Environmental Science, 2009. **2**(2): p. 216-219.

25.   Fu, Y.Z., R. Yuan, L. Xu, Y. Chai, X. Zhong, and D. Tang, *Indicator free DNA hybridization detection via EIS based on self-assembled gold nanoparticles and bilayer two-dimensional 3-mercaptopropyltrimethoxysilane onto a gold substrate.* Biochemical Engineering Journal, 2005. **23**(1): p. 37-44.

26.   Reis, F.M., H.G. De Melo, and I. Costa, *EIS investigation on Al 5052 alloy surface preparation for self-assembling monolayer.* Electrochimica Acta, 2006. **51**(8-9): p. 1780-1788.

27.   Feng, Y.Y., Chen, J. You, and W. Gu, *Investigation of alkylamine self-assembled films on iron electrodes by SEM, FT-IR, EIS and molecular simulations.* Electrochimica Acta, 2007. **53**(4): p. 1743-1753.

28.   Shervedani, R.K. and S. Pourbeyram, *Zirconium immobilized on gold-mercaptopropionic acid self-assembled monolayer for trace determination of phosphate in blood serum by using CV, EIS, and OSWV.* Biosensors & Bioelectronics, 2009. **24**(7): p. 2199-2204.

29.   Shervedani, R.K., F. Yaghoobia, A. Hatefi-Mehrjardia, and S.M. Siadat-Barzoki, *Electrocatalytic activities of gold-6-amino-2-mercaptobenzimidazole-Mn+ self-assembled monolayer complexes (Mn+: Ag+, Cu2+) for hydroquinone oxidation investigated by CV and EIS.* Electrochimica Acta, 2008. **53**(12): p. 4186-4192.

30.   Perrin, F.X., C. Merlatti, E. Aragon, and A. Margaillan, *Degradation study of polymer coating: Improvement in coating weatherability testing and coating failure prediction.* Progress in Organic Coatings, 2009. **64**(4): p. 466-473.

31.   Scharnagl, N., C. Blawert, and W. Dietzel, *Corrosion protection of magnesium alloy AZ31 by coating with poly(ether imides) (PEI).* Surface & Coatings Technology, 2009. **203**(10-11): p. 1423-1428.

32.   Gonzalez, J.E.G., F.J.H. Santana, and J.C. Mirza-rosca, *Effect of bacterial biofilm on 316 SS corrosion in natural seawater by EIS.* Corrosion Science, 1998. **40**(12): p. 2141-2154.

33.   Kavanagh, J.M., et al., *Monitoring fouling of reverse osmosis membranes using electrical impedance spectroscopy: measurements and simulations.* Desalination, 2009. **236**(1-3): p. 187-193.

34.   Deslouis, C., C. Gabriellia, M. Keddama, A. Khalila, R. Rossetb, B. Tribolleta, and M. Zidoune, *Impedance techniques at partially blocked electrodes by scale deposition.* Electrochimica Acta, 1997. **42**(8): p. 1219-1233.

35.   Gabrielli, C., M. Keddama, A. Khalila, R. Rossetb, and M. Zidoune, *Study of calcium carbonate scales by electrochemical impedance spectroscopy.* Electrochimica Acta, 1997. **42**(8): p. 1207-1218.

36.   Neville, A. and A.P. Morizot, *A combined bulk chemistry/electrochemical approach to study the precipitation, deposition and inhibition of CaCO₃.* Chemical Engineering Science, 2000. **55**(20): p. 4737-4743.

37.   Barchiche, C., C. Deslouisb, O. Gil, P. Refaita, and B. Tribollet, *Characterisation of calcareous deposits by electrochemical methods: Role of sulphates, calcium concentration and temperature.* Electrochimica Acta, 2004. **49**(17-18): p. 2833-2839.

38.   Devos, O., C. Gabrielli, and B. Tribollet, *Simultaneous EIS and in situ microscope observation on a partially blocked electrode application to scale electrodeposition.* Electrochimica Acta, 2006. **51**(8-9): p. 1413-1422.

39.   Marin-Cruz, J., R. Cabrera-Sierra, M.A. Pech-Canul, and I. González, *EIS characterization of the evolution of calcium carbonate scaling in cooling systems in presence of inhibitors.* Journal of Solid State Electrochemistry, 2007. **11**(9): p. 1246-1252.

40.   Rakitin, A.R. and V.I. Kichigin, *Electrochemical study of calcium carbonate deposition on iron. Effect of the anion.* Electrochimica Acta, 2009. **54**(9): p. 2647-2654.

41.   Marin-Cruz, J., R. Cabrera-Sierraa, M.A. Pech-Canuld, and I. González, *EIS study on corrosion and scale processes and their inhibition in cooling system media.* Electrochimica Acta, 2006. **51**(8-9): p. 1847-1854.

42.   Orazem, M.E. and B. Tribollet, *Electrochemical impedance spectroscopy.* The Electrochemical Society series. 2008, Hoboken, N.J.: Wiley.

43.   Horowitz, P. and W. Hill, *The art of electronics.* 1980, Cambridge, [Eng.] New York: Cambridge University Press.

44.   Jorcin, J.B., M.E. Orazemb, N. Pébèrea, and B. Tribollet, *CPE analysis by local electrochemical impedance spectroscopy.* Electrochimica Acta, 2006. **51**(8-9): p. 1473-1479.

45.   Pajkossy, T., *Impedance spectroscopy at interfaces of metals and aqueous solutions -- Surface roughness, CPE and related issues.* Solid State Ionics, 2005. **176**(26-28): p. 1997-2003.

46.   Skale, S., V. Dolecek, and M. Slemnik, *Substitution of the constant phase element by Warburg impedance for protective coatings.* Corrosion Science, 2007. **49**(3): p. 1046-1055.

47.   Emmanuel, B. and M.S. Grp, *Constant phase elements, depressed arcs and analytic continuation: A critique.* Journal of Electroanalytical Chemistry, 2008. **624**(1-2): p. 14-20.

48.   Schecher, W.D. and D.C. McAvoy, *MINEQL+: a chemical equilibrium program for personal computers- user's mannual.* 2003, Environmental Research Software: Hallowell, ME.

Chapter 9

1.   Leenheer, J. A.; Wilson, M. A.; Malcolm, R. L., *Org. Geochem.* **1987,** *11*, (4), 273.

2.   Orazem, M. E.; Tribollet, B., *Electrochemical impedance spectroscopy*. Wiley: Hoboken, N.J., 2008.

3.   Benjamin, M. M., *Water chemistry*. McGraw-Hill: 2002.

4.   Snoeyink, V. L.; Jenkins, D., *Water chemistry*. Wiley: New York, 1980.

5.   Vasquez, F. A.; Heaviside, R.; Tang, Z. J.; Taylor, J. S., Effect of free chlorine and chloramines on lead release in a distribution system. *Journal American Water Works Association* **2006,** *98*, (2), 144-154.

6.   Boyd, G. R.; Dewis, K. M.; Korshin, G. V.; Reiber, S. H.; Schock, M. R.; Sandvig, A. M.; Giani, R., Effects of changing disinfectants on lead and copper release. *Journal American Water Works Association* **2008,** *100*, (11), 75-87.

7.   Vasquez, F. A. Effect of free chlorine and chloramines on lead release in a distribution system (M.S. thesis). University of Central Florida, Orlando, FL, 2005.